

Wear of a Total Ankle Replacement

Alexandra Smyth

Submitted in accordance with the requirements for the degree of
Doctor of Philosophy

The University of Leeds

School of Mechanical Engineering

June 2017

The candidate confirms that the work submitted is her own, except where work which has formed part of jointly-authored publications has been included. The contribution of the candidate and the other authors to this work has been explicitly indicated below. The candidate confirms that appropriate credit has been given within the thesis where reference has been made to the work of others.

Chapters 2 and 3 were based on work from a jointly authored publication detailed below, all of the experimental work and analysis was directly attributable to me. Smyth, A., Fisher, J., Suñer, S., Brockett, C.L., 2017. Influence of kinematics on the wear of a total ankle replacement. *Journal of Biomechanics*, 53, pp.105–110.

This copy has been supplied on the understanding that it is copyright material and that no quotation from the thesis may be published without proper acknowledgement

© 2017 The University of Leeds and Alexandra Smyth

The right of Alexandra Smyth to be identified as Author of this work has been asserted by her in accordance with the Copyright, Designs and Patents Act 1988.

ACKNOWLEDGEMENTS

Submitting this thesis at the end of my ninth year in the School of Mechanical Engineering it's safe to say I've made myself at home here. Should I make it to ten someone needs to kick me out!

Firstly, my thanks has to go to Dr. Claire Brockett for taking me on as her first PhD student and proving to be the most thoughtful, supportive supervisor anyone could hope for. None of this would have been possible without your input and encouragement. Secondly to Prof. John Fisher for adding his endless wisdom and insight and pointing out when I was right and he was wrong so I didn't have to.

During this process I have had the opportunity to draw on so much expertise. Silvia and Chuck provided continued industrial input combined with the freedom to do as I pleased. Additionally, the ankle research group at Chapel Allerton Hospital and iMBE on the whole have provided a lot of enlightenment on this journey.

I owe a lot to the technical team; Phil, Rhys, Irvin and especially Lee for never refusing to help, even at short notice and only scoffing slightly at my ever-decreasing optimism.

I want to also acknowledge the Medical Technologies team, I hope the secondment opportunity has influenced my future career path for which I am grateful.

Extra thanks go to everyone I have shared an office with over the last four years. Your support and entertainment have made this such an enjoyable journey. Without you all to listen to my endless rants I don't know if the simulator would have lasted to the end.

I couldn't have kept this up without my wonderful friends; Lauren, Alice, Asa, Nick, Brendan, Mike and Dan who were always ready for a beer on a Friday evening and a special mention to Holly my ever-ready conference pal.

My family, although clueless to how I have spent the last four years of my life have continually supported me without question. I couldn't have asked for more.

Last, but definitely not least, my thanks go to Malcolm, my best friend and champion. You've been there for the endless ups and downs involved in a PhD and I couldn't have achieved this without you.

ABSTRACT

Ankle arthritis affects 1% of the population and can be a painful debilitating problem. One motion preserving treatment option is total ankle replacement (TAR). These devices are currently under researched and have poor clinical outcomes. Despite significant variation amongst device designs no pre-clinical test standards exist to allow comparison of tribological function.

Furthermore, malalignment of TARs is a potential result of surgical technique or failure to correct existing natural varus/valgus deformity. TAR malalignment can result in instability, deformity and is associated with increased wear and higher failure rates. Good alignment is considered instrumental for long term success.

The aim of this research was to develop clinically relevant wear test methodologies for both natural gait and adverse conditions.

First a parameterised test was undertaken to understand the critical parameters for the Zentih (Corin Group) TAR. A knee simulator was used to vary the combination of rotation and displacement and the change in wear rate was assessed gravimetrically.

The effects of malalignment were investigated biomechanically in terms of component lift-off, changing contact area and stress. Adverse conditions were defined based on these results and edge loading observed in retrieved TARs. One coronal malalignment condition and a 3mm translational offset were tested in the wear simulator previously developed.

Rotation proved to significantly increase the TAR wear rate while displacement had no significant effect. Implementing coronal malalignment alone resulted in a significant decrease in the wear rate, due to the reduced contact area while edge loading had no significant effect. This outcome may not translate to reduced wear in a complex biological environment, however simulation methods produced clinically comparable surface form.

This PhD highlighted the critical parameters for TAR wear simulation, however, TAR failure is bigger than wear alone. Further factors must be considered to develop a truly adverse pre-clinical test protocol.

CONTENTS

| | |
|--|-----|
| Acknowledgements | ii |
| Abstract | iii |
| List of figures | ix |
| List of tables | xv |
| 1.1 The natural ankle | 2 |
| 1.1.1 Bony anatomy..... | 2 |
| 1.1.2 Soft tissue anatomy..... | 3 |
| 1.2 Ankle biomechanics..... | 4 |
| 1.2.1 Motions at the ankle..... | 4 |
| 1.2.2 The role of the subtalar joint..... | 6 |
| 1.2.3 The axis of rotation..... | 8 |
| 1.2.4 Ankle forces..... | 8 |
| 1.3 Surgical intervention..... | 10 |
| 1.3.1 Ankle arthritis..... | 10 |
| 1.3.2 Ankle arthrodesis..... | 10 |
| 1.3.3 Total ankle replacement..... | 12 |
| 1.3.4 The Corin Zenith..... | 16 |
| 1.3.5 Comparing fusion and replacement..... | 17 |
| 1.3.6 Surgical complexity..... | 19 |
| 1.3.7 Complications..... | 22 |
| 1.4 Biotribology..... | 23 |
| 1.4.1 Friction..... | 24 |
| 1.4.2 Lubrication..... | 25 |
| 1.4.3 Wear..... | 26 |
| 1.4.4 Biological response to wear particles..... | 29 |
| 1.5 Wear simulation of total ankle replacements..... | 30 |
| 1.5.1 Simulator inputs | 31 |
| 1.5.2 Lubrication..... | 34 |
| 1.5.3 Wear rates and limitations..... | 34 |
| 1.5.4 Zenith wear performance..... | 36 |
| 1.6 Volumetric wear analysis in joint replacement..... | 37 |
| 1.6.1 Gravimetric wear measurement | 38 |
| 1.6.2 Geometric methods..... | 39 |

| | |
|---|-----------|
| 1.6.3 Coordinate measurement..... | 39 |
| 1.6.4 Micro CT measurements..... | 42 |
| 1.6.5 Measurement summary..... | 43 |
| 1.7 Surface metrology..... | 44 |
| 1.7.1 Methods of quantifying surface metrology..... | 45 |
| 1.7.2 Contact measurement..... | 45 |
| 1.7.3 Non-contact measurement..... | 47 |
| 1.7.4 Metrology summary..... | 50 |
| 1.8 Retrieval analysis..... | 50 |
| 1.8.1 Surface wear characteristics..... | 50 |
| 1.9 Summary..... | 55 |
| 1.10 Project rationale | 56 |
| 1.11 Aims and objectives..... | 58 |
| Chapter 2 Method development..... | 59 |
| 2.1 Introduction..... | 60 |
| 2.2 Materials..... | 60 |
| 2.3 Simulator..... | 61 |
| 2.3.1 Simulator kinetics and kinematics..... | 63 |
| 2.3.2 Translation to simulator..... | 74 |
| 2.3.3 Fixtures..... | 75 |
| 2.3.4 Component set up..... | 77 |
| 2.3.5 Contact areas..... | 78 |
| 2.3.6 Calibration..... | 79 |
| 2.3.7 Pre-test..... | 80 |
| 2.3.8 Lubrication..... | 80 |
| 2.3.9 Frequency..... | 81 |
| 2.4 Gravimetric measurement method..... | 81 |
| 2.5 The wear study..... | 82 |
| 2.6 Contact surface measurements..... | 82 |
| 2.7 Non-contact surface measurements..... | 84 |
| 2.8 Measuring coating damage..... | 85 |
| 2.9 Wear track analysis..... | 86 |
| 2.10 Comparison to retrievals | 87 |
| Chapter 3 Stratified wear test..... | 88 |
| 3.1 Introduction..... | 89 |

| | |
|---|------------|
| 3.2 Materials and methods..... | 90 |
| 3.3 Results..... | 91 |
| 3.3.1 Simulator performance..... | 91 |
| 3.3.2 Wear results..... | 94 |
| 3.3.3 Variation between stations..... | 98 |
| 3.3.4 Surface roughness results..... | 99 |
| 3.3.5 Wear track analysis results..... | 103 |
| 3.3.6 Polyethylene surfaces..... | 105 |
| 3.4 Discussion..... | 106 |
| 3.4.1 The wear effects of kinematics..... | 106 |
| 3.4.2 Comparing wear rates..... | 108 |
| 3.4.3 Comparing to retrievals..... | 111 |
| 3.5 Limitations..... | 113 |
| 3.5.1 Gait inputs..... | 113 |
| 3.5.2 Simulator..... | 113 |
| 3.5.3 Test protocol..... | 114 |
| 3.6 Conclusion..... | 117 |
| Chapter 4 Validation wear test..... | 118 |
| 4.1 Introduction..... | 119 |
| 4.2 Materials..... | 119 |
| 4.2.1 The simulator..... | 120 |
| 4.2.2 Simulator calibration..... | 121 |
| 4.2.3 Simulator kinetics and kinematics..... | 121 |
| 4.3 Methods..... | 122 |
| 4.4 Results..... | 123 |
| 4.4.1 Simulator comparison..... | 123 |
| 4.4.2 Wear results..... | 126 |
| 4.4.3 Roughness results..... | 129 |
| 4.4.4 Comparing wear scars..... | 129 |
| 4.5 Discussion..... | 131 |
| 4.6 Conclusion..... | 133 |
| Chapter 5 Malalignment biomechanics..... | 134 |
| 5.1 Introduction..... | 135 |
| 5.2 Materials..... | 139 |
| 5.2.1 Simulator commissioning..... | 142 |

| | |
|--|------------|
| 5.3 Methods..... | 146 |
| 5.3.1 Biomechanical test methods..... | 146 |
| 5.3.2 Pressure mapping test methods..... | 151 |
| 5.4 Results..... | 154 |
| 5.4.1 Biomechanics..... | 156 |
| 5.4.2 Contact area and pressure..... | 160 |
| 5.5 Discussion..... | 169 |
| 5.5.1 Effect of alignment and joint tension..... | 169 |
| 5.5.2 Comparison to literature..... | 171 |
| 5.5.3 Potential impact of malalignment..... | 173 |
| 5.6 Limitations..... | 174 |
| 5.7 Conclusion..... | 175 |
| 5.8 Influence of biomechanics study on the design of the wear study..... | 176 |
| Chapter 6 Malalignment wear test..... | 177 |
| 6.1 Introduction..... | 178 |
| 6.2 Materials and methods..... | 180 |
| 6.2.1 The simulator..... | 180 |
| 6.2.2 Malalignment wear test methodology..... | 181 |
| 6.2.3 Component preparation..... | 181 |
| 6.2.4 Simulator kinetics and kinematics..... | 183 |
| 6.2.5 Measuring lift-off..... | 183 |
| 6.2.6 Surface measurements..... | 185 |
| 6.2.7 SSKS3 validation..... | 186 |
| 6.3 Results..... | 187 |
| 6.3.1 Measured lift-off..... | 187 |
| 6.3.2 Coronal malalignment..... | 188 |
| 6.3.4 Coronal malalignment with translational offset..... | 192 |
| 6.3.5 Translational offset..... | 195 |
| 6.3.6 Comparison to retrievals..... | 199 |
| 6.4 Discussion..... | 201 |
| 6.4.1 Coronal malalignment..... | 201 |
| 6.4.2 Translational offset..... | 203 |
| 6.4.3 Comparison to retrievals..... | 205 |
| 6.4.4 Limitations..... | 208 |
| 6.5 Conclusion..... | 209 |

| | |
|---|-----|
| Chapter 7 Overall discussions, conclusions and future work | 210 |
| 7.1 Overall discussion..... | 211 |
| 7.1.1 Development of a wear simulation methodology..... | 212 |
| 7.1.2 Biomechanical effects of adverse alignment..... | 215 |
| 7.1.3 Wear effects of adverse alignment..... | 217 |
| 7.2 Overall conclusions..... | 219 |
| 7.2.1 Development of a wear simulation methodology..... | 219 |
| 7.2.2 Biomechanical effects of adverse alignment..... | 220 |
| 7.2.3 Wear effects of adverse alignment..... | 221 |
| 7.3 Future work..... | 222 |
| References | 224 |
| Appendix A Publications | 249 |
| Appendix B Engineering drawings | 252 |
| B.1 KS1 fixtures..... | 253 |
| B.2 SSKS3 fixtures..... | 255 |
| B.3 KS4 fixtures..... | 263 |
| Appendix C Simulator calibration record | 268 |
| C.1 KS1..... | 269 |
| C.2 KS4..... | 270 |

LIST OF FIGURES

| | |
|---|----|
| Figure 1.1 Coronal section through the left ankle and talocalcaneal joint..... | 2 |
| Figure 1.2 Lateral ligaments of the ankle..... | 4 |
| Figure 1.3 Motions of the ankle (A) dorsiflexion/plantarflexion, (B) adduction/abduction, (C) eversion/inversion..... | 5 |
| Figure 1.4 Ankle flexion and subtalar version during the gait cycle as 70s theory believed..... | 7 |
| Figure 1.5 Effect of walking cadence on the compressive ankle forces at 40 strides/minute compared to 60 strides/minute (dashed)..... | 9 |
| Figure 1.6. Example of ankle arthrodesis..... | 11 |
| Figure 1.7 Implanted TARs per year compared to primary hip and knee replacements based on NJR data for England and Wales..... | 12 |
| Figure 1.8 Schematic drawings of (A) mobile bearing MatOrtho Box TAR and (B) fixed bearing Wright Medical Infinity TAR..... | 13 |
| Figure 1.9 Corin Zenith titanium nitride coated TAR..... | 16 |
| Figure 1.10. BONIT fixation coating..... | 17 |
| Figure 1.11 Range of motion for ankles in normal and treated states..... | 18 |
| Figure 1.12. X-ray of a TAR a) neutrally aligned, b) talar centre anterior to tibial axis..... | 20 |
| Figure 1.13 Reasons for TAR revisions based on 189 revisions..... | 23 |
| Figure 1.14 The relative direction of friction compared to motion..... | 24 |
| Figure 1.15 Asperity contact in (A) boundary lubrication and (B) fluid film lubrication..... | 25 |
| Figure 1.16 Schematic of the effects of continued loading of a biomaterial. | 30 |
| Figure 1.17 One example of the motions and loading applied in a TAR wear simulator..... | 33 |
| Figure 1.18 Points collected during surface digitization with the coordinate measuring machine of one of the tibial inserts..... | 40 |
| Figure 1.19 Profile of the meniscus found by CMM measurements compared to the profile with form removed..... | 41 |
| Figure 1.20 Arithmetic roughness, R_a is the mean deviation from the mean line..... | 44 |
| Figure 1.21 Resolution of measurement methods..... | 45 |
| Figure 1.22 Simplified design of a white light interferometry microscope... | 48 |
| Figure 1.23 Sectioned tibial component..... | 51 |
| Figure 1.24 Surface damage compared to volumetric wear. | 54 |
| Figure 2.1 Leeds Knee Simulator I..... | 61 |

| | |
|--|-----|
| Figure 2.2 Positive simulator directions for FE, IER, AP and AF..... | 62 |
| Figure 2.3 Stance phase of gait with the relative force direction..... | 65 |
| Figure 2.4: Axial load profile derived from literature and implemented in simulator..... | 66 |
| Figure 2.5: Ankle plantarflexion (+) dorsiflexion (-) profile derived from literature and implemented in simulator..... | 69 |
| Figure 2.6: Internal (-) external (+) rotation of the ankle derived from literature and implemented in simulator..... | 72 |
| Figure 2.7 (A) Positive and (B) negative AP..... | 73 |
| Figure 2.8: Anterior (+) posterior (-) displacement of the ankle derived from literature and implemented in simulator..... | 74 |
| Figure 2.9 Schematic showing loads and motions at a left TAR relative to the inverted simulator position..... | 75 |
| Figure 2.10: Schematic of simulator cradles..... | 76 |
| Figure 2.11 Fixture alignment..... | 77 |
| Figure 2.12: Ankle simulator set-up..... | 78 |
| Figure 2.13: Contact areas of the insert (B) brought into contact with the tibial component (A) and talar component (C) demonstrating central alignment.. | 79 |
| Figure 2.14 Talysurf traces of the TAR surfaces..... | 83 |
| Figure 2.15 The analysis segmentation for the (A) talar surface and (B) superior insert roughness traces..... | 84 |
| Figure 2.16 Bruker measurement area on the flat bearing surfaces..... | 85 |
| Figure 2.17 Traces taken on the tibial components across damaged region.. | 86 |
| Figure 2.18 1mm ball bearings in the surfaces of a TAR insert..... | 87 |
| Figure 3.1 Simulator inputs compared to the mean output profiles across all stations for the duration of Stage 2 and their 95% confidence limits..... | 92 |
| Figure 3.2 (A and B) Mean displacement and rotation profiles for the 2Mc driven to zero and (C) the input profile for the reduced AP displacement profile compared to the mean output..... | 93 |
| Figure 3.3 Wear rates with 95% confidence limits for each test condition... | 94 |
| Figure 3.4: Two tibial components which experienced coating damage..... | 95 |
| Figure 3.5 Tibial interferometer images (A) worn surface without damage (B) damaged region..... | 97 |
| Figure 3.6 Relationships between the volumetric wear, station and insert.... | 98 |
| Figure 3.7 Simulator rotation outputs for stage two..... | 99 |
| Figure 3.8 Pre-test photograph of aTAR insert and magnified NPFLEX image of the machined surface compared to a photograph of the same insert surface after 4Mc where the machining lines are no longer visible accounting for the change in surface roughness measurement..... | 101 |

| | |
|---|-----|
| Figure 3.9 Typical component surfaces after 4MC with insert imprint on tibial component and unidirectional scratches on the talar component | 101 |
| Figure 3.10 Optical microscope images of the worn insert footprint compared to unworn tibial edges..... | 102 |
| Figure 3.11 Stills from the video footage showing both posterior and anterior edge contact throughout the gait cycle..... | 103 |
| Figure 3.12 Scratched surfaces from wear track analysis..... | 104 |
| Figure 3.13 Photos of the superior insert surfaces at the end of 12Mc with edge loaded areas highlighted..... | 105 |
| Figure 3.14 Volumetric wear for n=5 inserts per million cycles..... | 107 |
| Figure 3.15 Kinematics in (A) mobile bearing and (B) fixed TARs..... | 110 |
| Figure 3.16 Wear tested surfaces of the Zenith tibial articulation compared to that of two mobile bearing retrievals..... | 112 |
| Figure 3.17 Similar titanium nitride damage observed in (A) the damaged TAR tibial component and (B) a TKR retrieval. | 116 |
| Figure 4.1 Three stations of KS4 filled with serum..... | 120 |
| Figure 4.2 KS4 load and rotation/displacement calibration set up..... | 121 |
| Figure 4.3 Ankle kinematic to be implemented in KS4..... | 122 |
| Figure 4.4 Contact areas after set up in KS4 showing the central alignment of polyethylene insert imprint on tibial components..... | 123 |
| Figure 4.5 The input profile (black) and output profiles for each station of KS4 (blue) and KS1 (orange) for A: axial force (AF), B: anterior/posterior displacement (AP), C: rotation (TR) and D: flexion/ extension (FE)..... | 125 |
| Figure 4.6 Gravimetric wear rate measured in the validation of KS4 (orange) compared to the wear rate under similar conditions for KS1 (blue)..... | 127 |
| Figure 4.7 Wear rates for each individual insert from 1 to 6 for each million cycles colours representing the simulator station..... | 128 |
| Figure 4.8 Rotation across stations of KS4 for each of the individual Mcs.. | 128 |
| Figure 4.9 Comparing wear scars from (A) KS1 and (B) KS4..... | 130 |
| Figure 4.10 Worn inserts with less polished, raised central region visually compares to retrievals from two different TAR designs..... | 131 |
| Figure 5.1 Examples of TAR malalignment measured from x-rays collected from TAR retrieval patients at Chapel Allerton Hospital Leeds..... | 135 |
| Figure 5.2 Posterior view of ankle valgus, neutral and varus alignments..... | 136 |
| Figure 5.3 Severe coronal malalignment between components..... | 137 |
| Figure 5.4 Coronal plane through the Zenith TAR and lack of freedom..... | 138 |
| Figure 5.5 Leeds single station knee simulator III..... | 140 |
| Figure 5.6 Tekscan sensor..... | 141 |

| | |
|--|-----|
| Figure 5.7 Comparing simulator outputs for complex and smoothed kinematic inputs..... | 143 |
| Figure 5.8 Frictional shear force for dummies under smooth and complex kinematics $\pm 95\%$ CL for n=3 in SSKS3..... | 145 |
| Figure 5.9 Biomechanics test set-up..... | 146 |
| Figure 5.10 Coronal malalignment angles to be investigated..... | 147 |
| Figure 5.11 Variation in simulator inputs tested shown by dashed lines..... | 149 |
| Figure 5.12 The Tekscan sensor set up in the single station simulator..... | 151 |
| Figure 5.13 Sensitivity setting used to avoid oversaturation..... | 152 |
| Figure 5.14 Tekscan force outputs from two cycles of pressure recording highlighting the three time points for data collection..... | 153 |
| Figure 5.15 Force input profile..... | 154 |
| Figure 5.16 (A) Change in ad/abduction resulting in lateral followed by medial lift-off at 2.5 degrees malalignment (B) The experimental set-up of the TAR compared to the orientation of the output pressure plots..... | 155 |
| Figure 5.17 Effect of malalignment direction on lift-off with ab/adduction less than the malalignment offset angle showing lateral lift-off..... | 156 |
| Figure 5.18 Mean effect of AP displacement on lift-off (n=3) with ab/adduction less than the malalignment offset angle showing lateral lift-off..... | 157 |
| Figure 5.19 Mean effect of peak load on lift-off (n=3) with ab/adduction less than the malalignment offset angle showing lateral lift-off..... | 158 |
| Figure 5.20 Mean effect of swing load on lift-off (n=3) with ab/adduction less than the malalignment offset angle showing lateral lift-off..... | 159 |
| Figure 5.21 Pressure plots for cycle showing SPL of 50N and load peaks showing lateral lift-off as in Figure 5.16..... | 160 |
| Figure 5.22 Pressure plots for cycle showing SPL of 100N, 1st load peak and max load showing lateral lift-off as in Figure 5.16..... | 161 |
| Figure 5.23 Pressure plots for cycle showing SPL of 100N, 1st load peak and max load with a 3mm translational offset showing lateral lift-off..... | 162 |
| Figure 5.24 Pressure plots for cycle showing SPL of 300N, 1st load peak and max load showing lateral lift-off as in Figure 5.16..... | 163 |
| Figure 5.25 Pressure plots for cycle showing SPL of 500N, 1st load peak and max load showing lateral lift-off as in Figure 5.16..... | 164 |
| Figure 5.26 Pressure plots for cycle showing SPL of 1000N and load peaks showing lateral lift-off as in Figure 5.16..... | 165 |
| Figure 5.27 Mean peak contact pressure (n=3) for each tested coronal malalignment and swing phase load..... | 166 |
| Figure 5.28 Mean peak contact pressure (n=3) for each tested coronal malalignment at 100N swing with an addition 3mm translational offset..... | 166 |

| | |
|--|-----|
| Figure 5.29 Mean average contact pressure (n=3) for each tested coronal malalignment and swing phase load..... | 167 |
| Figure 5.30 Mean contact area (n=3) for each coronal malalignment and swing phase load..... | 168 |
| Figure 5.31 Mean contact area (n=3) for each tested coronal malalignment at 100N swing with an addition 3mm translational offset..... | 169 |
| Figure 5.32 Comparing the average contact pressure between the superior and inferior insert surfaces of the DePuy Mobility in coronal malalignment..... | 172 |
| Figure 5.33 Mean Average contact pressure (n=3) \pm standard deviation at heel strike (HS), midstance (MS), heel off (HO) and toe off (TO) at neutral alignment, 2.5, 5 and 10 degrees coronal malalignment..... | 172 |
| Figure 5.34 Abduction/adduction between the tibia and talus measured during stance phase with invasive marked placement in healthy subjects..... | 175 |
| Figure 6.1 Radiographs showing component malalignment..... | 180 |
| Figure 6.2 Diagram of component set-up for each tested condition..... | 181 |
| Figure 6.3 Component set-up..... | 182 |
| Figure 6.4 Zenith components showing lack of clearance highlighted..... | 183 |
| Figure 6.5 Apparatus for measuring abduction/adduction..... | 184 |
| Figure 6.6 Example trace from oscilloscope demonstrating both outputs..... | 184 |
| Figure 6.7 Infintefocus microscope (Alicona, AT) measurement set up..... | 185 |
| Figure 6.8 SSKS3 Profile input (solid) compared to average output profile (dashed) for 100N swing load..... | 187 |
| Figure 6.9 Ab/adduction cradle motion as measured with a potentiometer...188 | 188 |
| Figure 6.10 Mean measured wear rates aligned and malaligned..... | 189 |
| Figure 6.11 Wear volume at each station under each condition with the well aligned Mcs highlighted in grey..... | 189 |
| Figure 6.12 Changes in insert form after 3Mc aligned compared to 3Mc coronal..... | 191 |
| Figure 6.13 Mean medial/lateral surface profile of inserts 1 -5..... | 192 |
| Figure 6.14 Wear rate for coronal malalignment with and without translational offset..... | 193 |
| Figure 6.15 Coronally malaligned and edge loaded insert height maps..... | 194 |
| Figure 6.16 Mean medial/lateral profile from the five inserts..... | 195 |
| Figure 6.17 Comparing wear rate in neutral alignment to that after 4Mc translational offset..... | 196 |
| Figure 6.18 Comparing height maps after 2Mc neutral alignment to after 4Mc with 3mm translational offset..... | 198 |
| Figure 6.19 Mean medial lateral profiles comparing the surface after 2Mc bedding in to the effects of 4Mc edge loading..... | 199 |

| | |
|---|-----|
| Figure 6.20 Abbott Firestone curves comparing retrievals surface profiles of those categorised as normal (n=9) and Edge loaded (n=25) to simulator samples under well aligned (TARs 1-6) and after 4Mc neutral coronal alignment and translational offset (TARs 7-12) | 200 |
| Figure 6.21 Comparing mean contact area measurement from TAR tested in SSKS3 (n=3) for the equivalent tested conditions with standard deviation... | 202 |
| Figure 6.22 Effect of edge loading on the measured contact area in neutral coronal malalignment with standard deviation..... | 204 |
| Figure 6.23 Retrieval Hingtegra and AES TARs compared to simulator Zenith components..... | 208 |

LIST OF TABLES

| | |
|--|-----|
| Table 1.1 Primary TAR prostheses implanted in the UK in 2015..... | 14 |
| Table 1.2. Range of motion for TAR wear simulation..... | 32 |
| Table 1.3 Comparison of wear rates across tested designs..... | 35 |
| Table 1.4 Polyethylene worn surface characteristics as described by Hood et al. (1983) | 52 |
| Table 2.1 Simulator controls..... | 62 |
| Table 2.2 Maximum ankle compressive force for healthy individuals as a multiple of body weight (BW) | 63 |
| Table 2.3 Approximations of Peak Ankle Sagittal Plane Motion for the natural ankle..... | 67 |
| Table 2.4 Ankle rotational motions reported in literature..... | 71 |
| Table 3.1 Test Conditions..... | 91 |
| Table 3.2: Comparing medial/lateral (ML) traces for different tibial components, one worn, one unworn and two with visible coating damage. The difference in height was calculated for the profiles shown and also for the anterior/posterior (AP) profiles not presented here. | 96 |
| Table 3.3 Insert pathway around simulator stations each Mc..... | 98 |
| Table 3.4 Mean Ra values and 95% confidence limits for the articulating surfaces with significant ($p < 0.05$) changes from previous roughness measurement highlighted by *..... | 100 |
| Table 3.5 Comparative Ankle Wear Rates with similar 3/4mm AP..... | 109 |
| Table 4.1 Bearing details..... | 119 |
| Table 4.2 Average surface roughness for each component and 95% confidence limits alongside the percentage change in roughness between the stages..... | 129 |
| Table 5.1 Bearing details..... | 139 |
| Table 5.2 Simulator Controls..... | 140 |
| Table 5.3 Loads at similar points in the gait cycle defined by Espinosa et al. (2010)..... | 171 |
| Table 6.1 Malalignment wear test conditions..... | 172 |
| Table 6.2 Changing roughness measurements from well aligned to coronal malalignment with 95% confidence limits..... | 190 |
| Table 6.3 Change in surface roughness, Ra with the addition of translational offset and 95% confidence limits..... | 193 |
| Table 6.4 Mean Ra roughness measurements for translational offset test with 95% confidence limits..... | 197 |
| Table 6.5 Comparison between some retrieval height maps with their implantation time and activity level and those from in-vitro testing. | 207 |

CHAPTER 1
INTRODUCTION

CHAPTER 1

INTRODCTION

1.1 The natural ankle

1.1.1 Bony anatomy

Together twenty-six individual bones form 33 joints to make up the foot and ankle complex which allows us to walk, run and go about our daily activities (Sheehan 2010). All of these separate components work together in order to transfer loads and ensure smooth and stable walking gait (Nordin et al. 2001).

The ankle joint complex consists of multiple articulations; the talocrural (tibiotalar), talocalcaneonavicular (transverse-tarsal) and subtalar (talocalcaneal) joints. The talocrural joint is typically what is meant when referring to ‘the ankle’, a complex joint, itself consisting of multiple articulations (Figure 1.1). Situated between the lower leg and the foot, the ankle comprises of three bones; the tibia, fibula and the talus which together enable motion in three planes with a changing centre of rotation (Hintermann 2005; Standring et al. 2005; Vickerstaff et al. 2007).

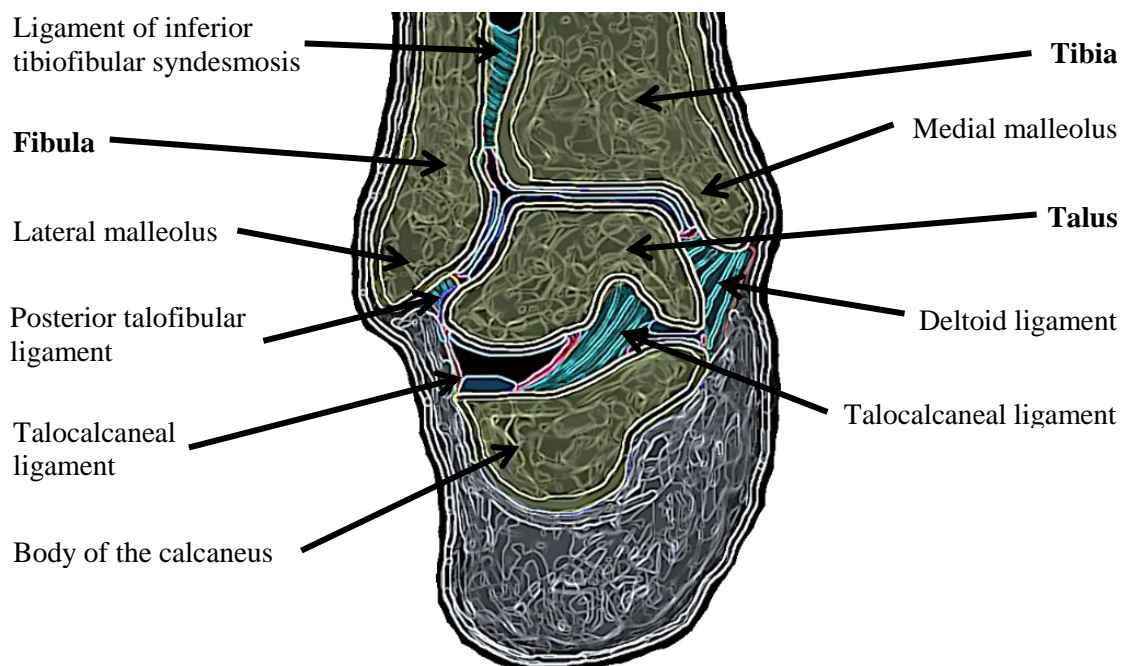


Figure 1.1 Coronal section through the left ankle and talocalcaneal joints

The anatomy of the talus is important. It is believed the shape of the ankle joint and its conformity allow motion and the ligaments and tendons hold the surfaces together (Teeter et al. 2011). The talus is understood to be marginally wider anteriorly compared to the posterior by 4.2mm and this anatomical contour guides the motion maintaining stability through dorsiflexion (Sarrafian 1993; Nordin et al. 2001). Historically the talus was also believed to be larger laterally, shaped like a truncated cone with a medial apex (Inman 1976). However, Inman's primitive calculation relied on one axis of rotation. A study of healthy computed tomography (CT) ankles, considering just geometry recently disproved this long assumed convention. Siegler et al. instead showed the opposite, the lateral talar radius to be significantly smaller than that of the medial, thus a truncated cone with its apex located laterally. This investigation also defined the shape of the talus to be saddle like rather than the dome it is often described as (Siegler et al. 2014).

The medial and lateral malleoli constrain the talus while the distal end of the tibia fits with the talar mortise (Brockett et al. 2016). The conformity of the tibiotalar joint is believed to be responsible for approximately "70% of the antero-posterior stability, 50% of inversion/eversion stability and 30% of internal/external rotation stability" (Kakkar et al. 2011). In the loaded position the joint was thought to provide full resistance to version (Nordin et al. 2001), however, the saddle description could potentially allow some inversion during dorsiflexion or neutral alignment (Siegler et al. 2014). The rest of the stability is left up to the ligaments, tendons and syndesmoses to maintain (Yamaguchi et al. 2009; Snedeker et al. 2012; Siegler et al. 2014).

1.1.2 Soft tissue anatomy

Ligaments play a key role in the ankle joint function, directing the motion path and limiting its range (Jackson et al. 2003). The syndesmosis provide critical stability between tibia and fibula (Figure 1.1). Then below there are three important lateral ligaments acting on the ankle; the calcaneofibular and the anterior and posterior talofibular ligaments (Figure 1.2). Together these provide resistance to the internal rotation, varus stresses and inversion (Nordin et al. 2001; Standring et al. 2005). The anterior and posterior ligaments also have to withstand large tensile forces in plantar and dorsiflexion respectively while the calcaneofibular ligament extends to the subtalar joint ensuring its stability. When the rotational motions are reversed

it is the superficial and deep deltoid ligaments on the medial side which must oppose the motions, limiting the range and reducing valgus stresses (Nordin et al. 2001). The lateral ligaments are at the greatest risk of injury, mainly sprains which result in an increase in joint laxity (Standring et al. 2005).

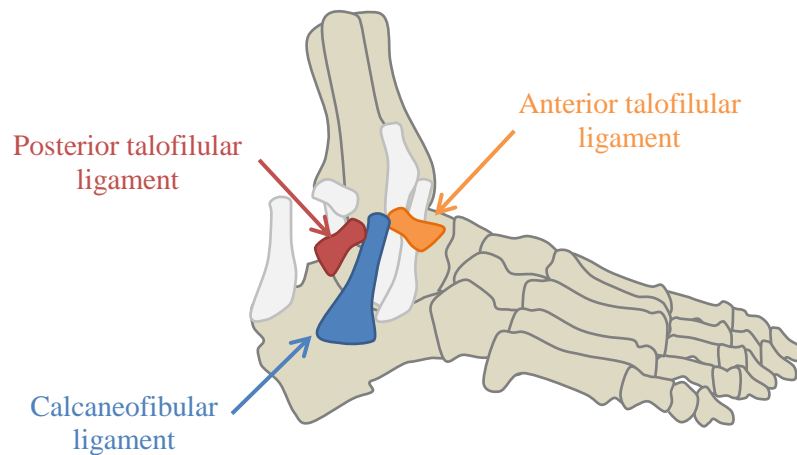


Figure 1.2 Lateral ligaments of the ankle

1.2 Ankle biomechanics

1.2.1 Motions at the ankle

The anatomy dictates the ankle biomechanics. The majority of the ankle motion occurs in the sagittal plane allowing a relatively large range of motion, typically from 20° dorsiflexion to 25°-35° plantarflexion (Figure 1.3). However, only half of this range is required for the typical gait cycle (Figure 1.4) (Michael et al. 2008). The abduction/adduction motion, also referred to as internal/external rotation lies primarily in the transverse plane with a little movement medial or lateral (Dugan et al. 2005). This motion, due to the lateral malleolus of the talus being longer than the medial, provides the small rotational components of ankle motion (Kingston 2000). Then in the coronal plane the motion of the ankle complex is known as inversion/eversion, believed to be primarily facilitated by the subtalar joint (Stauffer et al. 1977). The subtalar joint is a functional unit comprising of the three articular facets between the talus and calcaneus (Inman 1969; Leardini et al. 2001; Standring et al. 2005). Its range of motion is largest in inversion with a maximum of about 30°, compared to 10° in eversion. Again only about 10-15° of this motion is necessary for the typical gait, inverting at heel strike and everting to

allow the heel rise to push off phase (Figure 1.4) (Stauffer et al. 1977; Sarrafian 1993).

Combinations of individual planar orientations (Figure 1.3) at both joints create the three dimensional motions known as supination and pronation, consisting of plantar flexion, inversion and adduction, and dorsiflexion, eversion and abduction respectively (Standring et al. 2005). The coronal plane version motions, facilitated by the subtalar joint, allow the foot move smoothly into the pronation and supination positions experienced throughout the gait cycle. The degree of flexion will depend on the magnitude of the calcaneal inclination, the greater the angle the larger the range of flexion will be (Sarrafian 1993).

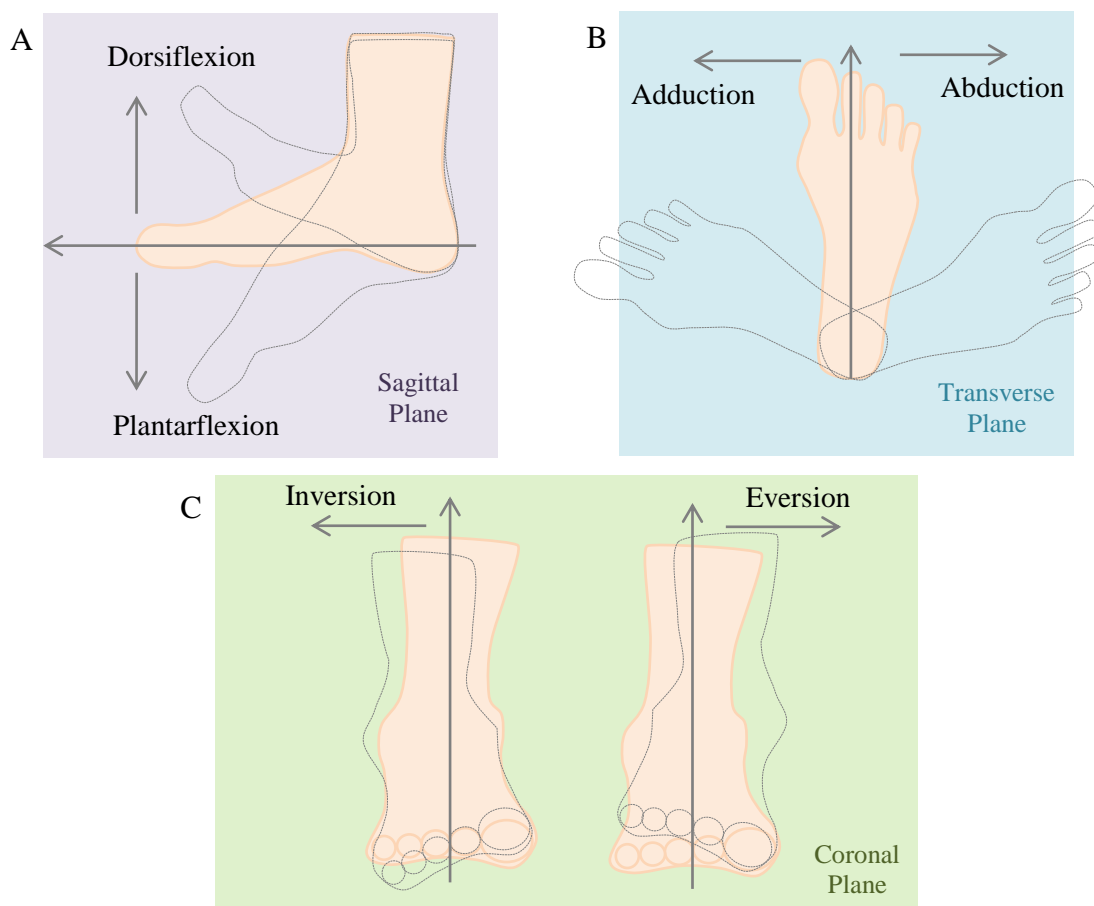


Figure 1.3 Motions of the ankle (A) dorsiflexion/plantarflexion, (B) adduction/abduction, (C) eversion/inversion

1.2.2 The role of the subtalar joint

The ankle's movements alone are not enough to facilitate what we consider normal walking. In order to provide the full range required for daily activities, the ankle joint works in partnership with the subtalar joint. Often the ankle is measured as the gross motion of the foot making the individual bone motions difficult to distinguish (Cenni et al. 2013). The contribution of the subtalar and ankle joints to ankle function have been explored by numerous sources since Inman (1969). Early investigations established a convention in which dorsiflexion and plantarflexion occurred exclusively at the talocrural joint and similarly inversion/eversion were confined to the subtalar joint (Figure 1.4) (Siegler et al. 1988; Sheehan et al. 2007; Funk 2011; Choisine et al. 2012). Some debate has surrounded the rotational components of motion (abduction/adduction), whether they are, as history dictates, allied to inversion and eversion at the subtalar (Sheehan 2010), split across both joints (Arndt et al. 2004; Funk 2011) or as Sheehan et al. (2007) believed, more prominent in the talocrural joint.

More recently the theory of these divided motions is being disputed, the majority of plantarflexion/dorsiflexion is still considered to occur at the ankle/talocrural but with a few degrees accounted for at the subtalar joint for some individuals (Arndt et al. 2004). Inversion/Eversion is much more controversial. Sheehan et al. (2007) used dynamic MRI to visualise the motions of the ankle as the patient repeatedly moved through a range of flexion. They concluded that the majority of the eversion to occur at the subtalar joint as expected whereas inversion and rotation were more likely to occur at the ankle (talocrural) articulation. Conversely Arndt et al. (2004) carried out a highly invasive study which showed that in weight bearing the inversion and rotational components of motion were divided proportionally between both the ankle and the subtalar joints. There are limitations to this study due to the large amount of variability amongst the small cohort of individuals tested and similarly the non-weight-bearing conditions of the MRI test limit the relevance of the results. Nester et al. (2007) have also developed a cadaveric model to investigate ankle motions, these give a good idea of the motions at the individual articulations, showing no more than four degrees of subtalar rotation in any plane during the stance phase but the results are dependent on the motions applied to the cadaveric foot. Developments in the understanding of the talar geometry mean

some of this motion perceived to occur at the subtalar joint may actually be occurring at the ankle due to the saddle shape. Siegler et al. (1988) hypothesised that the natural ankle was likely to experience a certain degree of inversion during the dorsiflexion and neutral orientations which includes a substantial proportion of the gait. This is in some agreement with both the MRI conclusions from Sheehan et al. (2007) and invasive gait analysis by Arndt et al. (2004). Current evidence suggests the ankle motions are less divided than it was once believed.

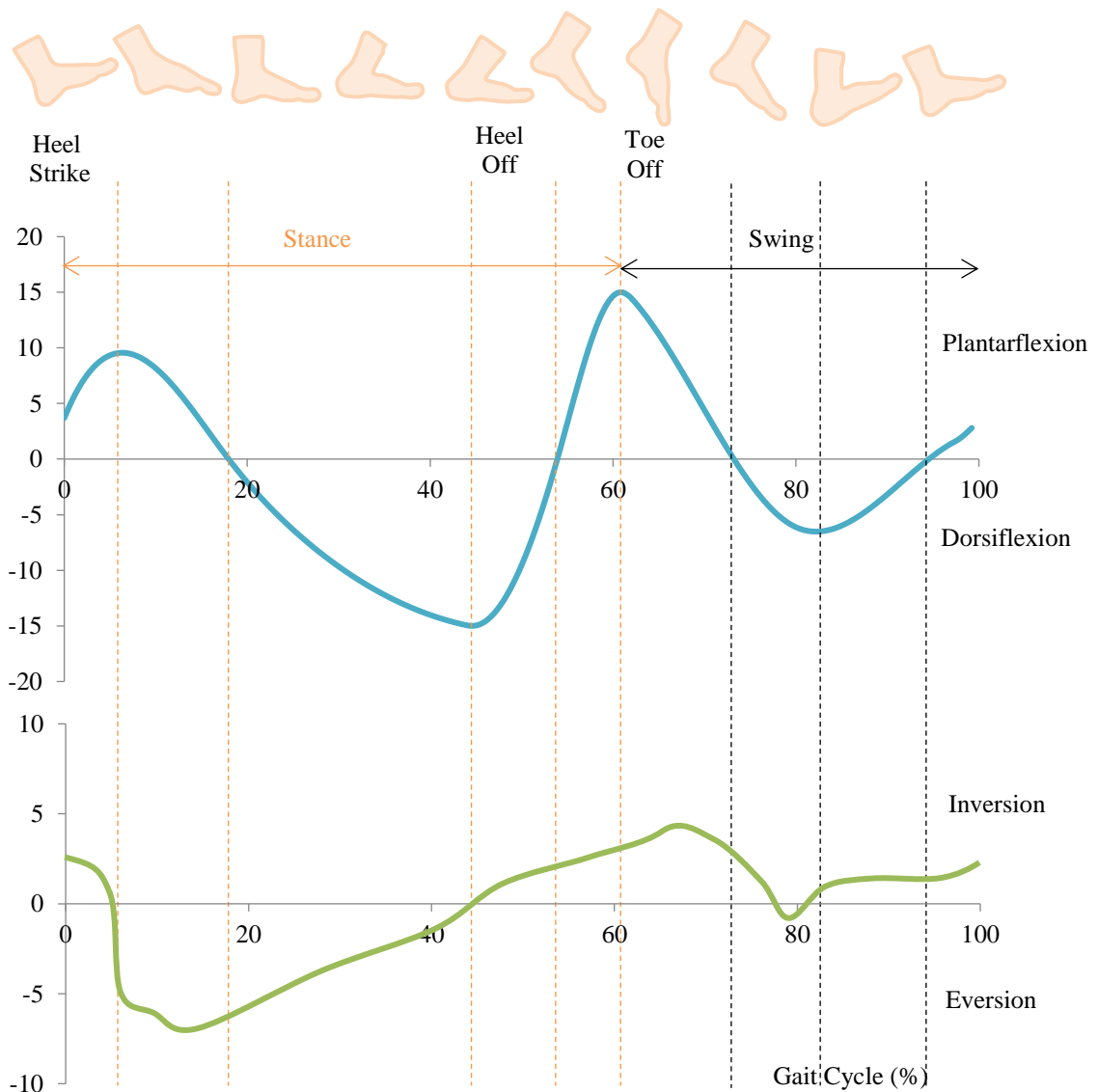


Figure 1.4 Ankle flexion and subtalar version during the gait cycle as 1970s theory believed (Stauffer et al. 1977)

1.2.3 The axis of rotation

The axis of rotation is another bone of contention when it comes to understanding the ankle. Whether it is a simple hinge or multiaxial has been a topic of debate. In the early 1950's Barnett et al. defined the axis to change with flexion, inclined downwards pointing laterally with dorsiflexion and downwards towards the medial malleolus with plantarflexion (Barnett et al. 1952). Twenty years later Inman (1976) contradicted this finding that a hinge action better described the rotational axis for their investigated population. This idea of the fixed axis hinge was then contested by Siegler et al. (1988) and Lundberg et al. (1989). By taking x-rays of patients with their foot aligned in known orientations Lundberg et al. (1989) found the axis of rotation to be continually changing but often crossing through a similar point near the midpoint of the malleoli. The majority of evidence points to this changing centre of rotation making ankle gait difficult to interpret.

1.2.4 Ankle forces

The gait cycle comprises of approximately 62% stance and 38% swing. During activity the compressive forces on the ankle joint, mainly through the tibia to the talus, are considered to be high over a contact area of 11-13 cm² (Michael et al. 2008). Throughout the gait cycle a high level of contact is maintained (Teeter et al. 2011; Siegler et al. 1988) but the weight bearing force per cm unit area is higher than any other joint (Thomas et al. 2003). The mobile axes of these joints allow the alignment of the ankle complex to change with the level of weight bearing reducing some of the stresses (Nordin et al. 2001).

Through the weight bearing stage the force will increase to its peak at approximately 70% of the stance phase and then release for swing (Figure 1.5) (Stauffer et al. 1977; Michael et al. 2008). Some authors have estimated forces during the loading phase by mathematical transformation of the ground reaction force measurement to the relative joint (Stauffer et al. 1977; Procter et al. 1982). It is common practice to simplify the joint model by considering that some muscle actions are negligible as the complexity is too much to manage so many unknown forces individually (Burdett 1982). When walking the ankle compressive forces have been reported to reach between 4-5.2 times the individual's body weight (BW) (Stauffer et al. 1977; Calderale et al. 1983; Thomas et al. 2003; Hintermann 2005). The results of these studies represent an estimation of the possible

magnitudes whereas in reality this will vary with the individual affected by factors such as cadence and disease. Stauffer found that degenerative ankles reduced the axial forces to be closer to 2 x BW with a similar force profile in terms of BW. Conversely the force profile presented is noted to vary in shape depending on the cadence (Figure 1.5), however, there is minimal difference in the magnitude of the peak force between an normal walking pace and one 50% faster (Stauffer et al. 1977).

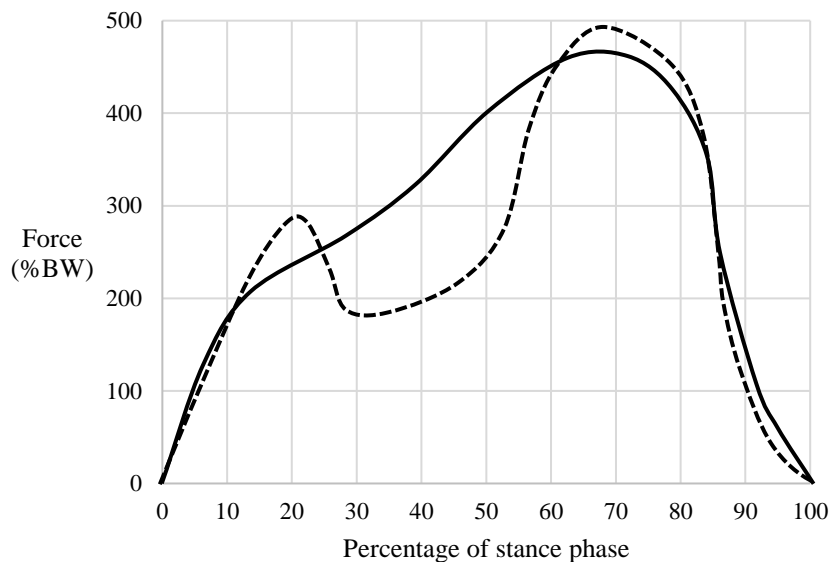


Figure 1.5 Effect of walking cadence on the compressive ankle forces at 40 strides/minute compared to 60 strides/minute (dashed) (Stauffer et al. 1977)

When the cadence and velocity are increased further to what is considered a run a third phase is added to the gait cycle during which neither foot is on the floor. During running the centre of gravity is shifted forward which will impact the forces experienced in the ankle (Dugan et al. 2005). An individual's specific running style will vary the gait cycle and peak forces. Burdett (1982) estimated localised forces to reach 13 times BW when the activity level be increased to running, such high loading is bound to take its toll on the natural articulation.

1.3 Surgical intervention

1.3.1 Ankle arthritis

The high impact forces, ankle anatomy and reliance on ligaments leave the ankle vulnerable to injury (Nordin et al. 2001). These incidences will, in some cases, be responsible for the onset of degeneration within the joint. Trauma is considered to be the most frequent cause of ankle arthritis (Thomas et al. 2003). Cases of osteoarthritis which often plague aging hips and knees are less common in ankle joints often leaving it the last of the main lower body articulations to require replacement (Vickerstaff et al. 2007; Snedeker et al. 2012). This channels the belief that the cartilage of the ankle is less responsive to age than hips and knees (Snedeker et al. 2012). However, as trauma affects all ages post traumatic ankle osteoarthritis can be unfortunately common in younger individuals. Rheumatoid arthritis and even abnormal joint biomechanics can also result in ankle degeneration. There are conservative treatments available for ankle arthritis including pain management, bracing, orthotics and arthroscopic debridement (Thomas et al. 2003). Generally the cause of degenerative changes will become indications for ankle surgery due to functional impairment and reduction in mobility that comes with it (Hintermann 2005). The majority of sources cite post traumatic arthritis as the biggest indicator for surgical intervention (Thomas et al. 2003; Hintermann 2005; Michael et al. 2008; Kakkar et al. 2011).

The increasing prevalence of sports injuries in young individuals and the aging population are likely to make natural ankle degeneration more common, cementing the need for a treatment option which can be relied upon for long term success. Current options range from conservative pain relief methods and physiotherapy to immobilisation of the problem joint or replacement of the natural articulation with a motion preserving alternative.

1.3.2 Ankle arthrodesis

Ankle arthrodesis is the most common invasive treatment for degenerative problems. The process involves restriction of the ankle's motion through the fusion of the tibia with the talus which can be achieved in a variety of manners using both external fixation and the preferred internal stabilisation methods. Both can include a variety of screws and plates in order to immobilise the joint in an ideal orientation

of neutral dorsiflexion with 5° of hindfoot valgus (Figure 1.6) (Thomas et al. 2003).



Figure 1.6. Example of ankle arthrodesis. Figure adapted from Iwasa et al. (2014) Arthroscopic ankle arthrodesis for treating osteoarthritis in a patient with kashin-beck disease. Case reports in medicine, 2014, p.931278

This procedure will aim to alleviate pain, correct deformity and stabilise the foot (Wu et al. 2000; Coester et al. 2001) and patient outcomes are generally positive as they experience immediate pain relief. However, arthrodesis is not without its complications. The fusion of the bones limits the joint function and changes the gait pattern which reduces the overall walking efficiency (Valderrabano et al. 2003). These changes may have a knock on effect on the individual's hips or knees (Coester et al. 2001), although it has proven to be minimal (Valderrabano et al. 2003). To continue to facilitate walking, the surrounding joints compensate for the motionless ankle resulting in high stresses in these joints (Wu et al. 2000). Just like in the spine these stresses cause shear forces which accelerate the degenerative process in the compensating joints (Lee 1988; Coester et al. 2001; Thomas et al. 2003; Hintermann 2005; Krause et al. 2012). In turn the only way to treat the further arthritic problems developed from fusion is with additional immobilisation creating a chain reaction. It is not uncommon for the end result to be amputation of the lower limb. Despite these complications the majority of authors still consider ankle arthrodesis as the gold standard treatment for ankle arthritis (Jackson et al. 2003). The alternative operative treatment is arthroplasty which is trying to build a reputation for itself to rival fusion.

1.3.3 Total ankle replacement

In 2015 just 582 Total Ankle Replacements (TAR) were carried out by the National Health Service in England and Wales, the equivalent to 0.7% of the joint registry's reported statistics for hips and even less for knees (Figure 1.7) (NJR 2016).

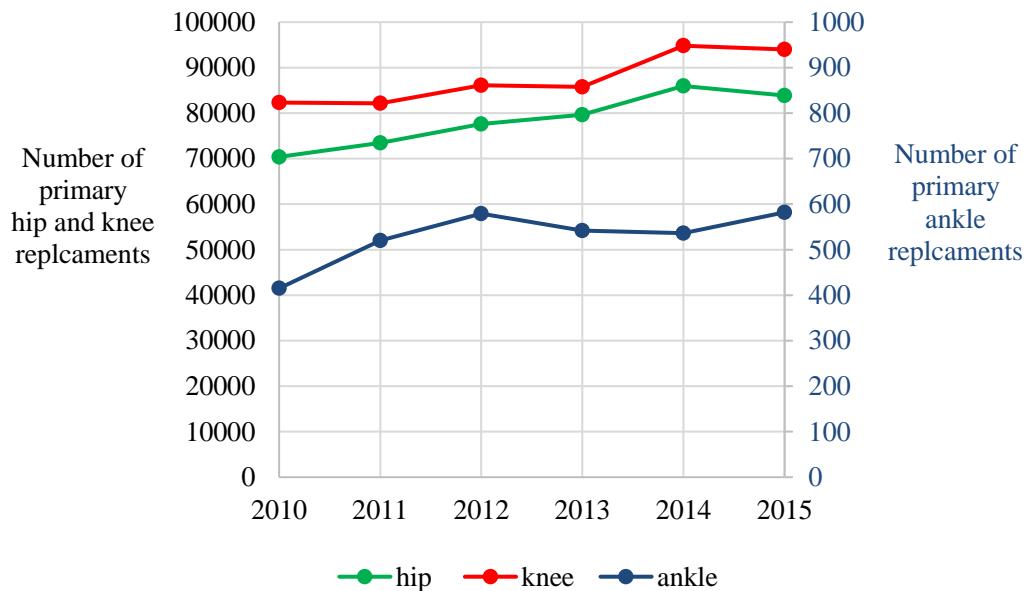


Figure 1.7 Implanted TARs per year compared to primary hip and knee replacements based on the National Joint Registry data for England and Wales (NJR 2016)

This less common procedure involves a similar concept to the other joints, replacing the natural articulating surfaces of the ankle with a mechanical alternative. The initial designs of the 1970s had poor outcomes to the point that TAR surgery was abandoned for over a decade (Vickerstaff et al. 2007; Gougoulas et al. 2010). However, this did provide a better insight into the demands from a TAR design. Hypotheses were defined that ideally the device should be relatively small because the bone quality in a diseased ankle is notoriously weak, the stiffest bone is located at the distal end of the tibia therefore as little of this should be removed as possible (Hintermann 2005). This dictated the fixation method to be porous coated to encourage osteointegration rather than cementation which requires a lot more space. The device should be positioned in order to restore the centre of rotation to that of the healthy ankle (Barg et al. 2010). A large range of motion about a varying axis is required from the device if this cannot be facilitated other joints try to compensate applying unnecessary stresses to them (Barg et al. 2010; Cenni et al. 2013). The geometry of the design should

be relatively anatomical and spherically congruent to keep the wear rates and contact stresses low and highly constrained designs should be avoided as they have been associated with stress shielding at the bone-implant interface (Hintermann 2005). All of these design factors must be applied whilst also maintaining ligamentous tension, the anatomical positioning and avoiding leg length inequality which are vital for implant success (Leardini 2001). Taking these lessons into consideration a second generation of designs saw its revival as a treatment method, tackling the problems from the previous designs by opting for a two component semi-constrained philosophy with the talus and the polyethylene implanted with primarily uncemented fixation to reduce bone resection. These TARs followed the natural geometry more closely than the initial attempts and were designed so the tibial component, which was larger than the talus, had a built in polyethylene layer (Figure 1.8B) to allow some axial rotation alongside flexion (Vickerstaff et al. 2007). The Tornier Salto ankle and Wright medical's Inbone and Infinity are the only one of this design concept still implanted in the UK according to the 2015 national joint registry statistics (Table 1) (NJR 2016).

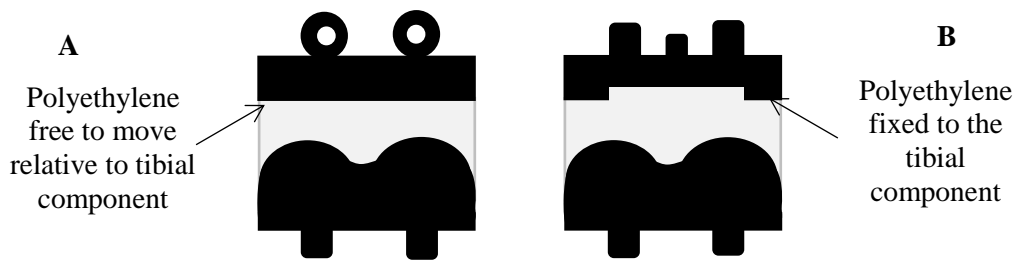


Figure 1.8 Schematic drawings of (A) mobile bearing MatOrtho Box TAR and (B) fixed bearing Wright Medical Infinity TAR

Shortly after the semi constrained design came the three component unconstrained TAR (Figure 1.8A). These consist of flat tibial component and curved talar metal components separated by a conforming polyethylene insert. A large contact area, with the talar radius of curvature longer than that of the natural ankle stops the occurrence of edge loading (Buechel Sr. et al. 2003; Hintermann 2005; Affatato et al. 2007). Currently the majority of the market share in TARs comprises of unconstrained designs (Table 1), these include; the Corin Zenith, Finsbury Box, SBI Star and Integra Hintegra (NJR 2016).

Table 1.1 Primary TAR prostheses implanted in the UK in 2015 (NJR 2016)

| <i>Manufacturer</i> | <i>Brand</i> | <i>Number of Procedures</i> | <i>Relative Percentage</i> |
|---------------------|--------------|-----------------------------|----------------------------|
| Corin | Zenith | 149 | 25.6% |
| Matortho | Box | 130 | 22.3% |
| Wright | Infinity | 90 | 15.5% |
| Sbi | Star | 75 | 12.9% |
| Tornier | Salto | 54 | 9.3% |
| Integra | Hintegra | 51 | 8.8% |
| Wright Medical | Inbone | 22 | 3.3% |
| Biomet | Rebalance | 4 | 0.7% |
| Lavender Medical | Akile | 4 | 0.7% |
| Unknown | | 6 | 1% |
| DePuy | Mobility | 0 | 0% |

Across Europe these mobile bearing designs are preferred, allowing rotational and translational freedom, aiming to reduce stress at the bone interface, protect the ankle ligaments and reduce wear and loosening due to the improved motion patterns (Tochigi et al. 2005; Barg et al. 2010). Meanwhile in America the surgeons prefer semi constrained designs with the STAR being the only FDA approved three component alternative. There is one obvious inconsistency across the available designs; the shape of the fixation surface which has companies opting for a variety of different solutions (Hintermann 2005; Kakkar et al. 2011). This wide variation suggests a problem and as of yet none of these solutions have proved themselves the obvious choice. Long tibial stems increase the likelihood of stress shielding due to the material stiffness compared to that of bone (Kakkar et al. 2011) and with the removal of bone required to fit these designs a weakening of the tibial cortex is often experienced (Gougoulis et al. 2010). In contrast the STAR design has a relatively small fixation, consisting of two bars to encourage osteointegration, although these should reduce the probability of stress shielding they will also lower the area for stress distribution. The Hintegra uses a screw fixation which aims to provide early stability but has shown limited success with problems of implant loosening before the screws have been fully integrated with the bone (Kakkar et al. 2011). Each of the methods discussed have both opposing and supporting arguments for their applicability as functional fixation geometries,

however, the only certainty is that secure fixation of the implant is vital to the implant longevity and functional success.

Comparing the clinically available devices it quickly becomes apparent that there is still no consensus on the ideal shape for a TAR with varying component constraints, fixation surface configurations and materials being marketed. The Salto Talaris and recently launched Integra Cadence design claims the talar component shape to be anatomical with a larger lateral radius but that is based on understanding prior to the 2013 discovery by Siegler et al. which contradicts that (Siegler et al. 2014; Morris et al. 2015). Building on the new understanding of the natural joint geometry the Bologna research group originally responsible for the design BOX TAR are taking a more considered approach to developing a more anatomically accurate mobile bearing TAR design rather than making incremental changes to the existing designs (Belvedere et al. 2017).

The reason the most recent TAR designs still are not an automatic choice of treatment is a result of the strict indications for surgery alongside the relatively high reported clinical failure rates (Thomas et al. 2003). The clinical success rate varies across the various devices and the surgeon implanting them. One study of over 500 TARs quoted the average five-year survival rate to be 83% irrespective of design or surgeon (Easley et al. 2011). Similarly a systematic review by Gougoulis et al. (2010) of 1105 showed a five year failure rate of 10% but the range varied from 0% to 31%. The poor performance and high failure rates have not reached the extent where recall is required, however, some designs have been taken off the market. These include the Biomet Ankle Evolutive System and the DePuy Mobility both of which had be implanted in relatively high numbers prior to their withdrawal (NJR 2016). Both of these devices were stemmed cobalt chromium designs but did not necessarily perform significantly worse than other devices. There is a high level of uncertainty in terms of the factors that cause failure and success in different designs in different patients and a lack of understanding of the causes of revision even in 2017.

1.3.4 The Corin Zenith

As the Zenith produced by Corin Group PLC holds the largest market share according to the National Joint Registry for England and Wales (NJR 2016) it was selected as the focus of this research.

Unlike any of the other commercially available TARs the Corin Zenith which consists of a titanium nitride (TiN) coated bulk titanium on ultra-high molecular weight polyethylene (UHMWPE) articulation (Figure 1.9). TiN coating has historically been applied to both knee and hip replacements but with varied success. The earliest unconstrained TAR design, the Buechel-Pappas opted for this material combination and the Zenith has followed its lead. The bulk titanium provides a lower Young's modulus more similar to that of bone reducing the stress shielding effects. Meanwhile the titanium nitride coating aims to provide a ceramic surface with better wear properties, this gives the device its distinguishable gold colouring (Pappas et al. 1995; van Hove et al. 2015). This combination of materials is a solution which should deliver the best of both worlds, low wear rates and reduced stress shielding.



Figure 1.9 Corin Zenith titanium nitride coated TAR

In order to comply with the minimal bone removal for ankle replacements, Corin also opted for porous coating. Corin have their own coating method, known as BONIT (Figure 1.10). This method involves electrochemical-deposition of biphasic calcium phosphate (CaP) on the already porous titanium coated tibial and talar component back surfaces. Electrochemical-deposition encourages a thin, even coating of CaP across the complex geometry of the fixation surface whilst preserving the porous titanium underlayer. A thinner coating has also been associated with a reduction in the potential for coating delamination (Røkkum et al. 2002). The temperature at which the coating process occurs can impact the

interface failure rate, electrochemical-deposition occurs at room temperature which avoids any alteration to the crystal structure (Rößler et al. 2003).



Figure 1.10. BONIT fixation coating

1.3.5 Comparing fusion and replacement

As previously mentioned the intention of ankle replacement is to preserve a full range of motion whereas fusion relies on immobilisation. There has been much clinical debate about which is the preferred treatment but despite this comparative studies are limited. In a systematic review Haddad et al. (2007) found outcomes between TAR and fusion at an intermediate stage to have similar revision rates due to failure and non-union respectively. In addition, the percentage of patients reporting good to excellent results with each treatment was 68.5% for TARs and 68% for fusion. Early results from a controlled trial comparing the multicentre clinical outcomes of 158 TARs to 66 ankle fusions showed initial pain relief scores were no different and after two years the pain relief similarities remain while TAR patients reported better function. However the number of major complications and patients requiring secondary surgery were higher for TAR patients (Saltzman et al. 2009).

Some authors have also compared the differences in range of motion associated with the two treatment options. Valderrabano et al. (2003) explored the extent of this motion difference through applying non-load bearing motions in the typical planes to a cadaveric model, one normal, one fused and three fitted with a range of TAR designs in accordance with the alignment outlined in the surgical guide.

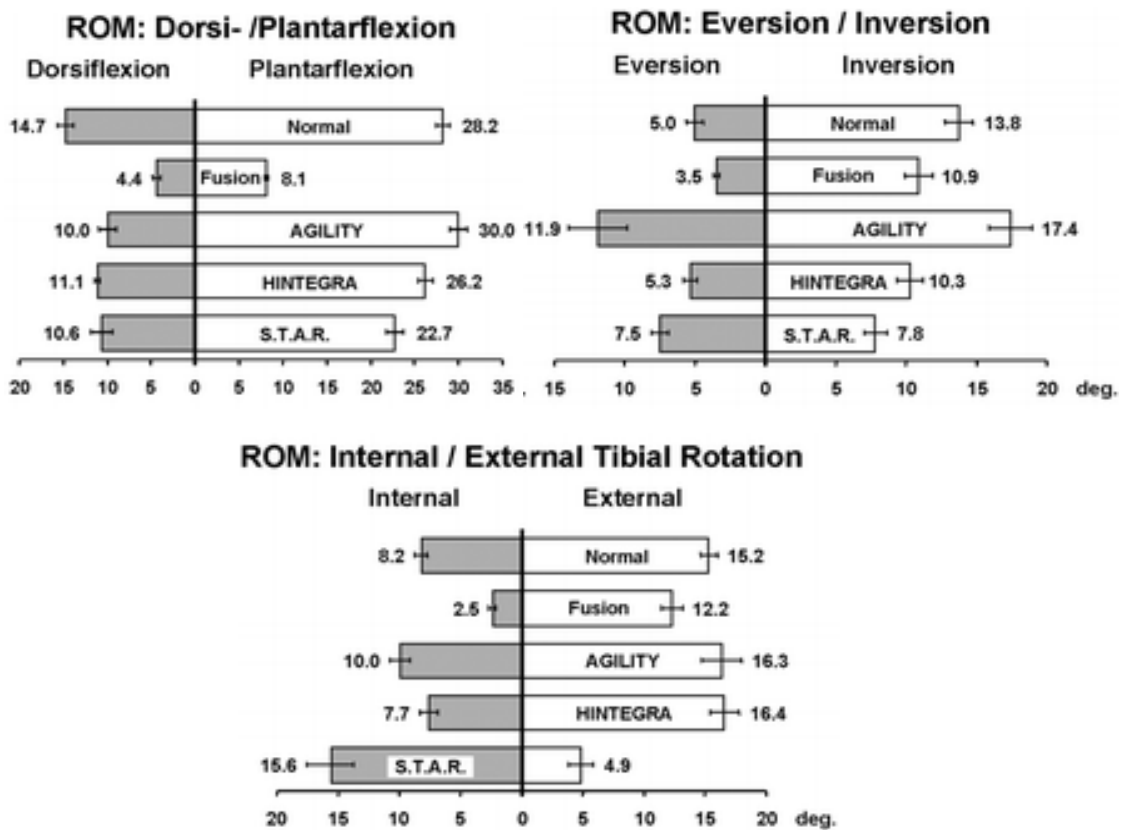


Figure 1.11 Range of motion for ankles in normal and treated states. Figure adapted from Valderrabano et al. (2003) Kinematic changes after fusion and total replacement of the ankle: part 1: Range of motion. *Foot Ankle Int*, 24(12), pp.881–887. Copyright © 2003 by SAGE Publications. Reprinted by Permission of SAGE Publications, Inc.

It is apparent from this visual representation (Figure 1.11) that under fused conditions there is substantially less motion in the ankle in all planes which will affect the gait pattern. This reduced motion is also the instigator of high stresses on adjacent joints. Comparatively TAR has, in most cases, achieved a more similar range of motion; however, this is highly dependent on the specific device. For example; the Agility provides a much greater range of eversion than inversion and the STAR allow substantially more internal rotation than the ankle is used to but much less external rotation (Valderrabano et al. 2003). None of the tested designs are perfectly in line with what we are used to naturally which is not necessarily a problem as the full passive range of ankle motion is not required for walking. Historically Lamoreux (1970) reported approximately 15° dorsiflexion during natural gait which all three of the devices tested would struggle to achieve. Aside from this reduced dorsiflexion at heel strike and possibly the STARs limitations in

external rotation the presented motions ranges mean the devices should have the potential to facilitate a relatively “normal” gait pattern.

In the first gait analysis study comparing cohorts of arthrodesis and fixed bearing replacement patients to healthy and arthritic controls Philippe et al. (2008) found both treatments to significantly diminish the range of flexion motion and walking speed compared to the healthy cohort. The range of motion following arthrodesis was also significantly less than that of the TAR group. Since, multiple authors have confirmed this trend for a larger, more natural range of motion with mobile bearing TARs compared to arthrodesis (Hahn et al. 2012; Singer et al. 2013). In contrast Flavin et al. (2013) found no significant difference between the flexion range of motion for similar sized cohorts in their gait study.

1.3.6 Surgical complexity

The location of the tibio-talar ankle joint makes the surgical procedure highly complex. As with all joint replacement surgeries the quality of the surgery can affect the success of the device. The small working area and notorious complexity often results in TAR reoperations to remove unforeseen malleolar impingements which will impact the recovery time (Henricson et al. 2007). It is vital to the joint function that the soft tissues are handled carefully (Hintermann 2005) and the device is implanted accurately, parallel to the ground (Jackson et al. 2003). Positioning can be difficult with the limited surgical access but malpositioning (Figure 1.12), in any or multiple planes, can be a serious problem (Jackson et al. 2003). Not only will this increase the possibility of lift-off (Tochigi et al. 2005), heighten contact stresses (Espinosa et al. 2010), affect the ligaments (Hintermann 2005) and functionality of the implant but should bearing impingement occur as a result the wear rates will be accelerated (Jackson et al. 2003; Hintermann 2005). Figure 1.12 displays an example of a well aligned implant compared to an anteriorly implanted talar component.

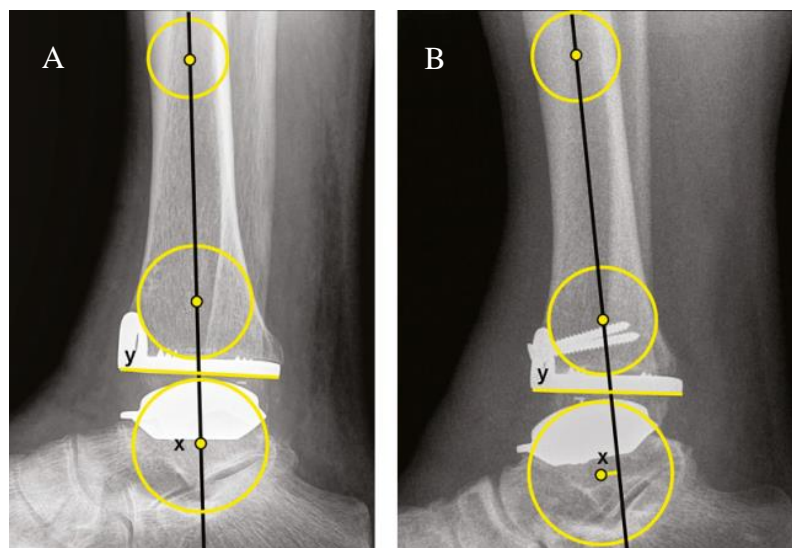


Figure 1.12. X-ray of a TAR (A) neutrally aligned, (B) talar centre anterior to tibial axis. Image obtained from: The effect of three-component total ankle replacement malalignment on clinical outcome: pain relief and functional outcome in 317 consecutive patients. Barg et al. (2011) J Bone Joint Surg Am, 93 (21): pp1969 -1978.

Anterior placement of the talus and reduction of the joint height can cause problems (Tochigi et al. 2005). Misalignments of greater than 5° in version could see the polyethylene components reach their yield stress long before the predicted time frame (Espinosa et al. 2010). Similarly, the challenges of correcting a heavily varus or valgus deformities have been recognised. Wood et al. (2009) defined a deformity of greater than 15° to dramatically increase the six year failure rate, especially in the Beuchel-Pappas design and for cases which did not result in direct failure a higher incidence of edge loading was observed. Morgan et al. (2010) reported a similar correlation between pre-op malalignment and post-op edge loading.

In terms of TAR surgical implantation there is a notable learning curve while the surgeon gets used to the device and operative technique (Haskell et al. 2004; Hintermann 2005; Henricson et al. 2007). The best outcomes have typically been published by the design surgeons themselves (Gougoulis et al. 2010). Henricson et al. (2007) used the Scandinavian Joint Registry to plot contrasting data for the revision rates for three surgeons for their first 30 STAR devices compared to those later. The five-year survival rate rose from 70% for the early implants to 86% for those after. This suggests the more experienced gained with the surgeon's

preferred implant the better the success rates will be expected to get, however, such inconsistent initial results may have an effect on the professional or public perception of the implant. This will impact low volume TAR centres which despite having similar functional results have been associated with a higher failure rates compared with the more experienced, high volume centres (Pinar et al. 2012). However, with low numbers of TAR procedures taking place at centres across the UK it is difficult for the surgeon to get the necessary experience (Henricson et al. 2007). This learning curve is likely to be partly responsible for the ranging success rates which are reported in literature. The Depuy Mobility was the most commonly implanted TAR in the UK despite its varying five year statistics; Ahluwalia et al. (2013) reported a relatively high, 92.6% success rate while at the lower end of the scale Blundell (2012) recorded 84.1% for a smaller study group. Despite these five-year success rates not being dissimilar to other marketed TARs this device has since been removed from the market.

The Corin Group's Zenith device, having been implanted since 2007 at this early stage there is limited published information regarding the medium or long term results. This evolution of the Buechal-Pappas is marketed on its "advanced coating technology" and novel instrumentation which allows for improved repeatability and may be the reason for its continued market placement (Millar 2012). Advances in surgical equipment may be able to curb the prominence of the surgical "learning curve". Mckenzie et al. (2012) have reviewed the 81 Zenith TARs implanted between 2007 and 2011 in what was an inventor study and reported a greater than 95% survivorship at 30 months and no evidence of radiographic loosening on radiographs. This centre published more recent survivorship statistics of 99.0% at three years (n=103), reducing to 94.0% at five years (n=50), and 93.8% at seven years (n=16) (Walter et al. 2015). Millar (2012) published a non-inventor study for the early follow up results for the first 50 implanted TARs outlining that 46 out of the 50 patients with the new TAR design were deemed happy. The alignment was reported within ± 5 degrees for 43 patients out of 50 in the coronal plane and 45 patients in the sagittal plane. After a mean follow up of 30 months only one revision surgery for loosening due to cyst formation was required. This was then followed up to medium term, an average of 5.3 years and showed 96% survivorship (Sinclair et al. 2015). Both of these centres showed encouraging

survivorship especially considering the learning curve which is associated with TAR surgery but further independent information is required to properly judge the implant performance. The midterm results will be interesting as this is where other designs have seen increasing osteolysis and failure.

Taking into consideration the complexity of this procedure combined with the high load bearing nature of the ankle joint it is no surprise the patient indications for TAR surgery are highly limited. The “ideal” patient for TAR is generally over 50 years of age, weighs less than 200 pounds, has failed to respond to the other non-invasive treatments and will only place low physical demands on the device (Mann et al. 2012). There are many more contraindications which are likely to contribute to the fact ankle fusion remains the preferred treatment method for many surgeons (Jackson et al. 2003). Ideally a TAR should be more widely available, especially for younger more active patients but limited confidence in current designs makes that a chance few are willing to take. If these devices are failing early in the ideal patient demographic this will no doubt be worse for any individual outside of this bracket.

1.3.7 Complications

The surgical challenges discussed only attribute to a certain percentage of the problems with TAR. For the majority of the ankle joint replacements the cause of complications with the TAR are down to mechanical failures, typically aseptic component loosening (Figure 1.13) (Bauer et al. 1996; Henricson et al. 2007; Glazebrook et al. 2009; Easley et al. 2011). Glazebrook et al. (2009) carried out a review of complications across all ankle implants comprising more than 25 studies with a follow-up time of at least 24 months. The most common complication observed was subsidence however, this complication did not necessarily lead to revision. Instead they found aseptic loosening, implant failure and most commonly a deep infection had the biggest impact in joint success, resulting in complete failure in over 50% of cases. More recently Sadoghi et al. (2013) also carried out a systematic review of published joint registry data between 1993 and 2007 of reasons for TAR revision. Based on the reason for failure in 189 revisions from 1113 primary cases it was found aseptic loosening to be the most prominent cause for revision at 38% (Figure 1.13). The loosening, especially common at the talar

component (Tomlinson et al. 2012), can be attributed to poor fixation or osteolytic lesions which in other joints have been the result of stress shielding or the immune host response to polyethylene wear debris (Bauer et al. 1996).

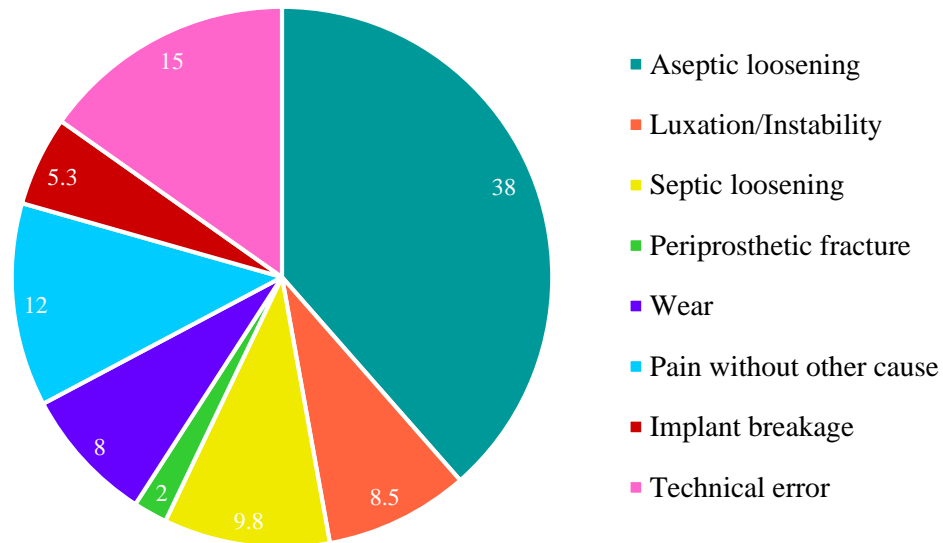


Figure 1.13 Reasons for TAR revisions based on 189 revisions (Sadoghi et al. 2013)

Technical error was the second greatest cause at 15%, found to be much more common than for hip or knee replacements at 3.8% and 4.6% respectively (Sadoghi et al. 2013). Technical errors include a variety of faults such as incorrect component positioning, impingement, wrong implant size and poor preparation.

1.4 Biotribology

Complications such as wear and implant breakage accounting for 13.3% of TAR failures have the potential to be improved by making correct design decisions. Biomaterial selection, bearing constraints and implant geometry will affect the TAR performance. It is vital to understand the biotribological implications of these design features in order to optimise the wear performance.

Tribology is defined as the science and technology of interacting surfaces in relative motion. Biotribology applies the same principal to a biological environment such as humans and animals, encompassing the properties of friction, lubrication and wear. Biotribology is most frequently addressed with respect to the hip joint; however, the theories are applicable to all synovial joints, both natural

and replacements, including the focus of this literature review, total ankle replacement (Hall et al. 2001; Davim 2010).

1.4.1 Friction

Friction is known as the resistance of motion (Figure 1.14). As far as records are concerned Da Vinci was the first person to formulate the current definition of friction. However, it was Amonton who went on to publish the two important laws regarding friction which state that the;

1. Frictional force (F) produced is directly proportional to the load (N) applied across the bearing surfaces
2. Frictional force is independent of contact area (Bowden et al. 2001).

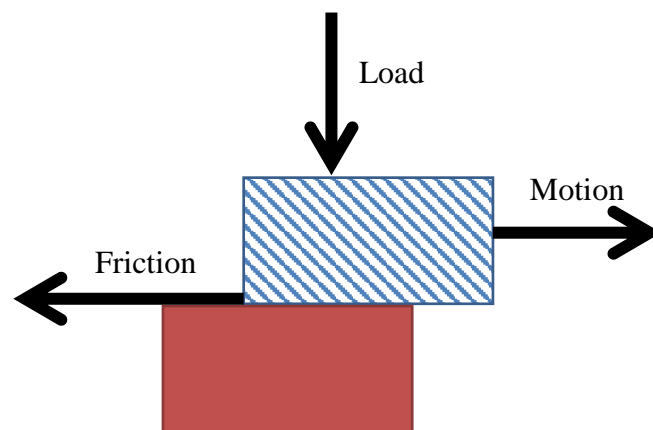


Figure 1.14 The relative direction of friction compared to motion (Hall et al. 2001)

For a metal on polyethylene articulation such as the majority of TARs the frictional forces are generated from the deformation of the contacting asperities, often adhesive bonds will occur at the contact areas between the two materials. Energy is required to break the physical and chemical bonds to allow articulation. It is this breaking of bonds which is considered the frictional resistance (Hall et al. 2001). The introduction of a lubricant has the ability to reduce the frictional forces. The frictional factor of a metal on UHMWPE total hip replacement in 25% bovine serum has been estimated as 0.06-0.08 (Jin et al. 2006).

1.4.2 Lubrication

The lubrication can dictate the level of friction and wear experienced by a bearing by controlling the level of contact between the two surfaces. This property can be influenced by the lubricant viscosity, loads applied to the joint and entraining velocity between components well as the implant geometry and material selection (Rabinowicz 1965).

The lubrication regime which can be achieved by a total joint replacement varies depending on the level of asperity contact between the bearing surfaces (Figure 1.15). The asperity contact will be at its highest in an unlubricated couple. The addition of lubricating fluid influences this contact dictating which regime the bearing will operate in (Bowden et al. 2001).

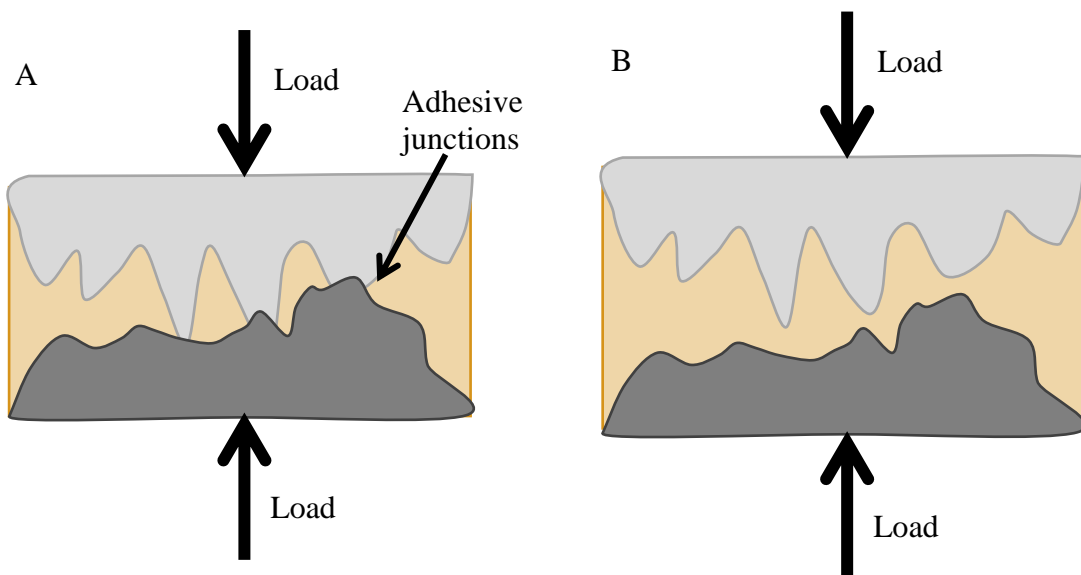


Figure 1.15 Asperity contact in (A) boundary lubrication and (B) fluid film lubrication

The first regime is known as boundary lubrication tends to be just a few molecules thick resulting in a high level of asperity contact through which all of the applied load must be supported. At the other end of the scale is fluid film lubrication in which the lubricant layer is thicker than the combined surface asperities completely separating the two components, protecting their surfaces. In this case the fluid takes the full force unless its viscosity is too high meaning minimal frictional force. Lying in between these regimes is the theory of mixed lubrication in which the load is distributed between both the surface contact and the lubricating

film in a ratio depending on the level of asperity contact (Bowden et al. 2001; Dowson 2001; Jin et al. 2006).

Typically, hard on soft bearings comprising of metal on polyethylene articulating components as seen in TAR will remain in the boundary lubrication regime. This high friction system is a result of the surface finish on polyethylene; this can only be machined to a certain resolution leaving a comparatively high surface roughness.

Another factor in the biological environment is the protein concentration as this will influence the friction and wear characteristics. *In-vivo* the proteins and polypeptides from the serum are known to preferentially adhere to the polyethylene bearing surfaces where they increase the friction through formation of a passivating layer (Heuberger et al. 2005). *In-vitro* the presence of proteins increases the wear rate relative to water or saline solutions (Brown et al. 2006). However, these proteins degrade over time in *in-vitro* simulation due to the heat generated which causes them to form a protecting layer which has been shown to affect the wear rate (Liao et al. 1999). Such protein films according to Brown & Clarke (2006) also caused with concentrations greater than 10-17g/L have been associated with reduced wear rates in joint replacements. This process is believed to not be physiologically relevant so should be mediated by controlling the temperatures, concentration and volume of lubricant.

1.4.3 Wear

The definition of wear is “the removal of material from solid surfaces as a result of a mechanical action”. In a simple system the level of volumetric wear (V) correlates directly with the applied load (W) and the sliding distance (x) (Rabinowicz 1965). Archard’s law defines the equation for the relationship with the addition of a wear factor (K) which relates to the materials hardness, roughness and lubrication (Equation 1)

Equation 1 Archard wear equation

$$V = K \times W \times x$$

The three most widely recognised mechanisms for wear for total joint replacement (TJR) include adhesion, abrasion and fatigue wear. These typically act in

combination but in some conditions one may become more prevalent (Hall et al. 2001). Adhesive and abrasive wear are considered to be responsible for the majority of the wear observed with polyethylene TJR clinically (Wang et al. 1998). Adhesive wear transpires from the shearing at the bonds across the points of asperity contact, if the force to break this junction is greater than the force required to tear the material surface material transfer will take place. Generally it is the less stiff material which forms fragments on the tougher surface. There is a risk that these will then come loose and can attribute to third body wear (Hall et al. 2001). This can be combatted with better lubrication (Wang et al. 1998). Abrasive wear is another problem for hard on soft bearings; if the hard surface is rough it will plough groves into its softer counterpart. This can result in the removal of polyethylene material which again contributes to the 3rd body wear. The level of abrasive wear is inversely proportional to the materials hardness (Affatato 2012). Improved surface finish can reduce abrasive wear (Wang et al. 1998). With the cyclic loading TJRs are subjected to high stresses which can fatigue the material. The level of surface fatigue depends on the magnitude of the applied load and how many cycles the implant had to endure (Teoh 2000). This can cause fatigue cracks either at the surface or below which will eventually result in pits.

There are many more wear mechanisms which have been documented on TJRs throughout their use which can involve the factors outside of the bearing surfaces. These individual mechanisms can be categorised into 4 modes of wear;

Mode 1: Simple articulation of the bearing surfaces under the ideal testing conditions

Mode 2: Articulation occurs between a bearing surface and a non-bearing surface such as the rim, known as edge loading

Mode 3: The presence of 3rd body wear particles in the joint space causing abrasion of the primary articulation

Mode 4: Articulation of two non-bearing surfaces such as the implant stem against the surrounding bone or surface fretting in modular components (Davim 2010)

It is unlikely to see one individual cause of wear for example particles generated from the articulations in mode 4 can be the cause of further 3rd body wear (mode 3).

From retrievals Hood et al. (1983) defined seven mechanisms of surface degradation visible on an UHMWPE knee insert and gave their physical appearance a description in order to be able to differentiate between them. These factors are combined below;

1. Abrasion- areas in which the polyethylene had a shredded or tufted appearance
2. Surface deformation- used to describe evidence of permanent deformation occurring on or around the articulating surfaces (and caused, presumably, by cold flow and/or creep of the polyethylene)
3. Pitting- describe depressions on the articulating surface usually of irregular shape and 1-2mm deep
4. Embedded PMMA debris (or other coating debris)- recognized by the colour and/or texture difference between PMMA and polyethylene.
5. Scratching- describes the indented lines (watch for marks from retrieval surgery)
6. Burnishing- areas that had become highly polished
7. Delamination- large amount of PE removed

Since these effects were initially outlined efforts have been made in order to reduce the wear mechanisms. Changing the method of sterilisation; moving away from oxidation towards inert atmospheres has substantially reduced the risk of delamination. The introduction of the highly crosslinked strain of polyethylene will change the wear properties depending on the level. With a moderate level of crosslinking the volume of wear debris can be reduced (Hall et al. 2001). Thus far only one TAR, the Trabecular Metal made by Zimmer has chosen to implement cross linking technology in their semi-constrained design. On the other hand, deviation from the ideal physiological conditions can result in highly accelerated wear of the device. The presence of 3rd body particles or edge loading components can see an increase in the prevalence of these wear mechanisms.

1.4.2 Biological response to wear particles

Over time the wear processes mentioned cause degradation of the implanted biomaterial which releases a certain level of wear particles. Due to the combination of wear processes which act on the UHMWPE the particle morphology vary in both shape and size from large flakes to small spheres. Although as a whole the body accepts the biomaterials, these particles can provoke an immune response from the biological environment (Figure 1.16). Seen as foreign bodies the particles attract leukocytes and macrophages to the implant site, their presence reduces the pH level and as a result the neutrophils increase their release of a chemotactic factor (Remes et al. 1992; Teoh 2000). The problem then extends with the host producing corrosive chemicals in response to the debris. These chemicals aggravate the initial fatigue problem causing further debris to be generated which in turn advances the host response and so the problem continues to cascade until the severity of the response it leads to failure (Teoh 2000).

As previously mentioned TARs typically constitute of cobalt chromium and ultra-high molecular weight polyethylene (UHMWPE) bearings. Conventional UHMWPE is renowned for generating more wear than some of the alternative bearing combinations. This debris has been heavily associated with the onset of osteolysis surrounding the implanted device and it is believed that the size and number of particles will dictate the immune response, these factors are dependent on both the material, implant design and the joint (Sethi et al. 2003). The larger the debris the more difficult they become for the giant cells to digest, however, it is the smaller particles of 0.1-10 μ m which have been reported as the most biologically active (Tipper et al. 2000). These small particles intensify the inflammatory response, attracting a large number of macrophages to the implant site which sees the release of cytokines (Tipper et al. 2001). A specific cytokine, TNF- α , is accountable for activating osteoclasts, the cells which destroy bone which is assumed to be the cause of bone resorption which leads to aseptic loosening in total joint replacements (Howling et al. 2001). As previously mentioned moderately crosslinked UHMWPE was developed to reduce the volume of wear debris in hips and knees, however, simulator studies show the particles it does generate lie in the most biologically active size range which puts its benefit in question (Howling et al. 2001; Endo et al. 2002). As of yet there have

been limited cases of wear mediated osteolysis across TAR publications despite simulator studies producing comparative wear volumes and particles with similar equivalent circular diameters to that of total knee replacements (Bischoff et al. 2015).

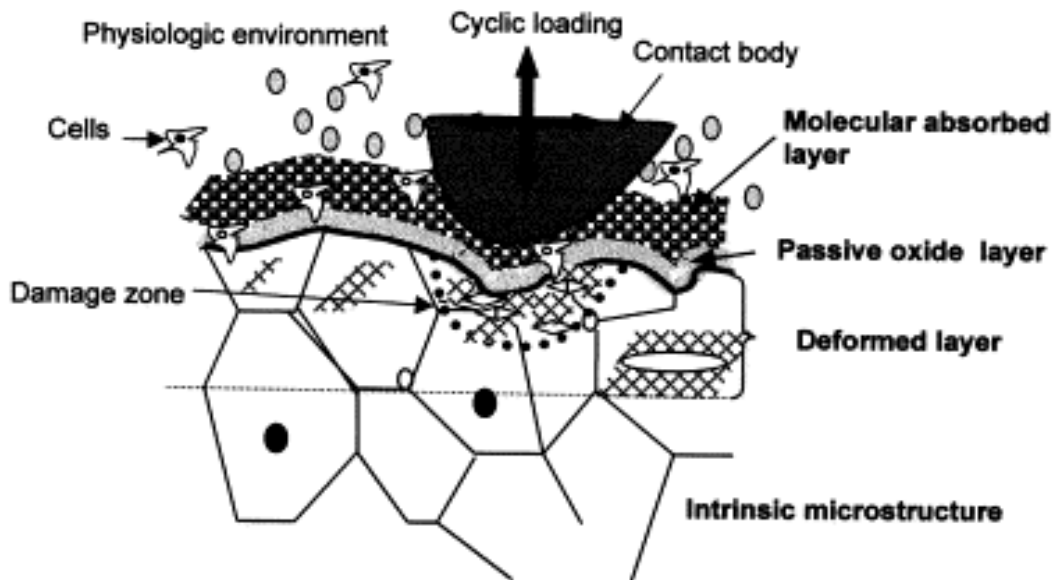


Figure 1.16 Schematic of the effects of continued loading of a biomaterial. Reprinted from Teoh (2000), *Fatigue of biomaterials: a review*, *IJ Fatigue*, 22(10), pp 825-837 with permission from Elsevier.

1.5 Wear simulation of total ankle replacements

Wear is a common primary failure mechanism in joint replacement but is often a secondary failure mode as it can result in mis-alignment, abnormal loading and fatigue (Affatato 2012). It is important to understand the wear of TARs and their possible impact on osteolysis but very little development has gone into simulating their wear. There is no widely recognised methodology, this is especially apparent when compared to the large volume of publications on hip and knee simulation. In these instances ISO standards dictate the input parameters; however, for TARs no such control has been implemented.

As with all joints, the input parameters such as the loading pattern, peak load, displacement and range of motion and phase of these inputs will impact the wear outcomes. These factors will vary across individual cases depending on the patient and/or the device design. In order to measure a clinically relevant wear volume

these need to be applied to the gait simulation with realistic magnitudes for the typical patient demographic. The information required to fulfil these inputs is limited and possibly somewhat outdated for the ankle joint. Without universal protocol it is no surprise there is a substantial variability across the few published studies investigating wear of total ankle replacements.

The first of the published wear simulation was investigated by Bell & Fisher (2007). Their method involved inverting the ankle prosthesis in an altered knee simulator testing the Buechel Pappas and the DePuy Mobility TARs. Around the same time Affatato et al. (2007) used a similar knee simulator based experimental setup for testing the Finsbury Box. A further ankle simulator publication from Postak et al. (2008) used what is described as “custom, single-station motion simulator” to test five Surgical Inbone STARs. Since Bischoff et al. (2015) have implemented a similar profile to that of Bell & Fisher (2007) in order to assess the afore mentioned semi constrained Zimmer device. All of these wear tests were carried out under displacement control. In the last two years Reinders et al. (2015) published results from the first force controlled TAR wear simulation. Each of these investigations used their own interpretation of the ankle gait inputs. Relative to the number of wear investigations in both total hip replacement and total knee replacement the number of TAR studies is greatly limited.

1.5.1 Simulator inputs

The input motion ranges (Table 1.2) vary subtly amongst the authors. These are generally similar aside from the reduced plantarflexion from Reinders et al. (2015) which aims for a range of motion based on gait data from individuals with TARs rather than a healthy gait as is the typical wear simulation convention. Bell & Fisher (2007) increased the maximum dorsiflexion to 15° whereas Affatato et al. (2007) and Postak et al. (2008) maintained the 10° and instead increased the plantarflexion by 5°. Postak et al. (2008) included minimal external rotation compared to the other authors with no reference of the clinical data it was obtained from. Instead Bell & Fisher (2007) and Affatato et al. (2007), with external rotations of 8° and 7.7°, cite motion ranges based on experimental measures by Calderale et al. (1983) involving electro-goniometric exoskeletons and Reggiani et al. (2006) from finite element modelling of TAR respectively. Internal rotation

is where the least variation within the figures lie. The relevant profile from Reinders et al. (2015) is difficult to compare as it is a force based input but estimating from the restraint model this is likely to be approximately 10 degrees of external rotation and minimal internal rotation.

Table 1.2 Range of motion for TAR wear simulation

| Author | Plantar-flexion | Dorsi-flexion | Internal Rotation | External Rotation |
|---------------|------------------------|----------------------|--------------------------|--------------------------|
| Bell 2007 | 15° | 15° | 2° | 8° |
| Affatato 2007 | 20° | 10° | 2.6° | 7.7° |
| Postak 2008 | 20° | 10° | 2° | 2° |
| Bischoff 2015 | 16° | 15.2° | 2° | 8° |
| Reinders 2015 | 5° | 10° | 0° | 10° |

The combination of loads and motions experienced at the ankle joint is highly dependent on the exact moment within the gait cycle. It is important to recreate this for a realistic simulation of ankle wear. Postak et al. (2008) chose to use a highly simplified sinusoidal input. Conversely the other authors used a more complex, physiologically accurate profile such as that in Figure 1.17 in order to maintain the most realistic motions possible. The axial loading on the ankle will change from the swing to stance phases. Maximum forces have been measured to reach up to 5.2 times body weight on the ankle's small contact area (Hintermann 2005). In order to replicate this Bell & Fisher (2007) scaled the dynamic force profile presented by Stauffer et al. (1977) to the equivalent of five times body weight which was taken to be 70kg (Figure 1.17). This proved problematic when combined with the motion pattern so was reduced by 400N with the minimum force applied during the swing phase, just 100N in order to maintain joint contact (Bell et al. 2007). Bischoff et al. (2015) was in line with this while both Reinders et al. (2015) and Affatato et al. (2007). had a much reduced axial load varying between 100N in the swing phase to a maximum of 1600N, almost half of the maximum load selected by Bell & Fisher (2007). Perversely Postak et al. (2008) chose to avoid dynamic loading and instead applied a static loading method applying 3000N throughout the full range of sinusoidal motion.

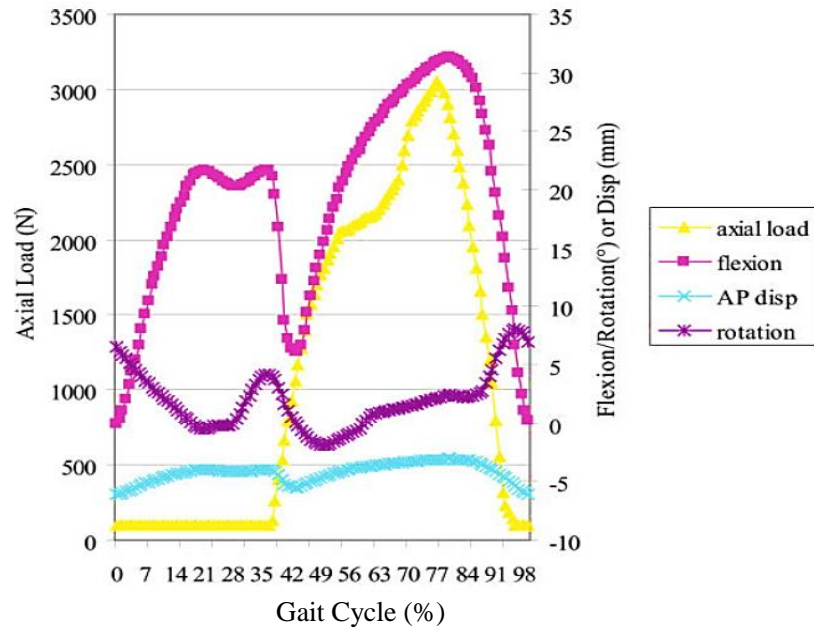


Figure 1.17 One example of the motions and loading applied in a TAR wear simulator. Reprinted from J Biomed Mater Res B 81B(1), Bell & Fisher (2007), Simulation of polyethylene wear in ankle joint prostheses, pp162-167.

Alongside the loading and range of motion the decision to include an Anterior-Posterior (AP) displacement is important in mimicking the natural gait, however, there appears to be no recognised magnitude of this motion. The majority of authors keep this relatively low to avoid dislocation problems with displacements of 2.5-3mm (Bell et al. 2007; Postak et al. 2008; Bischoff et al. 2015; Reinders et al. 2015). Bell & Fisher (2007) chose to apply the displacement with the same profile as the flexion but only for the last one million cycles (Mc) of the 6Mc of the experiment as evidence for a specific magnitude could not be found. In contrast to the small magnitudes Affatato et al. (2007) seem more decisive in choosing to induce a maximum of 8.45mm displacement over all of the gait cycles with a very different profile input decreasing throughout the gait cycle based on a computational output.

It is also important to note that none of the published studies address any version presumably on the assumption it is confined to the subtalar complex or the test apparatus could not drive inputs in six degrees of freedom.

1.5.2 Lubrication

Historically most investigators have agreed that bovine serum was the optimal lubricant producing similar wear rates to what has been observed *in-vivo* (Liao et al. 1999). In other more established joint replacement wear testing the ISO14242-2 (2016) standard has changed the bovine serum concentration recommendation. Initially suggesting bovine serum diluted to 25% in 2002 but because the protein concentration varies depending on the stage at which it is obtained the ISO standard now specifies the protein concentration of 20g/L for knees and 30g/L for hips. Synthetic serum alternatives are being explored but have not yet been widely adopted (Bortel et al. 2015).

In the TAR wear tests Reinders et al. (2015), Bischoff et al. (2015), Postak et al. (2008) and Bell & Fisher (2007) all used bovine serum. Bell & Fisher (2007) specify the serum from new born calves making up 25% combined with 0.1% sodium azide in deionised solution whereas Postak et al. (2008) and for Reinders et al. (2015) the lubrication requirement was a protein concentration of 20g for every litre. For Bischoff et al. (2015) this was the same with the addition of ethylenediaminetetraacetic acid (EDTA). Affatato et al. (2007) recognised their lubrication choice to be a limitation of their experimental procedure as deionised water has been proved to be poor at replicating the lubricant properties experienced *in-vivo*. It is important to use an organic serum to ensure the development of any tribofilms which may occur in a biological setting to improve the lubrication, guaranteeing more realistic wear rates.

1.5.3 Wear rates and limitations

All of these studies have significant limitations in terms of their physiological accuracy. In each case the number of samples is low, as low as three for all types of prosthesis except for the STAR where five were compared. Affatato et al. (2007) running their test for just two million cycles and not using the optimal lubricant is a definite drawback of their experimental testing. Postak et al. (2008) using a static loading pattern would not produce physiologically accurate wear volumes or wear scars and Bell & Fisher (2007) only applying the AP motion cycle for the last million cycles is not long enough to understand the effects of this parameter especially with such high variability.

The purpose of each of these studies is to quantify an average wear rate over the number of chosen cycles. The findings are laid out below in Table 1.3.

Table 1.3 Comparison of wear rates across tested designs

| Author | Implant | Samples | Cycles (million) | Wear Rate (mm³/MC) |
|---|------------------------|----------------|-------------------------|--------------------------------------|
| Bell 2007 (No AP) (With 1 MC AP) | BP | 3 | 5 | 10.4 ± 11.8 |
| | Mobility | 3 | 5 | 3.4 ± 10.0 |
| | BP | 3 | 1 | 16.4 ± 17.4 |
| | Mobility | 3 | 1 | 10.4 ± 14.7 |
| Affatato 2007 | BOX | 3 | 2 | 18.6 ± 12.8 |
| Postak 2008 | STAR | 5 | 10 | 5.7 ± 2.1 |
| Bischoff 2015 | Trabecular Metal (CPE) | 3 | 5 | 8.0 ± 1.4 |
| | (XPE) | 3 | 5 | 2.1 ± 0.3 |
| Reinders 2015 | Hintegra | 3 | 3 | 18.2 ± 1.4 |

These published wear rates should not be compared directly as all of the experimental conditions were highly variable. As highlighted by Affatato et al. (2008) different hip simulators will provide varying wear rates even when testing the same prosthesis. Factors such as lubrication, temperature, kinematic inputs, control system and centre of rotation specific to each centre's protocol will result in data disparity.

In each of the TAR wear tests the number of samples was small so as a result the variability in the recorded rates is high; with such large confidence limits it is difficult to draw any specific conclusions. The results from Postak et al. (2008) for the STAR have a lot less variability than the other designs, likely to be a result of the simplified conditions but also the extra experimental time and number of samples may be partly responsible. Although it cannot be considered significant there is a visible change in the wear rate with the addition of AP displacement to the wear simulation experiments by Bell & Fisher (2007). As this device had already been subjected to kinematic conditions any damage to the bearing surfaces could also be responsible for the increase. Wear rates from the force controlled simulator were comparable (Reinders et al. 2015) and the use of crosslinked

polyethylene produced much lower wear rates for the Zimmer Trabecular Metal (Bischoff et al. 2015).

It can be concluded that careful selection of the inputs is important to generate physiologically accurate data which can put confidence in the expectation for a device in a biological setting. It is likely some more research could be required in order to define some of these parameters accurately. However, defining these parameters is not enough it must then be ensured there is an acceptable 95% confidence in the ability of the system to generate the desired motions and forces throughout each gait cycle (Barnett et al. 2002).

1.5.4 Zenith wear performance

Due to the current classification of ankle replacement devices there have been no simulator studies carried out on the Corin Zenith device. As a class II device TARs do not have to undergo the same rigorous *in-vitro* testing as hips do before being approved in to the market. The Zenith as an evolution of the Beuchal-Pappas, consisting of the same biomaterials and therefore could be assumed to have a similar wear rate if subjected to the same simulator conditions.

Some knowledge of titanium nitride can provide an insight into the potential benefits and risks. The bearing coating increases the material hardness and can be highly polished providing the potential to reduce the friction between the components which should in turn improve the corrosion and wear resistance, reducing the number of biologically active particles released (Lappalainen et al. 2005; Sonntag et al. 2012). As well as a better wear performance the tibia and talar components are able to keep their bulk titanium properties, a Young's modulus much closer to that of bone. This in itself has the potential to be highly beneficial to this design as it should reduce the bone remodelling effects of stress shielding, hopefully reducing the osteolysis surrounding the fixation geometry. The positive attributes of a titanium nitride coated biological device have to compete with the negatives such as the high rate of fretting corrosion should the surface be infiltrated by any 3rd body particles (Sonntag et al. 2012). Such problems are hypothesised to generate stresses under the surface of the coating which has seen it delaminate from the titanium because of its brittle nature, this can affect the failure rate (Teresa Raimondi et al. 2000). Published results from titanium coatings have been varied

with some *in-vitro* studies producing lower wear rates but clinically wear rates have been higher with thin Titanium Nitride layers (Pappas et al. 1995). The measured surface roughness for such a coating was greater than that of the cobalt chromium alternative for both a pin and TAR (Kamali et al. 2005; Bell et al. 2007). Historically surface roughness has been correlated with the level of polyethylene wear (Pappas et al. 1995; Kamali et al. 2005; Bell et al. 2007). Kamali et al. (2005) tested a thicker TiN coating that that discussed clinically against UHMWPE in a multidirectional pin on plate test and the wear factor was not statistically different from that of cobalt chromium. The surface was deliberately scratched and the material hardness of the TiN meant the PE wear produced was significantly less for than the CoCr counterpart.

The titanium nitride tibial and talar components are separated by a polyethylene component. For the Zenith this is specifically GUR1050, which has a very high molecular weight of around 7.3×10^6 g/ml (Endo et al. 2002). UHMWPE has had a long successful history in joint replacement due to its simple structure, biocompatibility and wear resistance (Kurtz 2009). There have been some recent material advancements, introducing improved wear properties through crosslinking, however, conventional polyethylene seems to still be the preferred insert material selection for both knee and ankle replacement. Cross-linking has seen great success in total hip replacement as it greatly improves wear resistance but alongside this the material toughness is reduced (Kurtz et al. 2011). The high stresses in the ankle mean this could prove problematic. To the authors knowledge only the Zimmer TAR specify the use of crosslinked polyethylene.

1.6 Volumetric wear analysis in joint replacement

No matter what joint replacement is undergoing tribology testing in a simulator there is a need to quantify the wear effects of the components to understand its performance potential *in-vivo*. Wear of UHMWPE has historically been quantified in at least one of three ways:

- a) Measuring the dimensional changes
- b) Weighing the test specimen
- c) Weighing the debris produced in the lubricant

Each of these methods have their individual complications when trying to isolate the volumetric wear loss from factors such as creep and fluid absorption (McKellop et al. 1978).

1.6.1 Gravimetric wear measurement

To assess the wear of prostheses the ISO standard endorses gravimetric measurement (ISO14242-2 2016). This technique involves measuring the change in weight of the implant by weighing it before and after undergoing a wear simulation, and using the material density to calculate a volumetric wear loss (Affatato et al. 2013). In order to get the most reliable measurements ISO-14242 stipulates resting in a temperature and humidity controlled environment are required for 48 hours to ensure dimensional and fluid stability. Highest resolution balances are also beneficial in order to achieve the desired repeatability. All current wear studies use gravimetric wear assessment techniques although often in combination with alternatives. This method, although considered the gold standard in wear assessment, is only applicable to *in-vitro* implant studies and ignores the geometric implications of the wear process (Tuke et al. 2010; Affatato et al. 2013). The opinion is split in recent publications, with O'Brien et al. (2013) continuing to use a gravimetric method to validate their computational wear model and Blunt et al. (2009) are trying to discourage the reliance on it. Due to the low wear volumes, especially with the improved UHMWPE wear properties through crosslinking and very low wearing ceramics the change in weight due to wear will be so small the procedure is much more sensitive. Adhesive wear causing the transfer of material from the polyethylene to the metal components and the level of fluid absorption reduce the precision with which weight measurements dictate the wear (Blunt et al. 2009). Use of soak controls and correction factors are required to overcome gravimetric limitations, compensating for the effect of the attachment of proteins from the bovine serum lubricant and creep effects (Tuke et al. 2010). Ideally a method which excludes this variable and is inclusive of retrievals would be preferable.

1.6.2 Geometric methods

A number of geometrical methods for surface wear assessment have been developed. In its most simple form, the maximum penetration can be determined using a linear measurement device such as a mercer dial gauge. In this case the

minimum thickness is subtracted from the bearing thickness prior to insertion (Kendrick et al. 2010). This method is highly simplistic and can only be used in a comparative way either before and after simulation or between numerous retrievals of the same design and size.

1.6.3 Coordinate Measurement

For decades numerous centres have investigated the use of the co-ordinate measurement machine (CMM) in order to build a profile of the worn body and quantify volumetric wear (Derbyshire et al. 1994; Muratoglu et al. 2003; Blunt et al. 2009; O'Brien et al. 2013). The CMM is described as a "Cartesian robot" which combines a contact probe and a three dimensional digitiser (Affatato et al. 2013). The probe can be used to take many sequential co-ordinates across the surface of the implant, the denser the population of points the more accurate the profile of the wear scar will be, however, this is a time consuming process (Bills et al. 2005; O'Brien et al. 2013). Muratoglu et al. (2003) took approximately 7300 data points across the surface of a total knee replacement insert; equally spaced at 0.75mm in an anterior-posterior and medial-lateral direction to create the best surface profile (Figure 1.18). Blunt et al. (2008) specified that to be an applicable tool for three-dimensional wear assessment of a worn joint replacement device the CMM used requires a typical accuracy of 2 μ m. Both contact and optical CMM technology has been employed in an attempt to measure wear (Blunt et al. 2008; Tuke et al. 2010).

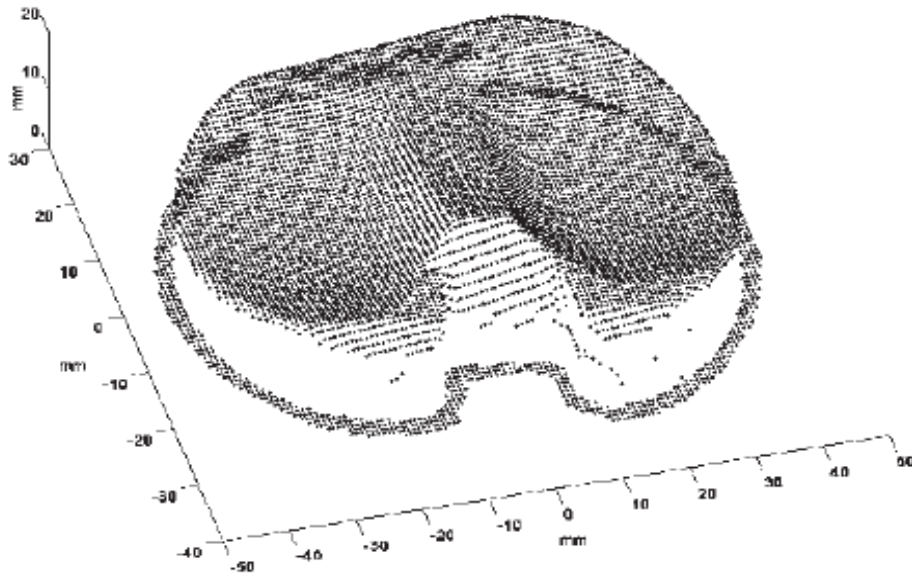


Figure 1.18 Points collected during surface digitization with the coordinate measuring machine of one of the tibial inserts Reprinted from Clin Orthop Relat Res, 410, Muratoglu et al. (2003), Metrology to quantify wear and creep of polyethylene tibial knee insert, pp155-164

One of the problems with characterising the surfaces of total joint replacement bearings, such as ankle implants, is their free form geometry, meaning they have no rotational symmetry or in some cases no symmetry at all. This reduces the number of reference planes making calibration difficult (Charlton et al. 2008). As a result Blunt et al. (2008) assumed the typical CAD–CMM manipulation would potentially lead to error. Instead their preferred method involved comparing the direct ASCII plain co-ordinates from both bearing surfaces using a surface interpretational software such as Talymap 3D (Taylor Hobson). Providing the surfaces are accurately aligned one can be ‘subtracted’ from the other to define a volume difference as demonstrated in Figure 1.19 (Muratoglu et al. 2003; Blunt et al. 2008). Blunt et al. (2008) reported a detailed methodology to quantify the wear which involves calculating the vertical z-shift; the vertical distance between the reference and the wear interval. This will define the linear penetration at each measured point. From this an average z-shift can be calculated for the bearing. Dividing this average by the measured area and multiplying it by the perpendicular cross sectional area should result in the volumetric wear (Muratoglu et al. 2003). The main difficulty with this method is the need for a pre-worn reference. For *in-vitro* wear studies this is simple as the surface of the implant can be assessed before

testing begins (Blunt et al. 2008). However, in the case of retrievals it is impossible to gain the information from the specific polyethylene insert.

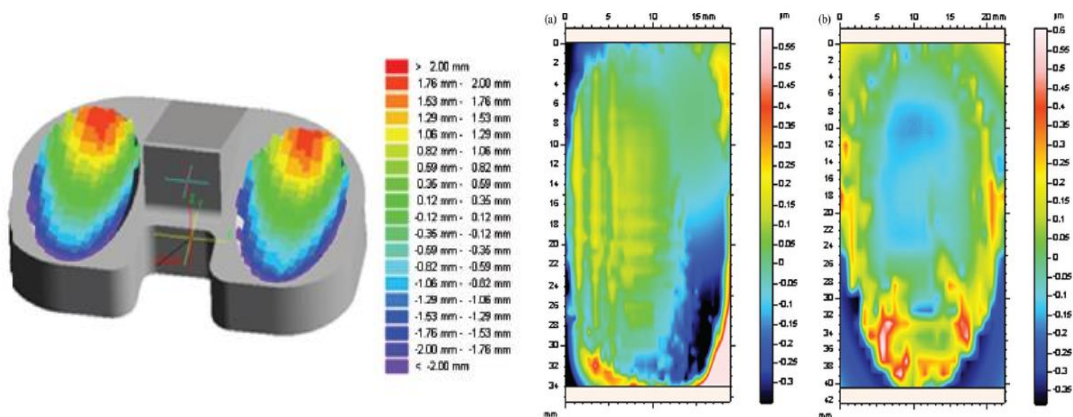


Figure 1.19 Profile of the meniscus found by CMM measurements compared to the profile with form removed. Image edited from Proc. Inst. Mech. Eng. H J. Eng. Med 222(3) .Blunt et al. (2008) Improvement in the assessment of wear of total knee replacements using coordinate-measuring machine techniques [Open Access]

With total hip replacements taking CMM readings from the unworn areas of the bearing surface is a viable method of creating a pre-wear surface however the knee insert was deemed too complex to create an original surface representation. Instead, using new polyethylene inserts of the same design is currently the best method of comparison (Blunt et al. 2008). It is still advised that an untouched surface of the tested bearing be used as a second reference plane along with the work surface for profile matching purposes (Bills et al. 2005). Knowlton et al. (2012) have since developed a method to estimate wear volume from retrieval knee inserts without the need for an unworn reference surface. High resolution optical CMM measurements were taken from the retrieval surface and curves were fitted to the unworn surface to define the unworn surface. From applying the technique to simulation components with known wear loss the authors found the error of this methodology to be less than 5mm^3 . Such accuracy could be considered reasonable having been implanted for many years but after just a short implantation time or 1Mc this error would not be acceptable.

When using this type of analysis creep must not be forgotten as it is assumed to account for 15-30% of polyethylene “wear” for knees having been *in-vivo* and this has been presumed to be similar for other total joint replacements with polymer bearings. The samples should be allowed a visco-relaxation period of at least 72

hours to ensure the majority of recoverable creep has had a chance to recuperate (Blunt et al. 2008). When carrying out an *in-vitro* simulator test the creep can be accounted for by taking measurements every million cycles for the test period. This is a viable solution to measure creep as it typically reaches a steady state after just one million cycles whereas the wear will be continuous throughout (Muratoglu et al. 2003). If this is not possible, as with retrieval testing, the non-recoverable creep percentage should be removed from the total wear volume reading in order to obtain a realistic polyethylene particulate wear reading.

Due to the highly conforming nature of the TAR insert the whole component will experience the effects of creep. The creep effects are known to reach a steady state after one million cycles (Estok et al. 2005), however, there would be no unworn surface to realign the post-test surface with that measured pre-test.

1.6.4 Micro computed tomography measurements

The application of micro computed tomography (μ CT) within biomedical engineering has been expanding. One development has been its use in the assessment of retrievals, especially the tibial insert of the knee (Teeter et al. 2011). This methodology could be applied to both implants retrieved from the body and those tested *in-vitro*. When measuring *in-vitro* wear volume the polyethylene insert may be scanned before, after and even during the desired cycle so long as the return of creep deformation has been allowed for. A direct comparison can be made between the surface morphology and a wear volume calculated through computational simulation of the recorded data. In comparing new and simulator tested components there was no significant difference between the wear rate compared to the gravimetric measurement and the between scan precision was 0.07% (Teeter et al. 2011). For cases of retrievals attempts have been made to use the unworn areas of the implant to generate a pre-operation profile but this had limited success. Another method of sourcing a model of a pre-surgery insert involves microCT scanning unused meniscal components of the same size and design (Teeter et al. 2011). The report on this method of creating a reference surface found that taking an average from a number, preferably as many as six, polyethylene inserts would reduce the error due to machining variations to an acceptable level. However, this method would only be practical if focusing on one

design of one size otherwise costs would escalate. Once a reference plane is obtained the profile from the retrieved bearing can be compared in order to find a good approximation of the volumetric wear. Use of μ CT technology is highly dependent on the resolution. Confidence in the results would be dependent on scanning parameters but Teeter et al. (2011) have indicated microCT may be a fast method of displaying the wear regions.

1.6.5 Measurement summary

Gravimetric wear measurement is a long established relatively reliable method but a geometric method of wear assessment is considered a “powerful tool” specifically when combined with an *in-vitro* wear model. Using CMM wear analysis provides a plateau for calculating linear and volumetric creep and wear for individual components. However, some of the high accuracy of this method for *in-vitro* testing will be lost for explanted bearings due to the information used to approximate the geometry of the un-deformed bearing (Muratoglu et al. 2003). In some cases the resolution of the machine will not be sufficient to compensate for the measurement errors. Spinelli et al. (2009) found the CMM method to systematically overestimate the wear highlighting the importance of the choice of the “time scale for creep evaluation”. There is generally very little information available on previous studies exploring the wear of TAR. Any studies which do consider ankle wear typically rely on gravimetric methods to quantify the volumetric loss (Affatato et al. 2007; Bell et al. 2007; Postak et al. 2008; Bischoff et al. 2015; Reinders et al. 2015).

Until a reliable high-resolution solution is developed the available techniques, similar to those described, will continue to be adapted for use with TAR just as they have for hip and knees retrievals previously. Ensuring the combination of volumetric wear, surface roughness and wear patterns are investigated in some capacity provides the important wider picture of what is happening under tribological testing.

1.7 Surface metrology

Surface metrology is defined as; “the science of measuring small scale geometrical features on a surface” (Jiang et al. 2007)

There are many different mathematical calculations which can define the metrology of a surface. These are either categorised as amplitude, spacing or hybrid parameters, as they depend on the vertical, horizontal or a combination of both profile characteristics respectively (Gadelmawla et al. 2002). The most widely used roughness parameter is the arithmetic average height, R_a (Akagi et al. 2007; Flannery et al. 2008). This is a two dimensional measurement summarising the “average absolute derivation of roughness irregularities from the mean line over one sampling length” (Figure 1.20). Alongside R_a there are various other commonly used terms, ranging from peak heights, R_p , troughs, R_v , and the sum of both R_{max} , to calculations such as skewness defining the sample symmetry and kurtosis explaining the profile sharpness in terms of the sample length (Gadelmawla et al. 2002). With so many options of parameters to define it is important the correct choice is made as some roughness estimates are more sensitive to the extreme peaks and troughs than others.

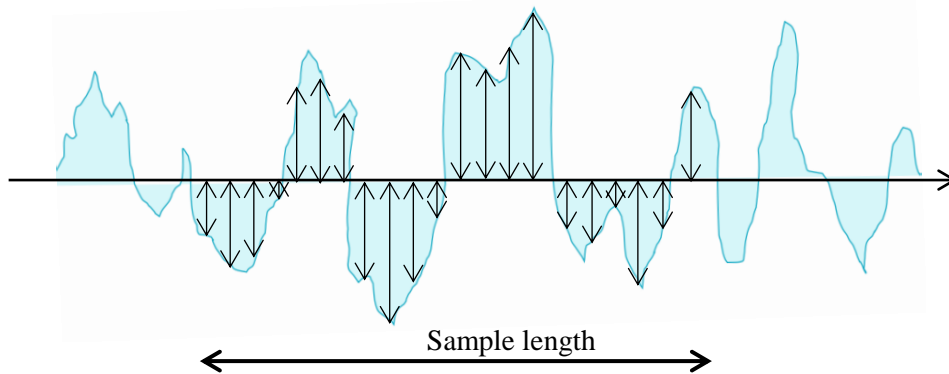


Figure 1.20 Arithmetic roughness, R_a is the mean deviation from the mean line

There is a selection of three dimensional parameters (areal roughness), with the prefix S , which as technology advances are becoming the preferred way to present surface measurements. Rather than relying on one profile which may not be an appropriate assumption for the whole surface they summarise an area. However, it is important to remember the recorded results can only be as accurate as the method used (Jiang et al. 1999).

1.7.1 Methods of Quantifying Surface Metrology

There is an extensive range of apparatus available designed for the purpose of measuring different properties of a surface to varying degrees of accuracy. Although the resolutions may have improved over the last decade, Figure 1.21 published by Myshkin et al. (2003) still outlines the measurement options available and gives an idea of the applicability. Scanning electron microscopy (SEM), optical and stylus methods all have the capability of measuring similar surface heights but the spacing which can be captured relative to roughness and form is variable. Both stylus and optical methods have proven valuable aids for explaining the development of wear during tribological investigation of joint replacement (Tuke et al. 2010).

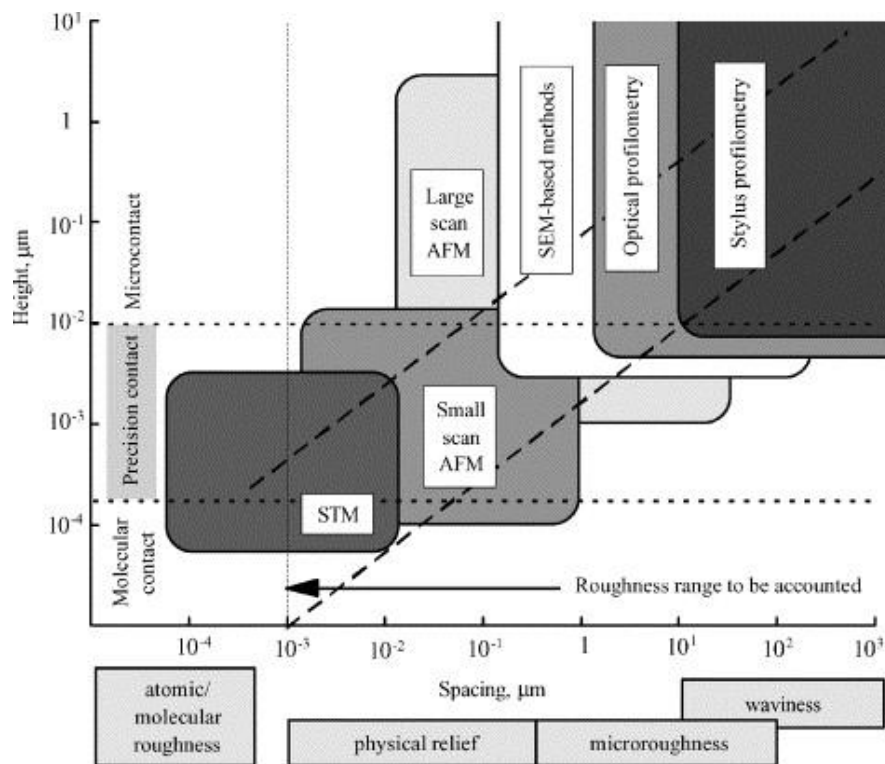


Figure 1.21 Resolution of measurement methods. Reprinted from Wear 254(10), Myshkin et al. (2003), Surface roughness and texture analysis in microscale with permission from Elsevier.

1.7.2 Contact Measurement

The most well established instrument for assessing a bearing surface profile is the stylus method (Atkinson et al. 1985). The stylus takes traces along the surface in question and from this highly accurate profile the surface roughness can then be

found manipulating the data to remove the form and waviness. For a new total joint replacement this can be on the nanometre scale so the resolution of the device must be sufficient to facilitate accurate measurement (Jiang et al. 1999). The surface, before it undergoes any articulations, will be dependent on the manufacturing process, whether it has been moulded or machined, however, this does not necessarily dictate the wear properties after it has been put to use (Benson et al. 2001). The roughness can be characterised in two dimensions or three. In two dimensions the profilometry of a total knee replacement is typically taken across a number of discrete locations along the wear scars on the femoral and tibial components (Flannery et al. 2008), with Brockett et al. (2012) specifying six. Ideally two of these profiles should be in the medial lateral directions and the other two perpendicular, travelling anterior to posterior. These profiles can be averaged across components and the R_a , R_p , R_v and R_{sk} of the surface, as previously defined can be established (Flannery et al. 2008). Like any measurement technique importance is placed on the repeatability of the readings to ensure the precision of the methodology. The choice of Gaussian cut-off which separates roughness from waviness will depend on the nature of the surface topography, changing with different materials. This choice should be made based on existing standards and combined with a 100:1 bandwidth and then fitted to a least squares arc or line depending on the profile shape is the preferred method to obtain the surface topography accurately (Brockett et al. 2012).

Three dimensional analysis is increasingly considered a more accurate method than the 2D profilometry (Jiang et al. 1999). In three dimensions both amplitude and special parameters can be defined to enable the device take a large number of equally spaced traces across the surface. This is a time consuming process, taking hours to cover a substantial area, with a small range in measurable height and the shape is restricted to a rectangular area (Mathia et al. 2011). There are problems with extending the typical data analysis method to 3D. The Gaussian filters could still be used but the residual surfaces are averaged, the effectiveness is reduced and surface defects are still included in the investigated surface despite the fact they are not components of roughness (Jiang et al. 1999). The additional time required for both data collection and analysis is often a deterrent for 3D surface profiling.

There are also cases where a contact measurement method may damage the material surface in which case it should be avoided.

1.7.3 Non-Contact Measurement

Non-contact analysis is typically used because of the speed at which an area can be visualised and without any surface damage. The most basic method of contactless wear measurement is photographic image analysis as explored by Puloski et al. (2001) investigating the wear on the tibial post. This method is a useful observational analysis to consider the component variability in terms of geometry but is not a quantitative method. More technical approaches are available which can provide more informative data about the surface texture.

Optical technology provides a good platform for non-contact surface analysis. Similar to contact measurements, in order to correctly interpret the readings a distinction between waviness and roughness characteristics must be realised through filtering (Kurtz et al. 2002). This is often seen as a preferable tool to contact methods due to the speed at which data can be collected across a relatively large area and the lack of contact means no surface damage will occur (Stout et al. 1995). One of the more widely used non-contact measurement technologies is white light interferometry. Interferometric devices typically use the emission of white light to map the discontinuity of the surface topography by recoding the change in two rays of light, of equal wavelength, out of phase, set up as shown in Figure 1.22 (Mathia et al. 2011). Limited success for total joint replacement assessment has been gained from white light interferometry, largely due to the curvature of many joint replacement articulating surfaces (Tuke et al. 2010). However, combining interferometry and microscopy has been found to produce better results. The addition of the microscope improved the possible measurement resolution, a limitation of the vertical scanning interferometer (VSI) (Mathia et al. 2011).

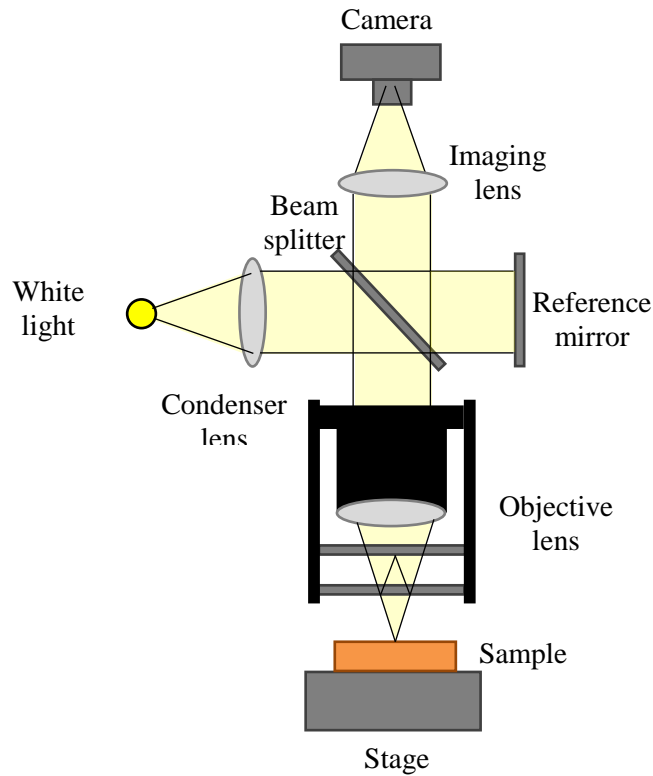


Figure 1.22 Simplified design of a white light interferometry microscope

The scan area size depends on the choice of objective lens. A compromise must be made between getting the best fringes and the largest area. The individual areas scanned can be knitted together to form a computational representation of the roughness of the whole surface. However, when applied over a large area this has been reported to generate high levels of error and distortion the real surface. Even if this is done correctly this method has its limitations. The shininess of a metallic surface reflects the light effectively but surfaces with limited reflectivity absorb a substantial amount of the incident ray into the material, reducing the quality of the signal returned. As a result it is a struggle to accurately define the surface of transparent or semi-transparent materials (Mathia et al. 2011). A small number of authors have used white light interferometry for analysing joint replacement wear. Kim et al. (2005) used white light interferometry to assess the surface topography of 15 retrieved ceramic femoral heads with both 20x and 40x lenses. Six, sub millimetre area measurements were taken from a variety of the most visibly damaged areas and those which appeared untouched. The two dimensional parameters, R_a and R_{pm} were used to represent the surface roughness. DesJardins et al. (2008) similarly measured four small samples of knee tibial and femoral

condyles using a non-contact method at 25x magnification recording a variety of two dimensional parameters from the three-dimensional data. More recently Scholes et al. (2013) have also employed the use of an optical profiler for knee retrievals with an x25 magnification. The parameters recorded in this case were three dimensional, areal parameters, the root mean squared S_q and the skewness S_{sk} . No information has been provided about the waviness and form filtering parameters used by any of the authors and currently there is no standard to apply.

Infinite focus microscopy is another alternative to white light interferometry. This produces morphological surface information using optical microscopy in combination with focus variation technology. Its measurement application relating to joint replacement has thus far been limited, mainly focused around corrosion. Publications document its suitability for imaging taper corrosion and providing surface form profiles (Cook et al. 2013; Gührs et al. 2015) as well as providing quantitative surface data and profiles from a TKR retrieval insert (Liza et al. 2011).

SEM testing can provide a good observation tool to further magnify features seen on the surface measurements so they can be analysed in greater detail (Liza et al. 2011). This technology provides a much more comprehensive idea about the wear mechanisms. The nature of SEM tests allow them to draw attention to any metal debris embedded in the polyethylene insert which could indicate potential third body wear mechanisms. SEM also has the ability to highlight any signs of the formation of biotribofilms which provides further insight into the functionality of the implant in its biological setting. SEM, unlike some of the other technologies discussed, is equally helpful whether analysing an implant which has been tested *in-vitro* or has come after retrieval from a patient and has the ability to be very insightful. In joint replacement SEM technology is most commonly used to quantify the wear debris size and morphology (Maloney et al. 1995).

1.7.4 Metrology Summary

There are weaknesses of stylus measurements. The stylus size can limit the ability to catch fine surface details and the contact risks damaging the surface and the relevance of a number of single line traces to the surface topography. A further limitation is their time-consuming nature, especially in three dimensions. As a result Mathia et al. (2011) believe the focus of surface measurement is shifting towards the optical methodologies which, despite some limitations, are proving to be able to measure roughness quickly and accurately while removing the risk of causing surface damage. The resolution of optical metrology devices has the potential to be much higher than standard contact measurements and are inherently three dimensional. However, its applicability to curved surfaces and the computing power required to process data generated from large areas is a limitation. However obtaining meaningful data through post processing is a challenge for both measurement technologies.

As trends in surface metrology develop, moving away from stylus measurement and towards optical methods the modes of analysing surface wear in joint replacement will undoubtedly develop.

1.8 Retrieval analysis

Retrieval analysis provides an important investigative tool to understanding potential causes of failure and *in-vivo* mechanics. Surface damage of total joint replacement results in wear debris and can lead to complications which reduce the life expectancy of the implant (Hood et al. 1983). Due to the lack of literature available for TAR, literature for total knee replacement has been explored. Various authors have investigated the surfaces of TKRs after they have been in action in the body or simulator. The studies vary in terms of number of samples and variety of implant manufacturer but the experimental approach remains relatively similar.

1.8.1 Surface Wear Characteristics

In 1983 Hood et al. defined the visible wear characteristics which should be assessed on the polyethylene component as listed below (Table 1.4). He also suggested a method of segmenting the insert surface into 10 sections (Figure 1.23) in order to define which wear features occur across the surface and scoring the wear severity accordingly. This historic assessment has had little advancement.

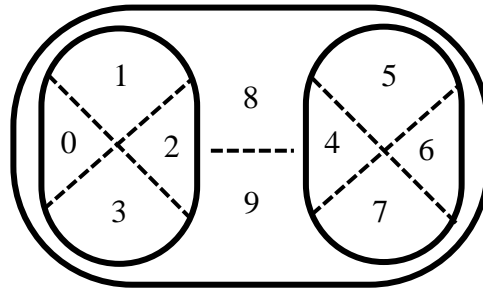


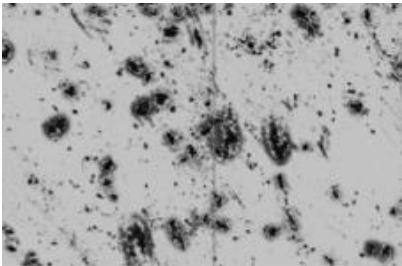
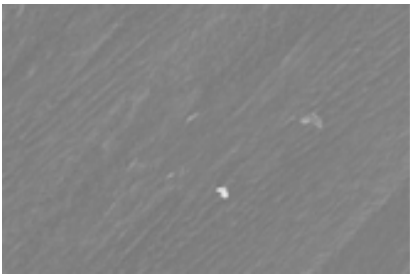
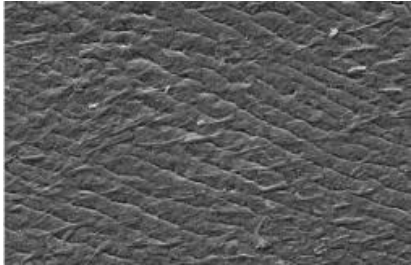
Figure 1.23 Sectioned tibial component (Hood et al. 1983)

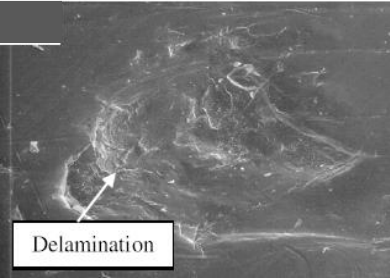
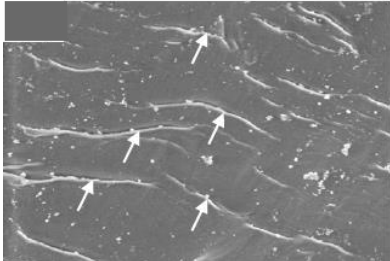
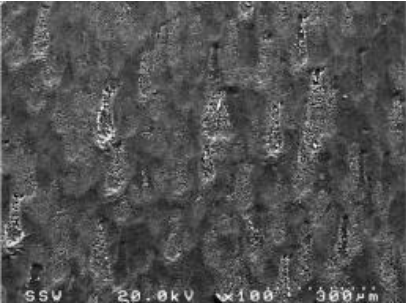
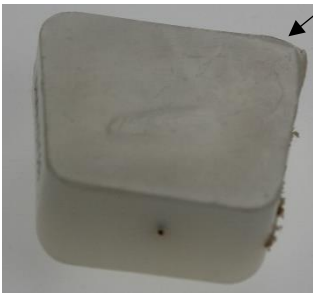
More recently Liza et al. (2011) used a similar approach and found delamination to be the most visually apparent damage in the single retrieved total knee replacement the authors assessed. Scratching, folding, pitting and 3rd body particles were also observed.

Delamination is underpinned by the adhesive and abrasive wear mechanisms compromising the integrity of sub-superficial layers of the UHMWPE. The compromised depth is dependent on the loading and the material properties on a microstructural level. The abrasive impact at the grain boundaries and application of high stresses can result in micro cracks under the surface. These cracks propagate as the deformation continuing until they reach a critical length at which point they tend to the surface detaching the delaminated region. High stresses and small contact areas due to minimal conformity are largely responsible for delamination, however, reduced material properties as a result of oxidation have historically had great impact. Improvements to the sterilisation process have seen reduction in the incidences of delamination (Affatato et al. 2013).

Pitting is assumed to result in the release of a large volume of UHMWPE debris which could be the cause of an immune reaction (Hood et al. 1983). Free particles are another problem, these can get trapped between the articulating surfaces, scratching in the anterior posterior direction often ending up imbedded at the end of the trace of the scratch (Hood et al. 1983; Malikian et al. 2014). Each of these features (Table 1.4), are visibly identifiable on a magnified surface of a retrieval.

Table 1.4 Polyethylene worn surface characteristics as described by Hood et al. (1983)

| Characteristic | Visual Description | Image |
|---|--|--|
| Pitting | Irregularly shaped depressions in the UHMWPE surface |  <p data-bbox="959 629 1362 667">NPFLEX image from retrieval</p> |
| Embedded particles | A change in colour on the SEM or texture is likely to be a PMMA or metal particle embedded in the insert surface |  |
| <p data-bbox="312 925 922 1048">Reprinted from Wear 154 (3) UHMWPE wear against roughened oxidized zirconium and CoCr femoral knee components during force controlled simulation pp245-256 with permission from Elsevier.</p> | | <p data-bbox="1070 965 1382 1003">(DesJardins et al. 2008)</p> |
| Scratching | Indented lines causing material removal. Typically parallel to each other in an anterior posterior direction in the regions of high wear and referred to as striations |  <p data-bbox="943 1357 1342 1395">NPFLEX image from retrieval</p> |
| Burnishing | Areas of the surface which have been highly polished over the time <i>in-vivo</i> characterised by shallow multidirectional surface ripples |  |
| <p data-bbox="312 1693 922 1816">Reprinted from The Knee 19 (4) Retrieval analysis of modular total knee replacements: Factors influencing backside surface damage. Pp306-315 with permission from Elsevier.</p> | | <p data-bbox="943 1715 1198 1753">(Brandt et al. 2012)</p> |

| | | |
|--|--|--|
| Delamination | The removal of sheets of UHMWPE |  <p style="text-align: right;">(Liza et al. 2011)</p> |
| <p>Reprinted from Eng Fail Anal 18 (6) Failure analysis of retrieved UHMWPE tibial insert in total knee replacement Pp1415-1423 with permission from Elsevier.</p> | | |
| Folding | A result of 3 rd body wear particles between articulations and often seen alongside scratches (Chang et al. 2007) |  <p style="text-align: right;">(Liza et al. 2011)</p> |
| Abrasion | A visible “shredded or tufted appearance” to the surface |  <p style="text-align: right;">(Brandt et al. 2012)</p> |
| Surface deformation | Any permanent deviation from the initial shape likely to be caused by creep |  <p style="text-align: right;">Photograph of edge loaded retrieval</p> |

Knowlton et al. (2016) combined their method of quantifying volume loss as an estimation for wear from retrievals with the visible damage mode (Figure 1.24). The authors found that aside from delamination the damage modes were only a moderate predictor of wear volume.

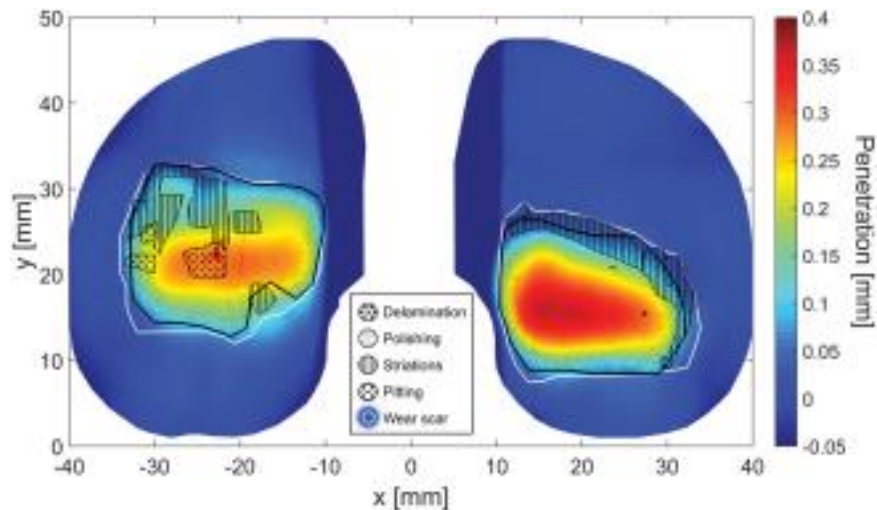


Figure 1.24 Surface damage compared to volumetric wear. Image reprinted from J Biomed Mater Res B Appl Biomater. Knowlton et al. (2016). Relationship of surface damage appearance and volumetric wear in retrieved TKR polyethylene liners.

Affatato et al. (2009) also carried out a small investigation comparing the wear of a TAR tested *in-vitro* in a knee simulator to three retrievals. SEM analysis showed similar wear patterns on both tested and retrieved inserts, but with scratching and pitting found to be more prevalent in the retrieved bearing. The wear for all worn polyethylene inserts was measured using the CMM and compared to the relevant nominal CAD models aligned using the unworn areas. The authors indicated this method of analysis was appropriate for quantifying the linear penetration of the *in-vivo* wear, ranging from 0.025 to 0.091 mm. This range was expected to be relatively large due to the small number of samples, just 3 and the varying implanted time. This CMM method may be a viable basis for the retrieval wear assessments however as previously discussed, the component variability should be accounted for where possible.

In a primitive analysis of a cohort of ten semi constrained DePuy Agility TARs Besse et al. (2009) unsurprisingly found polyethylene abrasive wear in the region in which the talar component was in contact with it. Pitting, and a talar footprint were observed on all of the tibial liners. While scratching was observed on over half of all of the constituent components. Another study by Cottrino et al. (2016) considered ten mobile bearing Biomet AES retrievals. Their observations from the articulating surfaces included prominent talar component scratches in the direction of flexion/extension as well as scratches on the UHMWPE articulating surface

both of which signified presence of third body particles. On the flat surface scratches measuring 100 μ m wide and 11 μ m were measured. Samples from the surrounding tissue were analysed for wear debris but the authors focused heavily on that relating to the coating surface as opposed to the UHMWPE which is a failure of this particular design rather than ankle replacements on the whole.

1.9 Summary

The ankle joint is complex and the understanding of it is limited. Discoveries are still being made about basic anatomy yet ankle replacement has been tried for almost 50 years. The demand for end stage treatment for ankle arthritis is expected to rise in coming decades and there is potential that a younger population will be affected. Fusion is often considered to be the gold standard treatment however the adjacent joint degeneration is less than ideal. TAR has the potential to restore the joint mobility but across the marketed ankle replacements there is very little consensus on the best design features and the success rates are highly variable. Aseptic loosening is the greatest cause of TAR revision. Alongside this, technical error and polyethylene wear appear to play significant roles in device failure.

Understanding of tribology has been considered extensively in hip and knee replacements with basic wear testing a requirement before any device reaches the market. Conversely, the use of wear simulation for ankle replacements is limited to articles from just five centres assessing six TAR devices and the effect of biomechanical, surgical and patient variables has received little attention. There are established wear measurement methods and metrology approaches. While retrieval analysis of ankle replacements has been limited surface identifiers for different polyethylene wear mechanisms have been clearly defined. The use of retrievals can help inform laboratory research to ensure the in-vitro wear simulation is producing outcomes relevant to the clinical environment which is especially important considering available literature surrounding the ankle gait cycle is both limited and dated.

Investigating preclinical testing of TARs has highlighted how far behind the curve they are and has highlighted a space for further investigation and increase in understanding.

1.10 Project rationale

With an ever aging, active population the demands placed upon our bodies are continually increasing and all the while our expectations for our future quality of life remain high. For a substantial proportion of the population surgical intervention will be necessary for this to be achievable.

Joint replacements have been carried out successfully since the 1960's, eliminating pain and restoring a natural range of motion to the affected joint. Hip replacements are considered to be one of the most successful operations. However, as a result of such a reputation, expectations after joint replacements have been heightened due to the long-term success from both hip and knee replacements. Of the data recorded by the national joint registry between 2003 and the end of 2015 the numbers of primary implanted hips and knees reached over 800,000 whereas for ankle replacements this number was just greater than 3100. Year on year the number of hip and knees implanted in England and Wales increases with the exception of 2015. The numbers of ankle replacements reported fluctuates between 500 and 600 with no obvious trend. Total ankle replacements are considered to be a cost-effective treatment option for the right patient yet instead fusion is maintaining its position as the gold standard treatment of ankle arthritis despite the resulting degeneration of surrounding joints.

The low numbers of TARs in the UK does not reflect the estimated 1% of the population suffering from ankle osteoarthritis (Barg et al. 2013). Goldberg et al. (2012) estimates that the UK sees 29,000 referrals for ankle arthritis annually yet despite the potential demand the relative number of ankle replacements is minor. It is anticipated that the demand for treatments for end stage ankle arthritis will increase for future generations. Typically ankle osteoarthritis is a secondary cause of joint degeneration, a result of pathological disorders such as haemophilia or dysplasia and injury (Saltzman et al. 2005). Recurrent ankle instability and sprains alongside fracture were responsible the majority of the posttraumatic cases. Allegra & El Boustany (2016) claim ankle trauma accounts for 12-15% of sports injuries. Given the current popularity of trends such as a long distance running or for wearing high heeled shoes the prevalence of ankle arthritis may rise further as both have be associated with repeated ankle sprains which leads to the onset of

posttraumatic osteoarthritis. Typically post-traumatic arthritis is associated with a younger subset of the population (Barg et al. 2013) so as this generation gets older it is vital there is a successful motion preserving alternative treatment available.

New designs have recently been released to market by a number of orthopaedic companies including, Integra Life Science Services SAS, Wright Medical and Ortho Solutions. Some of these devices even rely on the historical talar geometric convention which has since been disproved. However, none of these devices require the same vigorous preclinical testing as the equivalent designs for hips and knees.

A renewed interest in basic understanding of the ankle joint anatomy has resulted in more considered TAR development from basic principles (Siegler et al. 2014; Belvedere et al. 2017). Greater anatomical accuracy has the potential to see these devices last longer as the transmission of stress should be improved. The early failure of total ankle replacements has meant few make it to the point where wear debris mediated osteolysis may become a cause of failure. The longer new designs last the more important the wear characteristics become. With rising demand for ankle intervention in a younger patient demographic, other orthopaedic companies may also seek to redevelop their products. If this market is to grow successfully and benefit patients more stringent preclinical testing is critical to distinguish between these designs.

The value of preclinical wear testing has shown both strengths and weaknesses through decades of development in hip and knee replacement. The importance of considering conditions beyond the perfect placement has been established. It is taken seriously when designing new devices and many companies are choosing to go beyond compliance and standard tests in order to understand the implications under sub-optimal positioning and for larger patient demographics which may be critical to the device success. There have been a few such considerations in TAR design.

1.11 Aims and objectives

The main aim of this study was to develop an experimental model to simulate the clinical performance of total ankle replacements (TARs). In collaboration with an industrial sponsor (Corin Group PLC) the primary aim was to develop experimental simulation methods to evaluate TARs in ways that better replicated *in-vivo* function. Given the imminent reclassification of TAR devices from class II to class III medical devices it is important simulation methods are developed and implemented in order to better understand these devices in their optimal and adverse conditions and with the potential to define an ISO standard.

The objectives included to:

1. Develop an experimental wear simulator method for the analysis of TAR, implementing an experimental set-up and constraints in order to replicate clinical conditions
2. Explore the effects of kinematics on the wear of a mobile bearing total ankle replacement
3. Investigate the stratified functional envelope for the alignment and positioning of TAR bearings and development of an experimental model for assessing the stability of TAR under a range of alignments and conditions
4. Draw on existing collection of TAR retrievals to produce clinically relevant malalignment conditions
5. Use the models generated to create a holistic model that will evaluate wear performance over test durations representative of several years of *in-vivo* use.

CHAPTER 2
METHOD DEVELOPMENT

CHAPTER 2

METHOD DEVELOPMENT

2.1 Introduction

In-vitro testing has previously proven to be a relatively good predictor of *in-vivo* wear in joint replacements providing the kinematic conditions mimic that of human gait. Wear simulation has been developed extensively for total hip replacement (THR) and total knee replacement (TKR) in order to represent the *in-vivo* condition as closely as possible and under a broader range of conditions and patient activities. Tribological simulation is thought to provide a useful tool to compare and analyse new material combinations or designs and define their functional envelope in order to ensure confidence in the potential clinical benefits for new devices (Affatato et al. 2008).

Knee simulators have been used successfully for total ankle replacement (TAR) wear testing over the last decade (Affatato et al. 2007; Bell et al. 2007; Bischoff et al. 2015; Reinders et al. 2015). In allowing six degrees of freedom the simulator can recreate ankle kinematics. In using a knee simulator rather than an ankle specific simulator the adoption of the test methods has potential for a wider reach.

This chapter aimed to use tribological testing of total ankle replacements (TARs), undertaken in a knee simulator, under different kinematic conditions to understand the critical parameters for physiologically relevant wear simulation. As knowledge surrounding ankle motions is limited it was important to understand the influence of input kinematics on the wear of a commonly implanted mobile bearing device.

2.2 Materials

As one of the most implanted TARs in the UK (NJR 2016) the Zenith TAR (Corin Group, Cirencester, UK) was tested throughout the simulator studies. These devices consist of two bulk titanium, titanium nitride coated components; one a dual condyle talus and the other a flat stemmed tibia. The metal components are separated by an unconstrained conventional ultrahigh molecular weight polyethylene (UHMWPE) insert, GUR 1050. One surface which conformed to that of the talus the other flat like the tibia. The fixation surfaces of the components

were uncoated for the purpose of fixturing. The most popular sized components were chosen for the simulator testing, size three of the available four. Despite the surgical option to up-size the tibial equivalent sized components were selected for testing. This is the most common combination and will also be the smallest clearance between the tibial and insert edges which may create a worst case scenario. The size three consisted of a talar component with a 26mm radius and maximum width of 33mm, the width matched that of the tibial component which was 37mm in length while the polyethylene insert was 31mm wide and 29.5mm in length. The thinnest polyethylene insert which has a minimum thickness of 5mm was selected to create the highest risk situation.

2.3 Simulator

Knee simulators have historically been used for *in-vitro* wear tests of TKR under testing a variety of conditions. The Leeds Knee Simulator I (KSI) was used in the initial investigation. This simulator has been used for over a decade of knee wear studies (Barnett et al. 2002; Brockett et al. 2011). KSI consists of six stations, divided into two groups of three (Figure 2.1). The load, rotation and displacement were all controlled pneumatically while the flexion was applied electromechanically. The stations are supplied with air in series within their banks of three so to achieve the best simulator replication of the input profiles the air flow must be balanced.

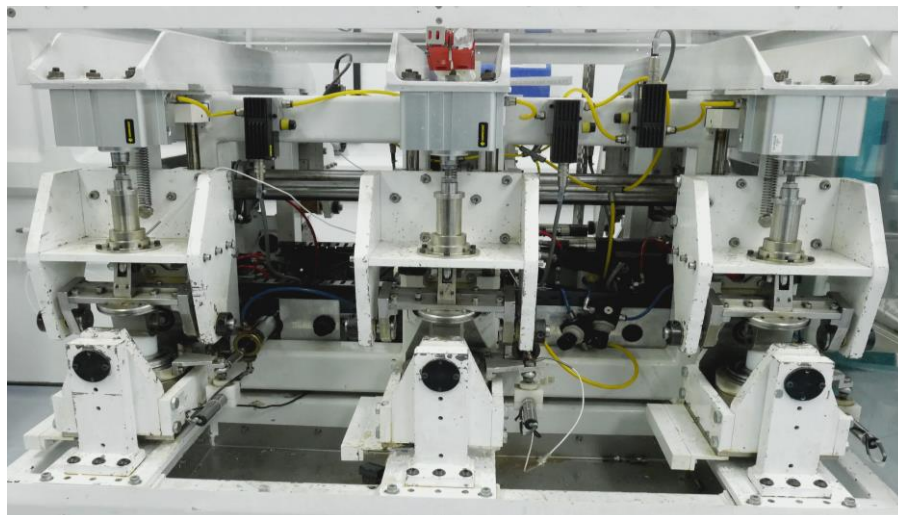


Figure 2.1 Leeds Knee Simulator I

Each individual station had six degrees of freedom, only four of which were controlled; axial load, flexion, rotation and anterior/posterior displacement. Through fixturing the medial lateral displacement was constrained and the adduction was allowed to move passively. Input profiles were defined from literature and applied with the controls listed in Table 2.1. Limitations within the existing ankle kinematic literature dictated the use of displacement controls as the forces at the tibiotalar articulation are not adequately documented. *In-vivo* the TAR is highly reliant on the surrounding soft tissues to provide constraint for the mobile bearing. As there were no such restraints in the simulator, displacement control provided these limits making it the preferable mode of simulation.

Table 2.1 Simulator Controls

| Input | Control |
|--------------------------------------|--------------|
| Axial Load (AF) | Force |
| Flexion/Extension (FE) | Displacement |
| Rotation (IER) | Displacement |
| Anterior/Posterior Displacement (AP) | Displacement |

The inherent direction of these motions within the simulator was an important factor to understand. The positive direction of these motions is highlighted in Figure 2.2.

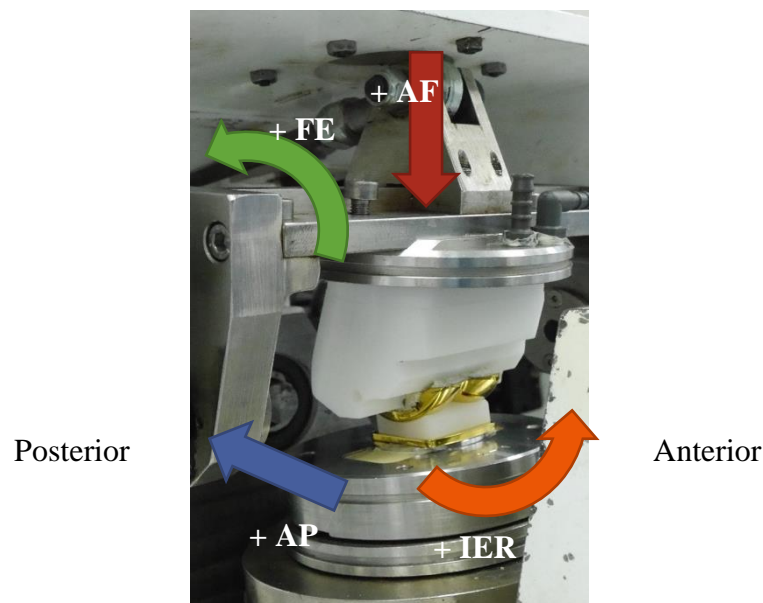


Figure 2.2 Positive simulator directions for FE, IER, AP and AF

2.3.1 Simulator kinetics and kinematics

The only guideline available for TAR is ASTM (2014) F2665 providing a standard specification for TAR. This standard highlighted the importance of understanding the wear performance but recommends pin on plate for new material combinations with a suggestion towards prosthesis wear simulation where this was not appropriate. Considering the variation in TAR designs, simple pin on plate tests were not deemed sufficient. As there were no standards in place for ankle gait inputs these had to be defined from the limited publications available assessing the motions at the natural ankle.

2.3.1.1 Force

Calculation of joint reaction force in the ankle is more complex than other joints due to the large number of bones and joints in the foot relating to the talus and the various ligamentous points of contact. The information required to define the load inputs is limited and has not been expanded upon in recent years.

To date it appears just six authors have presented original graphical representations of the loading in the ankle during the gait cycle. In each of these instances the force has been mathematically calculated in both two and three dimensions from the ground reaction experienced from individuals, taking into consideration various levels of acting muscle and tendon forces. Table 2.2 includes the maximum compressive forces these authors recorded.

Table 2.2 Maximum ankle compressive force during gait for healthy individuals as a multiple of body weight (BW)

| Author | Individuals tested | Mean age | Maximum Compressive Force (xBW) |
|-------------------------------------|--|----------|---------------------------------|
| Seireg & Arvikar (1975) | | | 5.2 |
| Stauffer et al. (1977) | 5 healthy males 9 disabling arthritis | 29 43 | 4.73 ~3 |
| Procter & Paul (1982) | 5 cadavers | | 3.9 |
| Simonsen et al. (1995) | 7 healthy males | 32 | 4.2 |
| Glitsch & Baumann (1997) | 1 healthy subject | 31 | 4-5 |
| Sharkey & Hamel (1998) | 1 healthy male | | 4.7 |

Authors Reinders et al. (2015) and Affatato et al. (2007) using the same inputs from an earlier computer model (Reggiani et al. 2006) both halved the peak force of the historical profile defined by Seireg & Arvikar (1975) to implement into their ankle simulators. The simulator was based on differences found between the hip and knee forces relative to more recent *in-vivo* measurements for joint replacements. *In-vivo* loads for TKRs have been measured using instrumented tibial components with peaks at a relatively low 2.2 x body weight (BW) (Zhao et al. 2007) compared to the Seireg & Arvikar (1975) mathematic calculation for the natural knee which predicts a peak force of three times that. Some of this variation may be the difference between natural joint and replacement forces. Stauffer et al. (1977) predicted a 30% decrease in ankle force with ankle replacements, however, due to advancements in TAR designs and improved fixation it is difficult to judge whether this difference would be of such magnitude for current postoperative patients. Brand et al. (1994) used similar instrumented technology in THR and found for one individual their mathematical models overestimated the peak force by 0.5 times body weight compared to the measured values, but the value was less than that of Seireg & Arvikar (1975). Bergmann et al. (1993) have defined the force profile for THR which has been widely adopted across wear simulation, the paper measures a peak force of 3-3.5 x BW for normal walking two thirds of the 5.2 prediction. There is much variation between measured forces in joint replacements and the mathematical calculations for the natural joint, however this relationship is not clear-cut. There is currently no evidence that ankle forces follow the same trends and without an instrumented prosthesis this will continue to be an unknown. Even if the force implemented is an overestimation this will potentially create a worse case simulation condition and will still be clinically relevant but for a heavier patient. The magnitude of the applied axial load would have greater implications in a force controlled simulator as it would alter the degree of rotation and displacement at the device.

The design of TARs aim to replicate the natural joint kinematics, however, across the devices currently in clinical use there are significant differences in design which will influence their ability to achieve this. In order to inform the best test standards for a range of TARs applying natural joint kinematics rather than those associated with joint replacement seems the most appropriate. To understand the

longevity of current TARs it is important that some of the more severe conditions are simulated.

Despite the variability relating to the maximum force at the ankle, there are many similarities across the force profile throughout the gait cycle. The general trend includes a steep increase in force from heel strike to approximately two times body weight at about 15% of the total gait cycle followed by a decrease in force at midstance. Coming out of this dip the force rises to its peak at 40-50% of gait at heel off and from there decreases to almost zero with toe off at around 64% where the swing phase begins (Figure 2.3).

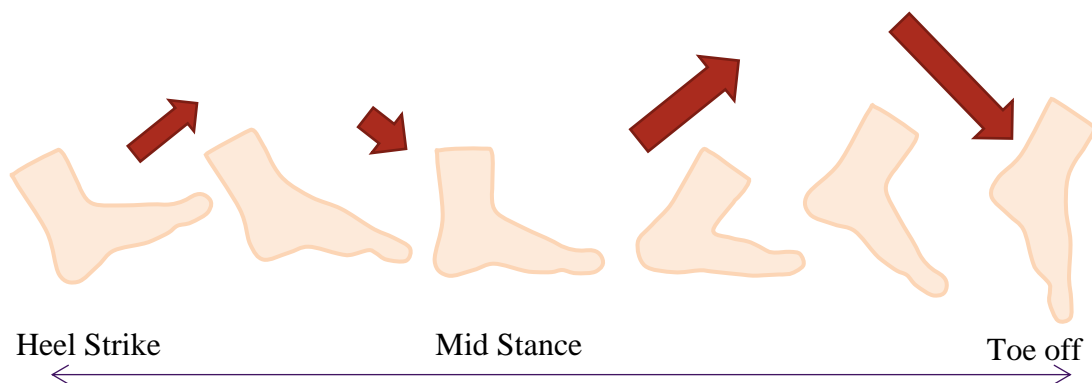


Figure 2.3 Stance phase of gait with the relative force direction

An initial input tibial-talar force profile was developed from the literature to represent the gait of one healthy individual. Due to the capacity of the simulator the profile was simplified. A maximum of 4.5 times body weight for a 70kg patient was chosen as it lay within the capacity of the simulator and the published values (Table 2.2). The peak force occurred relatively late in the stance phase in line with the Seireg & Arvikar (1975) profile. While the swing phase load is undocumented a 100N swing load was applied, aiming to replicate the soft tissue tension and ensure continued component contact, avoiding dislocation throughout the gait cycle. This was kept relatively low compared to the 300N swing phase load defined by the ISO standard for THR (ISO14242-2 2016) due to the weight of the simulator station itself applying a substantial load. This force was similar to the, almost zero swing forces reported by Seireg & Arvikar (1975). The specific magnitude of the force at 12 of the 128 time points was defined and a MATLAB

(Mathworks) coding function was used to interpolate the intermediary points (Figure 2.4).

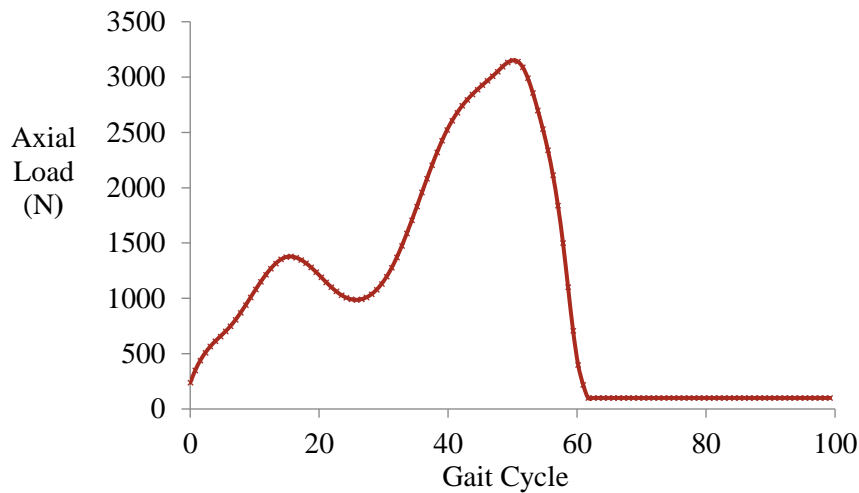


Figure 2.4 Axial load profile derived from literature and implemented in simulator

2.3.1.2 Plantarflexion/Dorsiflexion

Most ankle biomechanics studies have focussed on assessing plantar- and dorsiflexion. Of these (Table 2.3) twelve produced their profiles based on patients in a standard gait laboratory, Arndt et al. (2004) from an invasive marker placement gait analysis, (Lamoreux 1971) Lamoreux from electrogoniometric exoskeletons and Nester et al. (2007) from dynamic cadaveric assessment.

It is apparent that at heel strike, the start of the stance phase, the ankle moves out of dorsiflexion and into plantarflexion to an angle between three and 14.2° (Figure 2.3). As the foot falls flat after heel strike the level of plantarflexion decreases smoothly and then extends into dorsiflexion to a maximum. Ingrosso et al. (2009), Nester et al. (2007), Simon et al. (2006) and Lamoreux (1971) all present maximum dorsiflexion angles between 13° and 16° from a range of measurement techniques. Four authors measured the peak dorsiflexion as 12° (Table 2.3) whereas Stauffer et al. (1977) and Winter (1991) were closer to 10° and Jenkyn & Nicol (2007) measured the maximum angle to be just 5° . This semi plateau leads into a sharp change in direction around heel off to reach maximum plantarflexion on the cusp of the swing phase measuring between 10° - 19.8° (Lamoreux 1971; Winter 1991; Ounpuu 1994; Novacheck 1998; Simon et al. 2006; Jenkyn et al.

2007; Ingrosso et al. 2009; Singer et al. 2013). This change has only been documented by those authors who included the swing phase in their gait analysis.

Table 2.3 Approximations of Peak Ankle Sagittal Plane Motion for the natural ankle from literature

| Author | Plantarflexion (°) (stance) | Plantarflexion (°) (swing) | Dorsiflexion (°) |
|-------------------------------|--|---------------------------------------|-----------------------------|
| (Lamoreux 1971) | 7.5 | 17 | 15 |
| (Stauffer et al. 1977) | 14.2 | - | 10.2 |
| (Winter 1991) | - | 19.8 | 9.6 |
| (Ounpuu 1994) | 3 | 15 | 12 |
| (Ingrosso et al. 2009) | 3 | 13.37 | 15.89 |
| (Jenkyn et al. 2007) | 4 | 10 | 5 |
| (Nester et al. 2007) | 7 | - | 13 |
| (Novacheck 1998) | 5 | 16 | 12 |
| (Rao et al. 2006) | 12 | - | 7 |
| (Simon et al. 2006) | 3.6 | 10.4 | 13.1 |
| (Müller et al. 2006) | 7 | 3 | 12 |
| Singer et al. (2013) | 5 | 16 | 11.9 |
| Philippe et al. (2008) | | 27.3 (range) | |
| Flavin et al. (2013) | | 32.2 (range) | |
| Arndt et al. (2004) | | 24.7° (range) | |

During the swing phase the ankle goes from the peak plantarflexion, into dorsiflexion of approximately 5 degrees (Lamoreux 1971; Ounpuu 1994; Ingrosso et al. 2009; Singer et al. 2013), although Novacheck (1998) predicts it to be closer to neutral. Most depictions agree it remains in a dorsiflexed position for around 25% of the gait cycle before returning to a neutral position before the cycle starts again (Lamoreux 1971; Ounpuu 1994; Ingrosso et al. 2009). Across these studies few show any indication of interpersonal variability in the measured motion profile ranging from approximately $\pm 5^\circ$ (Ounpuu 1994; Rao et al. 2006; Ingrosso et al. 2009; Singer et al. 2013) to $\pm 1.5^\circ$ (Lamoreux 1971).

Multiple studies have addressed the relative motions for an ankle having undergone TAR. Ingrosso et al. (2009) showed that reduced stability associated

with TAR, specifically the BOX TAR (MatOrtho, UK), halved the range of motion in plantar/dorsiflexion. Conversely, Singer et al. (2013) saw no significant difference in the measured dorsiflexion for TAR patients but a significant reduction in the level of plantarflexion achieved by their mobile bearing TAR patients measuring $6.8^{\circ} \pm 5.0^{\circ}$ compared to $11.9^{\circ} \pm 5.2^{\circ}$. Müller et al. (2006) analysed results from two different multi-segmented computational foot models comparing TAR patients and normal individuals, from one model the TAR showed reduced plantarflexion whereas the other interpretation concluded similar plantarflexion but reduced dorsiflexion. In contrast Doets et al. (2007) observed a significant reduction in the passive dorsiflexion range of motion for TAR patients, however, there was no significant difference in the functional ankle motion during walking. From the existing research it can be concluded that a TAR may cause a reduction in range of motion compared to a healthy ankle, however, reports about the specific differences are conflicting. Despite the differences a range of motion more similar to that of a healthy natural joint was chosen for the range of motion input, just as is convention in both knee and hip replacement simulators. While an increased range of motion might improve some aspects of the TAR tribology, such as lubrication regime, it was assumed more likely that higher kinematic inputs would create more adverse wear conditions compared to the clinical performance.

Across all literature, the shape of the flexion profile was comparable, which only left the peak values to be defined. An initial plantarflexion peak was defined as 9° , one of the more variable parameters in the literature, the initial value selected for parameterisation has been made quite high. This value is substantially higher than that of 3° found by Ounpuu (1994) and Inghosso et al. (2009) but relative to the prediction of 14.2° by Stauffer et al. (1977) it could be considered small. From the available data the average angle is around seven degrees, however, the upper confidence limit on the existing graphs is closer to 9° (Lamoreux 1971; Inghosso et al. 2009). In order to implement this in the wear simulation a relatively large range of motion was selected as this would be assumed to create a more vigorous wear condition due to the increased sliding distance. The initial plantarflexion leads into maximum values of 15° dorsiflexion and 15° plantarflexion were defined as they were within the confidence limits for the majority of gait studies. The full range of 30° is also similar to some of the more recent publications by

Flavin et al. (2013) and Philippe et al. (2008) although the directional ratio of these ranges are unknown. Finally the swing phase is replicated by a five degree dorsiflexion based on the majority of the literature. These key features of the TAR flexion during gait defined a profile to me implemented within the simulator (Figure 2.5).

2.3.1.3 Rotation

Definition of the rotation, also referred to as abduction/adduction, input was more limited. Unlike flexion motions in the sagittal plane which are considered to occur

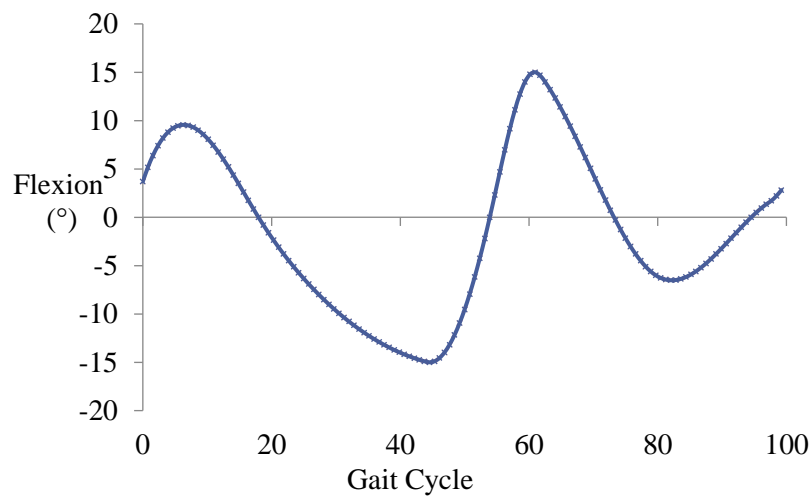


Figure 2.5 Ankle plantarflexion (+) dorsiflexion (-) profile derived from literature and implemented in simulator

predominantly at the tibial-talar articulation, the rotation in the transverse plane is not as well defined. It was important to distinguish between those sources presenting motions of the ankle complex rather than the talocrural articulation specifically and to ensure motions are applied corresponding to a similar coordinate system as that measured in the natural ankle (Table 2.4). Often the studies focused solely on the stance phase leaving the rotation during swing even harder to define. Nester et al. (2007), working with a cadaveric model of ankle gait, produced more pertinent results as more markers were implanted which made defining specific joint motions more precise. In this case the rotational, transverse plane motion was the smallest measured range of motion with around 2° internal rotation and 3° external rotation. This provided a reliable method of measuring the motions but these cadaveric results are highly dependent on the walking inputs applied to the model. Nester highlighted limitations in the load application,

especially of the second peak which is possibly why the profile does not respond as others do towards the end of the stance phase. When the rotation was compared with the profiles from Lundgren et al. (2008), following on from the initial investigation by Arndt et al. (2004) using invasive markers in living people there was very little similarity between the profile shapes in this plane. Three of the five individuals tested observed a clear internal rotation of the talus relative to the tibia at the start of stance followed by external rotation during stance. The other two individuals had small rotational changes throughout the stance phase.

At the other end of the scale Scott & Winter (1991) found peak rotations specifically for the ankle/talocrural joint during the stance phase of gait to be closer to 10° external and 8° internally. Both Smith et al. (2001) and Lamoreux (1971) lie in between both registering around 8° peak external rotation occurring before toe off and 2° internal rotation shortly after heel strike and again in the middle of the swing phase. These profiles were some of the few to consider the swing section of the gait cycle along with stance. Similarly, considering just the stance phase of gait Moseley et al. (1996) observed external rotation (abduction) of the rearfoot up to 8° and no internal rotation until the end of the stance phase and Reggiani et al. (2006) reported similar magnitudes generated from computational modelling of the joint with a TAR and gait analysis respectively with the peak rotation before toe off but the rotations act in the opposite directions. Although the rotation profile was not specified Singer et al. (2013) observed no significant difference in the rotation measured between normal individuals and those with an ankle replacement with the total tibial rotation measuring $10.6^{\circ} \pm 2.1^{\circ}$ and $10.5^{\circ} \pm 3.2^{\circ}$ respectively. This range of motion corresponds with the majority of the investigations discussed.

Table 2.4 Ankle rotational motions reported in literature

| Author | Number of Subjects | Internal Rotation (°) | External Rotation (°) |
|----------------------------------|---------------------|-----------------------|-----------------------|
| Lamoreux (1971) | | 2 | 8.5 |
| Ingrosso et al. (2009) | 20 controls | 0.05 | 20.75 (swing) |
| Nester et al. (2007) | 13 cadaveric feet | 2 | 3 |
| Arndt et al. (2004) | 3 subjects | 2 | 4 |
| Scott & Winter (1991) | 3 subjects | 8 | 10 |
| Smith et al. (2001) | 43 normal adults | 2 | 8 |
| Moseley et al. (1996) | 14 males walking | 0 | 8 |
| de Asla et al. (2006) | 5 healthy subjects | 3.8 ± 8.2 | 1.6 ± 5.9 |
| Winter (1991) | | | 6.8 |
| Arndt et al. (2007) | 4 men running | 8.7° (range) | |
| Flavin et al. (2013) | 14 normal adults | 13.0 ± 3 (range) | |
| Singer et al. (2013) | 10 control subjects | 10.5 ± 3.2 (range) | |
| Reggiani et al. (2006) | | 10.6 (range) | |
| Lundgren et al. (2008) | 5 subjects | 7.9 (range) | |

Despite some general agreement among the published ankle rotational profiles the variability of this parameter is especially apparent when looking at the results produced by Lundgren et al. (2008). There appeared to be no trends in the profile shapes or magnitudes. This should be one of the most reliable studies as the variability of marker placement on skin is removed as they used live individuals with gait markers fixed into the relevant bones. In addition, the information is not compromised by the motion input as it would in a cadaveric study, however, this study shows too much variability to be extracted to a simulator profile. With a need for a complete profile for both stance and swing phases a combination of the Smith et al. (2001) with the largest sample size and the historic Lamoreux (1971) profile were used following the general trend of greater external rotation. This magnitude of rotation totalling 10° also corresponds with that measured by Singer et al. (2013) for both healthy ankles and ankle replacements.

Due to the symmetrical nature of the TAR device this profile (Figure 2.6) can be applied in either direction but must be understood so that medial and lateral areas of the surfaces can be defined when carrying out the surface roughness assessment.

The sign convention for the rotation and its application to the tibial component defines that the gait input is simulating a left ankle.

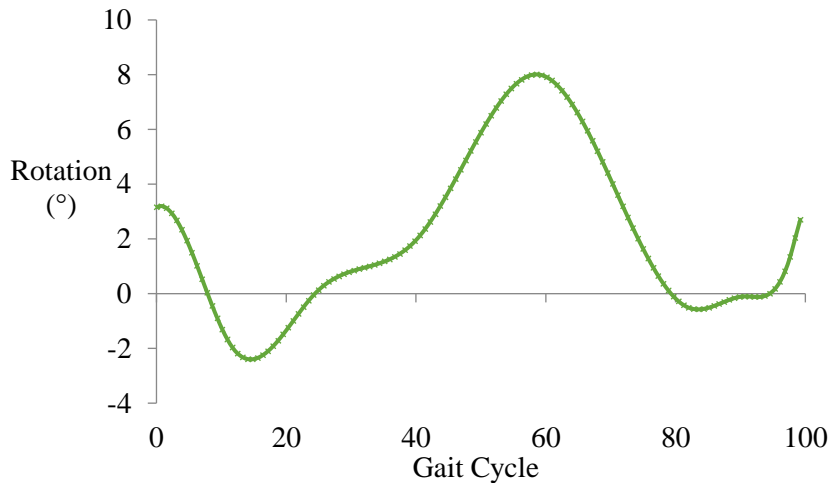


Figure 2.6 Internal (-) external (+) rotation of the ankle derived from literature and implemented in simulator

2.3.1.4 Anterior/Posterior displacement

The most difficult ankle motion to define was the anterior-posterior (AP) displacement. There was a distinct lack of publications defining the AP motions within either the natural or the replacement ankle joint.

Komistek et al. (2000) defined the position of the tibial-talar contact relative to the tibia during plantarflexion, dorsiflexion and midstance using fluoroscopy. Whilst weight bearing the test subjects moved from maximum plantarflexion to maximum dorsiflexion and fluoroscopic images were recorded. The AP displacement measured greater with the addition of a TAR device with the talar contact moving a mean of 7mm posteriorly at plantarflexion with some as high as 10mm but minimal displacement during dorsiflexion and midstance. Reggiani et al. (2006) found maximum insert displacements of approximately 5.6mm while the talar component moved 8.3mm in the AP direction in their computational model of a TAR and similarly Conti et al. (2006) measured a maximum of 10mm of AP displacement through analysis of fluoroscopic video of a natural ankle during gait. In contrast de Asla et al. (2006) found minimal translation at the natural ankle joint; during the stance phase the talus translating posteriorly 0.2mm from heel

strike to midstance and anteriorly 0.3 mm from midstance to toe off. Unlike Komistek et al. (2000), Conti et al. (2006) found no TAR to translate more than 3.5mm during stance. Similarly Leszko et al (2008) found the maximum displacement for the Salto TAR to be just 1.5mm. Reggiani et al. (2006) specified the insert moved posteriorly which suggests the talus also moved posteriorly. Conti et al. (2006) reported more anterior contact relative to the talus midpoint which also suggests the talus moved posteriorly. In contrast Komistek et al. (2000) reported the contact remained posterior. This was dependent on the relative measurement. Both groups defined positive as the contact point between the tibial and talus remaining anterior to the centre line of the talus (Figure 2.7) which does not explain the discrepancy in direction between these investigations. Harris et al. (2008) notes that the talus bone is known to translate posteriorly under plantarflexion and Reggiani et al. (2006) specifically stated it was the meniscal bearing which moved posteriorly although the AP displacement of the talus was 8.3mm with no directional information, going on the general consensus of the insert/talus moving posteriorly.

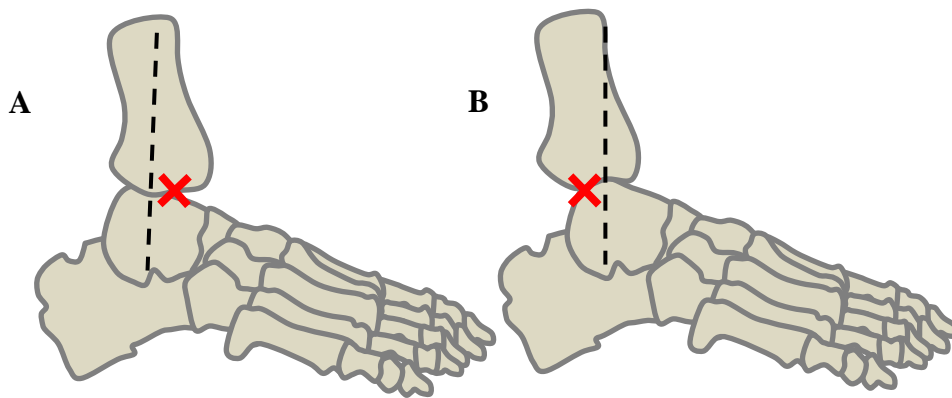


Figure 2.7 (A) Positive and (B) negative AP displacement

As the initial intention was to parameterise the effects of the inputs opting for a maximum displacement value at the larger end of the scale should be one of the considerations. The values provided by Conti et al. (2006) taken at four time points during the stance phase for the natural ankle helped define a profile shape. The main data points were interpolated relative to the flexion profile and reach magnitude of 7mm at peak plantarflexion (Figure 2.8). Within the simulator the AP displacement was applied to the tibial component driving it in the opposite direction, moving it anteriorly to facilitate the equivalent to the talus moving posterior, with this input it would result in a similar distance observed computationally by Reggiani et al. (2006) in the talus. With such limited physiological information available it is difficult to be confident that this may be a realistic representation of the AP displacement, however it is important to understand the effects of this parameter on the wear.

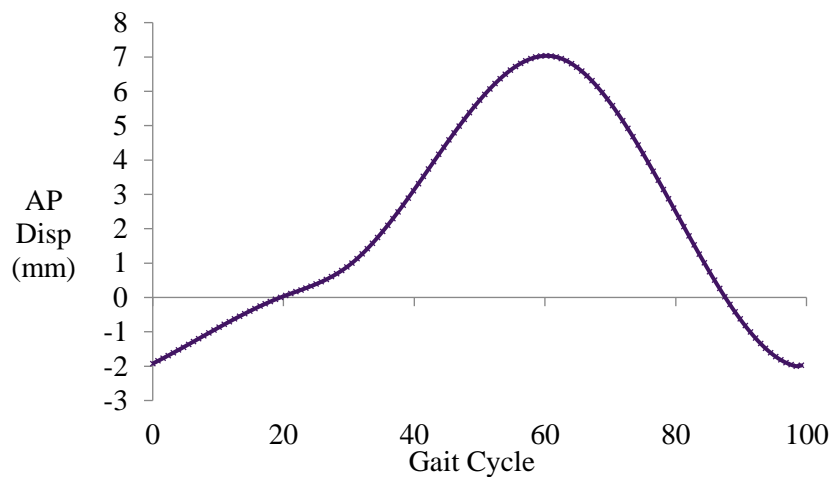


Figure 2.8 Ankle anterior (+) posterior (-) displacement derived from literature and implemented in simulator

2.3.2 Translation to simulator

Due to the inversion of the components within the simulator the relative motions had to be considered (Figure 2.9). As a result the direction of the flexion was altered. The rotation at the tibiotalar joint is considered as the motion of the foot relative to the tibia, occurring at the tibial articulation in a TAR. As the rotation was applied to the tibial component the direction of this also had to be reversed. Similarly, as the AP displacement was created by the talar component moving posteriorly this had to be created by the tibial component moving anteriorly in the

simulator. As the sign convention for the simulator defines this direction as negative (Figure 2.2) this also required inversion.

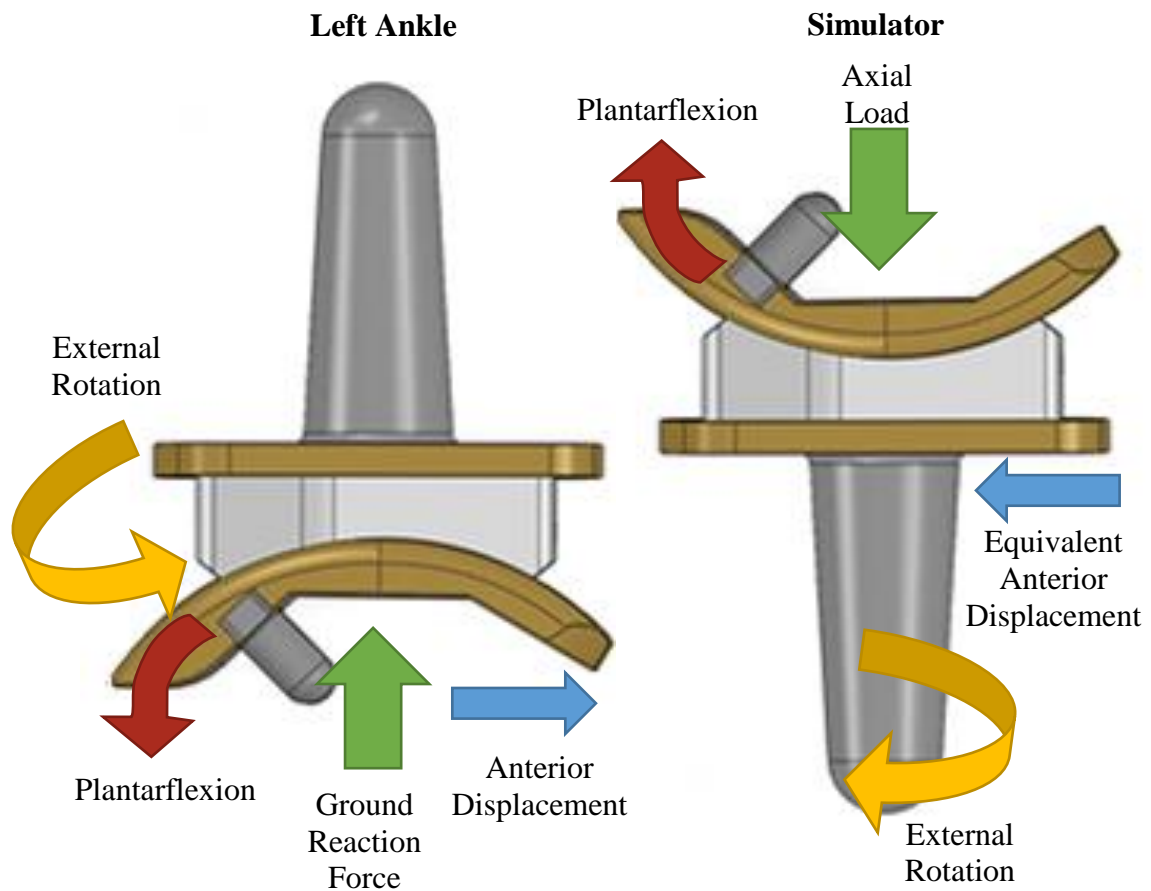


Figure 2.9 Schematic showing loads and motions at a left TAR relative to the inverted simulator position

2.3.3 Fixtures

The main priority in defining the simulator set up was to ensure alignment between the centres of rotation of the simulation and those of the TAR. Due to the available degrees of freedom there are two cradles to align the components with; flexion and version (Figure 2.10).

The talar fixture had to consider four important parameters; aligning the centre of rotations, compensating for the neutral alignment of the flexion cradle, conformity to the shape of the talar component and incorporating the surgical positioning of the TAR.

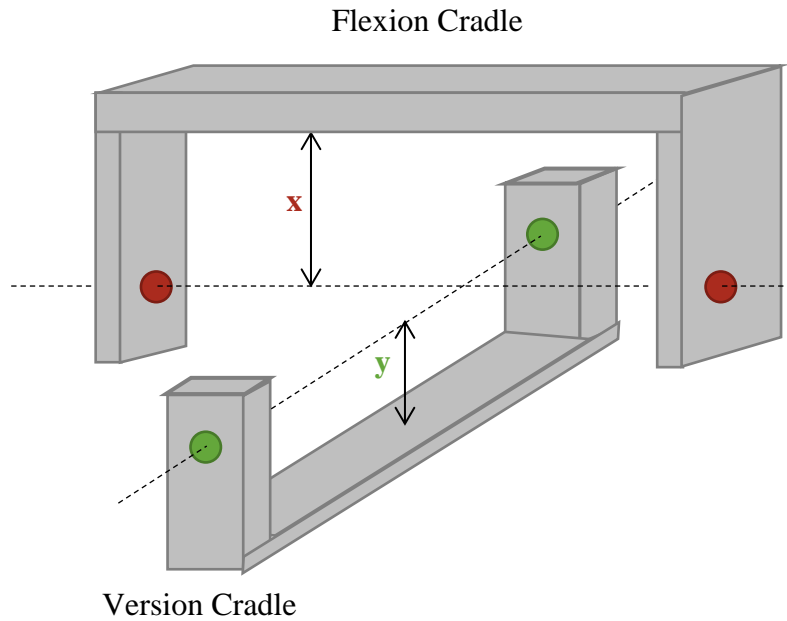


Figure 2.10: Schematic of simulator cradles

In order to achieve maximum stability there were design considerations relating to the ideal position of the centre of rotation. The TAR was inverted so the flexion could be applied to the talar component. This had a constant radius of 26mm to the bearing surface. The talar component measured 5mm thick at the centre and in order to fix the component to the fixture a 1mm layer of cement had to be accounted for. Taking this into consideration the fixture had the measure 20mm from the centre of rotation. This centre of rotation had to be aligned with that of the flexion cradle defined as length x (Figure 2.10), fixed at 36mm due to the simulator dimensions (Appendix B).

Fixturing of the talar component had to compensate for the neutral alignment of the Prosim Knee Simulator I which is offset at 30 degrees to allow for a full range of TKR motion. As changing this alignment was not possible and the simulator requires the gait profile to start at the zero position the components had to be aligned with the neutral position at 15° so at peak dorsiflexion the gait cycle will pass through zero. This angle was applied from the centre of rotation (Figure 2.11).

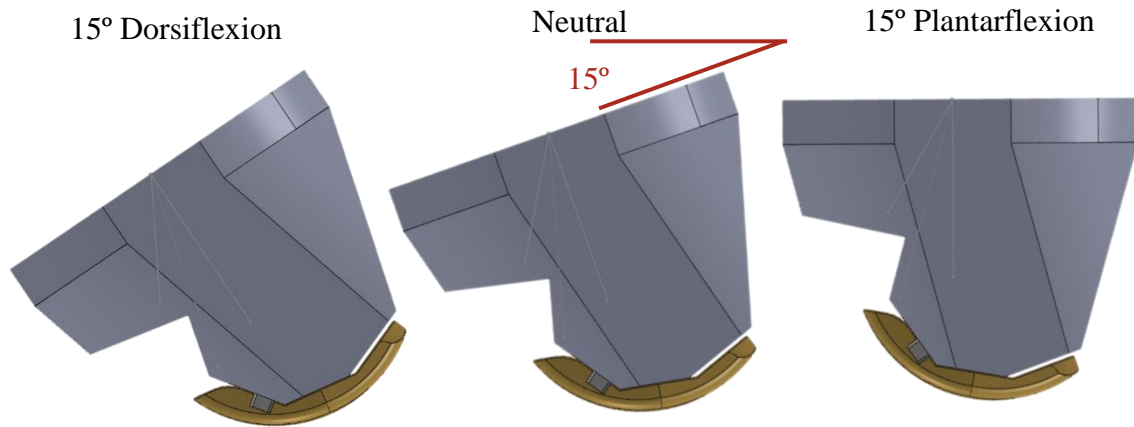


Figure 2.11 Fixture alignment

The surgical technique was also considered as the parallel cuts for the TAR are made with the foot in a five degree equinus position, this angle was applied at the fixation surface (Appendix B).

To ensure the components remained stable during testing and to minimise the vibrations affecting the floating inversion/eversion cradle it was important the components were aligned so the talar contact with the insert lies at the centre of the cradle. This was achieved through adjustment of the height of the tibial component. As the fixtures which fit the specific simulator are readily available, a low cost solution to insert a ring of metal was devised. This raised the component the necessary 2.2mm, calculated from subtracting the polyethylene and tibial thickness and fixture height from distance y, Figure 2.10. The ring was designed to be wide enough to sit on the edge of the extrusions on the holder but not protrude too far to avoid any obstruction. This simple part was then cemented between the component and the fixture.

2.3.4 Component Set Up

The talar components were cemented with Poly(methyl methacrylate) (PMMA) into the slots of the fixtures and secured with grub screws. With the rotation and displacement in the neutral position the cavity of the tibial fixture was filled with PMMA cement, and the spacer was set centrally and the tibial component placed on top of the spacer into the cement. The TAR insert was placed on the tibial component and the talar component, positioned neutrally aligned at 15degrees to

the vertical, lowered on to the insert. With the three components of the TAR in contact the tibial component was repositioned so the insert was, by eye, centrally located (Figure 2.12). A weight was then applied to hold the tibial component in place while the cement cured. It was important each station was aligned individually and would maintain partnered throughout the investigation, to account for variation between simulator stations.

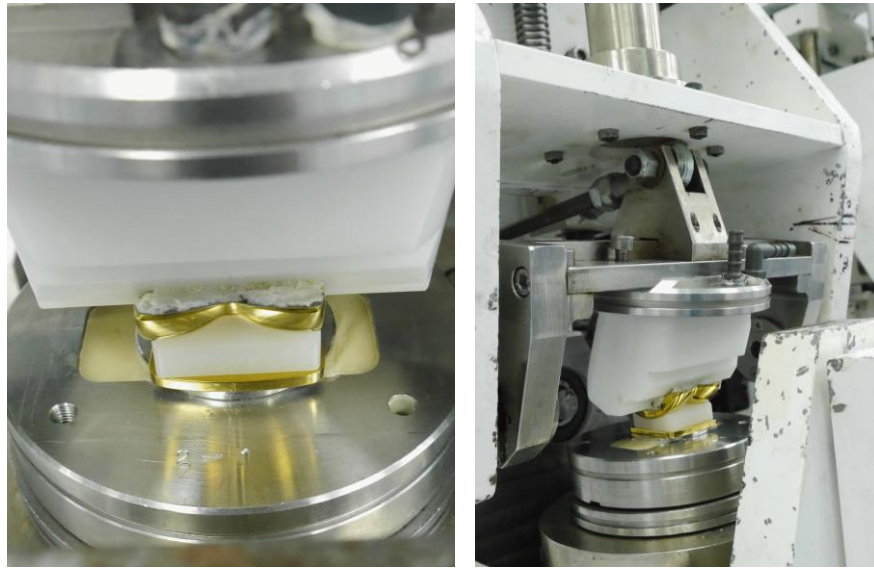


Figure 2.12: Ankle simulator set-up

2.3.5 Contact Areas

To ensure alignment of the components the contact areas for each implant were visualised under neutral alignment. Microset, a two part silicone polymer was applied to both the flat insert surface and the talar surface. The inset was set approximately in the correct position on the tibial component and the talar component lowered to make initial contact. A load of over 1000N was then applied to ensure the components aligned and achieved full contact. This outlined the contact area on the metal surfaces. This process was then repeated after each million cycles to ensure the alignment was maintained as the samples were rotated around the stations during the study. Across the sample the results were relatively similar to those depicted in Figure 2.13, although in some incidences the insert was difficult to remove from the tibial so its position was less well defined.

There was a distinct area on each of the components displaying contact across the majority of both of the insert surfaces with the imprint centrally aligned on both tibial and talar components. This indicated a successful set-up protocol. Although the insert contact area may appear to be located anteriorly in Figure 2.13a, any further posterior translation of the insert with respect to the tibial component would have been a risk of edge loading at the medial or lateral surfaces.

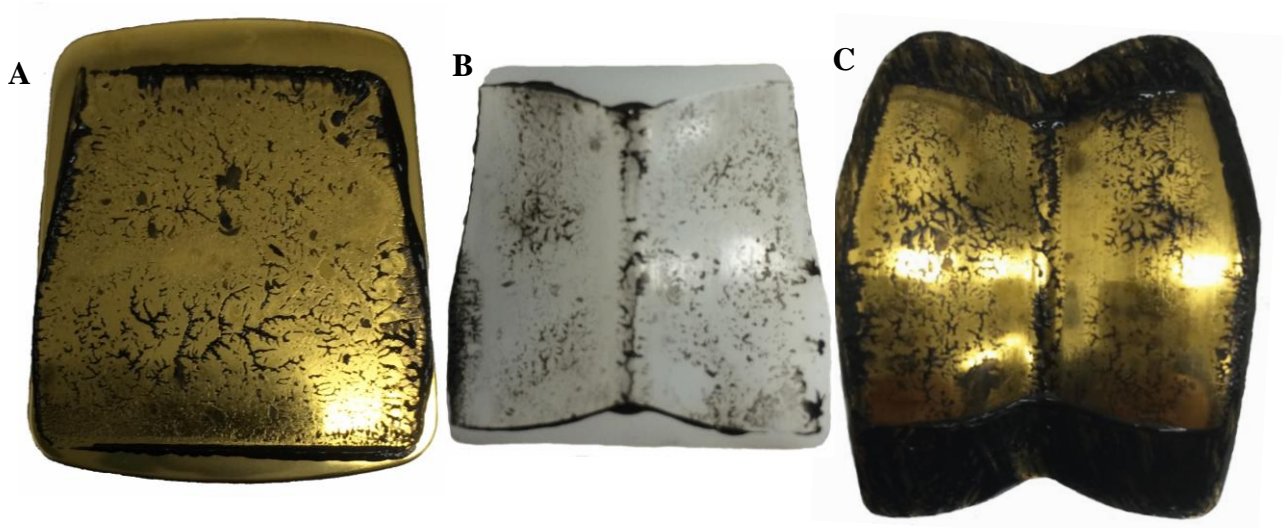


Figure 2.13: Contact areas of the insert (B) brought into contact with the tibial component (A) and talar component (C) demonstrating central alignment

2.3.6 Calibration

Prior to experimental wear testing the simulator was first calibrated. A standard iMBE protocol was followed, which involved setting the simulator at known forces, angles and displacements and monitoring the LVDT positional output in the simulator software. Existing fixtures allowed the rotation to be calibrated at 5° increments and displacement at 0mm and 10mm. With the simulator in the neutral position the axial load was then increased to 4000N in 500N intervals and the simulator reading recorded. This process was repeated as the load was reduced to zero and an average recorded. These values allowed calculation of a scaling factor so the software knew its physical position throughout the range of motion (Appendix C). The only exception was when assessing the sagittal plane motion as there is no integrated LDVT. Instead a potentiometer was attached to the flexion cradle and a digital inclinometer used to position it through five degree increments

between the zero and vertical position which defined the maximum and minimum angular points. The ankle gait profile was applied and the potentiometer readings observed. Testing both sides of the simulator the full range of motion was not seen on the display, approximately 10% at both ends of the range of motion was absent. This is likely a result of the speed at which the display updates with its relative position or alternatively the flexion profile is not quite fully replicating the input profile of Figure 2.5. As the defined inputs were at the higher end of the documented scale the simulator can be deemed to be applying a physiological flexion profile.

2.3.7 Pre-test

Before any wear testing on the Corin Zenith total ankle replacement (TAR) the pre-soak mass for eight polyethylene inserts was recorded. Initially the inserts were washed according to the principles outlined in ASTM F1714 - 96 (2013), this involved three stages of cleaning; soapy water, Distel (Tristel, UK) disinfectant and ultrasonic washing. Once allowed to dry in air the inserts were placed in a balance room and allowed to equilibrate to the controlled environment of constant temperature of 20°Celsius and 40% humidity for 48 hours (Smith et al. 1999). After this rest period the inserts were weighed on the XP26 Analytical Microbalance (Mettler Toledo, Leicester, UK) under the conditions described in Section 2.4 Gravimetric measurement method. With a pre-test weight recorded the inserts were submerged in deionised water and stored at room temperature for a period of two months prior to testing in order to ensure fluid absorption effects were compensated for (Wang et al. 1998; D’Lima et al. 2001).

2.3.8 Lubrication

Bovine serum is largely considered to be the most clinically relevant lubricant for *in-vitro* studies and is recommended by both ISO and ASTM standards. Each of the TARs were tested in secured chambers filled with 330ml of lubricant consisting of 25% new born calf serum, 0.03% Sodium Azide aqueous solution. This combination resulted in a protein content of 15.46g/l, used to replicate that of the natural joint capsule as defined by Saari et al. (1993) . The testing was carried

out at room temperature and the temperature was measured at the end of the test with a calibrated thermocouple.

2.3.9 Frequency

The frequency had to correspond with that of the natural gait which is approximated to 60 steps per minute, 1Hz. This was verified by timing 100 cycles with a stopwatch to ensure it was running to specification.

2.4 Gravimetric measurement method

Before simulator testing, the inserts were removed from soak, cleaned using the protocol described previously and were left to dry and acclimatise in the controlled environment balance room for 48hours before the gravimetric measurement of the inserts. The weighing method was carried out repeatedly at each of the six experimental parameterisation intervals on XP26 Analytical Weigh Balance (Mettler Toledo, Leicester, UK). Before weighing the balance doors were opened and closed repeatedly and an internal adjustment was carried out to allow the balance equilibrate with the room environment. The temperature and humidity were recorded. Wearing gloves one of the components was set on the balance and left for a minimum of five minutes to warm it up. This was removed and any particles were cleaned from the components using compressed air. The balance was calibrated by repeatedly weighing a metal control pin and this process was repeated again at the end of the weighing to ensure no change had occurred. Once the balance was set up the inserts could be weighed. With gloved hands the polyethylene inserts were turned under the active anti-static to remove any electrostatic charge from the inserts to improve measurement reliability. The components were set centrally on the weighing platform in a repeatable position. The anti-static ceased five seconds after the balance door shuts and the balance was allowed to settle before weights were recorded. Each time the tested and soak control samples were weighed sequentially from one to eight and repeated until five consecutive weigh measurements lie within $\pm 0.010\text{mg}$ of the first weight and the readings recorded. In between each measurement the balance was ensured to return and settle at zero. A mean for each insert was determined from the five recorded readings and was used to calculate the wear using Equation 2.1 which

compensates for the fluid absorption effects. This soak control accounted for changes between 0.03 and 0.4mg throughout the test therefore the sensitivity of the balance was able to account for these minor changes.

Equation 2.1 Volumetric Wear Equation

$$W_n = W_{an} + S_n$$

Where W_n is the net mass loss;
 W_{an} is the average uncorrected mass loss
 S_n average mass increase for the soak control

The net change in mass can be use calculate the average wear rate which will provide a comparative tool for the effect of the individual simulator input parameters.

2.5 The wear study

The simulator was run in million cycle (Mc) segments. The serum was changed every 0.3Mc to ensure a continued protein content and the load cell was moved between stations at each interval. Stations were washed thoroughly with soapy water and Distel disinfectant before being dried, fixed into the stations again and filled with fresh serum. Every Mcs the components were rotated around stations to compensate for any interstation variation. Components were visually inspected and photographed to provide record of the surface changes.

2.6 Contact surface measurements

A Form Talysurf PGI800 (Taylor Hobson, Leicester, UK) contact profilometer was used to evaluate the surface roughness of all of the TAR articulating surfaces at measurement points throughout the wear study. This method used a stylus to take two dimensional surface traces along the medial/lateral direction on each of the individual components for each of the stations. Three traces were taken on the unworn surfaces of the tibial and talar components prior to test. This was increased to six once the testing was underway in order to better represent the surface changes. Sample lengths were kept long, where possible, in order to ensure an accurate representation of the whole surface.

The measurements were taken as defined below relative to components (Figure 2.14);

- a) Tibia- Six medial-lateral 25mm traces spaced at 10mm, starting 5mm from the most medial point and 8mm from the most anterior point
- b) Superior Insert Face- Three traces of 18mm spaced at 5mm, starting 5mm from the most medial point and 5mm from the posterior
- c) Inferior Insert Face- Five traces of 20mm spaced at 5mm, starting 5mm from the posterior and 3mm from the most medial point
- d) Talus- With the talus fixture aligned at 18° three 24mm traces were taken from 1mm before the crest, 10 and 20mm from the posterior and 10mm from the anterior

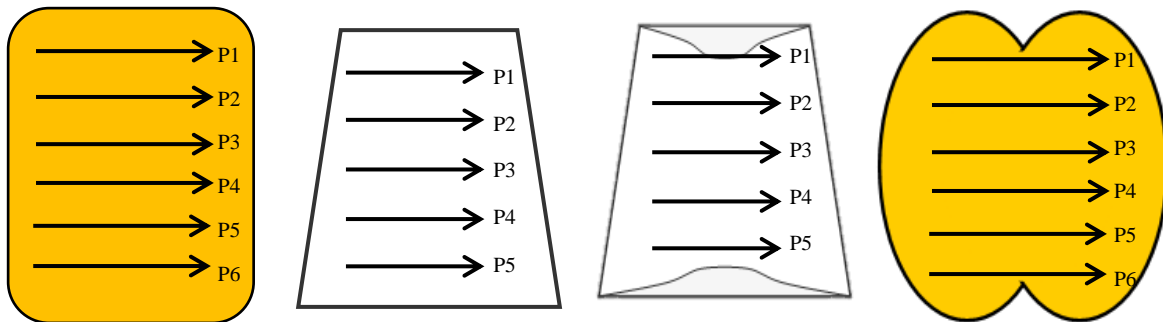


Figure 2.14 Talysurf traces of the TAR surfaces

The flat surfaces were fitted to least squares lines and the curved surfaces to arcs. Once the form was removed from the samples, a Gaussian regression filter was applied to isolate the surface roughness, for the metal components an upper cut off of 0.25 and for the polyethylene 0.8 both with 100:1 bandwidths based on the suggestions of the ISO standard from the initial roughness measurement ISO 4288 (1996). Despite later changes in roughness this parameter remained constant to ensure the results were comparable. The industry standard, average surface roughness (R_a) values were recorded alongside the relevant peak, valley and skewness values.

During the test it was realised that the single trace across the curved surfaces of the talar component and the inferior insert surface were not the best representation of the R_a value. The ability of the Gaussian regression to solve for the form was compromised by the big changes in the arc radius and individual condular changes

could not be compared. As this was the same throughout the first wear test these value could be compared, however, for the latter simulations the single trace was segmented into three (Figure 2.15); the medial slope (blue), central region (green) and lateral slope (red).

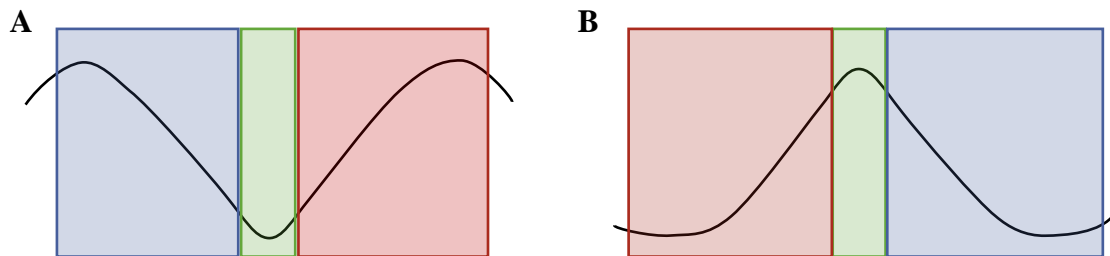


Figure 2.15 The analysis segmentation for the (A) talar surface and (B) superior insert roughness traces

Every two Mcs the contact surface measurements were repeated to observe any changes in the surfaces and averaged for comparison.

2.7 Non-contact surface measurements

To be able to visualise the surface roughness changes further non-contact surface measurements were taken of the flat tibial and superior insert surfaces at the start and the end of the test using the NPFLEX (Bruker, Coventry, UK). The centre of the components were located using the coordinates of the outer edges and a 12x12mm measurement area was defined (Figure 2.16).

The VXI setting which is a universal scanning mode suitable for stepped, smooth and rough surfaces was used. The coordinates at the widest point of the components were defined and from this the centre point was located. With a 2.5x objective lens and a 0.55x multiplier the same region was imaged with white light interferometry stitching together individual measurements. As the result of a sensitivity analysis threshold value of 3% was used for the polyethylene surface and 5% for the tibial component to ensure maximum data was captured. The threshold value defines the point at which data is excluded based on the quality of the fringes. Lower values ensure data is captured but with this there is a risk of noise presenting as erroneous data. The same measurement conditions were used for each of the components.

Just as for the two dimensional contact measurements filtering was used in post processing. The curvature and tilt were removed and any waviness was filtered out with a short wave pass Gaussian regression filter with a short cut off of 0.6.

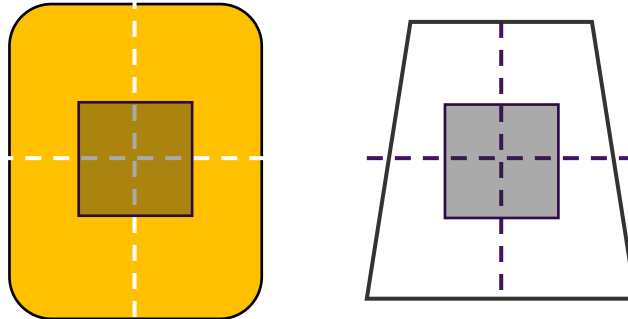


Figure 2.16 Bruker measurement area on the flat bearing surfaces

2.8 Measuring coating damage

In an attempt to understand more about the surface changes in two damaged tibial components their surface profile was also imaged with the white light interferometer, NPFLEX (Bruker, Coventry, UK). The NPFLEX could be used to gather a range of data including the change in roughness of this region as well as changes in form relative to unworn and worn tibial which showed no signs of coating damage. Using the lowest magnification, a 2.5x objective and a 0.55x multiplier, stitched traces limited to the imagefield width and height respectively were obtained in both anterior/posterior and medial/lateral directions including the damaged regions (Figure 2.17). The only post processing for this trace was the removal of tilt from the data.

With the 20x objective lens of a damaged region and intact region were imaged to compare roughness changes. The 3D surface roughness measurements from these images were derived with the application of a Gaussian filter with a lower cut off of 0.6 based on a convergence sensitivity test.

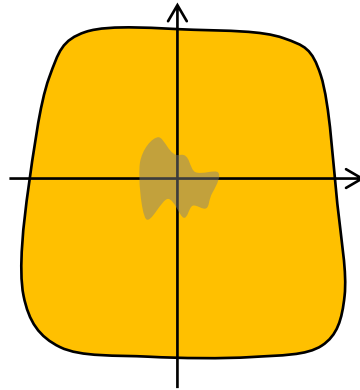


Figure 2.17 Traces taken on the tibial components across the damaged region

2.9 Wear track analysis

In order to further understand the motions on the different surfaces of the mobile bearing TAR and aid interpretation of the wear results methods were developed to quantify the displacement.

Once the testing was completed two stations were run lubricated by a thin layer of Vaseline rather than the serum capsule it was possible to visualise how the mobile nature of the TAR responded to the motions being applied. The most extreme conditions were applied and the stations were filmed from anterior and medial/lateral directions.

To further quantify this relationship 1mm ball bearings were partially embedded into the surface of two of tested inserts (Figure 2.18); two in the superior surface and two in the inferior, the simulator was again run for twenty cycles so the ball bearings would scratch the surfaces of the implant whilst under the range of motion implemented within the gait cycle. The scratches were then analysed to understand where the majority of the motions were occurring within the mobile bearing.

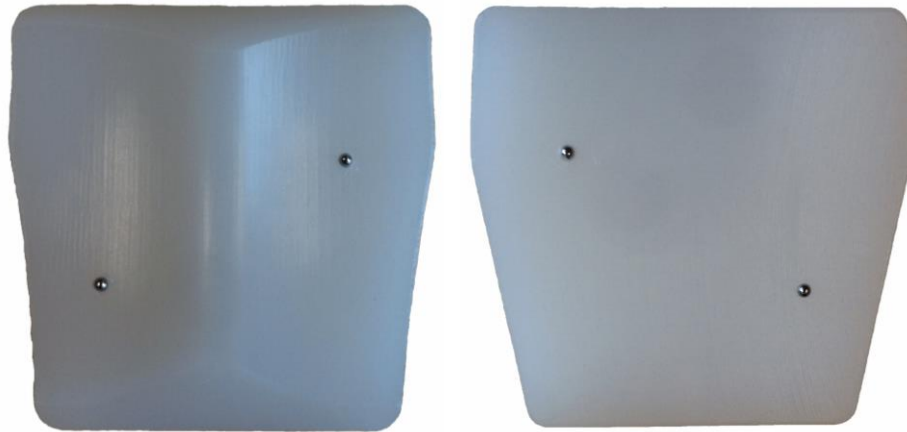


Figure 2.18 1mm ball bearings in the surfaces of a TAR insert

2.10 Comparison to retrievals

Where possible the components were visually compared to the collection of TAR retrievals within the retrievals bank at University of Leeds, collected from UK hospitals under ethical approval (HRA ethics ref: 09/H1307/60).

CHAPTER 3
STRATIFIED WEAR TEST

CHAPTER 3

STRATIFIED WEAR TEST

3.1 Introduction

As there is no defined standard for the simulator gait inputs for tribological testing of total ankle replacements (TARs) the aim of this chapter was to gain a broad understanding of the effects the gait profiles may have on the wear of the mobile bearing TAR.

There is a large variation in the published gait data for the talocrural articulation of the ankle joint and information for parameters such as displacement were especially limited. The available information also varies between healthy individuals and those with a TAR. In order to successfully preserve the motion at the ankle the ideal TAR device must be able to replicate the natural joint motions as opposed to limiting it. Through testing combinations of input conditions this chapter aimed to define which parameters had the greatest tribological effect on the wear rate for mobile bearing designs.

Wear testing has provided a useful method of directly comparing device designs and highlighting certain material benefits. In developing test methodologies which replicate the deformations and surface wear patterns found *in-vivo* assumptions can be made about the likely *in-vivo* wear rate of a device. It is critical wear simulations produce meaningful data which could be defined as reproducible, repeatable and clinically relevant (Affatato 2016).

At the start of the century Wang (2001) published the theory of cross-shear in polyethylene. This concept combined friction, cross-link density and cross-shear angle to explain polyethylene wear with crosslinking and multidirectional motion. The equation calculates the wear per unit sliding distance per unit load also known as wear factor (k) based on the lubrication coefficient of friction (μ), cross-sectional width of polyethylene fibrils (d), the material properties bond density (X_c) and bond energy (γ_c) and the degree of cross path motion based on the direction of the velocity vector relative to the x-axis (α) to account for the changing motion (Equation 1).

Equation 1 Wear factor relating to cross shear

$$k = k' \frac{\mu d}{2X_c \gamma_c} \times \left(1 - \frac{\sin 2\alpha}{2\alpha}\right)$$

This discovery highlighted the importance of inclusion of secondary motions in wear simulation (Wang 2001). Since knee replacements testing carried out by McEwen et al. (2005) showed a significant correlation between the wear rate and the degree of rotation and secondly the magnitude of the displacement. It was hypothesised that similar relationships would be apparent for total ankle replacements despite the device design potential to uncouple these different kinematic inputs.

Polyethylene wear has been linked with revision, cited as an indication for revision surgery in 8% of the 105 revision TARs operations logged on the National Joint Registry for 2016 (NJR 2016). This percentage matches that found from a wider review of TAR complications (Sadoghi et al. 2013). However, this does not include the much more prominent occurrence of aseptic loosening (38%) (Sadoghi et al. 2013) which has been associated with the immune reaction to polyethylene wear debris (Ingham et al. 2000).

Improving the understanding of the tribological performance of mobile bearing TARs is a vital stage in developing comprehensive pre-clinical test methodologies. There have been brief forays into TAR wear simulation using knee simulators in both displacement and force control to *in-vitro* wear test TARs (Affatato et al. 2007; Bell et al. 2007; Bischoff et al. 2015; Reinders et al. 2015). However, unlike the convention with hip and knee replacement none of these centres have continued investigation into the TAR wear beyond what each author deems a standard gait input.

3.2 Materials and methods

As outlined in the in-depth methods of Chapter 2 five Corin Zenith TARs were used in the wear testing. It is currently the most implanted TAR in England and Wales. The Zenith combines high congruency alongside an unconstrained articulation facilitating simultaneous rotation and displacement. This design philosophy applies to many devices marketed worldwide including the Small Bone Innovations STAR, Integra Hintegra, MATOrtho Box and Tornier Salto. These

three component mobile bearing TARs made up more than 70% of the TARs implanted in England and Wales in 2016 (NJR 2016).

In the adapted displacement controlled Knee Simulator I (KS1) the input conditions were applied in a total of five combinations through six test stages. The combinations of inputs aimed to provide examine the effects of both linear wear with isolated flexion and the addition of anterior/posterior (AP) displacement compared to multidirectional motion created by implementing a rotational input with and without of two different magnitudes of AP displacement (Table 3.1). Each condition was run for two million cycles (Mc). The first full kinematic stage was repeated at the end of the test to understand any changes which may have occurred.

Table 3.1 Test conditions

| | Test Stages (2Mc/stage) | | | | | |
|-----------------|-------------------------|------|---|------|------|------|
| | 1 | 2 | 3 | 4 | 5 | 6 |
| Force | ✓ | ✓ | ✓ | ✓ | ✓ | ✓ |
| Flexion | ✓ | ✓ | ✓ | ✓ | ✓ | ✓ |
| Rotation | ✗ | ✓ | ✓ | ✗ | ✓ | ✓ |
| AP Displacement | ✗ | ✓9mm | ✗ | ✓9mm | ✓4mm | ✓9mm |

In order to understand the statistical significance between the wear rates at each stage a one-way ANOVA post-hoc Tukey test was carried out with a null hypothesis that the kinematics would have no effect on the wear. A significance level of 0.05 was defined; when the P value calculated was less than or equal to the significance level the null hypothesis was rejected.

3.3 Results

3.3.1 Simulator performance

Generally, the simulator was able to reproduce the relatively high demands inputs replicating the ankle gait cycle. Feedback profiles were inspected visually at least once a day and were saved every few days during testing and averaged across all

stations to ensure the motions the components were experiencing were similar to that of the desired inputs (Figure 3.1).

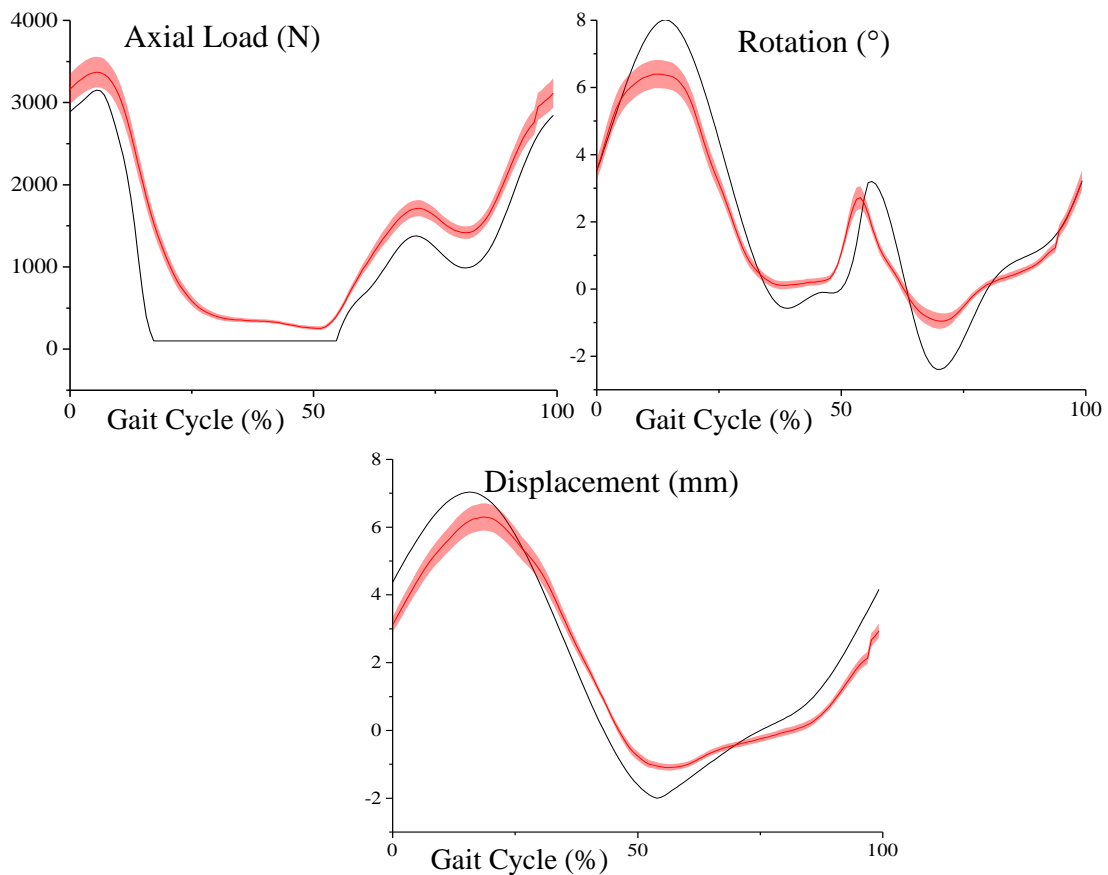


Figure 3.1 Simulator inputs compared to the mean output profiles across all stations for the duration of Stage 2 and their 95% confidence limits

As Figure 3.1 shows the simulator was adept at recreating the desired displacement, however there was a phase lag present. For the average profile the maximum phase lag was 0.06 seconds. When rotation was added to the inputs the simulator failed to reach all of the desired dynamic peaks, a limitation of the pneumatic control system with the mean rotation underperforming by 2° in the peaks. Typically, the load was well replicated however, it overloaded consistently with a mean of 407N throughout the cycle. This was especially apparent when the load was removed at a high rate and during swing phase loads which may be a limitation of the load cell calibration at these low levels. The tight confidence limits show all of the stations behaved similarly with the most variation occurring at the peaks in load rotation and displacement.

While the demands of Stage 2 were the greatest in terms of kinematic output the simulator also had to resist motion driving station to zero in the reduced kinematic stages one and four. While both the rotation and displacement were driven at zero all of the station were able to sustain this to $\pm 0.2^\circ$ and 0.1mm respectively. Similarly, Stage 3 required displacement driven at zero and Stage 4 rotation. While the rest of the simulator outputs remained in line with those presented (Figure 3.1) the mean displacement and rotation profiles were within 0.1mm of zero with minor variation throughout the cycle (Figure 3.2). With the reduced displacement of stage five (Figure 3.2C) there is a similar underperformance and phase lag and failure to obtain the profile peak as was observed with the higher AP displacement profile.

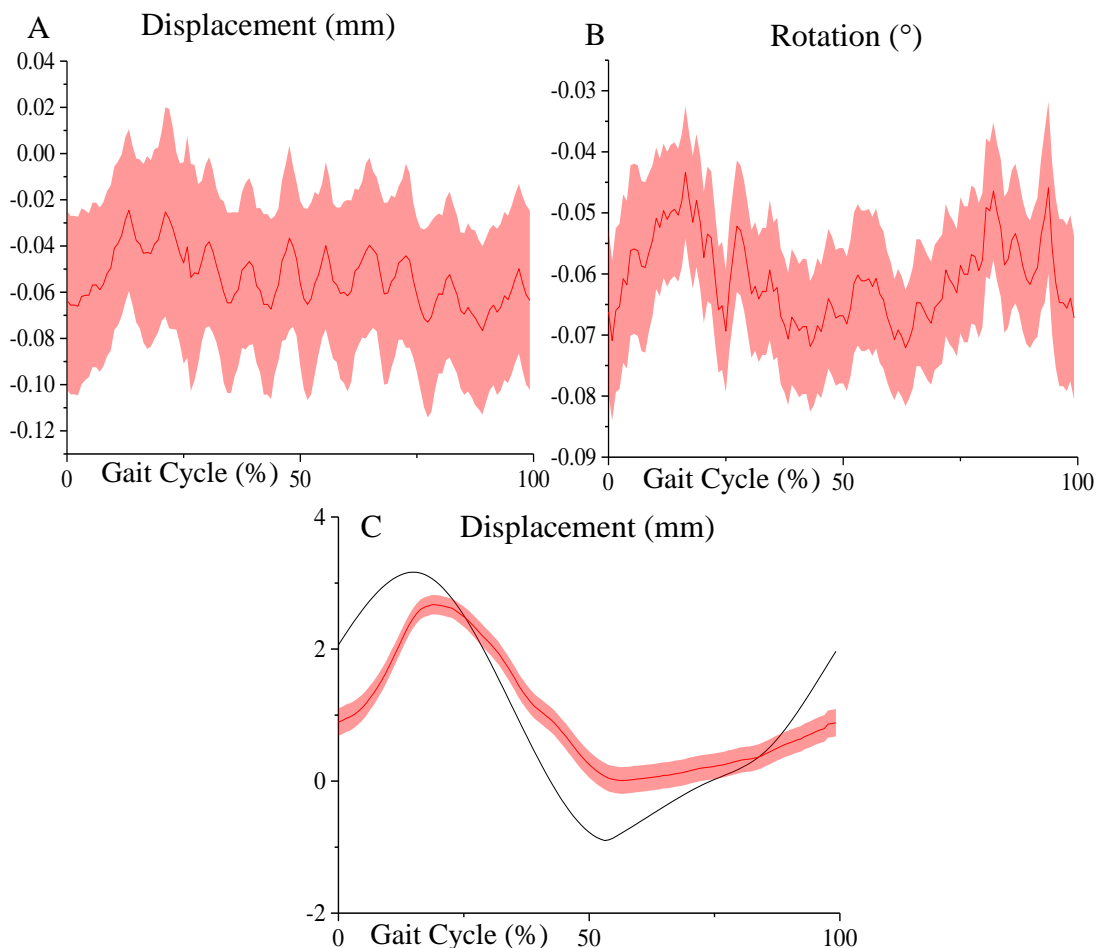


Figure 3.2 (A and B) Mean displacement and rotation profiles for the 2Mc driven to zero and (C) the input profile for the reduced AP displacement profile compared to the mean output

The simulator was not without intermittent flaws which were typically rectified within 24 hours. The AP displacement control failed at two different stations, one at the start of stage four which could not be rectified. To overcome this the components were moved to the unused station and the testing continued with all motions applied.

3.3.2 Wear results

The first test condition involved the lowest kinematic input limited to only flexion-extension with no additional AP displacement. The wear rate for this, Stage 1 was $1.16 \pm 0.55 \text{ mm}^3/\text{Mc}$ (Figure 3.3).

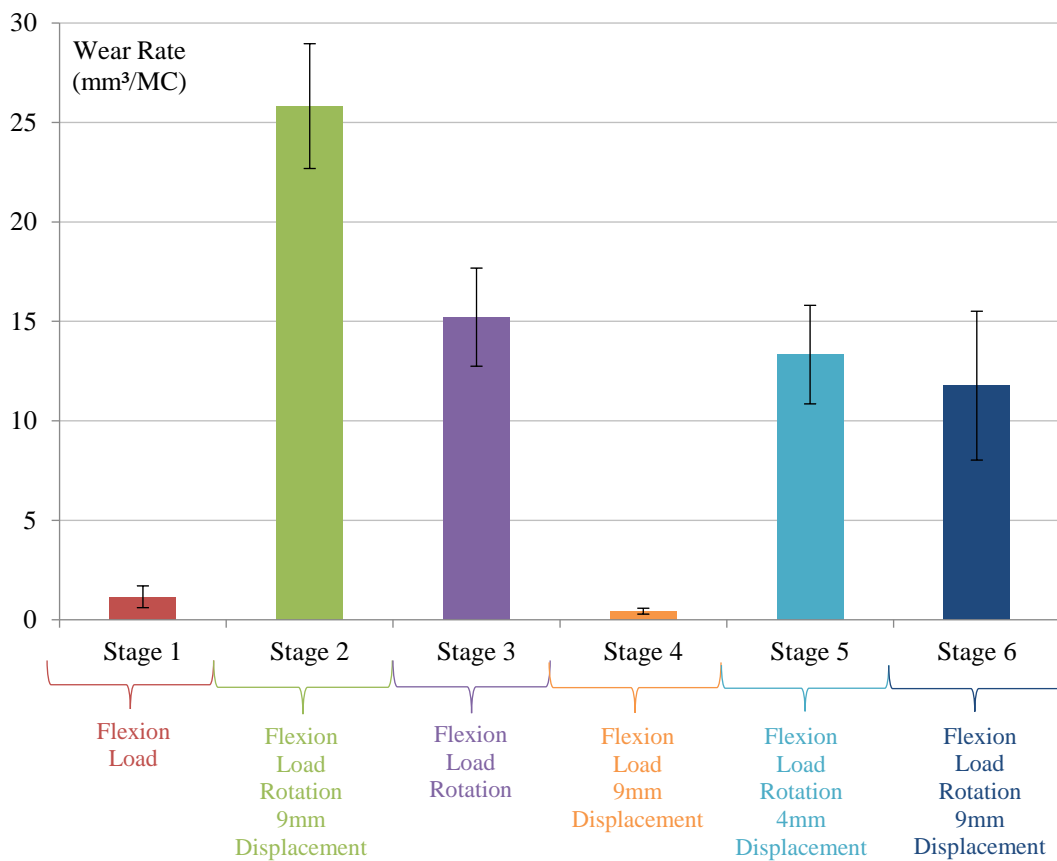


Figure 3.3 Wear rates with 95% confidence limits for each test condition

From the initial low kinematics of Stage 1 the addition of rotation and a 9mm displacement formed the highest kinematic input tested which resulted in the highest wear rate of $25.82 \pm 3.14\text{mm}^3/\text{Mc}$, significantly higher than any of the other test stages ($P < 0.001$). The testing under high kinematics damaged two of the tibial components with titanium nitride delamination uncovering visible signs of the bulk titanium (Figure 3.4). On the left-hand image, the bulk titanium base is very much visible in the centre of the component due to removal of the coating. The right-hand image the damage is not as severe but is still showing signs of the bulk titanium in a similar region.



Figure 3.4: Two tibial components which experienced visual coating damage

White light interferometry traces (Section 2.7) provided an insight into the curvature of the surface. In an anterior/posterior direction there was a similarity in the profiles observed, all concave including the unworn sample. However, this was not the same for the medial/lateral direction where prior to testing the surface was more of a convex shape (Table 3.2).

Table 3.2: Comparing medial/lateral (ML) traces for different tibial components, one worn, one unworn and two with visible coating damage. The difference in height was calculated for the profiles shown and also for the anterior/posterior (AP) profiles not presented here.

| Component | Medial/Lateral Trace | ML Depth Difference (μm) | AP Depth Difference (μm) |
|--|----------------------|---------------------------------------|---------------------------------------|
| Tibial 1-1 with visible coating damage at 4Mc | | 9 | 19 |
| Tibial 2-2 with visible coating damage at 4Mc | | 10 | 19 |
| Tibial 2-1 with no visible coating damage at 4Mc | | 3.5 | 13 |
| Tibial 2-3 unworn | | 9 | 9 |

In order to observe the surface roughness changes at the areas of degradation a higher magnification objective lens of 20x was used, a region with no visible damage was visualised alongside a region in which the coating was damaged (Figure 3.5). The areal roughness value for the undamaged worn area was 13.64 nm whereas the damaged region was five times that measuring 71.02 nm. However, the peak valley height is greater for worn region than the damaged region.

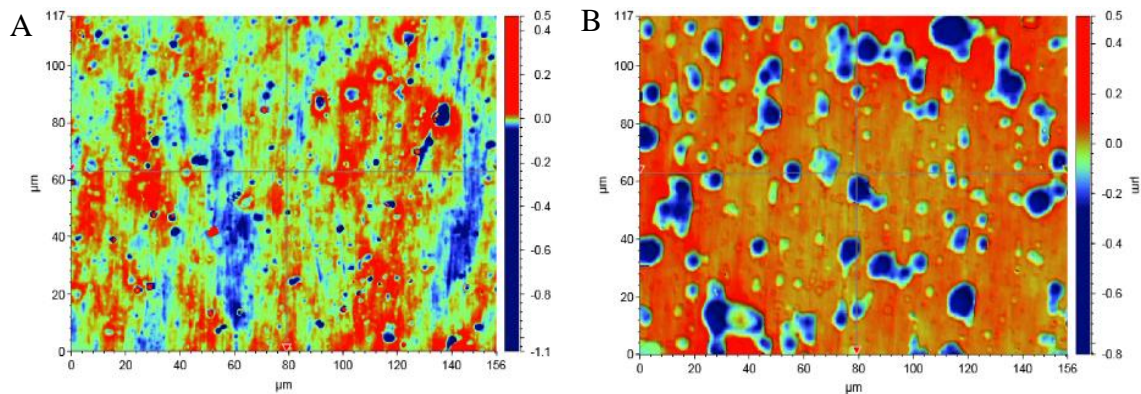


Figure 3.5 Tibial component interferometer images (A) worn surface without damage (B) damaged region

These components were replaced to ensure the coating damage did not impact the wear rates and keep the wear rate changes depended on the kinematic conditions rather than the varying changes in coating for specific tibial components. For these components there was no significant difference between the wear rates or change in surface roughness over this stage.

Stage 3 removed the displacement and with that the wear rate decreased to $15.21 \pm 2.47 \text{ mm}^3/\text{Mc}$, statistically lower than with the addition of 9mm AP ($P < 0.001$). Conversely at Stage 4 when the rotation was removed and the 9mm AP reinstated the wear rate was just $0.43 \pm 0.15 \text{ mm}^3/\text{Mc}$. This was not significantly different to Stage 1 ($P = 0.998$) despite the addition of the displacement. At Stage 5 a 4mm displacement was then implemented to create an intermediate condition between Stages 2 and 3 which resulted in a wear rate of $13.33 \pm 2.48 \text{ mm}^3/\text{Mc}$. There was no significant difference between the wear rates of Stages 3 and 5 with no displacement and 4mm respectively ($P = 0.886$). To understand whether there was a critical displacement value which elevated the wear significantly or the wear was the result of component changes over the testing time the Stage 2 conditions were

retested at Stage 6. The wear rate measured $11.77 \pm 3.74 \text{ mm}^3/\text{Mc}$, not statistically different to Stage 3 ($P=0.428$) or 5 ($P=0.961$) but significantly lower than the first time this condition was tested in Stage 2 ($P<0.05$).

3.3.3 Variation between stations

Some variation in wear rates between individual samples was observed, as demonstrated by the size of confidence limits (Figure 3.3). As the inserts moved stations (Table 3.3) there was a possibility that one station may apply more vigorous loads or motions which may affect the wear at that station. Relationships were plotted for the volumetric wear rate for both the inserts and stations each million cycle (Figure 3.6).

Table 3.3 Insert pathway around simulator stations each million cycle

| Station | 1 | 2 | 3 | 4 | 5 | 6 | 7 | 8 | 9 | 10 | 11 | 12 |
|---------|---|---|---|---|---|---|---|---|---|----|----|----|
| 1-1 | 3 | 7 | 6 | 5 | 4 | 3 | 7 | 6 | 5 | 4 | 3 | 7 |
| 1-2 | 4 | 3 | 7 | 6 | 5 | 4 | 3 | 7 | 6 | 5 | 4 | 3 |
| 1-3 | 5 | 4 | 3 | 7 | 6 | 5 | 4 | 3 | 7 | 6 | 5 | 4 |
| 2-1 | 6 | 5 | 4 | 3 | 7 | 6 | 5 | 4 | 3 | 7 | 6 | 5 |
| 2-2 | 7 | 6 | 5 | 4 | 3 | 7 | 6 | 5 | 4 | 3 | 7 | 6 |

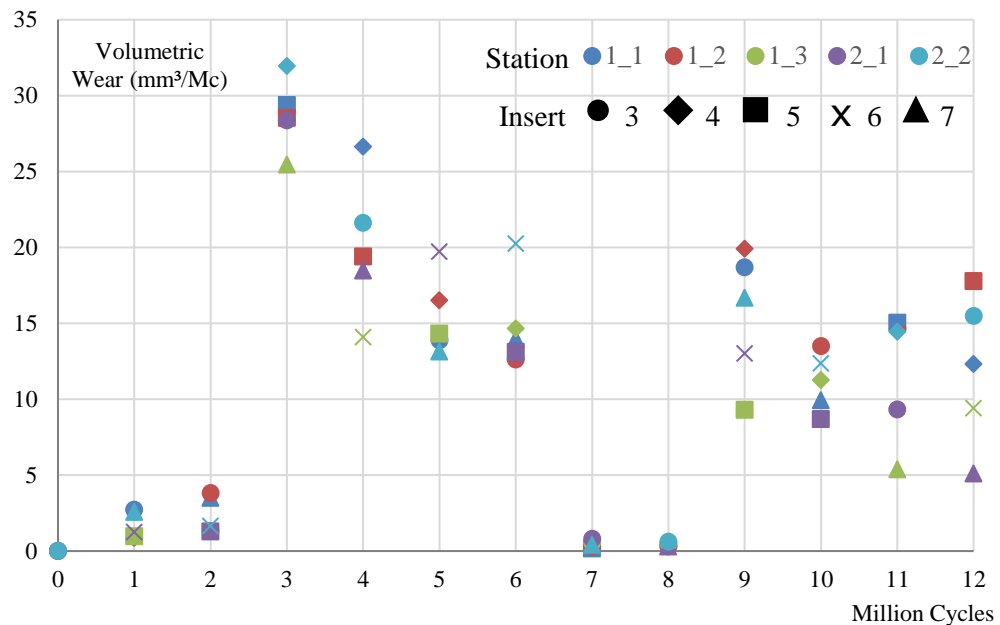


Figure 3.6 Relationships between the volumetric wear and the station and insert

In the earlier cycles the same insert experienced the highest wear rates for individual Mc; insert four during Stage 2 (3-4Mc) and insert six during stage three (5-6Mc). The same is notable for lowest wear with insert five continually low in Stage 5 (9-10Mc) and insert seven in Stage 6 (11-12Mc). Also during Stage 2 station 1-3 seemed to have a noticeably lower wear rate. To explain the cause of this disparity the rotation at individual stations during this stage was considered (Figure 3.7). This shows station 1-3 in green, to replicate the input profile least closely. At each of the peaks the output is a least 1° less than the demand. This small disparity may be enough to reduce the wear rates for both of the inserts tested in this station under the high kinematic inputs, highlighting the influence of the rotation.

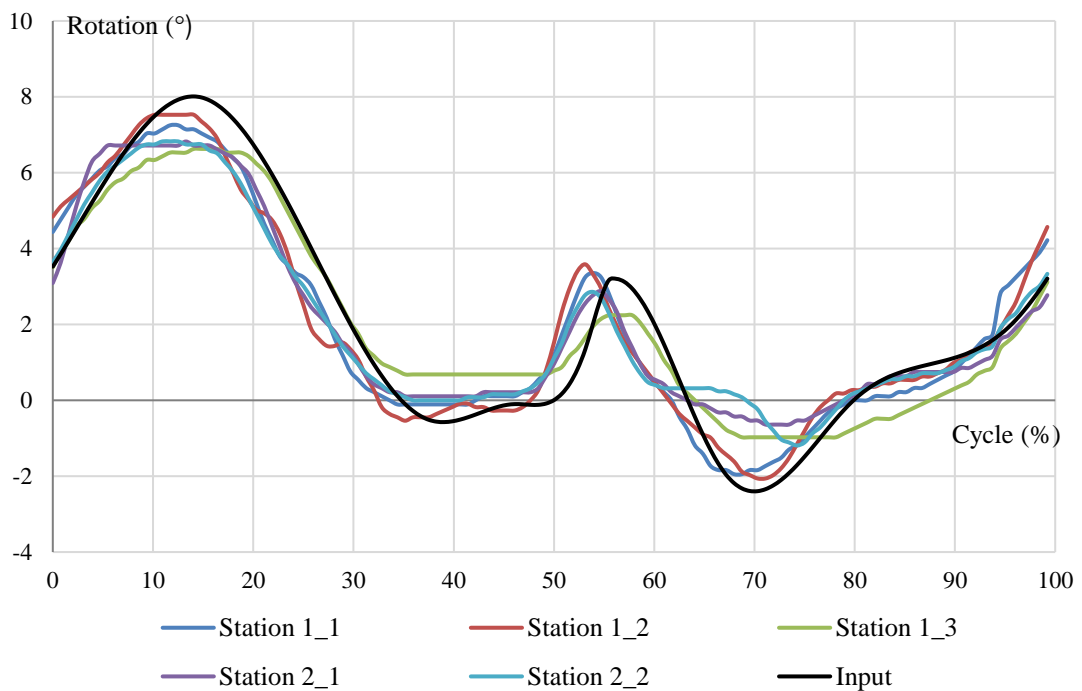


Figure 3.7 Simulator rotation outputs for Stage 2

3.3.4 Surface roughness results

Two-dimensional contact surface measurements were taken on all of the component surfaces and mean average surface roughness (R_a) values across the five samples for each articulating surface are presented in Table 3.4

Table 3.4: Mean R_a values and 95% confidence limits for the articulating surfaces with significant ($p < 0.05$) changes from previous roughness measurement highlighted by *

| Stage | Mc | Tibial R_a | Talar R_a | Superior Insert R_a | Inferior Insert R_a |
|----------|----|--|---------------------|---------------------------------------|-----------------------|
| Pre-test | 0 | 0.031 ± 0.001 | 0.126 ± 0.003 | 1.706 ± 0.043 | 1.995 ± 0.066 |
| 1 | 2 | 0.031 ± 0.002 | 0.155 ± 0.011 * | 1.343 ± 0.079 * | 1.379 ± 0.026 * |
| 2 | 4 | Worn 0.034 ± 0.005 * Damaged 0.37 ± 0.005 | 0.170 ± 0.032 * | 0.140 ± 0.037 * | 1.395 ± 0.054 |
| 3 | 6 | 0.023 ± 0.002 * | 0.169 ± 0.028 | 0.101 ± 0.023 | 1.277 ± 0.032 * |
| 4 | 8 | 0.022 ± 0.002 | 0.181 ± 0.030 | 0.189 ± 0.037 * | 1.257 ± 0.041 |
| 5 | 10 | 0.017 ± 0.002 * | 0.180 ± 0.032 | 0.080 ± 0.022 * | 1.255 ± 0.035 |
| 6 | 12 | 0.017 ± 0.002 | 0.188 ± 0.029 | 0.072 ± 0.019 | 1.259 ± 0.035 |

The most significant change in surface roughness occurred between stages one and two on the flat, superior insert surface where significant polishing resulted in a tenfold decrease from $1.343\mu\text{m}$ to $0.140\mu\text{m}$ (Table 3.4). Comparing a surface image of the pre-test superior insert surface to a photograph (Figure 3.8) the machining lines were highly visible but at the end of Stage 2 these have been worn away leaving a more overall polished surface with some scratches and pits.

At this stage there was no significant change in the measured roughness of the inferior insert surface whereas both the tibial and talar components had a significant increase albeit a relatively small change. Despite the roughness traces showing minimal changes in the measured R_a values for the rest of the components at this point there were some visible changes to the surface topography. On the tibial component there was a visible outline of the polyethylene contact area on the TiN coating (Figure 3.9). There were also obvious signs of adhesive wear within the polyethylene contact area, the radial orientation of which suggests the flat articulation facilitates any rotation applied as it was designed to. In comparison, the wear scars on the talar articulation were aligned in the anterior posterior direction with fine linear scratches visible on the TiN.

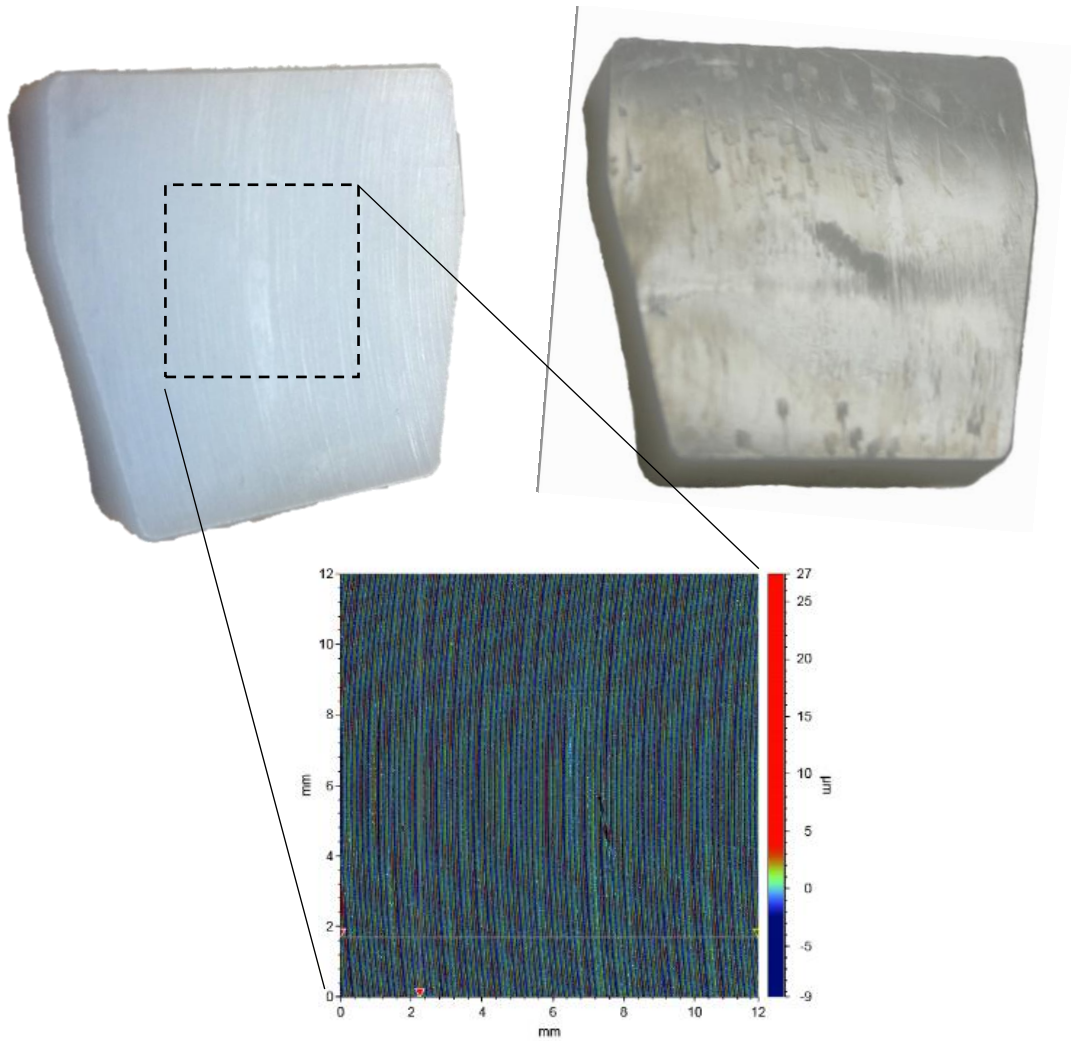


Figure 3.9 Pre-test photograph of aTAR insert and magnified NPFLEX image of the machined surface compared to a photograph of the same insert surface after 4Mc where the machining lines are no longer visible accounting for the change in surface roughness measurement



Figure 3.8 Typical component surfaces after 4Mc with insert imprint on tibial component and unidirectional scratches on the talar component

For the tibial components the most significant change in Ra was observed at stage three, this may result in some decrease in the polyethylene wear due to reduced asperity contact. Conversely, there was no significant change in the roughness measured at either the talar component or superior insert surface at the end of this stage. The mean inferior insert roughness also reduced significantly.

Following on from these earlier cycles the inferior talar articulations experienced no significant change in the roughness measurements. In contrast at the tibial articulation there was a significant reduction in Ra at both surfaces between the unidirectional kinematics of stage four and multidirectional at stage five.

At the end of the testing all of the components were in a similar condition to those presented in Figure 3.9 with an increased number of deeper scratches on the tibial component and more defined unidirectional scratches on the talar surfaces.

From the earlier component measurements in both directions (Table 3.2) there was an apparent difference between the maximum and minimum surface heights. For all of the worn components this corresponds with the images from the optical microscope (Nikon, Japan) which show a change in the surface coating where the polyethylene insert footprint lies (Figure 3.10).



Figure 3.10 Optical microscope images of the worn insert footprint compared to unworn tibial edges

This change in height varies depending on the specific component. In the anterior/posterior direction the step height increases from unworn to worn and further for both damaged tibial components. In the medial/lateral direction the unworn components are concave, this is worn down to create a more concave surface where the polyethylene footprint lies. For both damaged components, this difference is greater at approximately $10\mu\text{m}$, enough to penetrate the titanium nitride coating.

3.3.5 Wear track analysis results

Wear track analysis aided visualisation of the motions at each of the bearing interfaces. The most extreme conditions were applied and it was observed that the majority of the displacement seemed to occur at the flat, tibial bearing articulation. Within the simulator the conformity of the talus tended to keep the insert central and instead only the tibial component appeared to move with rotational motion input. With the relatively large 9mm displacement the insert was shown to experience some edge loading due to the small clearance on the tibial component. Figure 3.11 shows the edge loading occurring both anteriorly and posteriorly. However, after the initial running in period there was no significant increase in the wear rate with the addition of edge loading. Due to the continued applied motion, there was also no signs of deformations as a result of this condition.

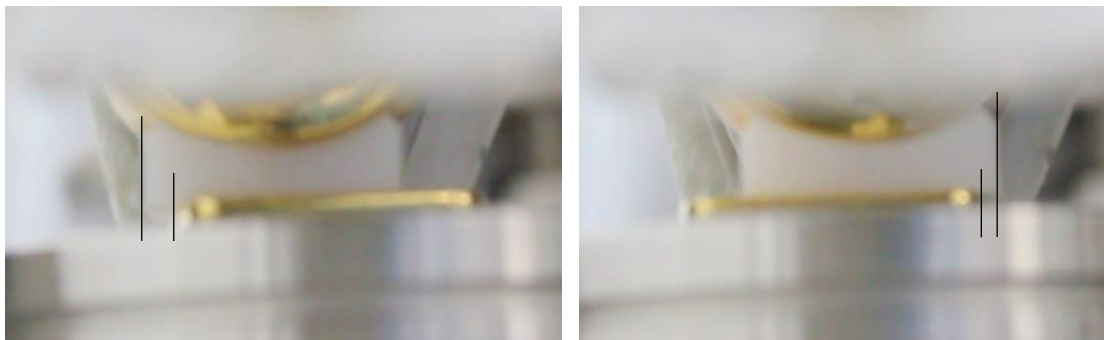


Figure 3.11 Stills from the video footage showing both posterior and anterior edge contact throughout the gait cycle

To further quantify this relationship 1mm ball bearings were embedded into the surface of two of tested inserts. The scratches were then analysed to understand where the majority of the motions were occurring within the mobile bearing (Figure 3.12).

As the simulator started up there was typically a jolt while it initialises, the effects of this are visible on the tibial component surfaces. Distinguishing between these scratches and those from the standard gait cycle proved relatively straightforward as the initialisation scratches were a single line rather than repeated as those from the gait cycle.



Figure 3.12 Scratched surfaces from wear track analysis

Under the most extreme displacement conditions it was observed that the majority of the displacement occurred at the flat bearing articulation. In this simulation, the conformity of the talus keeps the insert central and instead only the tibial component appears to move with rotational motion. With the 9mm displacement the insert experienced some edge loading due to the small clearance on the tibial component, however, after the initial running in period there was no significant increase in the wear rate with the addition of edge loading.

3.3.6 Polyethylene surfaces

The capability for comparing the existing components to retrievals was limited to those which have been collected by the existing retrieval centre at the University of Leeds. As there are no Zenith (Corin Group PLC) retrievals in our collection the simulator components were instead compared with the AES (Biomet) a similar three component design but a Cobalt Chromium on UHMWPE articulation. Due to the difference in material for the tibial and talar components the main focus of the comparison was the polyethylene surfaces (Figure 3.13)

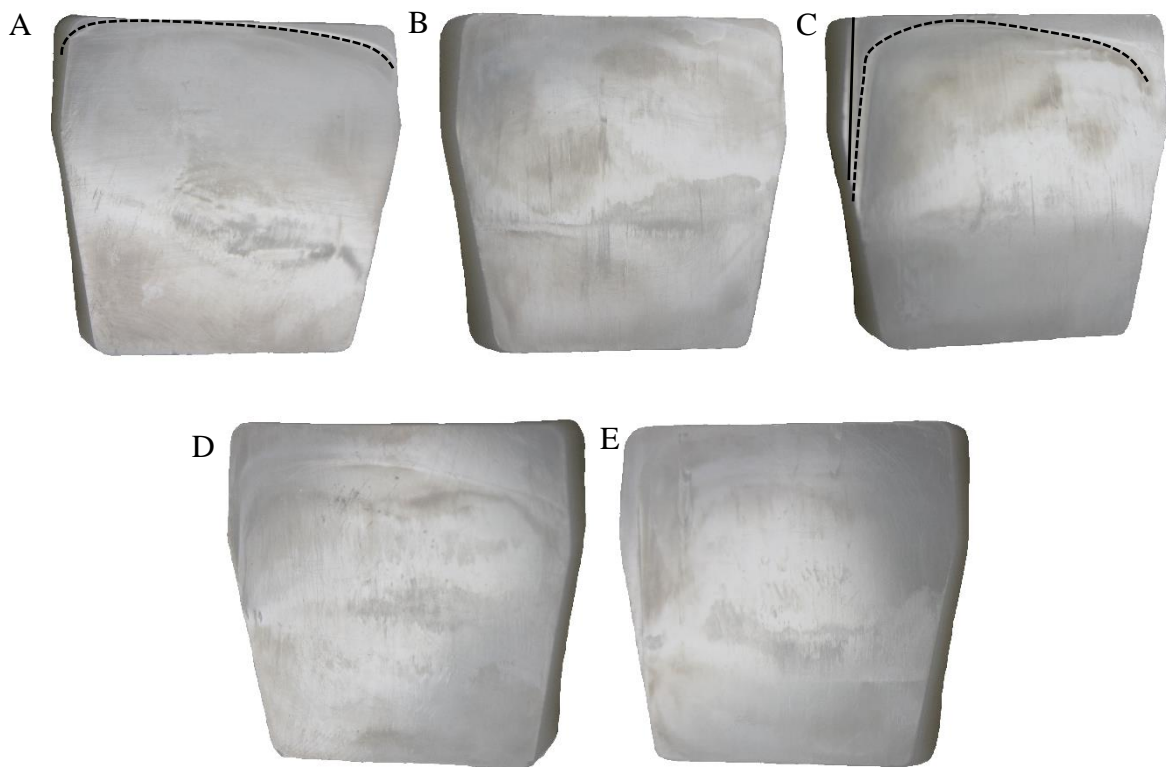


Figure 3.13 Photos of the superior insert surfaces at the end of 12Mc with edge loaded areas highlighted

It is apparent from Figure 3.13 that on some stations there was edge loading occurring. During stage three in which the displacement should have been zero, the AP displacement control failed at two different stations and the displacement went to approximately 8-10mm posterior where it was stopped by the physical stops, this affected Figure 3.13 A and C where there is some deformation and edge loading.

3.4 Discussion

The developed method provided an appropriate way to test the tribology of mobile bearing total ankle replacements under a variety of kinematic conditions.

3.4.1 The wear effects of kinematics

The most significant variations in wear rate were observed between those with constrained rotation resulting in linear wear and those with multidirectional gait inputs. Stages which were stripped back to flexion/extension with or without AP displacement (stages one and four) had significantly lower wear rates than those which allow some degree of flexion. The addition of rotation caused multidirectional motion which stopped the polyethylene from strain hardening in one direction, altering the orientation of the polyethylene fibrils and reducing its wear resistance (Wang 2001). Stages two, three, five and six all created significantly more wear with the wear rate measuring at least ten fold greater than that for the linear conditions.

The multidirectional kinematics of stage two resulted in the most dramatic decrease in mean surface roughness of the superior, flat insert surface rather than the simple flexion of stage one. Following this the changes in surface roughness thereafter are minimal, although not insignificant. After the significant change in superior insert surface roughness after four million cycles, three AP conditions were tested; 0mm, 4mm and 9mm repeated to understand the changes. From the results, it can be concluded that after the initial run in period the magnitude of the displacement does not have a significant effect on the volumetric wear rate for the polyethylene inserts. Although there were further significant changes in the surface roughness measurements which may have had some effect on the resulting wear rate the magnitude of these changes was not as large. Considering the average volumetric wear each Mc there was less variability across the two Mc of the latter stages compared to stage two (Figure 3.14). A portion of this variability may also correspond with the transition from unidirectional kinematics to a multidirectional gait input. Moving from stage one to two and again from stage four to five there is an increased wear rate for the first Mc. Potentially the result of the unidirectional alignment of the UHMWPE fibrils being disrupted due to rotation.

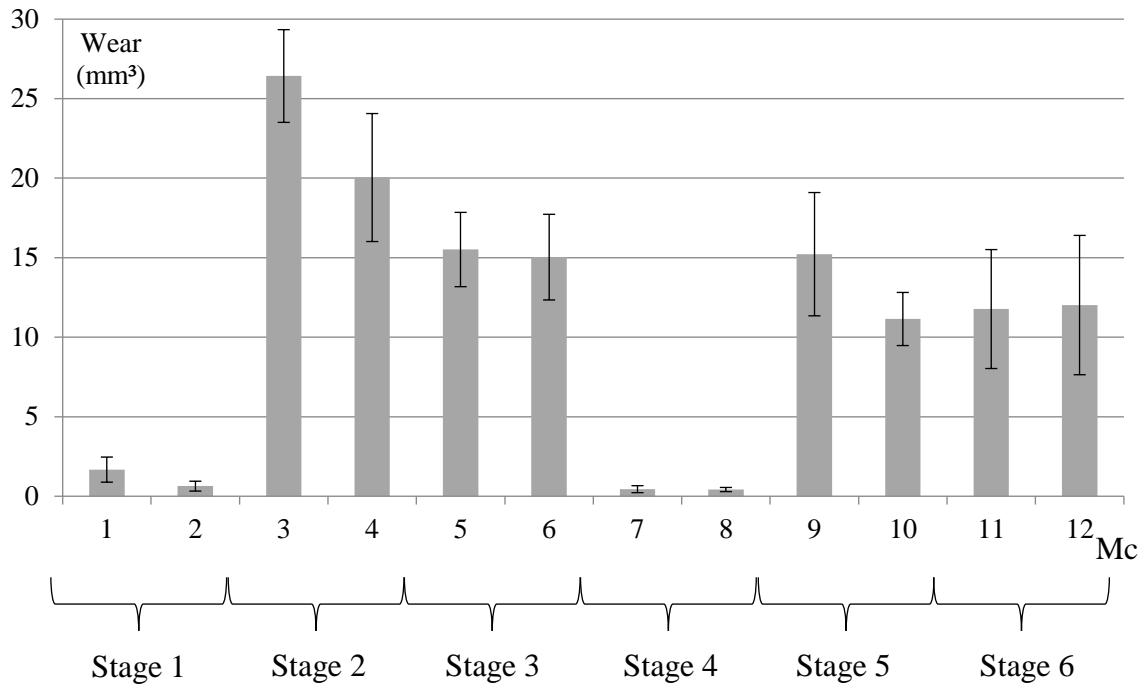


Figure 3.14 Volumetric wear for n=5 inserts per million cycles

These findings partially follow the same trend of those published by McEwan et al who in testing fixed total knee replacements found halving the rotation from ± 5 degrees to ± 2.5 degrees reduced the wear rate from $9.8 \pm 3.7 \text{ mm}^3/\text{Mc}$ to $3.9 \pm 2.9 \text{ mm}^3/\text{Mc}$ showing the magnitude of the rotation to have a significant effect just as in this study. The reduced kinematics are attributed to having reduced the cross-shear effects and allowing some strain hardening which will improve the wear rates, this effect will not be as significant as in this test as a degree of rotational motion was still present. However, the effect of displacement on the wear rate of the tested knee was also significant reducing the high kinematic wear rate from $16 \pm 4.0 \text{ mm}^3/\text{Mc}$ to $9.8 \pm 3.7 \text{ mm}^3/\text{Mc}$ when the displacement was halved due to the reduced sliding distance and the surface area being worn. The displacement trend observed by McEwan et al. (2005) is very different to what was experienced in the latter stages of the TAR testing where there was no significant difference in the wear rate for the selected conditions. This is a possible result of the mobile nature of the bearing allowing the increased sliding distance and thus sliding velocity which has been associated with improved lubrication and lower wear, such a relationship could potentially counteract the effects of the higher kinematics. However, the effect of the sliding distance has also been shown to have much less of an effect on polyethylene wear rate than surface roughness (Fisher et al. 1994).

It is possible the early changes in surface roughness resulted in the initial reduction of wear and the local kinematics at the tibial surface were not affected by the higher displacement inputs. Brockett et al. (2016) showed increasing displacement to significantly increase the wear rate for TKR tested under distal centre of rotation but not with the ISO centre of rotation for the same design. This highlights that the relationships is less straightforward than that of rotation. Additionally, D'Lima et al. (2001) found 25% greater loads in combination with doubled rotational and displacement kinematics to increase the wear rate of total knee replacements (TKR) from 3.1 ± 1.2 mg/Mc to 7.4 ± 2.7 mg/Mc, the equivalent to doubling. It is difficult to isolate from this where the increase in wear stemmed from. Whether it is the result of the combination of the increased displacement, rotation and load or if like the TAR in this study where one motion, in this case rotation plays a bigger role while the rest see no significant difference.

3.4.2 Comparing wear rates

The polyethylene wear rates for the three component TAR under multidirectional kinematics were comparable to the range measured from similar simulator testing of conventional polyethylene against metal in hip and knee replacements with respective ranges of approximately 10-80mm³/Mc (Affatato et al. 2007) and 2-20mm³/Mc (D'Lima et al. 2001; Johnson et al. 2003; McEwen et al. 2005; Schwenke et al. 2005) Such magnitudes are similar to those associated with wear debris mediated osteolysis and have been found by previous authors to be in a similar size range (Reinders et al. 2015).

Although relatively few TAR wear studies have been carried out previously the results of those which have been published are presented in Table 3.5. The many variations in the test protocols and device materials make it difficult to compare the individual wear rates directly, however, they do provide a useful benchmark. The wear results for this study were similar to the results presented by Bell & Fisher (2007), Affatato et al. (2007), Bischoff et al. (2015) and Reinders et al. (2015) although some of these wear rates have such sample variability that they lack confidence.

Table 3.5: Comparative ankle wear rates with similar 3/4mm AP

| Author | Constraint | TAR Device | Wear Rate (mm ³ /Mc) |
|------------------------|------------------|-------------------------------|---------------------------------|
| Smyth et al. (2017) | Unconstrained | Corin Zenith | 13.3 ± 2.5 |
| Bell & Fisher (2007) | Unconstrained | Buechel Pappas | 16.4 ± 17.4 |
| Bell & Fisher (2007) | Unconstrained | DePuy Mobility | 10.4 ± 14.7 |
| Reinders et al. (2015) | Unconstrained | Integra Hintegra | 18.2 ± 1.4 |
| Affatato et al. (2007) | Unconstrained | MatOrtho BOX | 19.9 ± 22.5 |
| Bischoff et al. (2015) | Semi-Constrained | Zimmer Trabecular Metal (CPE) | 8.0 ± 1.4 |
| Bischoff et al. (2015) | Semi-Constrained | Zimmer Trabecular Metal (XPE) | 2.1 ± 0.3 |

The most apparent difference in wear rate comes with the addition of highly cross-linked UHMWPE (XPE), reducing the wear rate to just 2.1 ± 0.3 mm³/Mc. Cross-linking eliminates the free radicals improving the material properties, it has a proven track record in reducing the measured wear rate *in-vitro* for both total hip and knee replacements (Muratoglu et al. 2001, 2004). This has been reflected in the THR clinical results with significantly reduced penetration and wear rates at 10 years compared to conventional polyethylene (Glyn-Jones et al. 2015), but the benefits of this on survival rates beyond 10 years are still to be determined. It must be remembered that alongside the wear benefits crosslinking can heighten the risk of fatigue failure due to reduced toughness (Baker et al. 1999), a trade-off which must be considered for each joint and bearing design individually. Within the simulator this material configuration in combination with the constrained nature of the Zimmer trabecular metal TAR presented substantially lower wear rates than the rest of the tested devices including the conventional polyethylene two component equivalent (Bischoff et al. 2015). However, the clinical performance of XPE in this design TAR has not yet been documented and currently no mobile bearing TARs have made the move towards XPE. Another notable difference between the tested designs is the tibial and talar component materials, only the Buechel-Pappas constitutes of the same materials as the Corin Zenith and was tested under similar conditions, yet there is no notable difference between these devices and the cobalt chromium designs.

In general, the semi-constrained two component TARs reported lower wear rates compared to the mobile-bearing alternatives in spite of the specific polyethylene. While aiming to reduce shear forces through minimal constraints, mobile bearing designs also aimed to split the ankle motions across two surfaces as has been shown to reduce wear in mobile bearing TKR when compared to a fixed bearing design (McEwen et al. 2005). However, instead of decoupling the motions so that only unidirectional motion occurs at each surface the unconstrained surface facilitates a range of both rotation and displacement which may otherwise be limited by the constraints of the fixed bearing design (Figure 3.15).

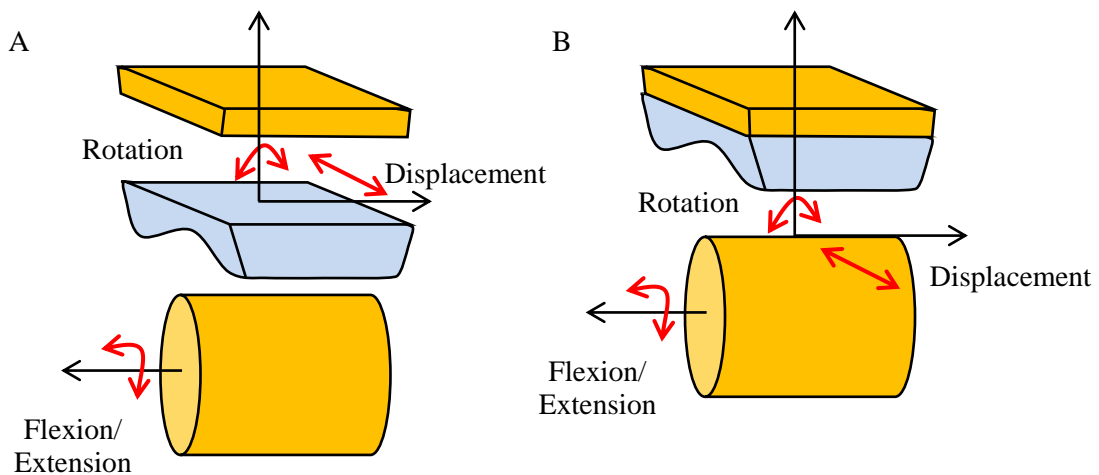


Figure 3.15 Kinematics in (A) mobile bearing and (B) fixed TARs

The use of displacement control ensured that the displacements applied to each station were of a similar magnitude although there was some inter-station variability due to the pneumatic control system. It allowed the input parameters to be changed by known amounts and simulated. Other studies have used force controlled simulation across joint replacement (Reinders et al. 2015), this is considered by some researchers to be the more physiological method of simulator control. As this research question was addressing the effects of kinematics on the wear rate, displacement control was the most reliable driving mechanism for this simulator investigation. Through wear testing of TKRs, the difference between force controlled and displacement controlled simulation has been explored. Implementation of the relevant ISO profiles; ISO 14243-1 and 14243-3 for force and displacement control respectively, has shown significantly lower wear when testing in displacement control (Schwenke et al. 2009) however this is due to integral differences in the input profiles. Whereas, comparing this study to that by

Reinders et al. (2015) the profiles were in phase with peak rotation and displacement occurring at the same time point in the loading which has resulted in similar wear rates. There were however, variations amongst the test conditions applied. Both Affatato et al. (2007) and Reinders et al. (2015) applied reduced loads of 2.57 and 2.32 times body weight respectively, almost half that applied by this study and by Kincaid (2013) and Bell and Fisher (2007). This change is not identifiable in the wear rate alone which may support the idea that the wear rate is not proportional to the load as the relationship between load and contact area is not linear (Liu et al. 2011). However, there are too many other differences between the simulations for this to be the only factor.

3.4.3 Comparing to retrievals

Retrieval TARs have been collected and studied at the University of Leeds (Stratton-Powell et al. 2016). Although there are no Zenith, titanium nitride coated TARs in the collection at present these examples of other three component mobile bearing TARs show similar wear scars and damage modes to those simulated *in-vitro* (Figure 3.16). The comparison between the tested components and the retrievals is limited for a number of reasons. The *in-vivo* components will have been subjected to a wider range of motion due to the activities of daily living and the potential return to higher impact activities. In contrast, the *in-vitro* tested inserts, whilst undergoing a variety of kinematic conditions, these were to simulate the motions of walking gait to varying degrees. On all of the simulator tibial components there is a visual imprint from the polyethylene articulation, this imprint is the likely result of adhesive wear from the insert. A similar imprint is visible on the retrievals after multidirectional kinematics were applied (Figure 3.16). This is somewhat similar to the stippling effect that has been observed on tibial base plates of fixed bearing TKR thought to be a result of rotation occurring due to inadequate locking mechanism (Naudie et al. 2007).

| | Tibial | Superior Insert |
|--|---|--|
| Biomet AES Retrieval |  |  |
| Corin Zenith <i>in-vitro</i> simulation |  |  |
| Intergra Hintegra Retrieval |  |  |

Figure 3.16 Wear tested surfaces of the Zenith tibial articulation compared to that of two mobile bearing retrievals

The most common difference between simulator and retrieval wear scars is the addition of third body wear particles such as cortical bone or titanium particles which can amplify the abrasive wear (Davidson et al. 1994). The TAR retrievals were no exception with prominent signs of deeper scratching from abrasive wear at the tibial articulation of the inserts as a result of third body wear in the biological environment. In both the retrievals and the *in-vitro* tested samples the machining lines have been worn away and there is strong evidence of burnishing.

3.5 Limitations

As with any investigation which involves *in-vitro* simulation of a human environment this study had limitations. These ranged from the input parameters to the test rig itself.

3.5.1 Gait inputs

While the lack of *in-vitro* test standards defined the need for this study to investigate the effects of specific inputs on the wear rate that also meant relying heavily on existing ankle gait literature. Gait input profiles depended on historic force data calculated for healthy individuals. However, instrumented implants in knees have shown this to overestimate the axial loads (Zhao et al. 2007). Based on the Archard wear law which described the proportional relationship between volumetric wear and load alongside sliding distance (Archard et al. 1956) it is possible the wear simulation is also overestimating the wear rate. However, this investigation considered the wear rate relative to the kinematics the applied force remained the same and thus was less critical. Similarly, there was a lot of variation across literature for each of the kinematic profile inputs and compromises between conflicting sources had to be made, however this research has provided a way to define the inputs with greatest influence.

3.5.2 Simulator

For conditions with no rotation or displacement these inputs were driven to zero. Initially this proved to be beyond the capacity of the simulator in combination with the high axial loads, this caused the circuit to break and the simulator to stop within the first number of cycles. In order to overcome this limitation of the equipment the number of samples was reduced to five and a dummy placed in the final station of the simulator which helped the simulator facilitate the required input.

There were some limitations in using the pneumatic simulator over a prolonged period. Short term failure of the rotational and AP displacement axes drivers resulted in periods where the ideal gait input was not being applied on individual stations and some insert deformation. Due to daily simulator checks these problems were always corrected by readjusting the airflow tuning within 24 hours. In order to use a conventional knee simulator the TAR had to be inverted so the flexion could be applied about the constant radius of the talar component. Although a standard method in the limited displacement controlled TAR wear tests (Affatato et al. 2007; Bell et al. 2007; Bischoff et al. 2015) this may alter the biomechanics. Similarly, inverted simulators have been accepted for hip replacement testing as it is assumed to maintain lubrication of the surfaces, however there were concerns about debris remaining between the counter faces. These issues were less pertinent for the TAR due to the constituent three components of the tested design.

3.5.3 Test protocol

The in-vitro test method eliminated the presence of third body debris and effects from surrounding tissues and aimed for optimal component alignment. In testing the same components sequentially under a variety of kinematic conditions the results will depend on the surface changes which have occurred prior to that stage therefore they are not strictly independent. This was certainly the case after the initial polishing of the components in the bedding in stages. By repeating the initial high AP displacement condition at the end of the investigation and routinely measuring the surface roughness at the end of each stage these effects can be understood. The simulation was performed at room temperature which resulted in an average capsule temperature of 30°Celsius. It has been suggest that for hip replacement simulation it should be ensured the environment measures 37 ± 2 °Celsius to represent body temperature (Affatato et al. 2008) However, Palmieri et al. (2006) measured temperatures at the ankle surface to be 29.6 ± 3.0 °Celsius compared to the core temperature of 36.4 ± 1.4 °Celsius so room temperature was deemed an appropriate approximation as the serum temperature measured an average of 30.4 °Celsius during testing. All tests were carried out in 25% bovine serum, a lubricant accepted to create a pseudo-synovial fluid *in-vitro* wear testing, providing clinically relevant wear rates and wear debris (Biggs et al. 1997;

Besong et al. 1999). It was assumed that, as for other joints, bovine serum would provide an approximation to the ankle joint synovial fluid, similar polyethylene adhesion observed between the retrievals and *in-vitro* tested inserts backed this up. However, there were no retrieval Zenith components within the collection to confirm the trend follows that of the cobalt chromium designs.

A further limitation of the test methodology was the reliance of gravimetric wear as the only method of wear quantification. Some of the effects of serum absorption were accounted for through the soak control, however as these inserts were not under load this may not be fully comprehensive. Loaded soak controls in THR have shown to have a fluid uptake of approximately 2mg/Mc (Bragdon et al. 1996) for the ankle unloaded soak this was typically an order of magnitude less. However, given the volume of polyethylene and surface area it is unlikely this would be comparable to a polyethylene cup for a hip. Quantifying this from weight measurements the volume of a Zenith insert is approximately 6cm³, compared to 18cm³ for a DePuySynthes 36mm UHMWPE cup. For a THR cup Smith & Unsworth (1999) found the fluid absorption of the loaded soak to be no more than 1mg greater than the unloaded soak. The real benefits of loaded soak controls come for geometric measurements as these allow the creep effects to be quantified, for gravimetric measurement this is not critical. As the process of correcting for fluid absorption for unloaded inserts was constant across the tested conditions this method can be considered robust enough for comparison. Due to the fully conforming nature of the TAR insert the use of typical surface mapping techniques using coordinate measurement machines were not appropriate. The existing methods rely heavily on calculating the surface change relative to the unworn portions of surfaces which equates to volumetric wear. As both the anterior and superior surface are bearing surfaces there is no unworn datum. Additionally, the sides of the insert will also be influenced by creep deformation. Obtaining the necessary resolution through micro CT measurement proved unsuccessful.

In removing the two tibial components which experienced coating damage from the test it was ensured this had no effect on the relationship between the kinematic conditions and wear. As stipulated in the design drawing the TiN coating should have had a thickness of 4 μm within a tolerance of 1 μm . Table 3.2 showed the majority of the surface of the worn but undamaged component to lie within a height of $\sim 2.5\mu\text{m}$ in the medial/lateral direction. For both of the coating damaged components this was more like $\sim 6\mu\text{m}$, exceeding the thickness of the coating. Failure of the TiN surfaces on two of the tibial components is a concern, TiN failure in hip replacements has been associated with adverse effects clinically. Teresa Raimondi et al. (2000) highlighted potential outcomes such as the release of both TiN fragments and debris from the titanium substrate into the surrounding area alongside an increase in the measured roughness of the femoral head which would increase the wear of the other articulating surface. In this case there was no significant difference ($P=0.474$) between the polyethylene wear rate for the two stations with damaged coatings compared with those with intact TiN surfaces for the stage when the coating damage occurred.

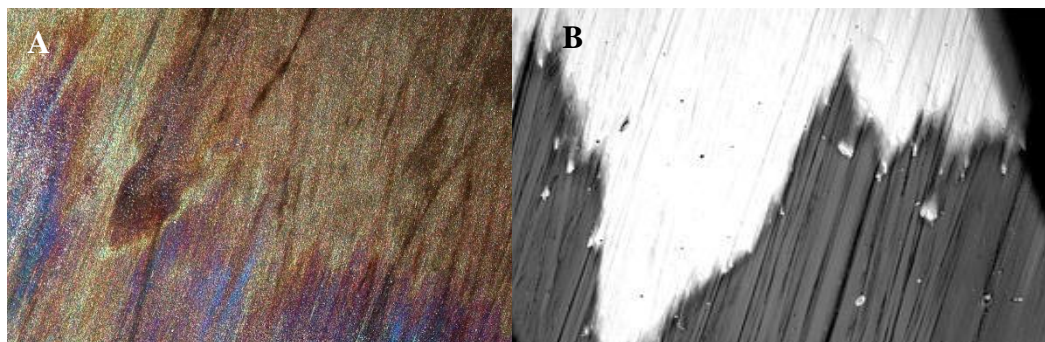


Figure 3.17 Similar titanium nitride damage observed in (A) the damaged TAR tibial component and (B) a TKR retrieval. Figure from: Fabry et al. (2017) High wear resistance of femoral components coated with titanium nitride: a retrieval analysis. *Knee Surg Sports Traumatol Arthrosc.*

In an analysis of TiN TKR retrievals, Fabry et al. (2017) found three of the 25 investigated components had signs of “coating breakthrough”, two of which were a result of metal on metal contact with a patella resurfacing resulting in irregular, rough coating damage. The third, however, was also in the patella region but in contact with natural tissue which showed similar smooth coating damage to that

observed in the TAR (Figure 3.17). Due to the location of the “coating breakthrough” it was not considered to be the reason for failure for these TKRs.

3.6 Conclusion

This study has established a method and furthered the understanding of the effects of the kinematic inputs in mobile bearing TAR devices which in future will allow us to test other device designs under a range of adverse conditions. Inputs which have the greatest influence on wear have been highlighted and thus should aim to be the most physiologically relevant.

Within the altered knee simulator, the Corin Zenith total ankle replacement (TAR) was able to perform the large kinematic range of motions implemented. The wear test demonstrated there was a significant running in period for the inserts which creates a high level of polyethylene wear. After the initial effects of this during the first four million cycles, the components were tested under three displacement conditions and one without rotation. For the latter displacement conditions the magnitude of the displacement had no significant effect on the polyethylene wear rate. Without rotation, the wear rate was an order of ten lower, this parameter should be considered vital for realistic wear testing. The wear results were comparable to those previously published for unconstrained TARs and a similar magnitude to the only semi constrained design tested. With increasing implant lifetimes *in-vivo*, wear rates of this magnitude may pose the risk of wear debris induced osteolysis a historic problem from hip and knee replacements.

Although multiple limitations have been highlighted the majority of these follow the typical limitations of *in-vitro* wear testing or have been accounted for in the fact it is the relationships between kinematic inputs and wear rates which were of most importance rather than the finite wear rates themselves.

CHAPTER 4
VALIDATION WEAR TEST

CHAPTER 4

VALIDATION WEAR TEST

4.1 Introduction

In the commissioning process for new simulators the testing convention was to compare the wear rate from the new simulator to that of an existing simulator (Barnett et al. 2002; Brandt et al. 2011) . By ensuring the same design of components were tested and similar kinematic inputs were implemented the expectation was to produce repeatable wear rates, with no significant difference due to the test simulator used. Wear scars have also been used to validate the kinematic performance (Barnett et al. 2002).

As the simulator used initially was decommissioned a change in simulator to a more recent pneumatic simulator, Leeds Knee Simulator IV (KS4) was required. Although this simulator was not new and had previously been validated for total knee replacements it had not been used for total ankle replacement (TAR) gait inputs prior to this test. Due to the high demands of the TAR kinematic profiles wear rates from KS4 had to be validated against the results from the Leeds Knee Simulator I (KS1).

Previous TAR testing (Chapter 3) showed high polyethylene wear rates for the first million cycles (Mc) under multidirectional kinematics. It was decided that in order to fully validate the simulator the TAR components should be tested for multiple millions of cycles to extend the study beyond this bedding-in phase.

4.2 Materials

Six Corin Zenith total ankle replacements (Table 4.1) with 5mm insert thickness were tested in the Leeds pneumatic multi-station Knee Simulator IV (KS4).

Table 4.1 Bearing details

| Bearing | Talar | Tibial | Insert |
|--------------|-----------------------------|-----------------------------|--------------------|
| Corin Zenith | 283119 / 298112 500.1003 | 287288 / 298111 503.1003 | 309126 506.1053 |

4.2.1 The Simulator

For this study, Leeds Knee Simulator IV (KS4) was set up to test six Corin Zenith total ankle replacements (TARs), one more than had been possible in the previous wear test. Similarly to the previous simulator (KS1), KS4 also consisted of six stations divided across two banks (Figure 4.1) and the components were set up in the inverted position. In order to carry out the validation test some of the existing knee replacement tibial component holders and top plates were used. To facilitate the change in height and zero position of the flexion/extension (FE) cradle six new delrin fixtures were designed and manufactured to ensure the talar component articulated about the centre of rotation (Appendix B). As in KS1 a steel ring was added to lift the height of the tibial component so that the anatomically inferior articulating (experimentally superior) surface of the polyethylene surface was aligned with that of the abduction cradle as it had been in the initial wear test.



Figure 4.1 Three stations of KS4 filled with serum

4.2.2 Simulator calibration

The calibration process varied in this simulator compared to KS1. A load cell was fixed between the FE cradle and a delrin block. As the simulator applied increasing loads the actual force as measured from the load cell was recorded. The simulator had more recent control software enabled the forces to be input directly into the calibration file. Bespoke fixtures also allowed the rotation and AP displacement to be calibrated more robustly at 5° or 5mm increments respectively (Figure 4.2). The motor positions at each of these known orientations were recorded and used to derive the relevant calibration constants. This process ensured the simulator outputs were a representation of the actual displacements and loads.



Figure 4.2 KS4 load and rotation/displacement calibration set up

4.2.3 Simulator kinetics and kinematics

The effect of displacement had no significant effect on the wear of TARs (Chapter 3.3.2) so it was decided that an input profile with a total of 4mm anterior/posterior displacement (Figure 4.3) would be the best input. This value is larger than the 1.5mm which has been measured for TARs (Leszko et al. 2008). However, it is similar to the 3.5mm maximum displacement for TARs observed by Conti et al. (2006) but less than the computational displacement published by Reggiani et al. (2006).

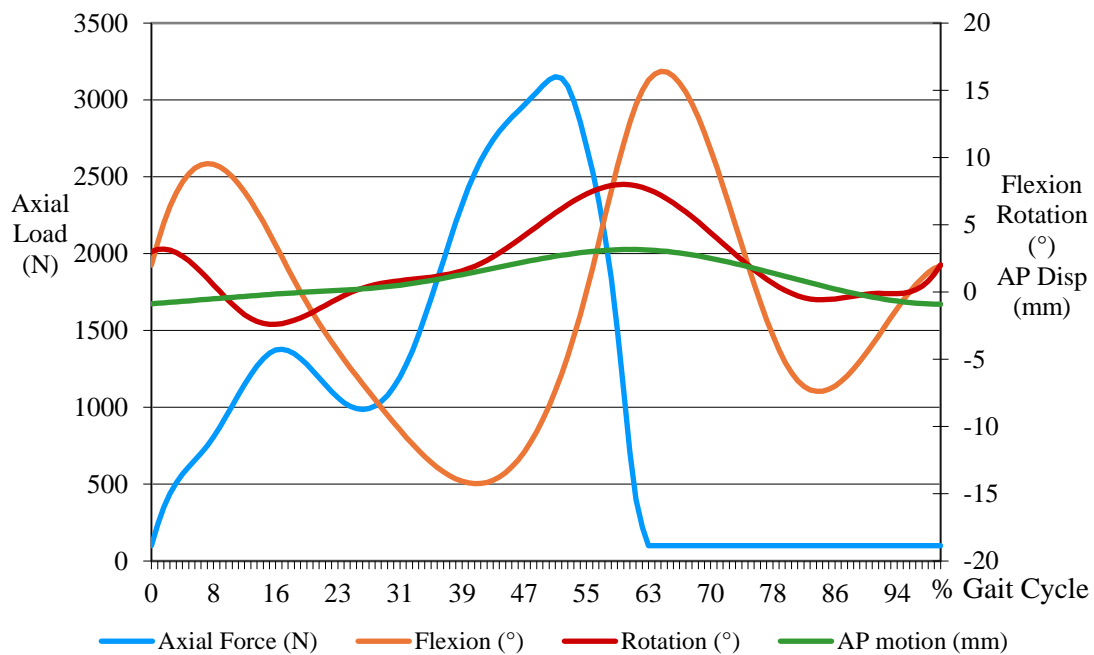


Figure 4.3 Ankle kinematics to be implemented in KS4

4.3 Methods

Three million cycles (Mc) were carried out on six TARs under defined test conditions in a 25% bovine serum, 0.3% Sodium Azide solution. The serum was changed every 0.33Mc and the wear was measured gravimetrically, as previously described, every Mcs. Two unloaded soak controls were used to compensate for any fluid uptake. Every Mc the components were moved along a station and contact area checks were carried out to ensure similar component positioning across the stations (Figure 4.4). After two MCs and at the end of the three Mcs of testing the same contact PGI800 Talysuf (Taylor Hobson, Leicester, UK) surface roughness measurements were taken to understand the topographical changes occurring. A one way ANOVA post-hoc Tukey test was used to compare the significance of the wear rates to the results from KS1. Wear scars were compared from photographs of worn components and similarities to TARs collected through the Leeds retrieval bank were also investigated (Stratton-Powell et al. 2016).

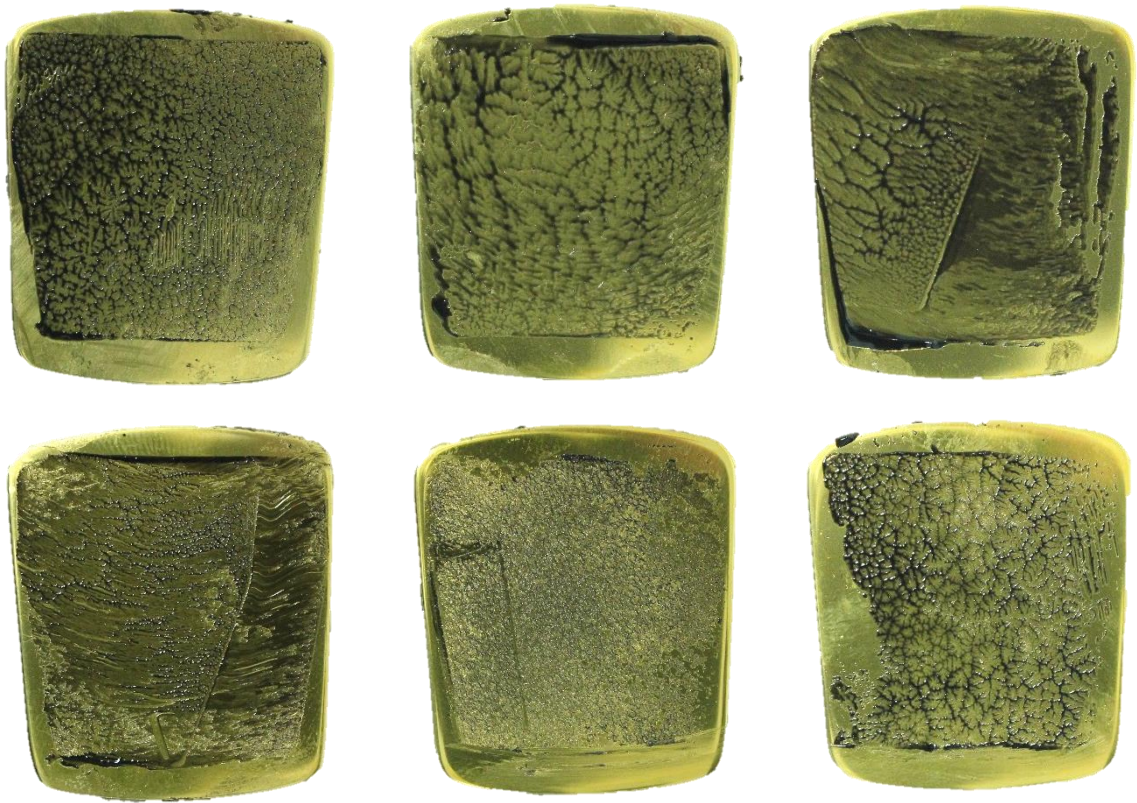
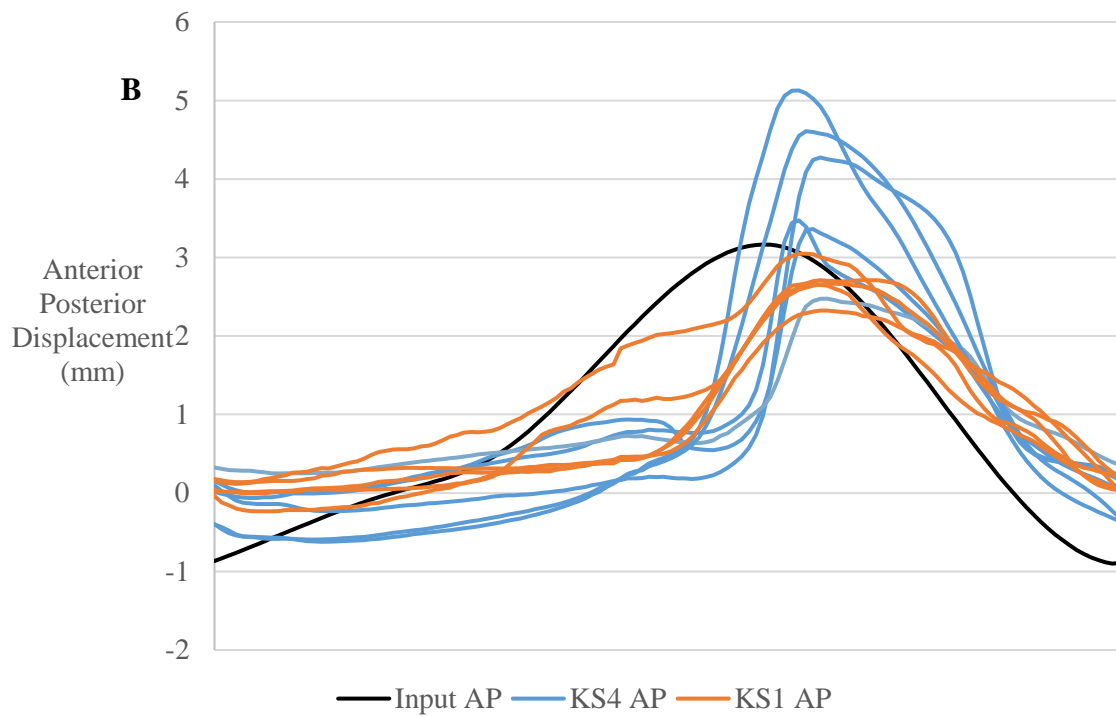
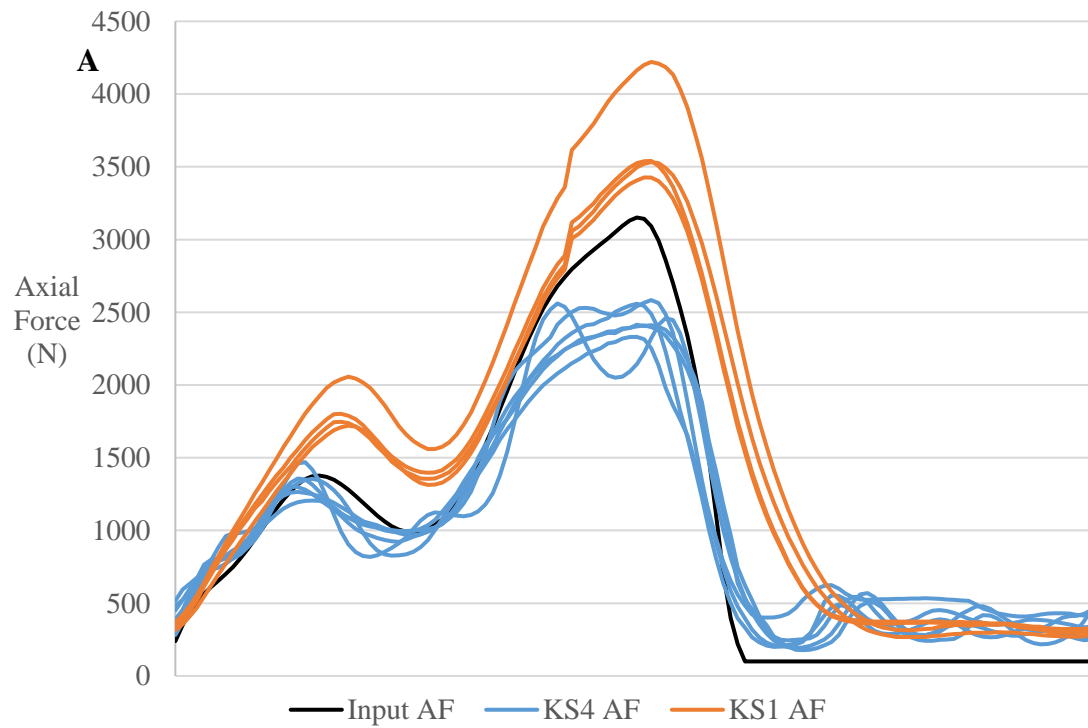


Figure 4.4 Contact areas after set up in KS4 showing the central alignment of polyethylene insert imprint on tibial components

4.4 Results

4.4.1 Simulator comparison

In order to understand how the simulators differ the kinematics between the early simulator (KS1) and KS4 to be used for the future testing were compared. With KS1 the gait outputs were recorded manually on a daily basis whereas this process was automated on KS4 to record one cycle every 20,000. These profiles were averaged for the length of the 2Mc and 3Mc stages for KS1 and KS4 respectively and plotted (Figure 4.5).



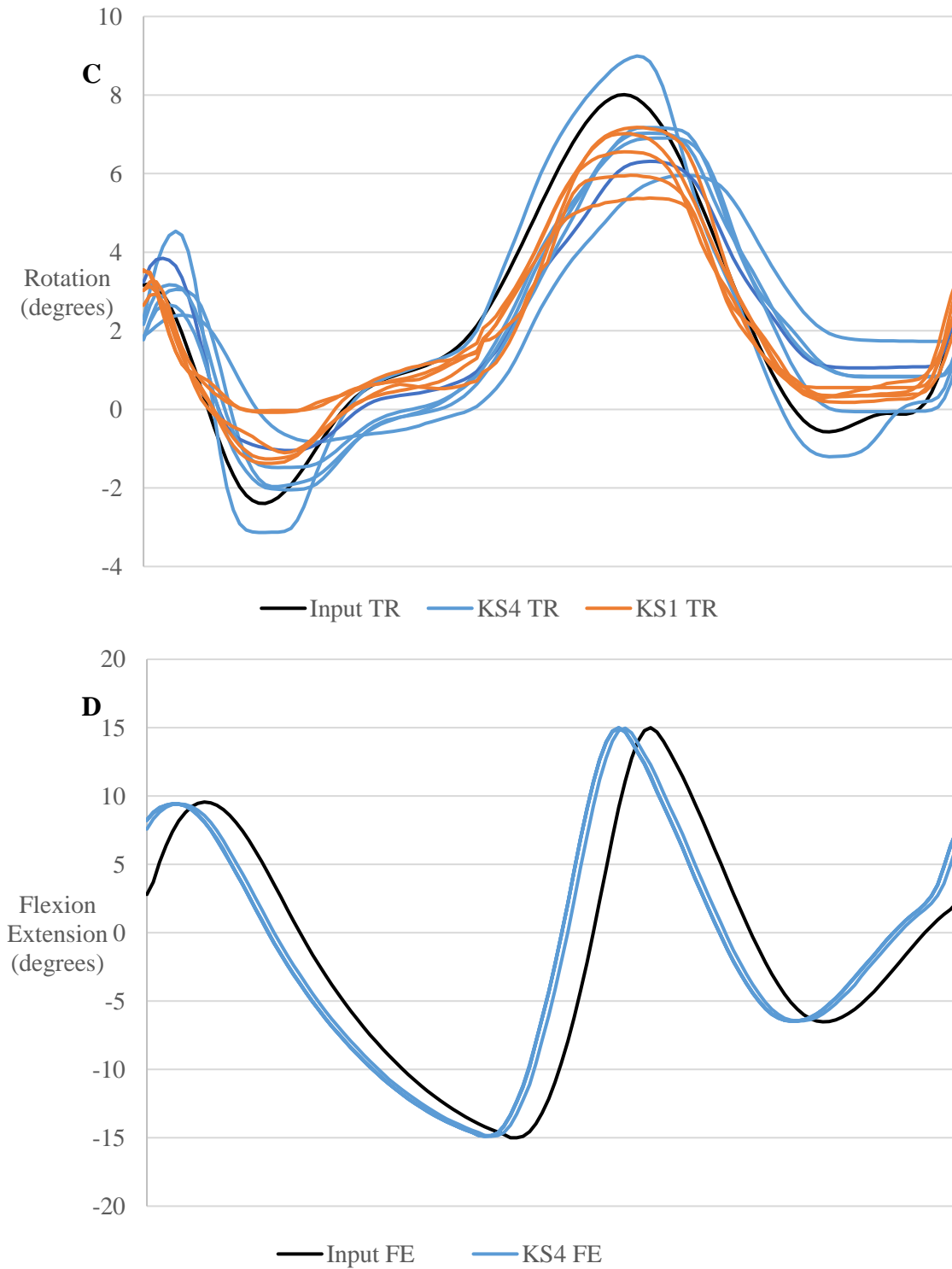


Figure 4.5 The input profile (black) and output profiles for each station of KS4 (blue) and KS1 (orange) for **A**: axial force (AF), **B**: anterior/posterior displacement (AP), **C**: rotation (TR) and **D**: flexion/ extension (FE)

There was visible variation between the simulators. This was especially apparent in the axial loading (Figure 4.5A). KS1 generally overloaded for peak forces compared to the desired input profile whereas KS4 underperformed. Both simulators were unable to facilitate the desired swing phase load of 100N, instead the force remained around 300N. For one station in KS4 (station 6) this was higher again measuring around 500N. This force remained constant for KS1 but was less stable in KS4 with some oscillation on all stations.

Balancing the AP displacement in the simulators was a continual challenge. Both simulators had a phase lag in peak AP displacement so that this occurred just after the peak load rather than in phase with it (Figure 4.5B). Three of the six stations on KS4 put the TAR through greater AP displacement than the demand requested.

The rotation profile was much more similar between the simulators with both pneumatic simulators typically underachieving on the maximum rotation angle but within a boundary of approximately 2 degrees (Figure 4.5C). Station one of KS4 was the only one to over perform on the maximum degree of rotation. There was a phase lead of around 0.05 seconds between the demand profile and the simulator output for all of stations. As this is this is leading the input this may be the result of a problem with the simulator data logging.

KS1 did not have the capacity to record the flexion/extension angle so this cannot be compared between simulators. However, relative to the input profile there was a 0.05 second phase lag throughout the gait cycle, in this instance the flexion was preceding the input (Figure 4.5D). Aside from this the variation between stations was negligible.

4.4.2 Wear results

The gravimetric wear measurements were separated into two groups, an initial bedding in million and the mean wear rate for the following two Mc. This was compared to the wear rates from KS1 at the most relevant stages (Figure 4.6).

The wear rate of the first Mc in KS4 measured 31.20 ± 5.35 mm³/Mc (Figure 4.6). This was not significantly different to the wear rate for the first Mc under multidirectional kinematics in KS1 ($p=0.306$). The kinematic inputs for these

simulators were different as the first multidirectional wear stage on KS1 consisted of a 9mm AP displacement input whereas in KS4 it was reduced to 4mm. After the initial Mc the wear rate reduced significantly to $18.90 \pm 2.42 \text{ mm}^3/\text{Mc}$ ($p=0.001$). This followed the same bedding in trend discussed in chapter 3. There was also no significant difference between the wear rates from the following two Mc under the same kinematic conditions in both simulators ($p<0.001$).

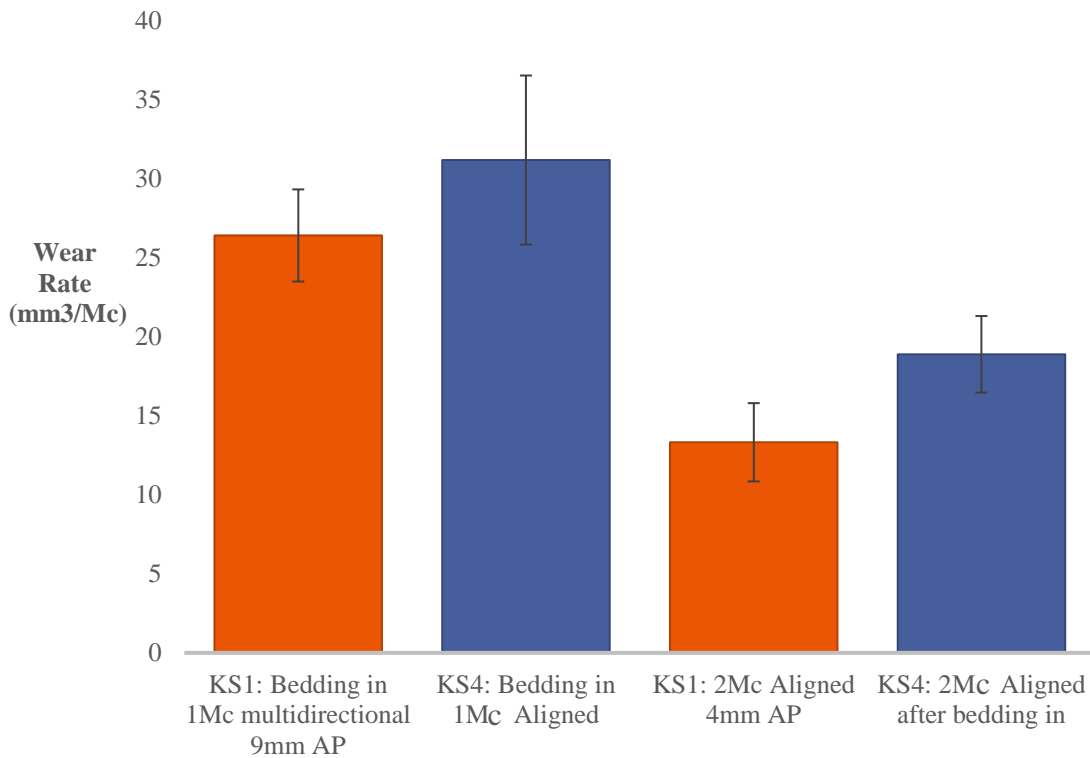


Figure 4.6 Gravimetric wear rate measured in the validation of KS4 (orange) compared to the wear rate under similar conditions for KS1 (blue)

By considering the individual insert wear rates relative to the simulator station in which they were tested (Figure 4.7) the impact of highlighted inter-station kinematic variations could be considered.

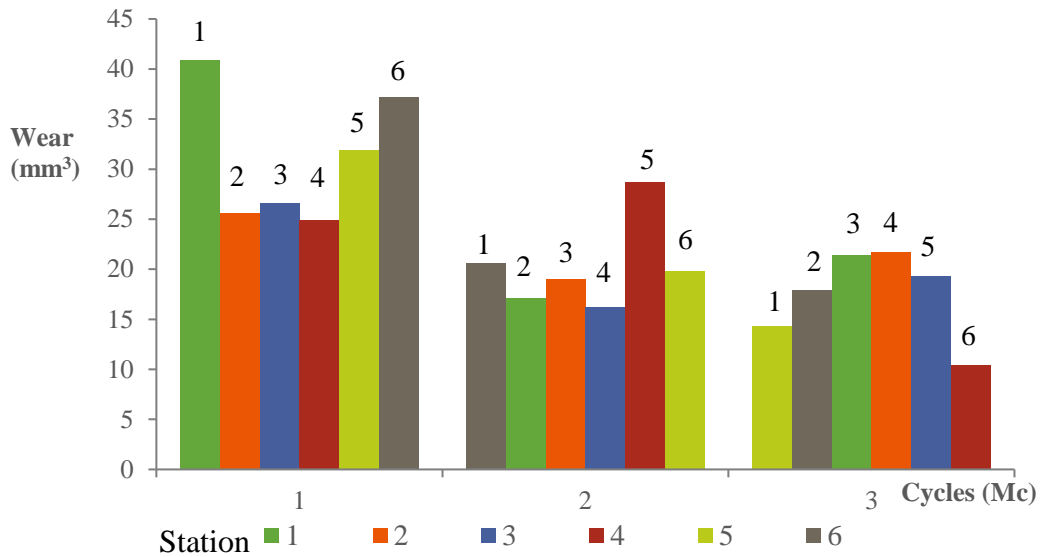


Figure 4.7 Wear rates for each individual insert from 1 to 6 for each Mc with the colours representing the simulator station

Initially the wear rates on stations one and six wear noticeably higher but this effect did not continue. Station one was the station which exhibited the highest rotation which may have affected the wear rate but this effect was not sustained throughout the further two Mcs. To ensure this was not the result of a change in rotation the input profiles were broken down into individual millions and no notable change between the dotted, dashed and full lines was observed (Figure 4.8).

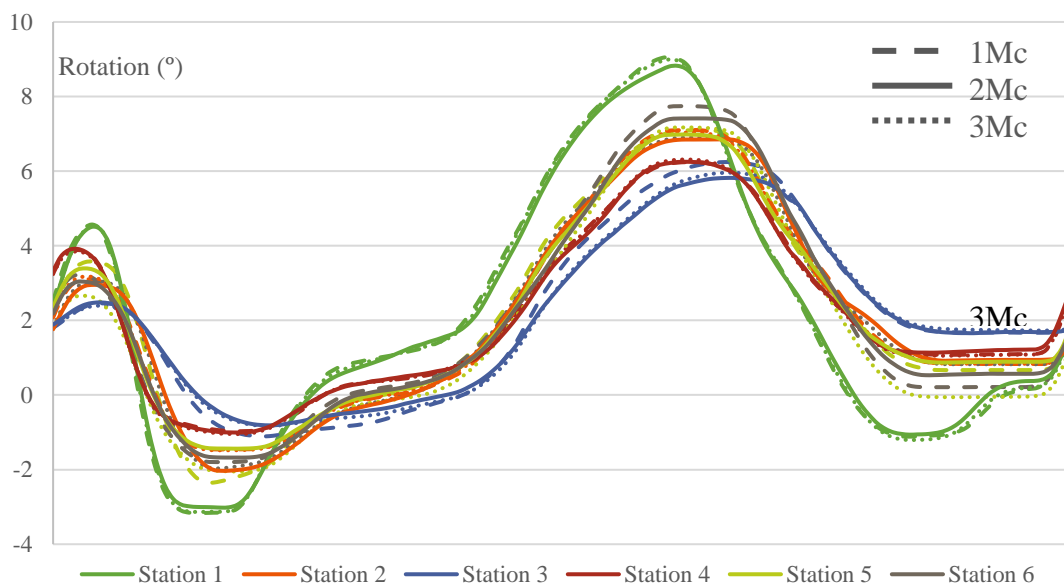


Figure 4.8 Rotation across stations of KS4 for each of the individual Mcs

4.4.3 Roughness results

Roughness measurements were taken prior to testing, after the first two Mc and again at the end of the validation period after the third stage (Table 4.2). There was a notable reduction in roughness for the polyethylene. Both medial and lateral insert curves reduced in surface roughness (Ra) by almost 60% while the flat superior insert surface was even lower with 86% reduction. This change suggests an indication that the peaks are flattening. On both of these surfaces the continued articulation caused the removal of machining lines and the polishing of the surface known as burnishing. The titanium nitride surface of the tibial component saw the measured roughness almost halved while in contrast there was a minimal observable change observed on the talar component. Compared to the initial surface polishing the change from 2Mc to 3Mc was minimal with the largest observed change for the tibial component.

Table 4.2 Average surface roughness for each component and 95% confidence limits alongside the percentage change in roughness between the stages

| | | 1Mc | | | 2Mc | | | 3Mc | | |
|----------|-----------------|-----------------|-----------------|-----------------|-----------------|-----------------|-----------------|-----------------|-----------------|-----------------|
| Ra (µm) | | centre | medial | lateral | centre | medial | lateral | centre | medial | lateral |
| Average | Talar | 0.111 ±0.009 | 0.038 ±0.003 | 0.035 ±0.003 | 0.119 ±0.006 | 0.038 ±0.003 | 0.045 ±0.005 | 0.124 ±0.009 | 0.042 ±0.004 | 0.048 ±0.005 |
| | Inferior Insert | 2.295 ±0.067 | 1.871 ±0.106 | 1.729 ±0.078 | 1.616 ±0.066 | 0.780 ±0.117 | 0.725 ±0.085 | 1.479 ±0.160 | 0.773 ±0.111 | 0.749 ±0.086 |
| | Superior Insert | 0.819±0.05 | | | 0.119±0.033 | | | 0.116±0.030 | | |
| | Tibial | 0.031±0.001 | | | 0.024±0.002 | | | 0.020±0.002 | | |
| | | | | | 1Mc → 2Mc | | | 2Mc → 3Mc | | |
| % Change | Talar | - | - | - | 6.7 | 0 | 22.2 | 4.1 | 10.9 | 8.0 |
| | Inferior Insert | - | - | - | -29.6 | -58.3 | -58.1 | -8.5 | -0.9 | 3.3 |
| | Superior Insert | | | | 15.3 | | | -16.3 | | |
| | Tibial | | | | -10.8 | | | -6.9 | | |

4.4.4 Comparing Wear Scars

It is important that as well as similar wear rates between the simulators the components display comparable wear scars. Figure 4.9 shows photographs from the tibial component and superior insert surfaces from KS1 after two Mc

unidirectional motion followed by two Mc multidirectional kinematics alongside the components tested in KS4 after an equivalent two Mc multidirectional wear.

Generally the components appear visually similar. There were, however, some notable differences. The imprint of the polyethylene component was more prominent across the KS1 components, Figure 4.9 shows the most prominent difference. This was likely a result of the initial stage of solely flexion and loading which will have kept the motion at this interface minimal. There is evidence of polyethylene transfer on both tibial components and scratches in similar directions. The insert surfaces show signs of burnishing and scratching. These were prominent in the anterior/posterior direction on the KS1 component whereas the equivalent from KS4 were more radial.

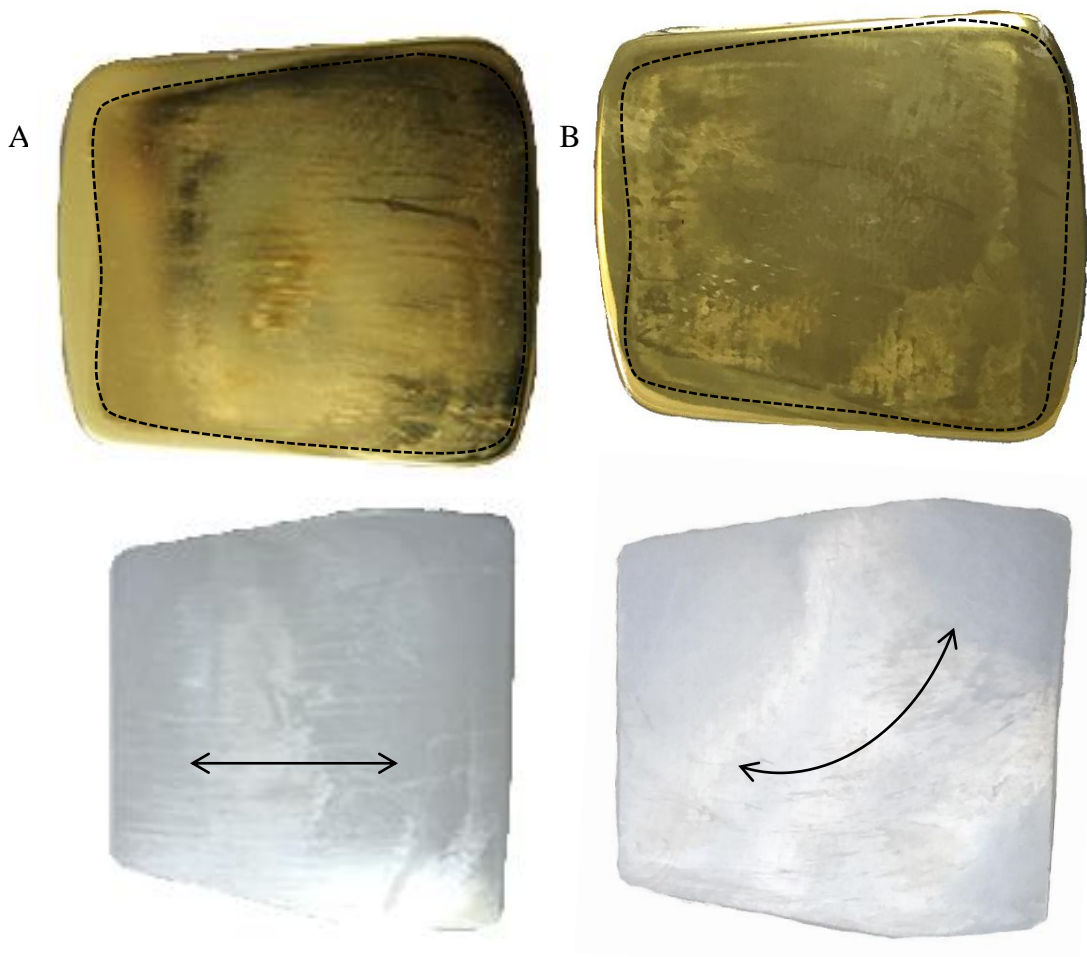


Figure 4.9 Comparing wear scars from (A) KS1 and (B) KS4

Two of the KS4 inserts also exhibited a less polished central region after two Mc (Figure 4.10). This phenomenon was not observed on any of the inserts in KS1 despite similar conditions. However, this has been observed on a number of retrieved components, providing confidence in the wear simulation.

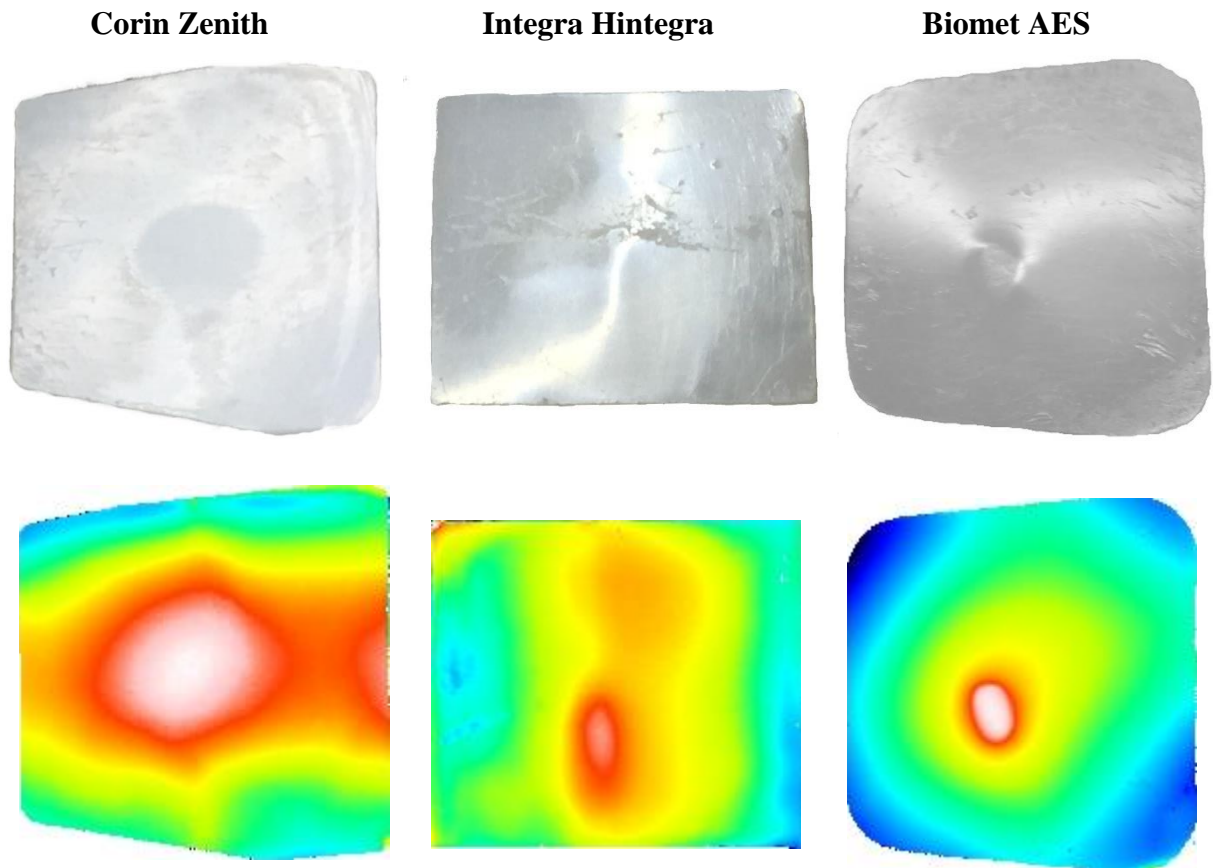


Figure 4.10 Worn inserts with less polished, raised central region visually compares to retrievals from two different TAR designs

4.5 Discussion

It is standard practice to validate a change in simulator by carrying out wear tests under comparable test conditions and comparing wear rates while observing the relevant kinematic differences. In this case the wear rates in the bedding in Mc and two Mc under equivalent input gait conditions were not significantly different between the simulators. However, the trend showed wear rates from KS4 were generally higher.

There were obvious differences between the kinematics applied from both simulators. The higher loads and lower AP displacement of KS1 compared to KS4

are likely to create some inconsistencies between the wear simulations. The reduced maximum load applied by KS4, an average of 2.48kN, the equivalent of 3.6 times body weight is a limitation of the experimental equipment. However this brings this simulation closer in line with the experimental inputs of Reinders et al. (2015) who opted for a 2.6 times body weight, (1890N peak force) arguing it to be more realistic than that of the historic force calculations.

The roughness values were somewhat comparable to the measured Ra values in KS1, presented in Chapter 3.3.4. However, the pretest roughness of the KS1 superior insert surfaces measured an average of 1.681 μm compared to only 0.843 μm for this set of tested components. Both such measurements are within the 2 μm maximum Ra manufacturing tolerance specified for this component. After undergoing multidirectional wear kinematic conditions these initial machined rough surfaces were polished to similar roughnesses of 0.140 μm and 0.119 μm respectively. In this case the pretest, unworn tibial surface of the components tested in KS4 had comparable surface roughness to the KS1 samples. At the first measurement interval this reduced to 0.024 μm but because two of the components in the KS1 test were removed from the test at the end of the first multidirectional stage this was more comparable to the measured roughness after the following stage of 0.023 μm . For both wear simulations the talar component roughness observed the least change and the inferior insert saw an initial reduction in roughness but minimal change subsequently.

Comparing the wear scars is complicated as both sets of components have undergone different kinematic conditions. The conforming nature of the anatomically inferior articulation of the talar component meant there were no observable differences between these components on both simulators. In contrast the superior tibial articulation demonstrated more of the effect of the different kinematic conditions. Despite this the similarities were especially apparent on the tibial components with some variation between the superior insert surfaces. However, as well as similarities between the simulator wear scars it is also important that the results are physiologically relevant. Comparing the in-vitro results to that of explanted TAR retrievals provided confidence that the simulation was replicating the natural environment to a large extent.

4.6 Conclusion

Although there were some apparent differences in the simulators this has not resulted in significantly different wear rates. The similarities to retrievals provided assurance that this simulator in combination with the kinematic inputs defined in Chapter 2 will provide a reliable TAR wear simulator.

CHAPTER 5
MALALIGNMENT BIOMECHANICS

CHAPTER 5

MALALIGNMENT BIOMECHANICS

5.1 Introduction

Malalignment is one of the many complications associated with total ankle replacements (TARs). This can be the result of surgical technique in implanting the device, failure to correct existing natural varus/valgus malalignment, ligament laxity or further degeneration of the hindfoot (Bonasia et al. 2010; Queen et al. 2013; Usuelli et al. 2016). It can occur in any plane (Figure 5.1). Malalignment of a TAR is suspected to be present in as many as 45% of patients (Usuelli et al. 2016).



Figure 5.1 Examples of TAR malalignment measured from x-rays collected from TAR retrieval patients at Chapel Allerton Hospital Leeds (HRA ethics ref: 09/H1307/60)

Alignment is critical to ensure optimal transmission of forces. Component malalignment may alter the joint mechanics often resulting in edge loading of the component, deformity, higher stresses, increased wear and potentially higher failure rates (Conti & Wong 2001; Bonasia et al. 2010; Mann et al. 2011; Uselli et al. 2016). A link between component malpositioning and occurrence of arthrofibrosis has also been observed (Hintermann et al. 2013). In general good alignment is considered to be instrumental for long term success (Frigg et al. 2010).

Hintermann et al. (2013) found malpositioning of components to be the direct cause for revision in 5% while osseous problems as a result of varus or valgus malalignment made up a further 14%. Wood & Deakin (2003) refer to this component malalignment as “edge-loading” and found this problem in just nine of 200 TARs analysed. One third of these required no further treatment, a further third needed surgery to correct the complication and the final third required fusion or revision suggesting that the severity of the problem varies across individuals.

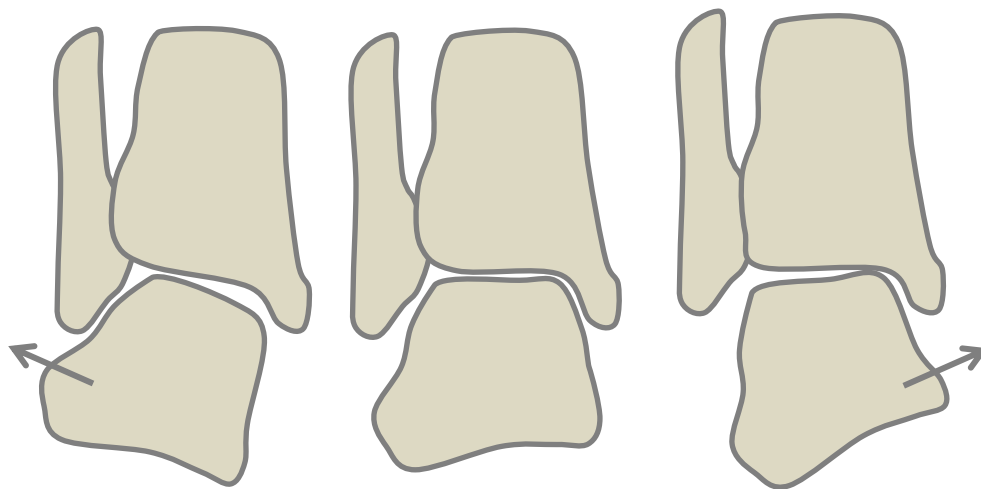


Figure 5.2 Posterior view of ankle valgus, neutral and varus alignments

Mann et al. (2011) assessed the post-operative alignment of a cohort of 84 STAR ankle replacements to find that in the coronal plane only 11% of tibial components were considered to be neutrally aligned. Of the rest 74% were in varus alignment in a range of 1-10 degrees while the other 15% in valgus alignment of 1-5 degrees with averages of 3.9° and 1.8° respectively (Figure 5.2). In the sagittal plane 96% of the tibial components were measured to be positioned at an average of 4.0° of dorsiflexion. However Hintermann et al. (2013) defined only malalignment of

greater than 5° from the physiological loading axis to be “clinically important misalignment”. Similarly looking at the talar component 78% of those were in varus alignment which suggests often the components are aligned with each other just not with the anatomic loading axis of the tibial (Mann et al. 2011).

There is a difference between the malalignment being observed at one component or both so they are aligned with each other but not the joint axis, which will affect the joint mechanics. Mann et al. (2011) found 25% of the patients with preoperative coronal plane deformity ended up with a coronal plane malalignment greater than 2° between the tibial and talar components post- operatively. Given that 43% of the cohort had a preoperative coronal deformity this may affect a substantial number of TARs patients. A third of these had to be revised to fusion yet no correlation was observed between failure and the degree of coronal malalignment. Only 2% of the investigated cohort developed a “prosthetic malalignment” without prior coronal plane deformities, presumably instead a result of surgical error. Koivu et al. (2017) specifically observed coronal incongruence between the components in eleven of the 35 patient cohort followed up, at almost one third this could be considered frequent. Morgan et al. (2010) refer to this coronal malalignment between components as “edge-loading” and observed it in 10 out of 45 patients followed up. Kim et al. (2016) also reported on talar subsidence resulting in a prosthetic malalignment of 20° resulting in the need for revision (Figure 5.3).

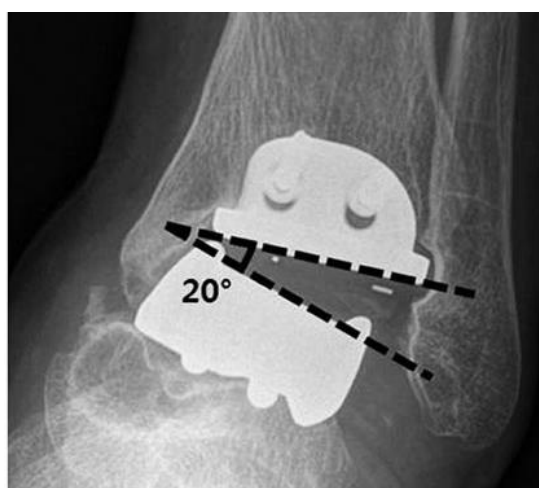


Figure 5.3 Severe coronal malalignment between components. Image adapted from: Total Ankle Arthroplasty: An Imaging Overview. Kim, D.R. et al. (2016) Korean j radiol, 17(3), pp.413–23.

As the term edge-loading has also been used to describe an inflection of material observed on retrievals caused by a translational malalignment this chapter will refer to such alignment as coronal malalignment only.

In addition investigations in total knee replacement, Liao et al. (2002) used computational modelling and found that increases in maximum polyethylene contact stress were greatest with valgus/varus tilt followed by mal-translation and least with a rotational malalignment. They suggested the surface wear would be worst for high conforming flat on flat knee designs and least for the equivalent curve on curve knee designs but concluded that valgus/varus would accelerate wear for any total knee design. Given the highly conforming design of the majority of mobile bearing TARs, including the Zenith (Corin Group PLC, UK) its function is unlikely to be compromised by a sagittal malalignment as the constant radius can compensate for the component set at relatively small degrees of dorsiflexion. While the mobile bearing design facilitates flexion, rotation and displacement through the two interfaces the congruency provides no flexibility in the coronal plane (Figure 5.4). As it appears to be an equally common problem due to the prevalence of preoperative coronal deformity gaining a better understanding of coronal malalignment biomechanics would be valuable. Braitto et al. (2015) believed that coronal alignment within a safe zone, which is yet to be defined may not increase failure rates, there may be significance in exploring and further defining this hypothesis.



Figure 5.4 Coronal plane through the Zenith TAR and lack of freedom of motion

Through use of a mechanical simulator the effects of known coronal malalignment on the biomechanical performance of a TAR were assessed in order to inform the most critical test conditions for the malalignment wear test. A maximum of 10° coronal malalignment was chosen based on clinical results and previous computational investigations in TKR and TAR (D’Lima et al. 2001; Espinosa et al. 2010). Observations in our local TAR retrieval cohort highlighted the prevalence of translational offset causing edge loading (Stratton-Powell et al. 2017). From a trial 3mm translational offset from neutral alignment appeared enough to cause deformation with the kinematic inputs. This offset was implemented in the single station simulator for the contact area assessment. Since, Koivu et al. (2017) have described an overhang between the components greater than 3mm to be “substantial”.

5.2 Materials

Three Corin Zenith total ankle replacements (Table 5.1) were tested in electromechanical Leeds Single Station Knee Simulator III (SSKS3).

Table 5.1 Bearing details

| Bearing | Talar | Tibial | Insert |
|--------------|----------|----------|----------|
| Corin Zenith | 298111 | 298112 | 291193 |
| | 500.1003 | 503.1003 | 506.1053 |

The simulator (Figure 5.5) had the capacity to drive axial load, flexion/extension, rotation, anterior/posterior displacement and abduction/adduction inputs using electromechanical motors (Table 5.2), however for this methodology the connecting arm was uncoupled from the abduction/adduction cradle to allow it to move freely. The medial/lateral displacement was fixed.

Table 5.2 Simulator Controls

| Input | Control |
|---------------------------------|--------------|
| Axial Load | Force |
| Flexion/Extension | Displacement |
| Rotation | Displacement |
| Anterior/Posterior Displacement | Displacement |
| Abduction/Adduction | Passive |
| Medial/Lateral Displacement | Fixed |

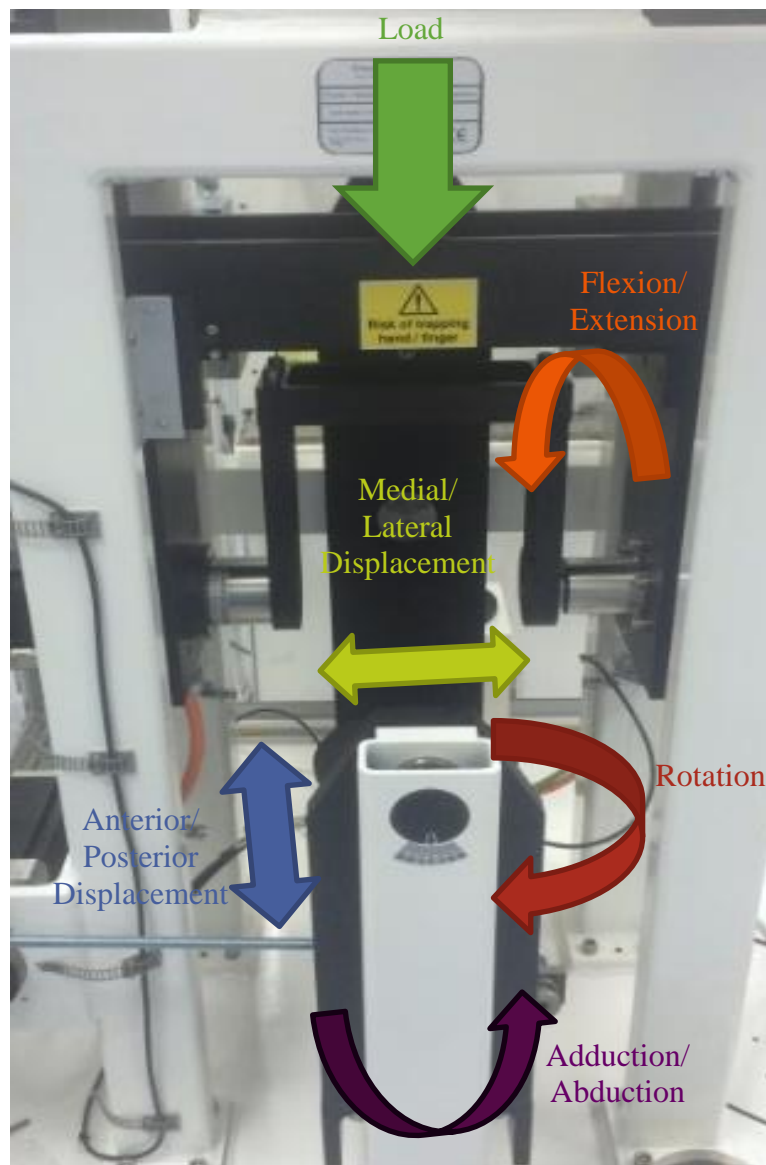


Figure 5.5 Leeds single station knee simulator III (SSKS3)

Wedged fixtures were designed to create an offset to tibial coronal alignment between 0 and 10 degrees whilst maintaining a consistent centre of rotation. Talar fixtures were also designed to ensure the talus articulated about the centre of rotation of the flexion/extension cradle of SSKS3. In order to avoid cam lift-off when applying the high loads a larger spring spacer was designed and modifications were made to the flexion cradle counterweights to ensure the components remained in contact reducing the risk of dislocation.

A Tekscan (Boston, USA) pressure sensor, receptor and I-scan software were required for the measurement of the pressure and contact area. The sensor consisted of two flexible polyamide sheets with electrically conductive material printed on the surfaces, one in rows the other in columns and coated with a semi conductive material. These, laminated together, create intersections between the rows and columns known as sensels. At each sensel the load is measured in terms of the resistance. This technology has a proven track record in biomechanics testing for both natural tissue and joint replacements under both static and dynamic loading conditions (Zdero 2017). Typically Tekscan measurements are used to validate computational models (Fregly et al. 2003; Catani et al. 2010; Mengoni et al. 2016). The model: 5076 (Figure 5.6), made up of 44 columns and rows and thus 1936 sensels, was deemed most appropriate for the size of the TAR insert. Although not as high resolution the size of the sensor allowed space for the component to realign under load.

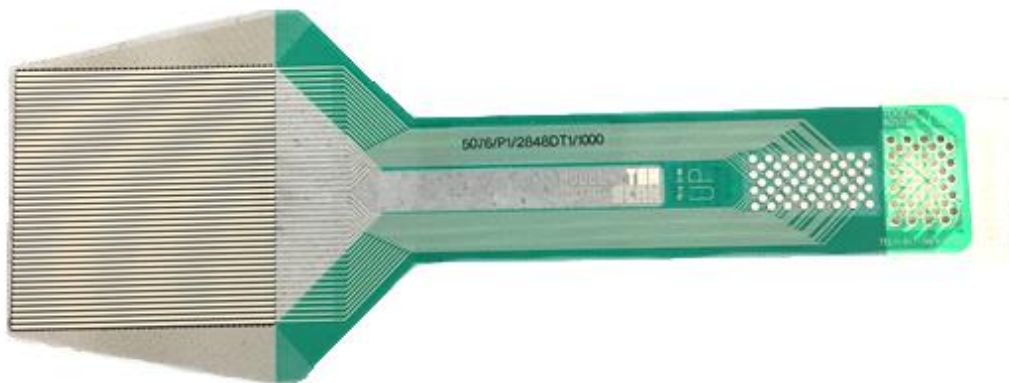


Figure 5.6 Tekscan sensor

5.2.1 Simulator commissioning

As the simulator had not been used prior to this investigation it had to be commissioned. This involved calibrating the axes of the simulator and running standard tests comparing the results to that of the earlier simulator generations. The forces and torques were all recorded from the six-axis load cell which sits beneath the components while a second load cell at the front of the station measured the shear force to estimate friction. The linear displacements such as anterior/posterior (AP) and medial/lateral (ML) displacement were monitored by magneto inductive position sensors. The radial displacements including flexion/extension, rotation and abduction/adduction, were all output from optical encoders in the motors.

In order to validate the simulator and assess its ability to deliver the kinematic inputs to the desired specification a standardised test was carried out (Liu et al. 2015). The single station knee simulator SSKS3 was run with dummies consisting of a stainless-steel cylinder of radius of 25mm articulating against a GUR1050 polyethylene flat under both smoothed and standard test conditions (Figure 5.7). The simulator outputs were analysed and compared against the data from corresponding SSKS1 data under the same test conditions from the commissioning process (Liu et al. 2015). Tests were run with the AP motion either constrained, constrained with only the spring connected or unconstrained without a spring. Each test was run for 300 cycles at 37 degrees in 25% serum. The average shear force was calculated for each condition.

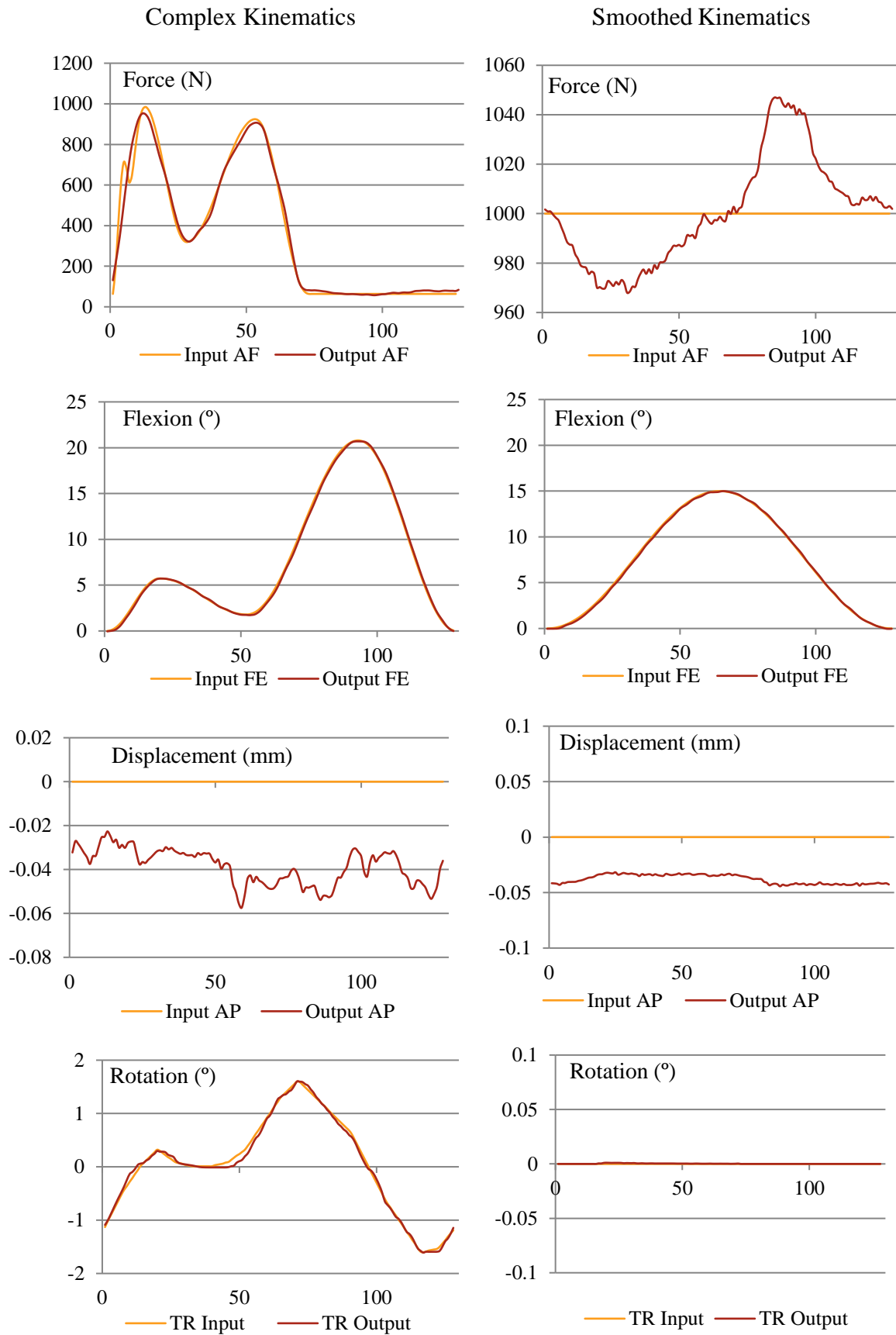


Figure 5.7 Comparing simulator outputs for complex and smoothed kinematics

This electromechanical simulator had additional load tuning capabilities which ensured the adherence to the axial force input profile was within 5%. The kinematic outputs also showed accuracy to 0.06mm and less than 0.1°.

Initially, the shear forces under the smoothed kinematics ranged between -86 and 40, -83 and 27, -40 and 16 [N] for the constrained, spring, and unconstrained configurations respectively. The corresponding measured shear forces under the complex kinematics were -47 to 33, -47 to 26, and -19 to 7 [N] respectively. The average shear forces for SSKS3 under the complex kinematics and constrained configuration showed a large amount of resistance in one direction compared to the readings from an equivalent simulator under the same test conditions (Liu et al. 2015).

The simulator was examined and it was noticed that in the posterior direction the AP sensor was in contact with the receptor. Further investigation found the sensor bracket to be bent which was obstructing the clearance and stopping the platform from moving freely. The sensor was straightened which appeared to reduce the friction felt manually in the system when moving the AP platform. Upon repeating the testing the shear force reading was still higher than expected. Further investigation showed the shear force load cell was much looser than that on the previous generation (SSKS2). The tension in this was adjusted in an attempt to improve the shear force results. These secondary adjustments brought the shear forces more in line with what was measured on SSKS2, although slightly higher than the published results for SSKS1 (Liu et al. 2015). The smoothed shear force profiles were comparable in shape although the peak forces were approximately 20N higher. From comparing with SSKS1 the AP displacement platform on SSKS3 appears to have more resistance to motion, moving less freely creating more friction which may cause the greater peak forces (Figure 5.8).

The complex results for the constrained and unconstrained tests were similar between the simulators although SSKS3 had more variation than SSKS2. There was more noticeable variation between the simulators when running the more complex kinematics under the spring constraint. This may be a result of the variation in load tuning or could be influenced by the cam lift-off which occurred

under the complex loading profile. The spring positioning may also have some bearing on these results.

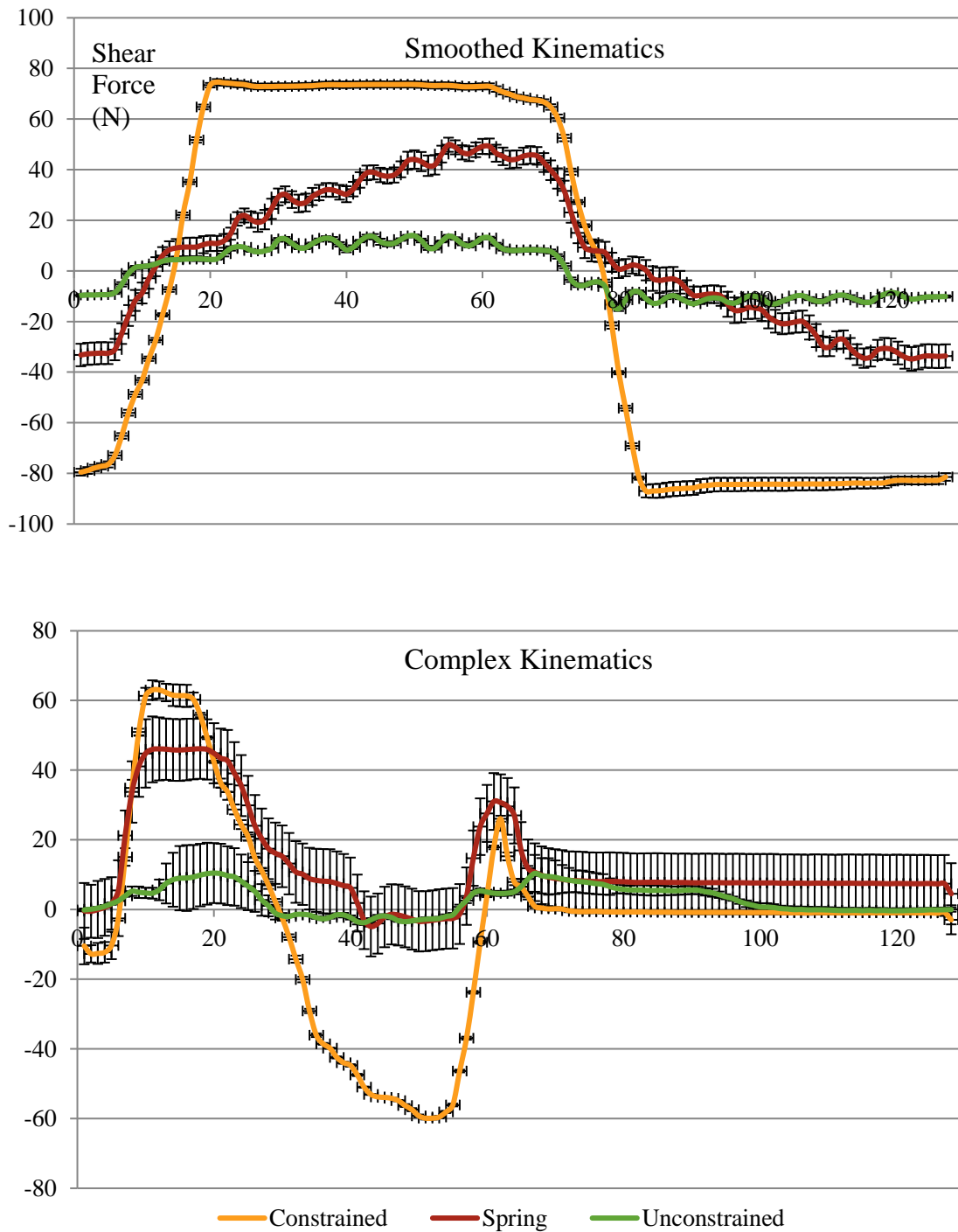


Figure 5.8 Frictional shear force for dummies under smooth and complex kinematics $\pm 95\%$ CL for $n=3$ in SSKS3

The complex results for the constrained and unconstrained tests were similar between the simulators although SSKS3 had more variation than SSKS2. There was more noticeable variation between the simulators when running the more complex kinematics under the spring constraint. This may be a result of the variation in load tuning or could be influenced by the cam lift-off which occurred under the complex loading profile. The spring positioning may also have some bearing on these results.

After a series of simulator adjustments, the measured shear forces from SSKS3 were generally similar to that reported for SSKS2. The differences in shear forces between the two simulators were attributed to the axial force tuning of the SSKS2 simulator which was adapted to smooth cam mechanism performance and the positioning of the spring system.

5.3 Methods

5.3.1 Biomechanical test methods

Within the newly commissioned simulator the three TARs were tested within chambers filled with 25% bovine serum, 0.03% Sodium Azide aqueous solution (Figure 5.9).

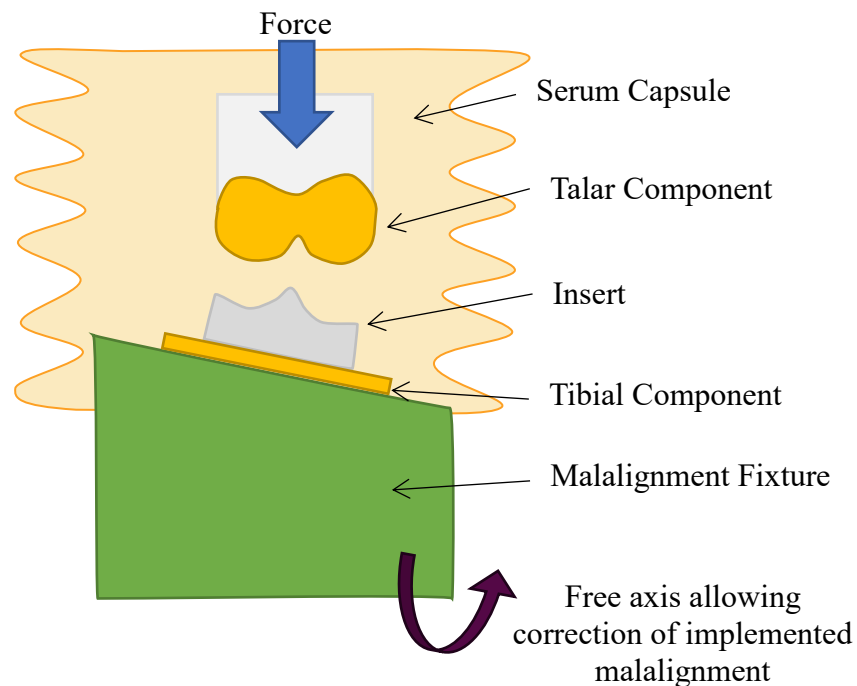


Figure 5.9 Biomechanics test set-up

Before commencing testing the abduction/adduction cradle was aligned in the zero position using a digital inclinometer before initialising the simulator to realign the sensor. Gait conditions were applied to the TARs for 300 cycles while the gait outputs were recorded and averaged. The mean abduction/adduction output between TARs was plotted to observe the changing contact. Maximum and minimum profile values were used to define the degree of lift-off.

This process was repeated for each of the three TARs under the five alignment conditions equally spaced between 0 and 10° (Figure 5.10) for the kinematic conditions described to create varying degrees of component lift-off. Within the simulator these components were inverted with malalignment applied to the tibial component which has the ability to correct itself during the loading cycle.

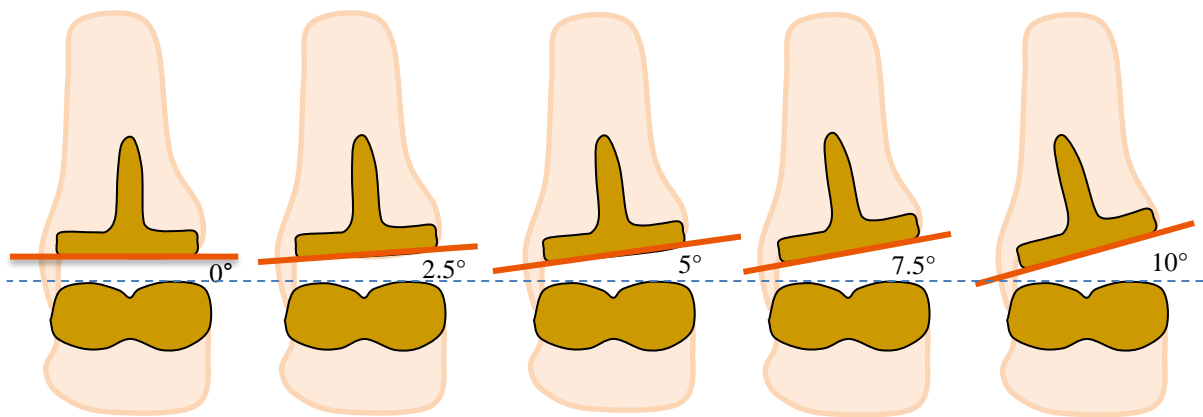


Figure 5.10 Coronal malalignment angles to be investigated

The standard gait input defined in Chapter 4 with load, flexion/extension and rotation was applied (Figure 5.11). When testing the effects of conditions other than displacement the 4mm displacement was used as standard. The fine-tuning capabilities were employed to ensure the best possible replication of the force inputs.

5.3.1.1 The effect of valgus and varus malalignment

As it was important to understand the effect of the direction of malalignment, testing with the malalignment wedge was undertaken in both directions. To ensure the differences observed were not caused by minor differences in the component set-up this was verified by recreating the same condition by keeping the wedge

direction constant and inverting the rotation input. The results of this comparison defined the orientation for the rest of the tests.

5.3.1.2 The effect of displacement

Secondly the effect of displacement on the biomechanical outputs was assessed. The range of AP displacements from chapter 3 were employed; 9mm, 4mm and 0mm.

5.3.1.3 The effect of peak load

The effect of the peak load was also an important consideration. There is some variability across publications in what is believed to be the actual force through the ankle. Mathematically it has been calculated to represent 4-5 times bodyweight however instrumented prostheses have shown these calculations tend to overestimate the contact forces (Bergmann et al. 1993; Zhao et al. 2007). Due to the limitations of the pneumatic multi-station simulator the TAR is unlikely to experience the desired peak loads so understanding the effects of this variable is important.

5.3.1.4 The effect of swing phase load

Due to individual variability and the lack of data surrounding the swing phase of gait in the ankle, it was difficult to be confident the 100N previously applied is an appropriate assumption. This is assumed to be an important parameter when considering malalignment as it may dictate the level of component lift-off and the potential for dislocation. After joint replacement surgery ligament tensioning is a critical factor which will influence the swing forces experienced (Conti & Wong 2001). This will vary from patient to patient depending on whether the joint is left relatively lax to ensure full range of motion or is over-tensioned, for example using a very thick insert which can decrease mobility and increase stresses (Hintermann & Valderrabano 2003). As the ankle goes through a substantial range of motion during the swing phase there are likely to be multiple muscle forces active however, there was no literature available to define the range of forces experienced. In order to better understand the implications of this variable the profile was scaled to a range of swing phase loading conditions were investigated; 50N, 100N, 300N, 500N and a positive control of 1000N (Figure 5.11). These

values aimed to cover a variety of situations as the ankle force during swing has not been directly measured. During the swing phase however, the ankle is known to move through plantar and dorsiflexion, this will require muscle actions at the ankle which will see additional force transmission between the tibia and talus.

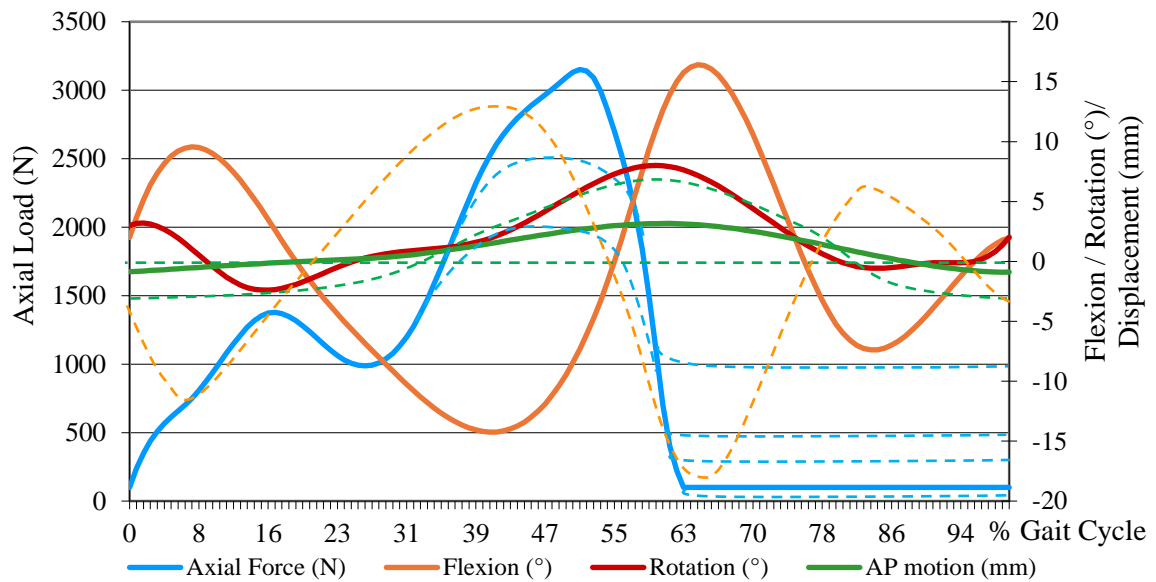


Figure 5.11 Variations in simulator inputs tested shown by dashed lines

The standard gait input defined in Chapter 4 with load, flexion/extension and rotation was applied (Figure 5.11). When testing the effects of conditions other than displacement the 4mm displacement was used as standard. The fine-tuning capabilities were employed to ensure the best possible replication of the force inputs.

5.3.1.1 The effect of valgus and varus malalignment

As it was important to understand the effect of the direction of malalignment, testing with the malalignment wedge was undertaken in both directions. To ensure the differences observed were not caused by minor differences in the component set-up this was verified by recreating the same condition by keeping the wedge direction constant and inverting the rotation input. The results of this comparison defined the orientation for the rest of the tests.

5.3.1.2 The effect of displacement

Secondly the effect of displacement on the biomechanical outputs was assessed. The range of AP displacements from chapter 3 were employed; 9mm, 4mm and 0mm.

5.3.1.3 The effect of peak load

The effect of the peak load was also an important consideration. There is some variability across publications in what is believed to be the actual force through the ankle. Mathematically it has been calculated to represent 4-5 times bodyweight however instrumented prostheses have shown these calculations tend to overestimate the contact forces (Bergmann et al. 1993; Zhao et al. 2007). Due to the limitations of the pneumatic multi-station simulator the TAR is unlikely to experience the desired peak loads so understanding the effects of this variable is important.

5.3.1.4 The effect of swing phase load

Due to individual variability and the lack of data surrounding the swing phase of gait in the ankle, it was difficult to be confident the 100N previously applied is an appropriate assumption. This is assumed to be an important parameter when considering malalignment as it may dictate the level of component lift-off and the potential for dislocation. After joint replacement surgery ligament tensioning is a critical factor which will influence the swing forces experienced (Conti & Wong 2001). This will vary from patient to patient depending on whether the joint is left relatively lax to ensure full range of motion or is over-tensioned, for example using a very thick insert which can decrease mobility and increase stresses (Hintermann & Valderrabano 2003). As the ankle goes through a substantial range of motion during the swing phase there are likely to be multiple muscle forces active however, there was no literature available to define the range of forces experienced. In order to better understand the implications of this variable the profile was scaled to a range of swing phase loading conditions were investigated; 50N, 100N, 300N, 500N and a positive control of 1000N. These values aimed to cover a variety of situations as the ankle force during swing has not been directly measured. During the swing phase however, the ankle is known to move through

plantar and dorsiflexion, this will require muscle actions at the ankle which will see additional force transmission between the tibia and talus.

5.3.2 Pressure mapping test methods

With all of the displacement controlled axes constrained to zero a dynamic loading input was applied. The three TARs were tested under a range of conditions with a 5076 pressure mapping sensor (Tekscan, Boston, USA) placed between the tibial component and the polyethylene insert in order to record the changing contact area and pressure throughout the loading cycle. The sensor connected to data acquisition electronics which fed the captured information back to the software, this was carefully secured to the abduction/adduction cradle (Figure 5.12). A thin layer of vaseline was applied between the insert and sensor surface to mimic some lubrication and care was taken to align the insert square to the parallel lines of the sensor.

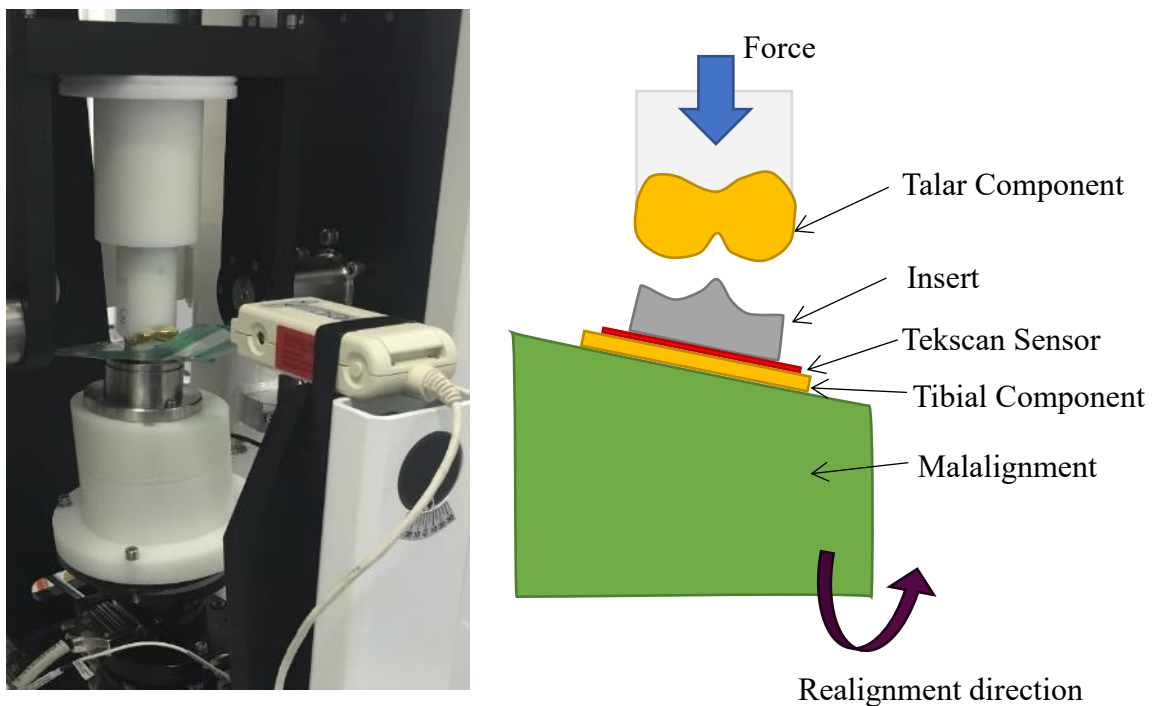


Figure 5.12 The Tekscan sensor set up in the single station simulator

Based on the manufacturer recommendations each time the sensor was used it was first conditioned. A force around 20% greater than the maximum force to be tested under was applied, in this instance 3700N was used with the TAR in the neutral alignment condition. This process was repeated three times with unloaded rests in

between. This ensured the sensor was warmed up to measure the loads which were applied.

On the first use, before any data was collected, the Tekscan sensor underwent a calibration procedure to improve the sensor accuracy. The sensor was calibrated with the two-point power law calibration deemed better for changing loads. In order to achieve the range of loads this was carried out within the simulator on a TAR aligned in the neutral orientation. Loads at 20% and 80% of peak were used based on the manufacturer's recommendation, a first static load of 630N was applied. After a relaxation period a second load of 2500N was applied which defined the two-point power law load calibration.

The software provides a series of sensitivity settings which can be optimised depending on the range of forces being applied. As the range of forces applied reached 3.15kN this resulted in sensor saturation at high sensitivity levels when subjected to peak loads. As a result, a "low -1 minimum" sensitivity was used throughout (Figure 5.13).

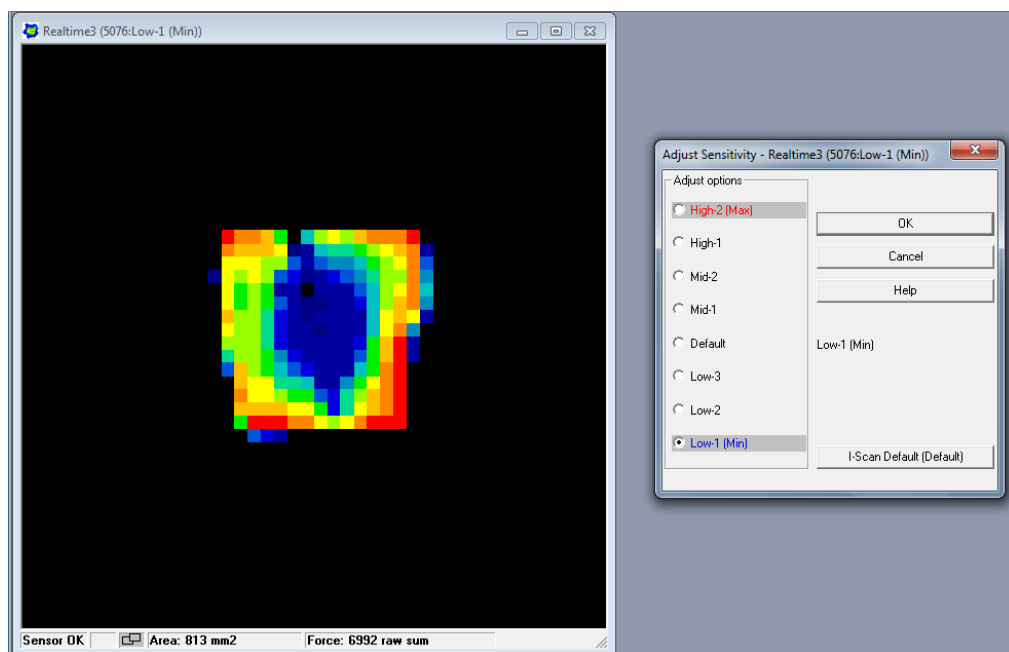


Figure 5.13 Sensitivity setting used to avoid oversaturation

Prior to each loading and alignment condition the simulator's axes were sent to zero and the loading profile was initiated. In order to ensure the peak loads were achieved at least ten cycles were applied before any data was collected. Recordings were taken for two seconds, the equivalent of two seconds, the equivalent of two loading cycles, at a rate of 100 frames/second. This process was repeated for the range of swing load profiles at each alignment and for three TARs. The effect of translational offset was also considered under the standard input.

The data from the two second pressure recordings was analysed by exporting the measured load profile, contact pressure and contact area for the whole two cycles. As each recording was not made repeatedly at the same point within the gait cycle the output profiles had to be realigned. In order to achieve this the force increase at the end of the swing phase and the peak loads were used to bring the profiles into phase with each other so they could be compared.

Pressure map outputs were exported from the Tekscan software at three time points in the loading cycle; end of the swing phase before the load starts to increase, first load peak and overall peak load (Figure 5.14).

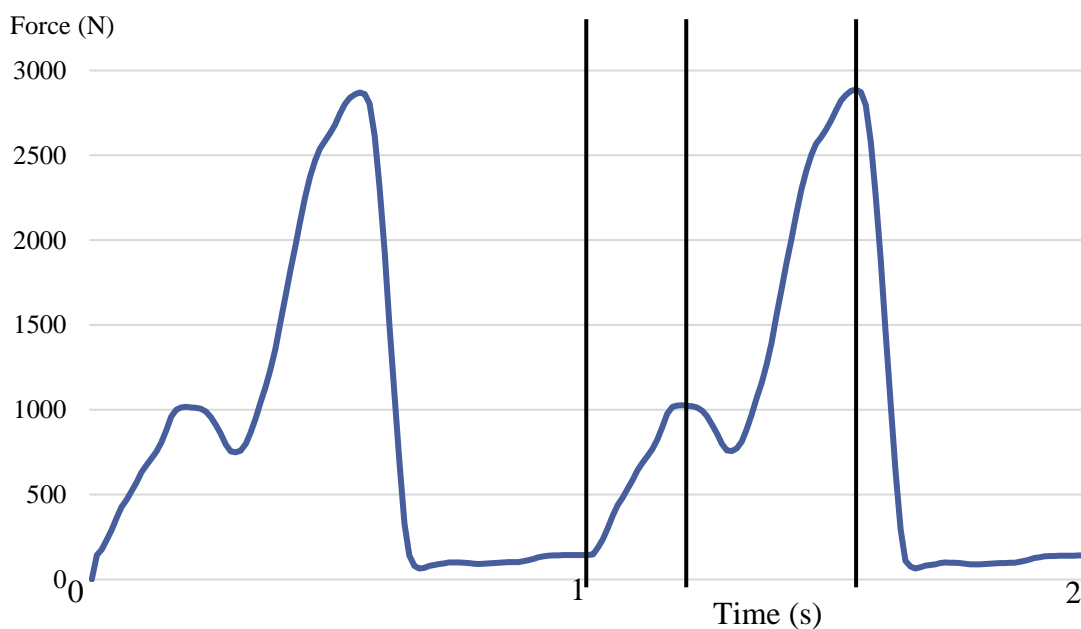


Figure 5.14 Tekscan force outputs from two cycles of pressure recording highlighting the three time points for data collection

These three points were believed to give sufficient insight to describe the changes across the whole profile and were considered to be repeatable across all measurements. For each individual recording this data was collected and combined for comparison purposes using a Matlab (Mathworks, Natick, USA) script.

At the same loading points (Figure 5.14) the pressure and contact area data was exported relative to the rows and columns of the sensor in order to understand how these parameters changed across the surface throughout the loading cycle.

The Tekscan sensor typically underestimated the peak load by 10%, this is assumed to be a result of the relatively small area of the sensor used when calibrating. It is important this is considered when analysing the pressure outputs.

5.4 Results

In each of the graphical results which follow the changing element; swing force, peak load, AP displacement and direction have represented by the changing coloured lines. They are presented relative to the degree of malalignment implemented at 0°, 2.5°, 5°, 7.5° and 10°. For each condition, the lift-off has been presented changing relative to the force input profile (Figure 5.15), stance followed by swing.

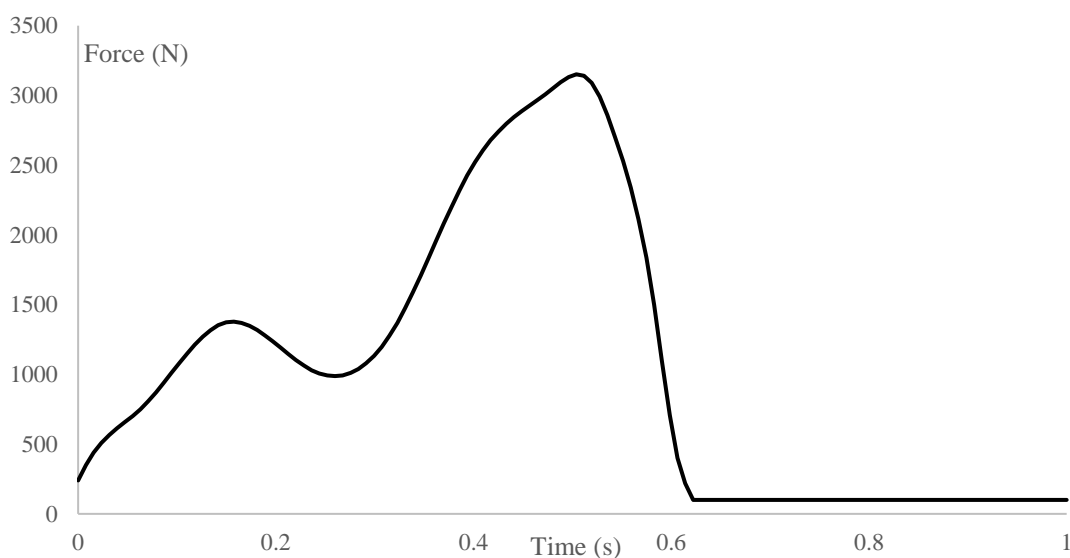


Figure 5.15 Force input profile

To understand the effect of the direction of the malalignment, whether varus or valgus the fixture and direction of rotation were reversed to account for set up variability. As standard, the fixture was tested in valgus therefore any ad/abduction less than the degree of malalignment was lateral lift-off and greater this was medial (Figure 5.16A). When testing the varus offset inverting the direction of the rotation created a direct comparison whereas when rotating the fixture the swing changed from positive to negative. In order to be able to compare these outputs graphically the negative abduction for the reversed set up was made absolute, however the relative swing is a mirror image of the reversed rotation profile. The lift-off is shown relative to the force input profile (Figure 5.15) at 0°, 2.5°, 5°, 7.5° and 10°. The pressure plots which follow are inverted relative to the direction of the malalignment due to sensor position (Figure 5.17B).

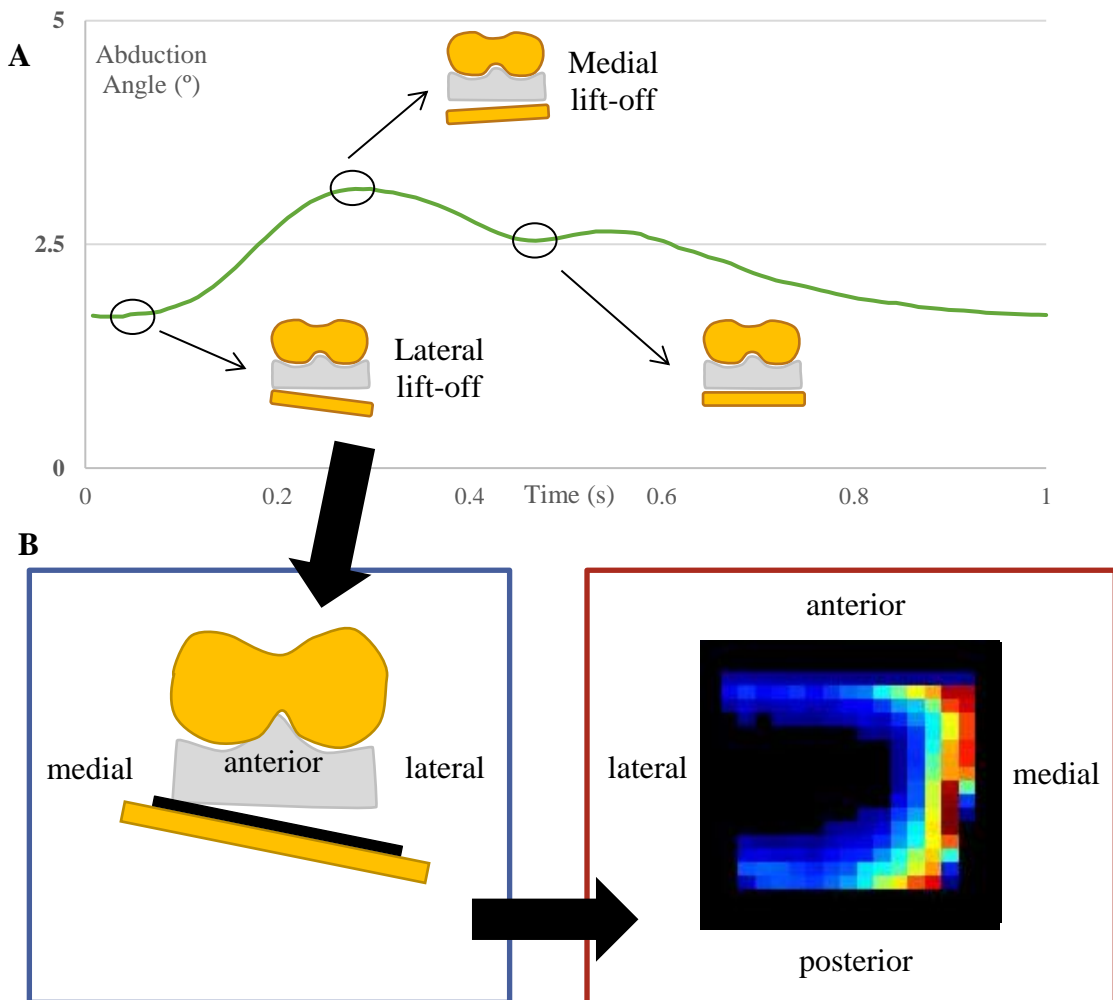


Figure 5.16 A) Change in ad/abduction resulting in lateral followed by medial lift-off at 2.5 degrees malalignment B) The experimental set-up of the TAR compared to the orientation of the output pressure plots

5.4.1 Biomechanics

At zero there was no difference between the ad/adduction swing with the fixture aligned in either direction (figure 5.17). However, when a degree malalignment was applied there became an apparent difference between the valgus (green) and varus malalignments (blue and red). Valgus malalignment caused a greater lift-off effect this reached a maximum of 2.2° occurring with 5° malalignment. For varus conditions replicated with the reversed fixture and rotation input the lift-off effect was reduced with maximum lift-off at 10° measuring 0.85° and 0.82° respectively. Generally, the profile with the rotation reversed (blue) showed less lift-off.

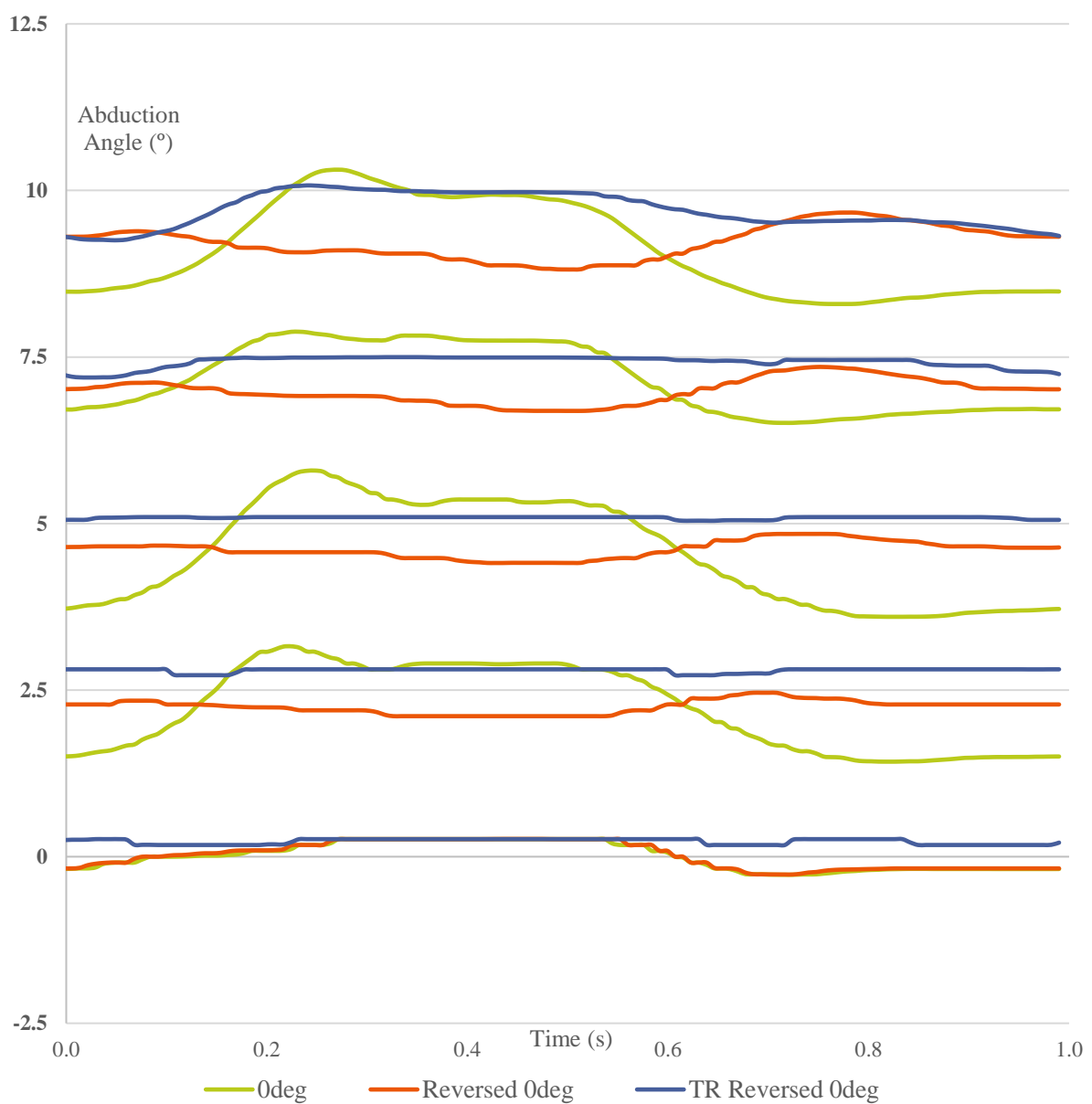


Figure 5.17 Effect of malalignment direction on lift-off with ab/adduction less than the malalignment offset angle showing lateral lift-off as in Figure 5.16

The effect of the different anterior/posterior displacements previously tested in the wear simulation were considered in combination with the range of coronal malalignment offsets. At lower malalignment angles the degree of lift-off was relatively similar despite the magnitude of the displacement applied (Figure 5.18). At higher malalignment angles such as 7.5 and 10° the 4mm displacement (green) was more comparable with the outcomes with no displacement (red) with lift-off between 0.7° and 0.9°. Conversely the larger displacement of 9mm saw much lift-off at these angles measuring 1.2° to 2.1° at 7.5° and 10° malalignment respectively. There is also a greater oscillatory effect with the large AP displacement and malalignment angles.

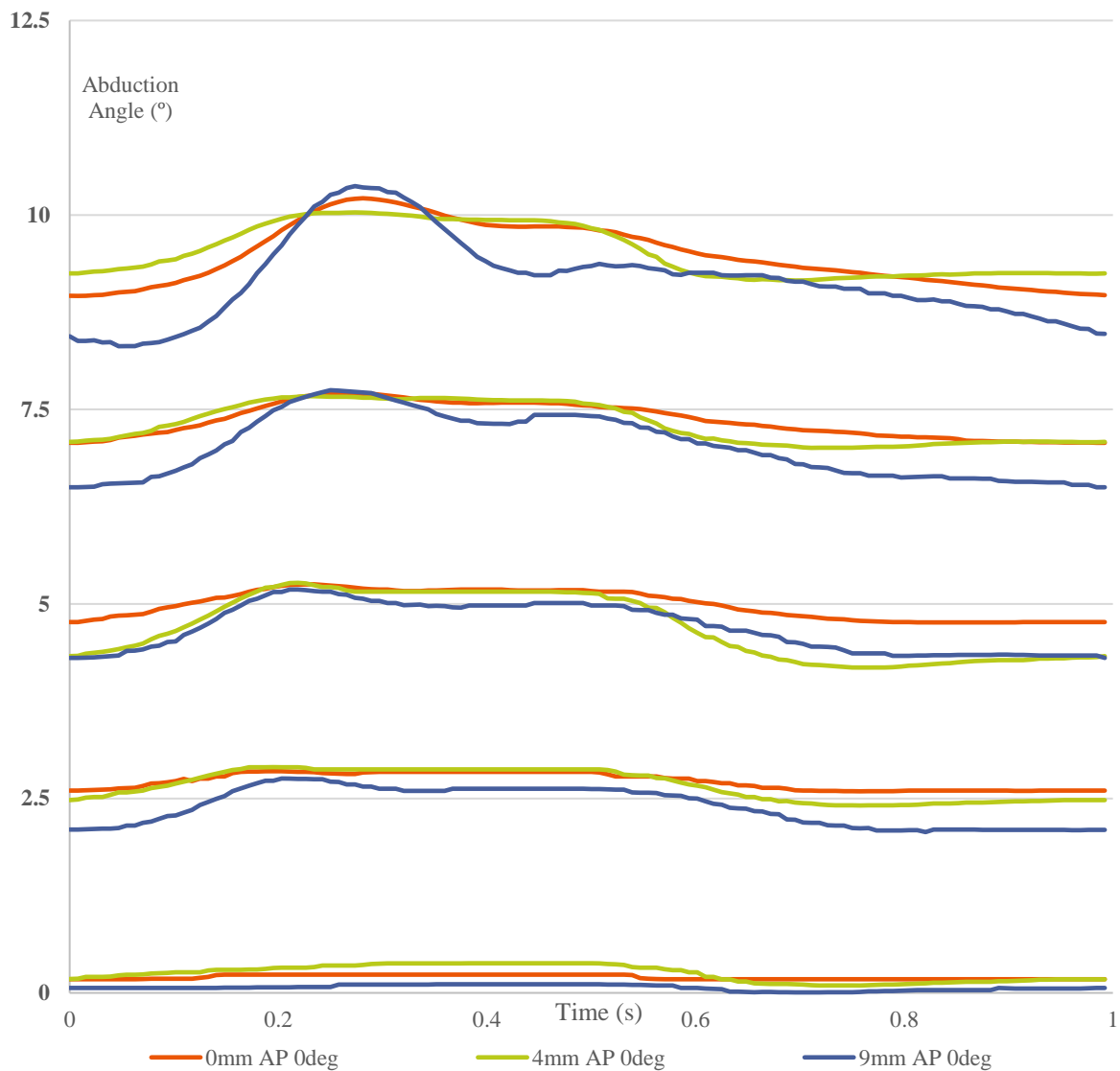


Figure 5.18 Mean effect of AP displacement on lift-off (n=3) with ab/adduction less than the malalignment offset angle showing lateral lift-off as in Figure 5.16

Generally, the difference with the changing peak loads was negligible between the 2kN and 2.5kN peaks (Figure 5.19). Both these lower loads caused dislocation in combination with a 10° malalignment angle. With the higher load of 3.1kN (green) the degree of lift-off was notably lower at both 2.5° and 7.5° measuring just 0.5° and 0.7° respectively. In comparison, the lower peak loads resulted in lift-off of 0.9-1.1° and 1.7° with the same alignment conditions applied. The same trend was not observed with 5° malalignment.

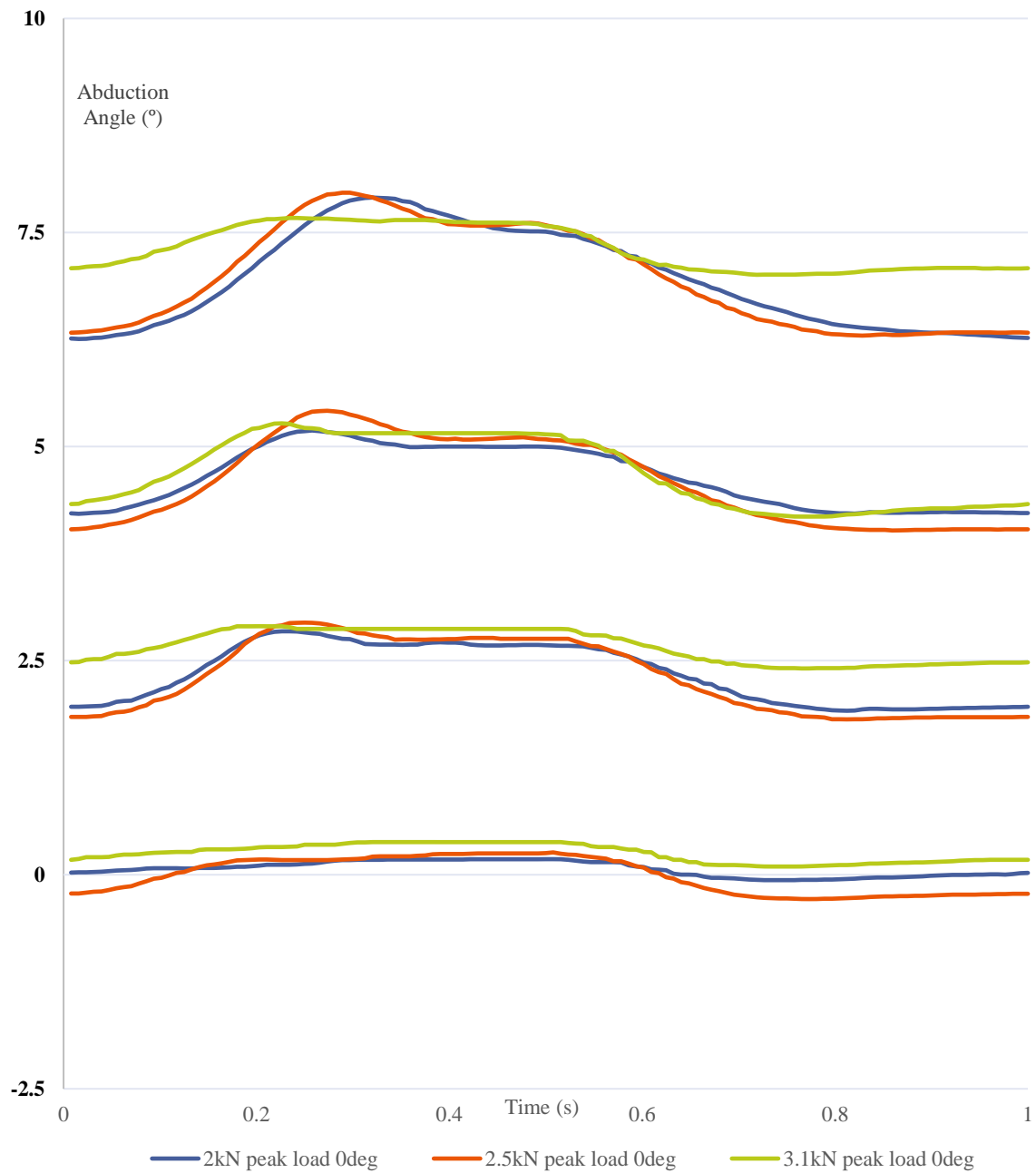


Figure 5.19 Mean effect of peak load on lift-off (n=3) with ab/adduction less than the malalignment offset angle showing lateral lift-off as in Figure 5.16

Finally the effect of swing phase load was investigated (Figure 5.20). With a 50N swing phase load (green) there was too much oscillation in the system which resulted in dislocation at 10° malalignment. Across each of the malalignment conditions the same trend was observed with smaller swing phase loads causing the lift-off at the start of the swing phase which continued to the first load peak. As the swing phase load was increased to 300N, 500N and 1kN the duration of this lift-off effect reduced sequentially. However, the degree of lift-off remained similar despite the swing phase load. Generally, the degree of lift-off increased with the malalignment angle with the exception of 100N swing phase load at 5° malalignment.

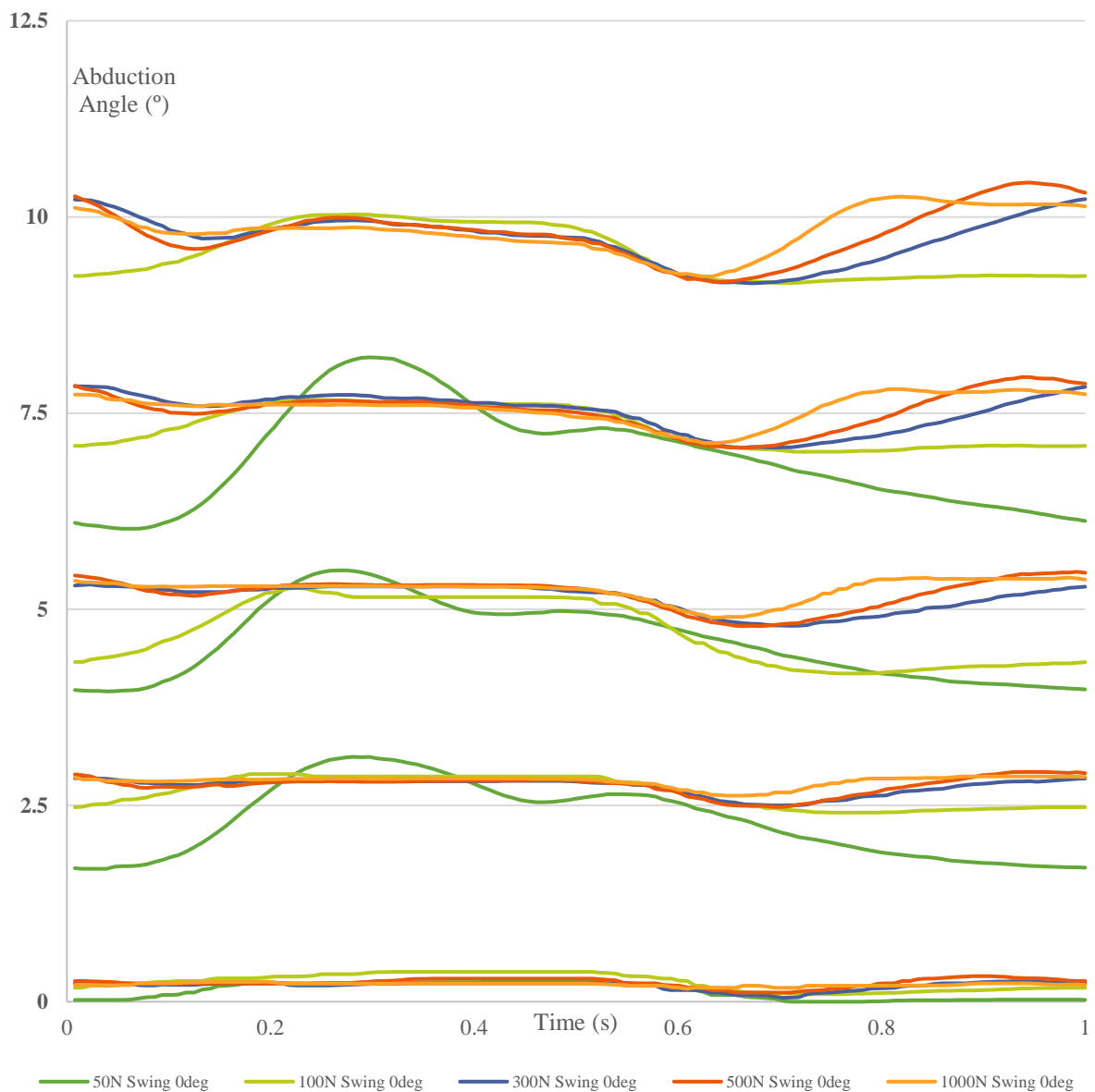


Figure 5.20 Mean effect of swing load on lift-off (n=3) with ab/adduction less than the malalignment offset angle showing lateral lift-off as in Figure 5.16

5.4.2 Contact area and pressure

For each loading condition the example of TAR2 has been used to demonstrate the pressure plots as this was the only TAR which did not dislocate with 50N swing and 10° coronal malalignment. The plots are presented in columns at a time point during swing and the two stance load peaks and in rows at each of the tested alignments; neutral and 2.5°, 5°, 7.5° and 10° coronal malalignment.

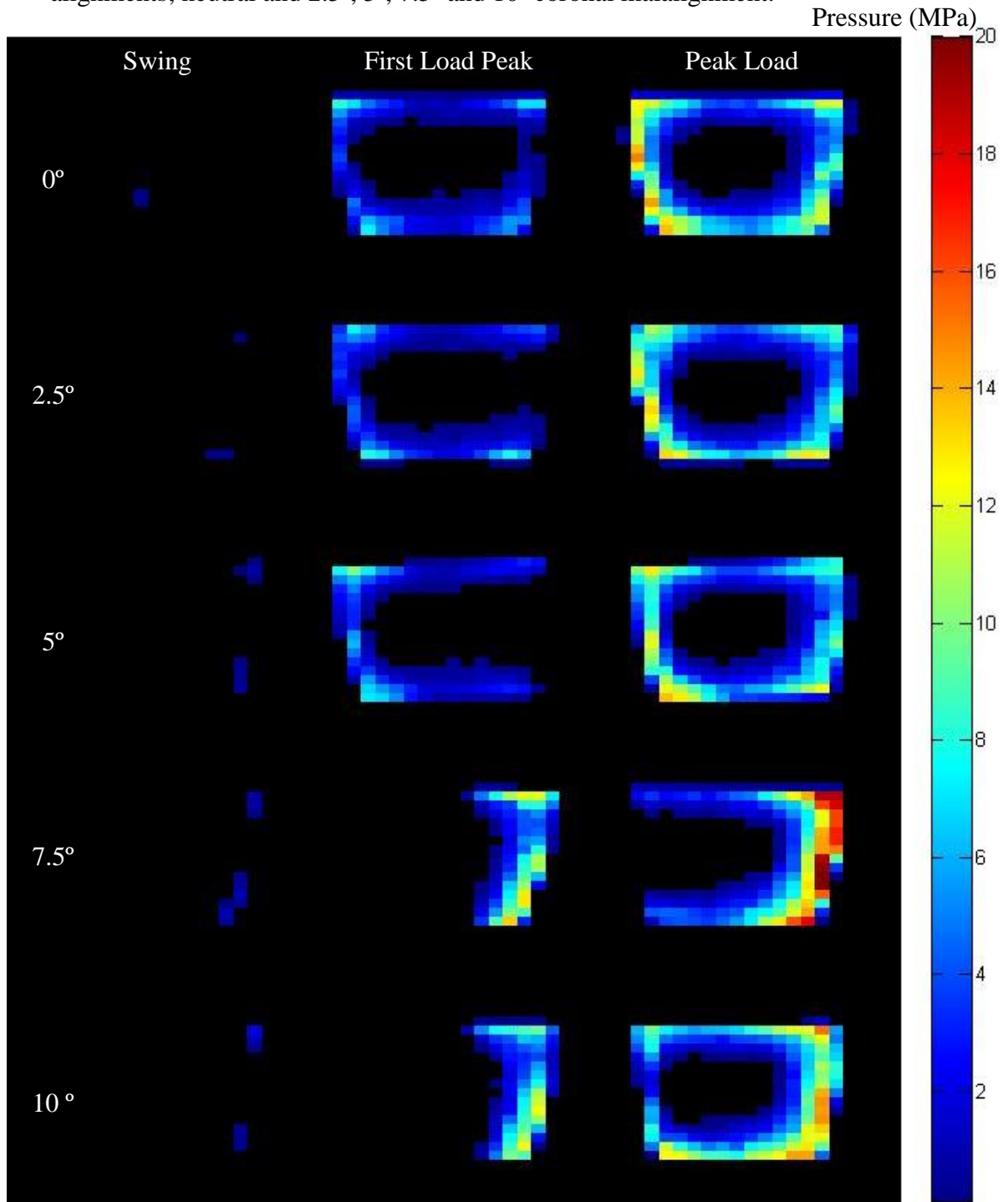


Figure 5.21 Pressure plots for cycle showing SPL of 50N, 1st load peak and max load showing lateral lift-off as in Figure 5.16

With the lowest swing phase load of 50N, a small contact area was measured across all alignment conditions including neutral alignment (Figure 5.21). The low swing phase influenced the contact at the first load peak in all malaligned conditions, at 7.5° this continued to the maximum load peak, however the same problem was not observed at 10°. The combination of ~3kN loads and small contact area resulting from the 50N swing saw peak pressure reach 21MPa. When the swing phase load was increased to 100N there was increased contact area during swing (Figure 5.22). During the stance phase there was little variability between the malalignment conditions.

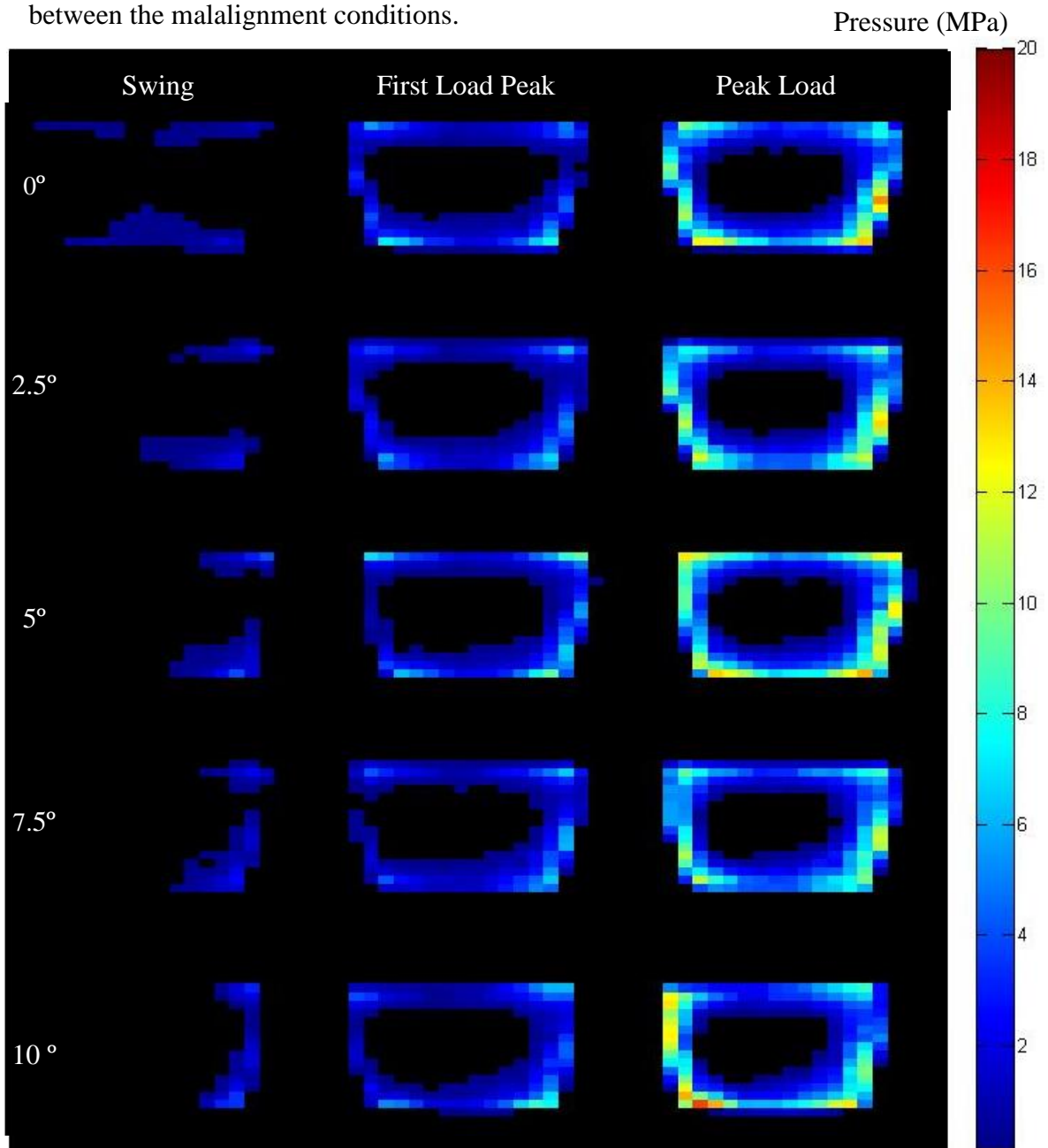


Figure 5.22 Pressure plots for cycle showing SPL of 100N, 1st load peak and max load peaks showing lateral lift-off as in Figure 5.16

The addition of 3mm translational offset causing edge loading saw an increase in the peak pressures focused medially (right) when the insert is brought back in contact rather than laterally (left) where it was in contact with the tibial edge, with the values up to 20MPa in all alignments (Figure 5.23). Combined translational offset and edge loading resulted in very little swing contact and more uneven loading at the first load peak especially at 5°, 7.5° and 10° malalignment.

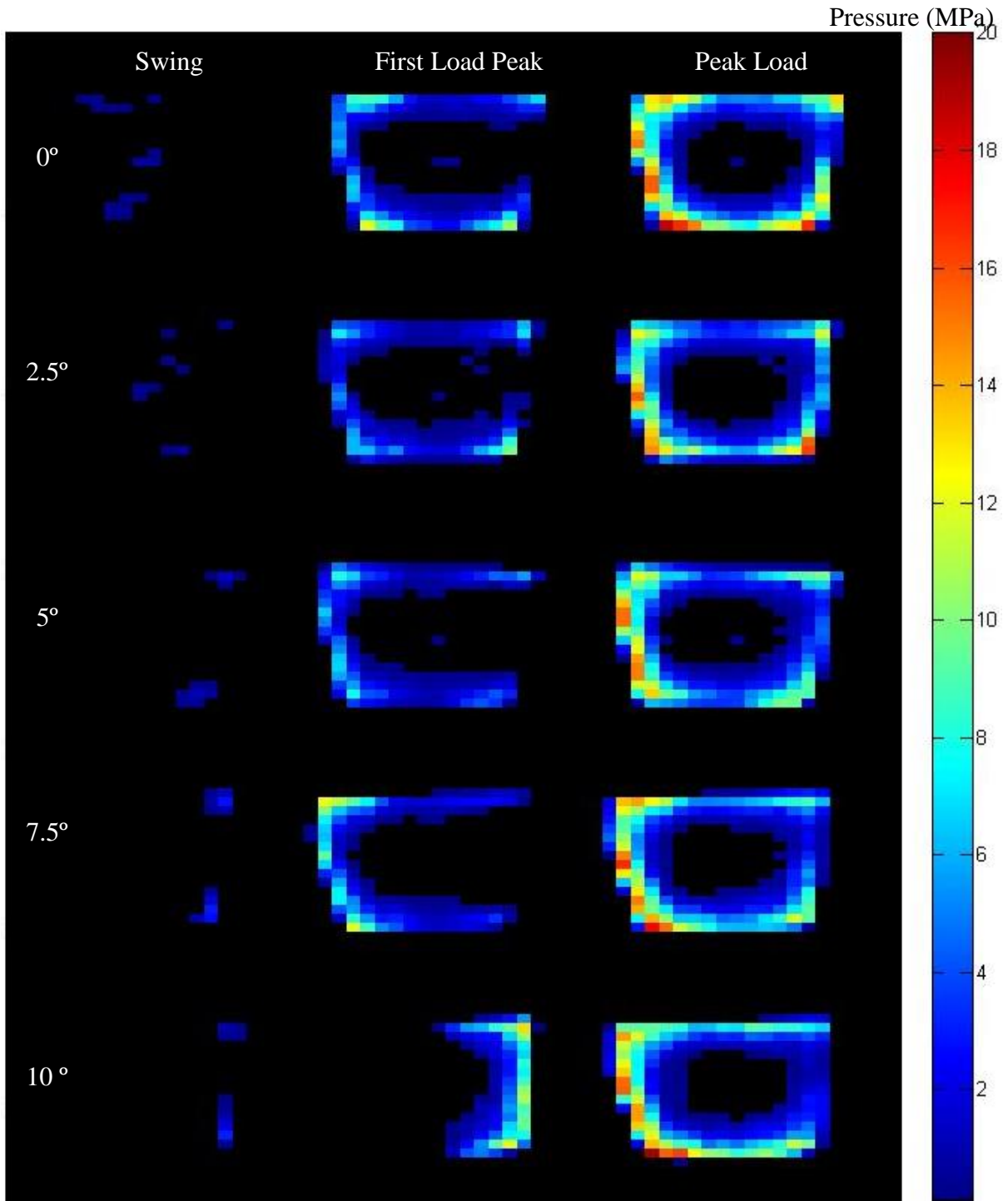


Figure 5.23 Pressure plots for cycle showing SPL of 100N, 1st load peak and max load with a 3mm translational offset showing lateral lift-off as in Figure 5.16

A swing phase load of 300N was closest to that seen in KS4 so these contact pressures and areas (Figure 5.24) may be representative of those expected when testing these alignments within the wear simulator. At 7.5° and greater the contact area during swing phase was located only on half of the insert and contact pressure on the other side was elevated at peak load. With a larger swing phase load the effects of the malalignment during the stance phase peak loads were considered negligible in this static condition.

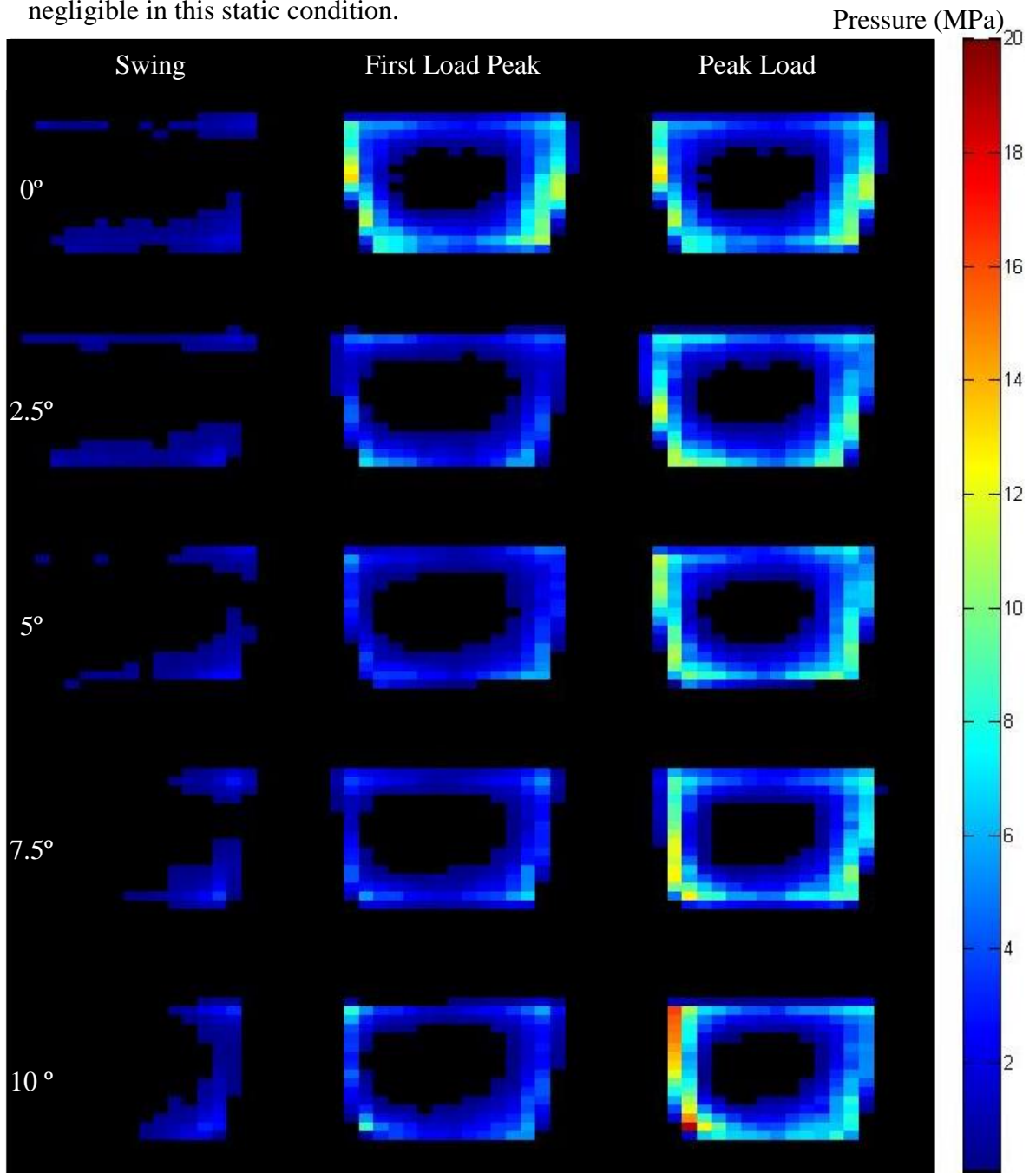


Figure 5.24 Pressure plots for cycle showing SPL of 300N, 1st load peak and max load showing lateral lift-off as in Figure 5.16

A similar trend occurred with swing phase loads of 500N (Figure 5.25) with the effects of the malalignment only substantial at 10°. As expected the positive control of 1000N reduced the swing phase lift-off the most (Figure 5.26). These conditions saw marginal increases in the regions experiencing peak pressures of 17.2-18.3MPa more concentrated at the medial insert edge.

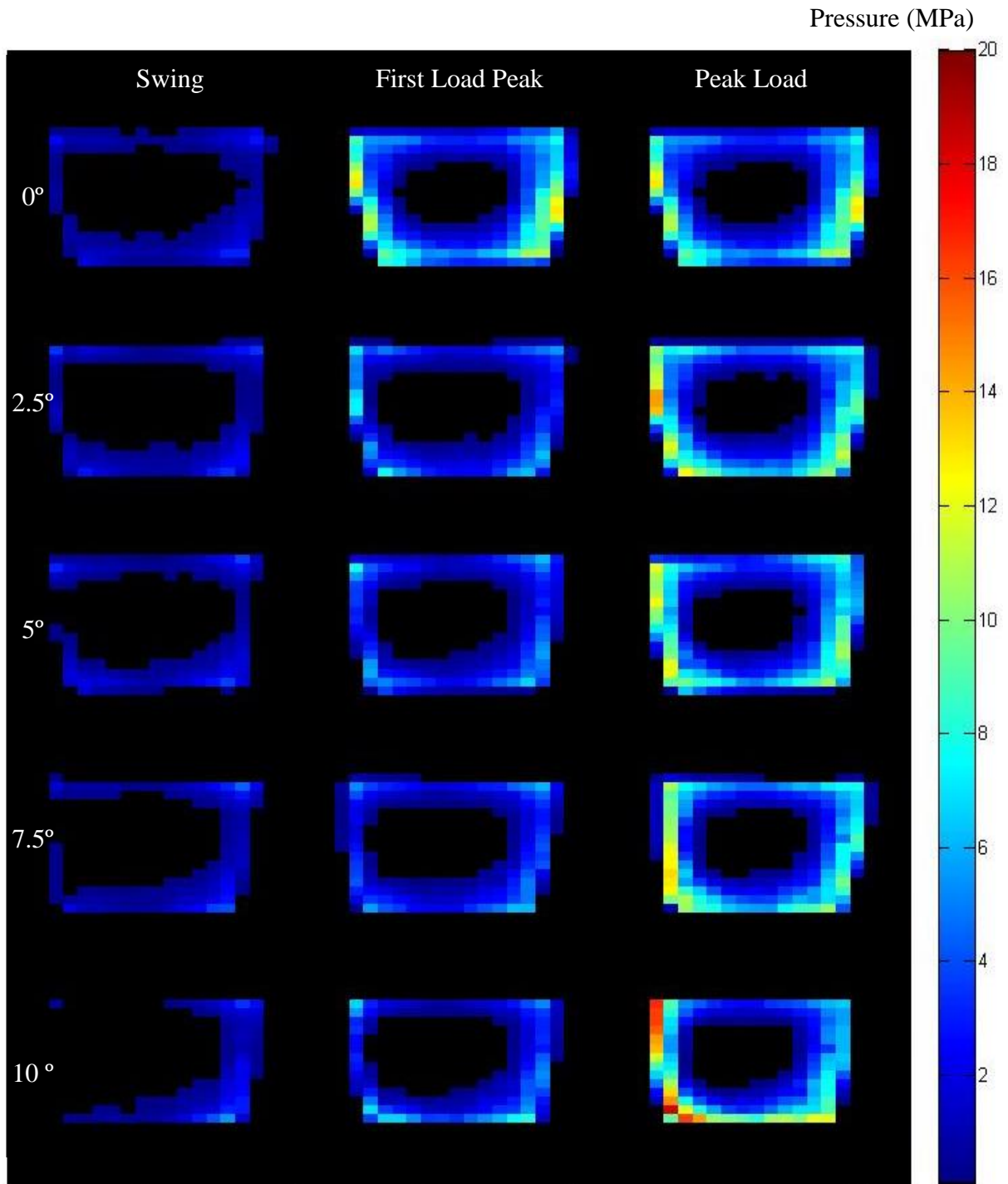


Figure 5.25 Pressure plots for cycle showing SPL of 500N, 1st load peak and max load showing lateral lift-off as in Figure 5.16 peaks

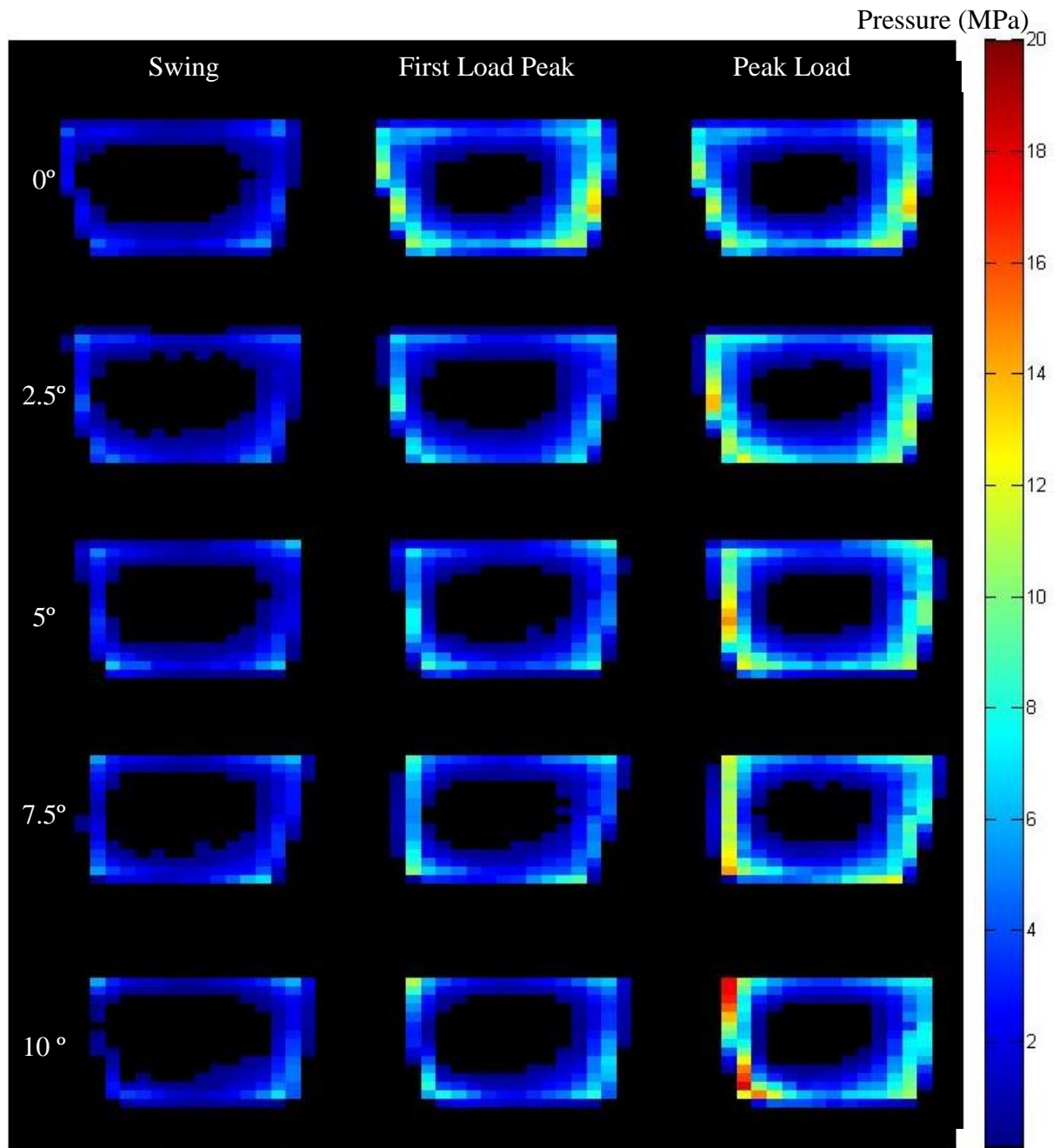


Figure 5.26 Pressure plots for cycle showing SPL of 1000N, 1st load peak and max load showing lateral lift-off as in Figure 5.16

In order to better quantify these variations across all three TARs tested the mean peak pressure throughout the two cycles was plotted (Figure 2.27). As only one TAR did not dislocate at 10° with 50N swing this combination was not plotted. The main trend apparent was the elevated peak pressures with 10° coronal malalignment at the peak load, which was independent of the magnitude of the swing phase load. In general, the swing phase peak pressure increased with the swing phase load and to some degree the increased malalignment angle.

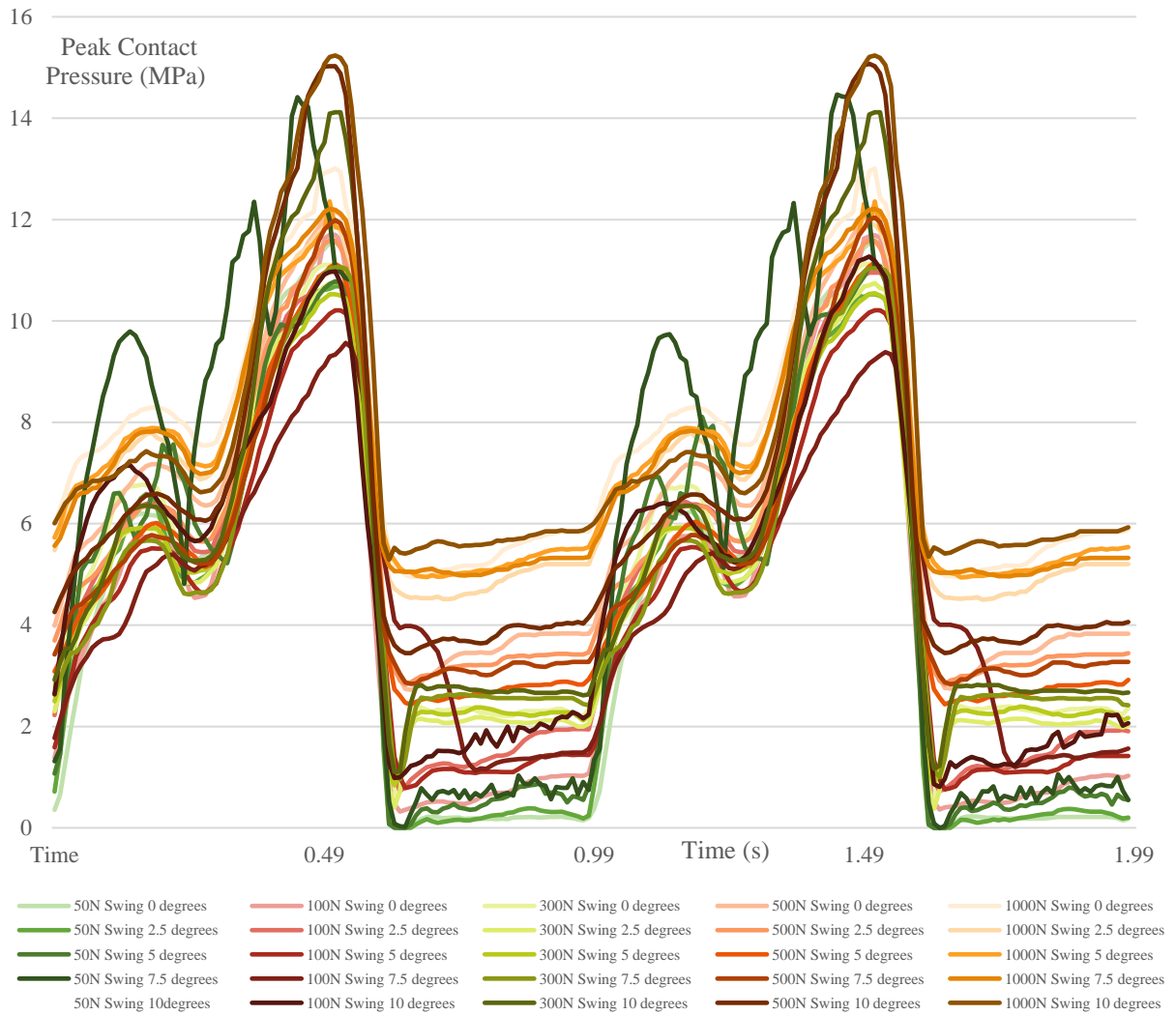


Figure 5.27 Mean peak contact pressure (n=3) for each tested coronal malalignment and swing phase load

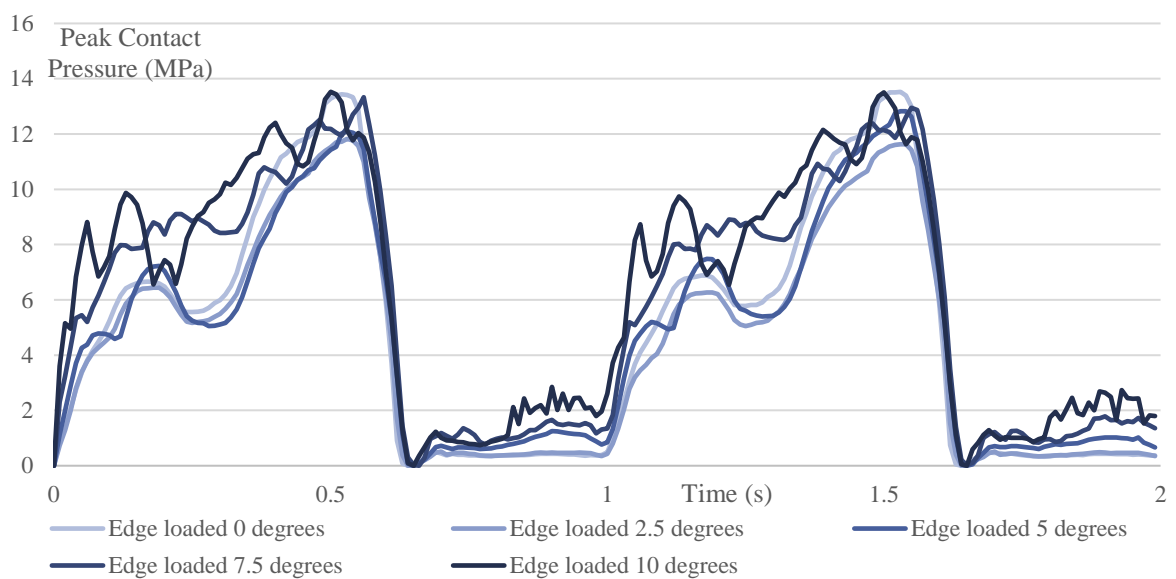


Figure 5.28 Mean peak contact pressure (n=3) for each tested coronal malalignment at 100N swing with an addition 3mm translational offset

With the addition of edge loading (Figure 5.28) the measured peak contact pressure was much more inconsistent at both 7.5 and 10° coronal malalignment. In the edge loading condition the peak contact pressure in the neutral alignment (0°) was the same as that measured at 10°. The peak contact pressures with edge loading were less than those with no translational offset, high swing loads and 10° malalignment. They were also marginally higher than the equivalent kinematic inputs with 100N swing but without edge loading (red).

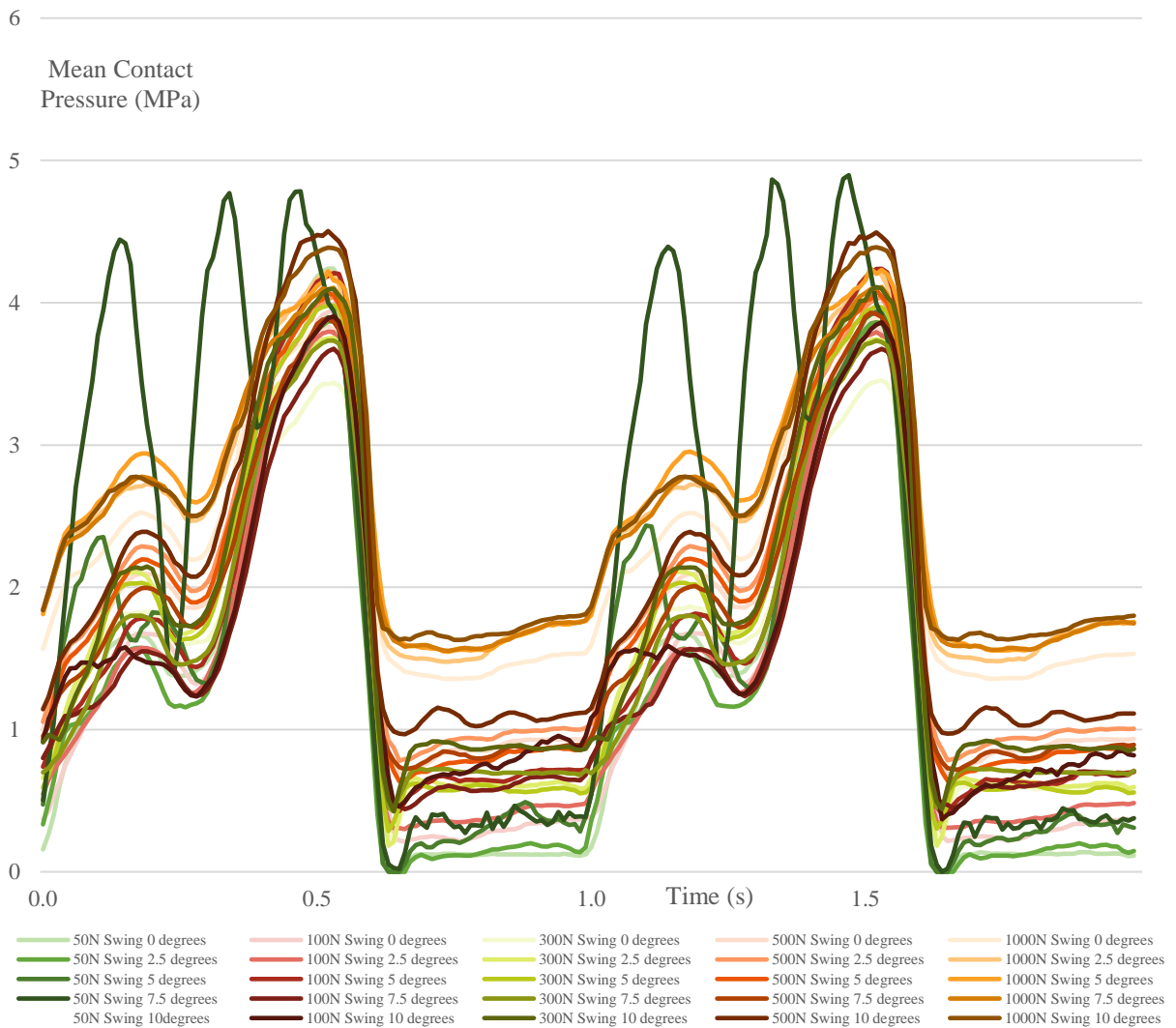


Figure 5.29 Mean average contact pressure (n=3) for each tested coronal malalignment and swing phase load

The maximum mean contact pressure was much lower than the peak contact pressure, measuring between 3 and 5MPa for all of the conditions tested (Figure 5.29). The increased peak pressure at greater coronal malalignment has increased the peak average contact pressures for these conditions also. While there were clear

difference in the mean contact pressure between 1000N and 50N swing phase loads, but between the other swing phase loads the differences were less apparent.

Conversely the contact area (Figure 5.30) was greatest in neutral alignment. The swing phase load had a greater effect on the contact area than the degree of malalignment during the swing phase. During the stance phase of the loading cycle the variation in the contact area was minimal. The 50N swing caused a complete component lift-off when transitioning from stance to swing. At 7.5° there was a substantial reduction in contact area as the load increased. These points of increase and decrease aligned with the oscillation observed in the ab/adduction (Figure 5.20), however the same was not prominent at smaller degrees of malalignment.

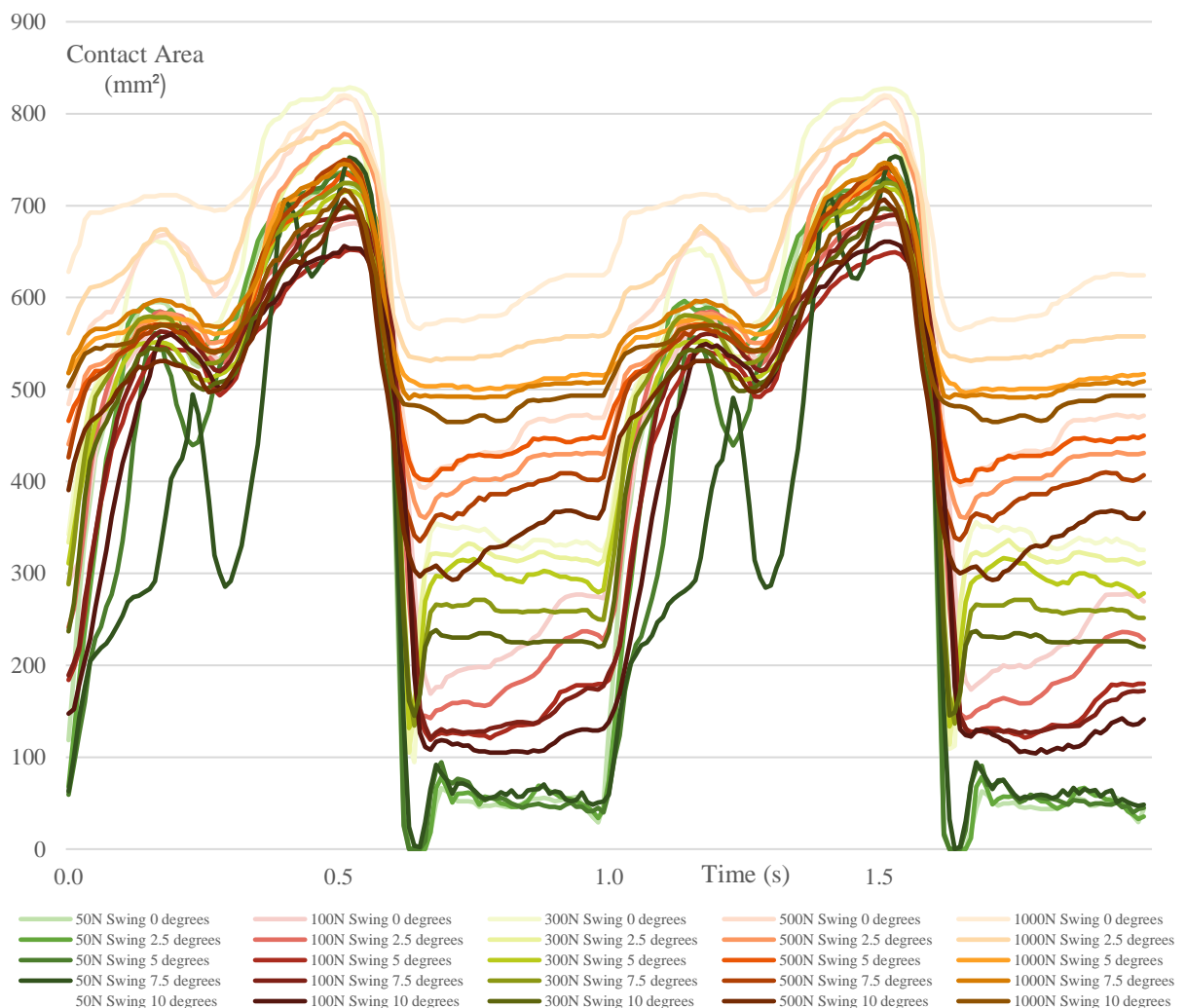


Figure 5.30 Mean contact area (n=3) for each coronal malalignment and swing phase load

The edge loading caused complete component lift-off at the start of the swing phase (Figure 5.31). This is comparable to the 50N swing phase load. The contact area remained low even for the well aligned component. At 7.5° and 10° malalignment there were sharp changes in the contact area until peak stance where it was comparable to other alignments.

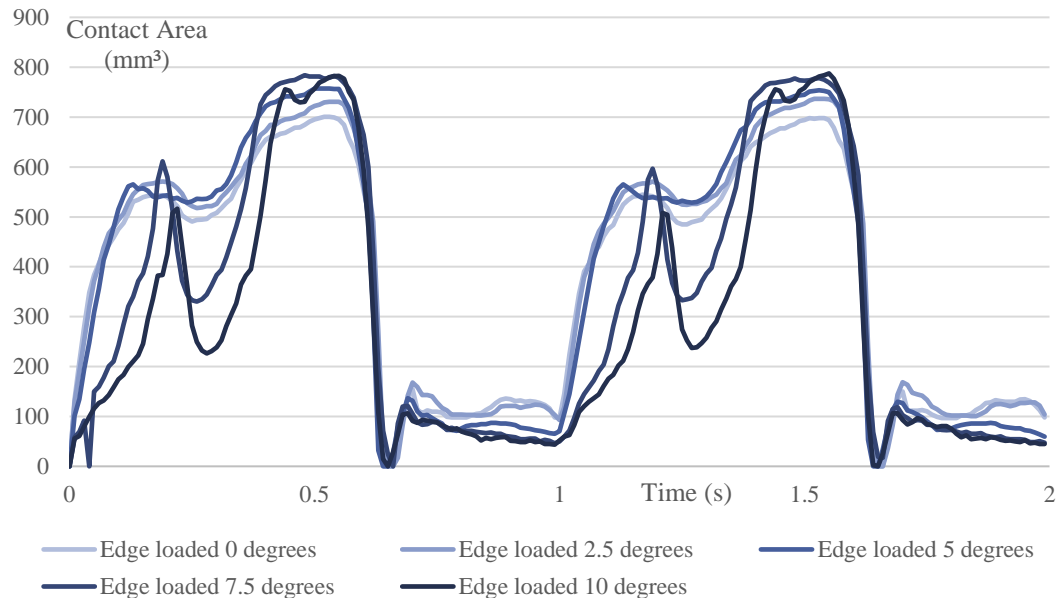


Figure 5.31 Mean contact area (n=3) for each tested coronal malalignment at 100N swing with an addition 3mm translational offset

5.5 Discussion

A single station electromechanical knee simulator proved a valuable apparatus for testing a TAR under a wide range of alignment and loading conditions. The occurrence of dislocation within this biomechanical investigation was relatively uncommon. However, the combination of 50N swing phase loads and 10° coronal malalignment did heighten the risk. This suggested that a mobile bearing TAR, despite having no freedom in adduction/abduction, can facilitate a certain degree of coronal malalignment before dislocation becomes a risk. This also highlights the importance of ligament tensioning.

5.5.1 Effect of alignment and joint tension

While the angular mismatch between the tibial and talar are unlikely to mimic the exact effects of similar alignments *in-vivo*, this model was able to recreate a

component lift-off effect up to 2.2°. Generally, as the degree of malalignment got incrementally greater from 0 to 10 degrees the contact area reduced and the contact pressure increased throughout the gait cycle. The degree of component lift-off in this set up was influenced even more by whether the malalignment was in the varus or valgus direction. While varus malalignment has been observed to be more common for joint replacement alignment (Mann et al. 2011) valgus malalignment is considered to be much harder to correct surgically (Roukis 2016). Valgus deformities are typically more lax (Roukis 2016), this may further amplify the risk. It has been suggested that the ankle can cope better with valgus deformities compared to varus alignment (Conti & Wong 2001), therefore a device could potentially last longer in this condition increasing the importance of the contact areas and stresses. The force inputs including peak force and swing phase load and, at higher malalignment angles, the displacement input also had an effect on the contact with the insert during the loading cycle.

While the degree of lift-off did not necessarily decrease with the increased swing phase loads the duration of the lift-off did decrease. In combination with 50N swing phase loads there was some increase in the degree of lift-off especially at larger malalignment angles. When considering the effect of the swing phase load this study further highlighted the importance of soft tissue balancing. For coronal malalignment in combination with low swing phase loads of 50N, which are proposed to simulate joint laxity, the peak contact pressures were at their highest. With valgus malalignment this is a concern (Roukis 2016). In this condition the contact areas were also the most erratic which could be a risk for stability. This also increased the probability of dislocation in the simulator, this may pose a subluxation risk *in-vivo*.

A similar effect was observed with translational offset, despite a 100N swing phase load this condition showed a similar biomechanical response to the lowest swing phase load of 50N. This included reduced contact areas throughout the gait cycle, greater individual sensel pressures and more erratic pressure profiles at malalignment angles of 7.5 and 10°. The edge loading appeared to amplify the instability of the TAR. A combination of valgus malalignment ligament laxity and translational offset could be considered high risk for a TAR.

In comparison higher swing phase loads, simulating an oversized insert provided some more stability. With the higher load inputs there were increasing pressures observed over a larger area of the medial insert edge at high malalignment angles.

5.5.2 Comparison to literature

Espinosa et al. (2010) used computational modelling of a similar mobile bearing TAR design, the Mobility (DePuy-Synthes, USA), to investigate the effects of malalignment. Their results showed average contact pressures on the superior surface between 3 and 14MPa (Figure 5.32). This can be compared directly to this experimental study under similar conditions; neutral alignment, 2.5, 5 and 10 degrees coronal malalignment (Figure 5.33), the equivalent to version. The same approximate time-point definition of heel strike, mid-stance, heel off and toe off defined by Espinosa et al. (2010) were used in combination with a swing phase load of 100N. The equivalent mean force measured by the Tekscan sensor was comparable (Table 5.3). Due to the steep decrease in force in the input profile used the force at toe off is higher in the experimental instance.

Table 5.3 Loads at similar points in the gait cycle defined by Espinosa et al. (2010)

| | Espinosa et al. (2010) | Smyth (2017) |
|-------------|------------------------|--------------|
| Heel Strike | 800N | 666N |
| Midstance | 2000N | 1576N |
| Heel off | 2800N | 2637N |
| Toe off | 800N | 1212N |

The computational simulation saw the biggest change at the superior surface with a version angle of 5 degrees where the average pressure at heel strike was greatly increased compared to the rest of the gait cycle, a trend which only occurred at this angle. With the mean pressure on the superior surface measuring above 10MPa throughout the stance phase of the gait cycle and upwards of 25MPa at 10° with the highest contact pressures focused at the edge of the insert where it is in contact and on the central convex region (Espinosa et al. 2010).

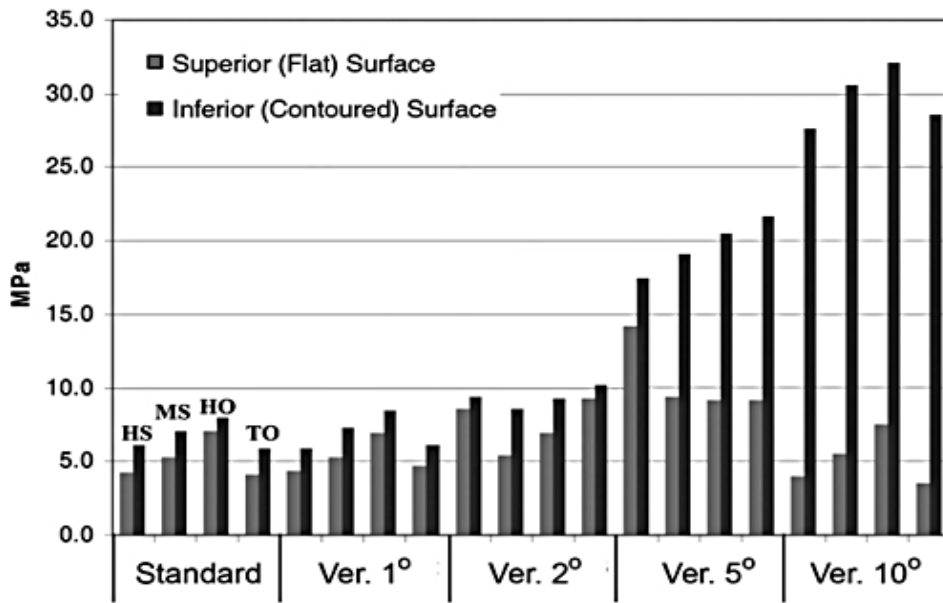


Figure 5.32 Comparing the average contact pressure between the superior and inferior insert surfaces of the DePuy Mobility TAR under coronal malalignment. N. Espinosa et al., Misalignment of Total Ankle Components Can Induce High Joint Contact Pressures, *J Bone Joint Surg Am*, 2010; 92 (5): pp1179 -1187. <https://www.ncbi.nlm.nih.gov/pubmed/20439664>

By comparison the experimental set up follows a similar trend for the average contact pressure throughout the gait cycle at all of the tested alignments (Figure 5.33).

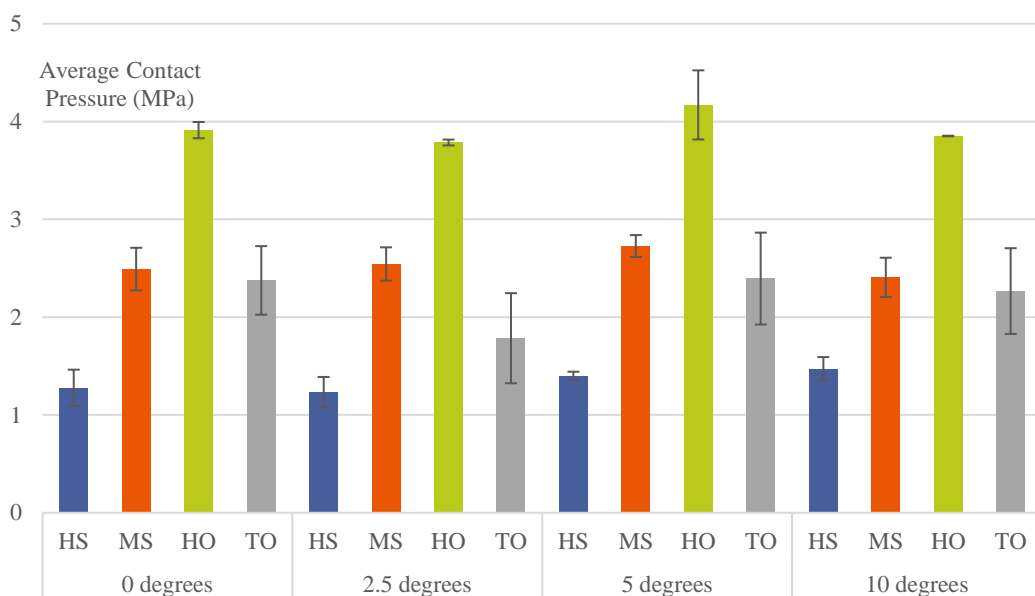


Figure 5.33 Mean average contact pressure (n=3) \pm standard deviation at heel strike (HS), midstance (MS), heel off (HO) and toe off (TO) at neutral alignment, 2.5, 5 and 10 degrees coronal malalignment

Typically, the pressure at toe off is higher than at heel strike in the experimental test set up, this is presumably a result of the higher force at this time point. Despite the fact Espinosa et al. (2010) used lower force inputs than this study the measured tekscan sensor force at the same points in the cycle are comparable due to its underestimation of the input force. In the experimental simulation the gait cycle was applied at the standard 1Hz so the lift-off effects aligned with the biomechanical testing. This high speed load application combined with the unworn insert shape which is slightly higher at the edges compared to the centre caused a central area where pressure was generally not registered. In the computational model the tibial and talar components are both rigidly fixed and thus do not allow any component reorientation unlike the simulator model which allows realignment, to varying degrees, depending on the force input. This is the likely cause of the discrepancy as the force will be highly concentrated on much smaller contact areas if the device cannot realign.

The computational model had the benefit of being able to quantify the contact pressure on both surfaces of the polyethylene insert and observed greater average contact pressures on the curved contact surface for all test conditions. This was significantly larger at both 5 and 10° malaligned conditions compared with the flat and in some cases it was almost ten times higher (Espinosa et al. 2010). Continued cyclic loading at such high pressures which would severely increase the polyethylene failure risk (D'Lima et al. 2001).

5.5.3 Potential impact of malalignment

D'Lima et al. (2001) found that in their finite element investigation of high and low conformity TKRs single condyle loading as a result of lift-off increased both the mean and peak polyethylene stresses observed. In this investigation component lift-off was highly prevalent with lower swing phase loads of 50-300N reducing the contact area substantially. This lift-off results in peak pressures occurring at the medial insert edges only noticeably higher at the greatest malalignment angles.

Taking an average across the three tested TARs showed peak forces of around 16MPa with 10° malalignment, however from the contact pressure maps the peak sensor pressures in the TARs were as high as 21.1MPa (50N swing and 10° malalignment). The discrepancy arises as the peak pressure is derived from four

sensels rather than individually. The individual sensel peak pressure is just short of the yield stress of polyethylene, thought to be 21.7MPa for GUR1050 (Hunt & Joyce 2016). Given the underestimation of the force applied by the simulator it is possible the pressure outcomes may be 10% higher which would reach towards the polyethylene yield stress in more conditions increasing the risk of fatigue failure. This investigation suggests that in valgus malalignment the fatigue risk would be most likely at the medial insert surface where the stresses are highest when the components are brought back into contact.

The component lift-off caused by the coronal malalignment may result in increased wear as has been seen in TKR (Jennings et al. 2007). Alternatively, lower contact areas and increased contact pressure may result in reduced surface wear as has been seen when comparing less conforming, flat, high contact stress TKR insert to a standard curved insert (Galvin et al. 2009).

It must be remembered the problem with malalignment is greater than the surface biomechanics. In the clinical environment such lift-off whether a result of malalignment or ligament imbalance has been associated with micromotion which can lead to loosening (Hintermann & Valderrabano 2003). Component malalignment has also been associated with arthrofibrosis, reducing the motion at the joint and causing pain which can result in early revision (Hintermann et al. 2013). Furthermore, both the malalignment and translational offset could result in bony impingement which has been associated with early complications (Kurup & Taylor 2008).

5.6 Limitations

As with any attempt to model a complicated biological structure mechanically, the limitations come from the assumptions and simplifications.

The weight of the simulator abduction/adduction cradle was assumed to have a similar effect on lift-off effect to the weight of the foot. The effects of the natural ankle ab/adduction during gait were considered negligible whereas in reality these may improve the joint's ability to correct the malalignment or accentuate it further. When measuring during stance Lundgren et al. (2008) found much variability between individuals (Figure 5.34). To the author's knowledge this has not been

documented for the swing phase where the most lift-off is observed. Additionally, the in vitro model does not replicate soft tissue forces or constraints.

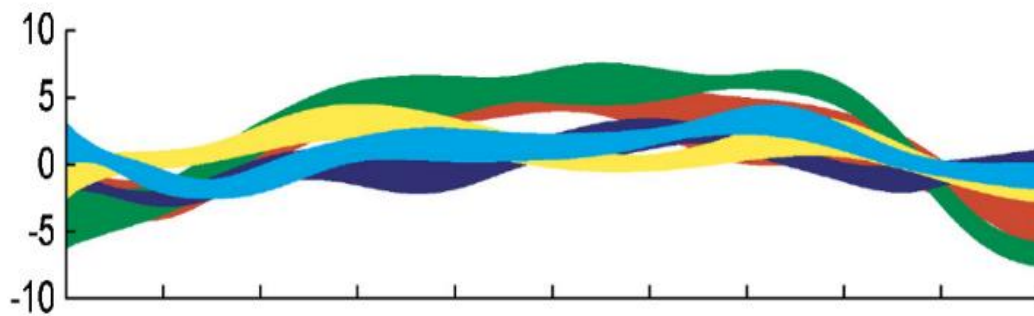


Figure 5.34 Abduction/adduction between the tibia and talus measured during stance phase with invasive marked placement in healthy subjects. Reprinted from *Gait & Posture*, 28 (1), Lundgren, P. et al., Invasive in vivo measurement of rear-, mid- and forefoot motion during walking (2008), pp.93–100, with permission from Elsevier.

Further limitations come from the Tekscan sensor. Measurements could only be taken at the flat on flat interface. These were taken under dynamic loads but otherwise static conditions. High rate of loading reduced some of the sensor sensitivity. As the biomechanics test showed the degree of lift-off was affected by the rotation and to some extent by the displacement yet these were not considered.

Components are aligned optimally aside from the imposed coronal malalignment—this would be clinically unlikely given the ankle complexity. Introducing the addition of translational offset provided some insight into the effects of additional alignment problems.

5.7 Conclusion

The alignment of a TAR combined with soft-tissue joint tension will influence the contact mechanics. The highly conforming design of most three component mobile bearing TARs have no flexibility to accommodate coronal malalignment causing component lift-off during swing. This resulted in uneven loading and lower contact areas, elevating the stress which has been associated with polyethylene fatigue failure and both increasing and decreasing the surface wear of polyethylene. Computational studies showed that the average contact pressure at the curved inferior insert was far greater than at the flat superior surface measured in this

investigation so the risk of fatigue failure may be higher than that observed in this investigation.

5.8 Influence of biomechanics study on the design of the wear study

One of the aims of this biomechanical test was to define the conditions to investigate in terms of wear. Ideally the gait profile would be implemented with a 50N swing phase load in order to observe the most severe lift-off effects. However, the simulator which was allocated for this test relies on pneumatic load control, reducing the sensitivity at these lower forces. As the force limit is closer to 300N the biomechanics results under this condition was considered (Figure 5.24). Figure 5.24 In order to create the full condylar lift-off in this condition a malalignment greater than 5° was required. The AA cradle in KS4 weighs less than in SSKS3 therefore the lift-off is likely to be reduced further. The machine structure would obstruct a 10° malalignment therefore the 7.5° was deemed the best choice to recreate the observed effects on a multi-station wear simulator.

CHAPTER 6
MALALIGNMENT WEAR TEST

CHAPTER 6

MALALIGNMENT WEAR TEST

6.1 Introduction

The need for advanced preclinical testing of total joint replacements (TJR) which goes beyond the optimal conditions has been highlighted (Fisher 2012). It is important that we learn from the expensive mistakes of total hip replacements (THR) not to assume a joint replacement will be implanted perfectly every time. Instead the wear will depend on the surgical precision and the individuals' demands. Embarking on a stratified approach to the wear testing has shown valuable insight. Using observations from retrievals it was noticed that hard on hard THRs were experiencing a strip wear on the femoral component which corresponded with a worn area on the rim of the acetabular cup (Nevelos et al. 2000). By altering simulator conditions, using translational offset to create a microseparation Stewart et al. (2001) showed it was possible to recreate this wear phenomena in hip wear simulation which increased the wear rate significantly compared to well aligned conditions. This was later confirmed by Clarke et al. (2007) but with the addition of a vertical distraction which created an additional wear scar. These early simulations have provided a platform to further investigate a range of clinically relevant alignment conditions relating to edge-loading (Al-Hajjar et al. 2013; Clarke et al. 2016). Computational modelling of similar conditions in metal-on-polyethylene THRs suggested the same problem was likely due to increased contact stresses, and plastic strain (Hua et al. 2014) and a simulator study by Ali et al. (2017) has confirmed this hypothesis with edge loaded wear simulation of the metal on polyethylene bearing combination. Whereas Harris (2012) believed the retrieval literature provides enough evidence to conclude that the common occurrence of edge loading in hard-on-soft bearings does not accelerate the overall wear rate. The observation of polyethylene cracking at the rim of steep cup inclined retrievals suggests there is a fatigue risk with thin highly cross linked liners under edge-loaded conditions (Tower 2007). Similarly for total knee replacements (TKR) D'Lima et al. (2001) showed varus malalignment to result in elevated wear compared to a standard condition, Zietz et al. (2015) corroborated this and found the same relationship for rotational

malalignment. Meanwhile Hermida et al. (2008) showed artificially aged highly crosslinked polyethylene to perform well regardless of severe malalignment conditions, however this was not compared to a standard alignment. Additionally by applying an adduction/abduction torque Jennings et al. (2007) showed coronal lift-off to significantly elevate wear rates

With the lack of pre-clinical test standards for total ankle replacements (TARs), there is an opportunity to learn from the decades of research investment in preclinical hip and knee testing and implement the most appropriate test conditions to consider malalignment. It is the author's belief that it is critical that this opportunity is harnessed from an early stage in preclinical test development.

Having explored the effects of coronal malalignment within the single station simulator and through pressure mapping many variations were highlighted depending on the degree of component malalignment and the magnitude of the swing phase load. From the evidence provided a decision was made to test a 7.5° malalignment angle, to understand the effects of the lift-off and high contact pressures on the wear. However, this is not the only malalignment clinically observed. The collection of retrievals at Leeds has been investigated by Stratton-Powell et al. (2017) with 53% of the components being identified as 'edge loaded'. In this case edge loading was defined as "a depressed area in the insert surface indicative of articulation with the edge of the tibial component". The assumed cause of such deformation was relative translational component positioning to the tibial component in both the medial/lateral and anterior/posterior directions. Buechel Sr. et al. (2003) revised one such posteriorly edge-loaded insert from their cohort of 50 citing the posterior edge-loading to cause premature polyethylene wear and osteolytic cysts (Figure 6.1). While Karantana et al. (2010) reported fracture due to edge loading in two mobile bearing STAR inserts after 52-60 months. Deorio & Easley (2008) explained edge loading as the contact between the polyethylene and the metal edge, explaining that recent designs have addressed this problem by reducing the surface area of the superior polyethylene or increasing the size of the tibial component. In their systematic review Zhao et al.

(2011) grouped edge loading and malalignment together when reporting this reason for failure in 18% of STAR devices.



Figure 6.1 Radiographs showing component malalignment. Image reprinted from Buechel et al. (2003) Ten-year evaluation of cementless Buechel-Pappas meniscal bearing total ankle replacement. FAI 24 (6) pp462-472. Copyright © 2003 by SAGE Publications. Reprinted by Permission of SAGE Publications, Inc.

Due to the high prevalence of this edge deformation within the local retrieval cohort, despite the insert width being substantially smaller than the width of the tibial component which should provide suitable clearance this alignment was also considered.

This chapter aimed to use the standard simulation methods developed earlier to test conditions replicating coronal malalignment and translational offset within the *in-vitro* test environment in terms of polyethylene wear. The retrievals collection was used to validate the clinical relevance of the test methodology.

6.2 Materials and methods

6.2.1 The simulator

Having been validated for testing of TARs (Chapter 4) Leeds Knee Simulator IV (KS4) was again employed to test the Zenith TAR under a defined range of malalignment conditions.

6.2.2 Malalignment wear test methodology

To ensure the effects of elevated wear due to the bedding in of the components observed with this design in both Chapter 3 and 4 before any malalignment condition was implemented all components were initially tested in the neutral alignment. Based on the limitations of the TAR design, the biomechanical investigation and the existing literature a coronal malalignment of 7.5° and translational offset of 3mm in the medial direction were implemented by altering the fixtures (Chapter 5.8). The sequential test plan is outlined in Table 6.1 with diagrams of the component set-up in Figure 6.2.

Table 6.1 Malalignment wear test conditions

| Components | Conditions |
|------------|--|
| TAR 1-6 | 3Mc neutral alignment Validation (Chapter 4) |
| | 0.6Mc malalignment setup refinement (A) |
| | 3Mc with 7.5° coronal malalignment |
| | 2Mc with 7.5° coronal malalignment and additional 3mm translational offset (B) |
| TAR 7-12 | 2Mc neutral alignment bedding in (C) |
| | 2Mc 3mm translational offset (D) |
| | Further 2Mc 3mm translational offset (D) |

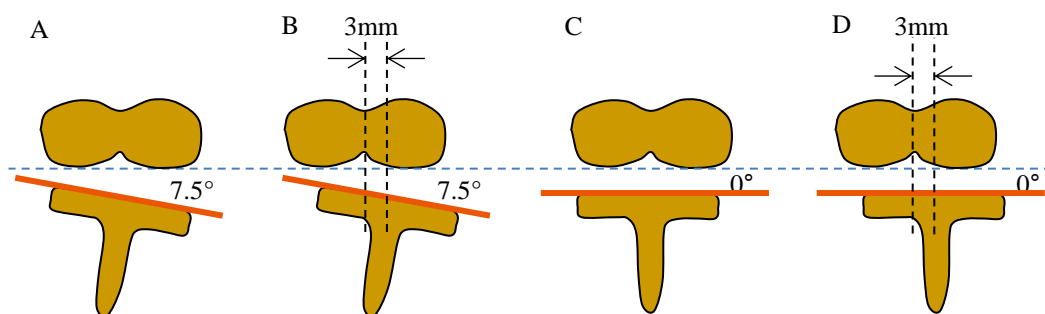


Figure 6.2 Diagram of component set-up for each tested condition

6.2.3 Component preparation

Fixtures with the desired angular offset were designed for KS4 in order to create the coronal malalignment (Appendix B). After the simulator validation cycles (Chapter 4) the tibial components were removed from their holders and realigned

and cemented into the malalignment fixtures with the adduction/adduction cradle propped at 7.5° to avoid any translational malalignment (Figure 6.3). Once the cement had set this support was removed. To add a further translational offset new talar fixtures were designed, the talar surface appeared the same but a displacement was applied to the lateral side when fixing it to the talar plate. This ensured the talar could be cemented centrally to the fixture as it would be typically.

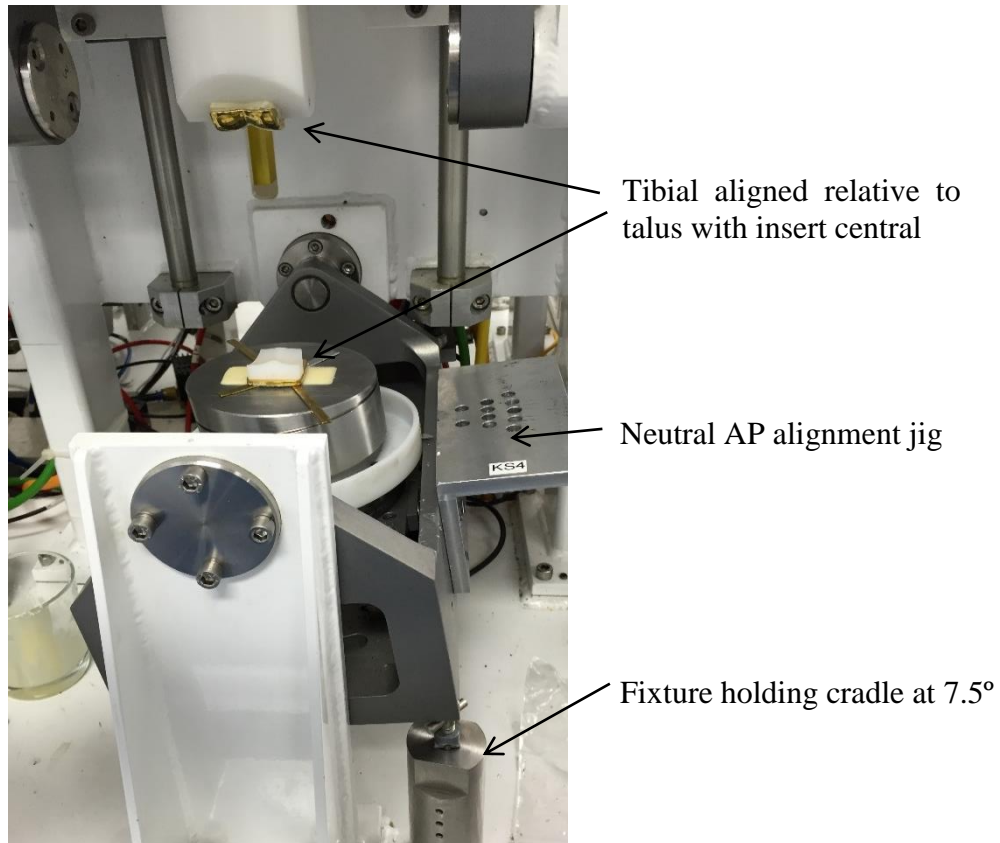


Figure 6.3 Component Set-up

The tibial components maintained their prior alignment thus creating an offset between the components. There are no measurements of translational offset published in literature, so the test aimed to recreate the more severe examples observed amongst the retrievals. By trial, varying the talar position in the single station knee simulator (SSKS3) 3mm seemed to provide the desired deformed lip. The Corin Zenith design has a small clearance between the tibial component and the widest point of the insert in the medial-lateral direction (Figure 6.4) which allows this value to remain relatively small but with the potential for substantial

deformation with translational malalignment. A similar procedure was followed to transition from neutral alignment directly to the translational offset condition.

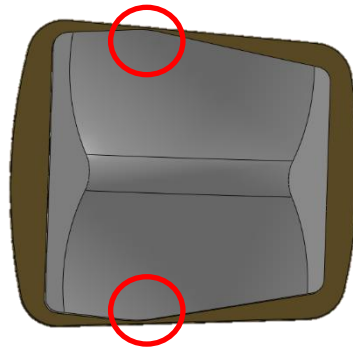


Figure 6.4 Zenith components showing lack of clearance highlighted in red

6.2.4 Simulator kinetics and kinematics

As previously n=6 TARs were tested under the same input kinematics in a 25% bovine serum, 0.3% Sodium Azide solution. The serum was changed every 0.33Mc and the wear was measured gravimetrically, as previously described in Chapter 2.4, every Mcs. Again, two unloaded soak controls were used to compensate for any fluid uptake. While testing coronal malalignment the components moved stations every Mc. When the translational offset was applied this procedure was stopped and the components remained in the same station in order to concentrate the location of the deformation.

6.2.5 Measuring lift-off

The degree of lift off was measured for each station using a potentiometer. To accurately measure about the centre of rotation of the abduction/adduction cradle a fixture was designed and manufactured to align to the potentiometer centre (Appendix B). The arm of the potentiometer was fixed in a retort stand which was secured with weights (Figure 6.6). The potentiometer was validated by applying know abduction (eversion) angles between 0 and 9 degrees measured with a digital inclinometer and recording the potentiometer output. The linear relationship enabled conversion of potentiometer output to the actual angle. In all cases the R^2 value was greater than 0.989, providing confidence in the linearity.

Using a second retort stand an LVDT was set up to intersect with the flexion/extension cradle at peak dorsiflexion. This provided a bench mark for the gait cycle. Readings from both the LVDT and potentiometer were fed into an oscilloscope (Tektronix, Oregon) (Figure 6.5).

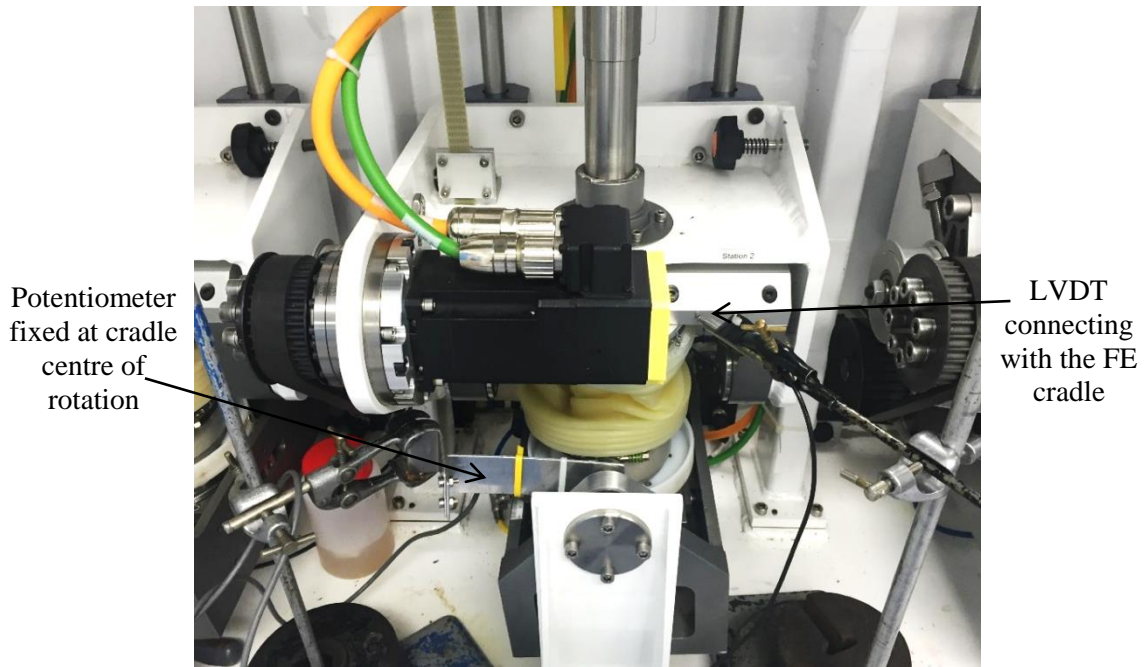


Figure 6.6 Apparatus for measuring abduction/adduction

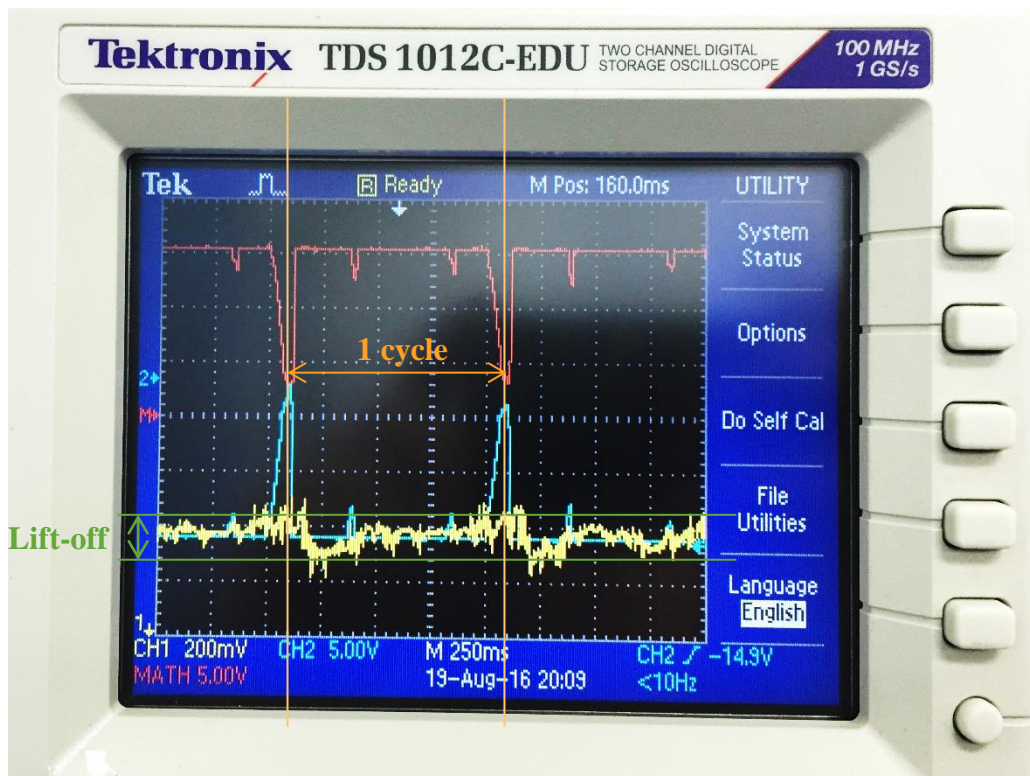


Figure 6.5 Example trace from oscilloscope demonstrating both outputs

The simulator was run for at least 100 cycles to ensure it had reached a steady loading profile after which data from the oscilloscope was saved to a USB. This process was carried out sequentially to obtain data for all simulator stations.

6.2.6 Surface measurements

Before testing and every two Mcs or prior to any change in condition contact Talysurf (Taylor Hobson, Leicester, UK) surface roughness measurements were taken to understand the topographical changes occurring.

Alongside the contact profilometry, Infinite Focus (Alicona, Austria) non-contact measurements were taken of the complete superior insert surface. This equipment uses focus variation technology combining white light, an optical microscope system to decipher the best focus and a vertical scanning capability to provide topographical information (Danzl et al. 2011). The components were fixed in a custom-made jig. At key measurement points in the test all of the components' superior insert surfaces were imaged. This aimed to provide a comparison between the neutral and malalignment conditions (Figure 6.7).

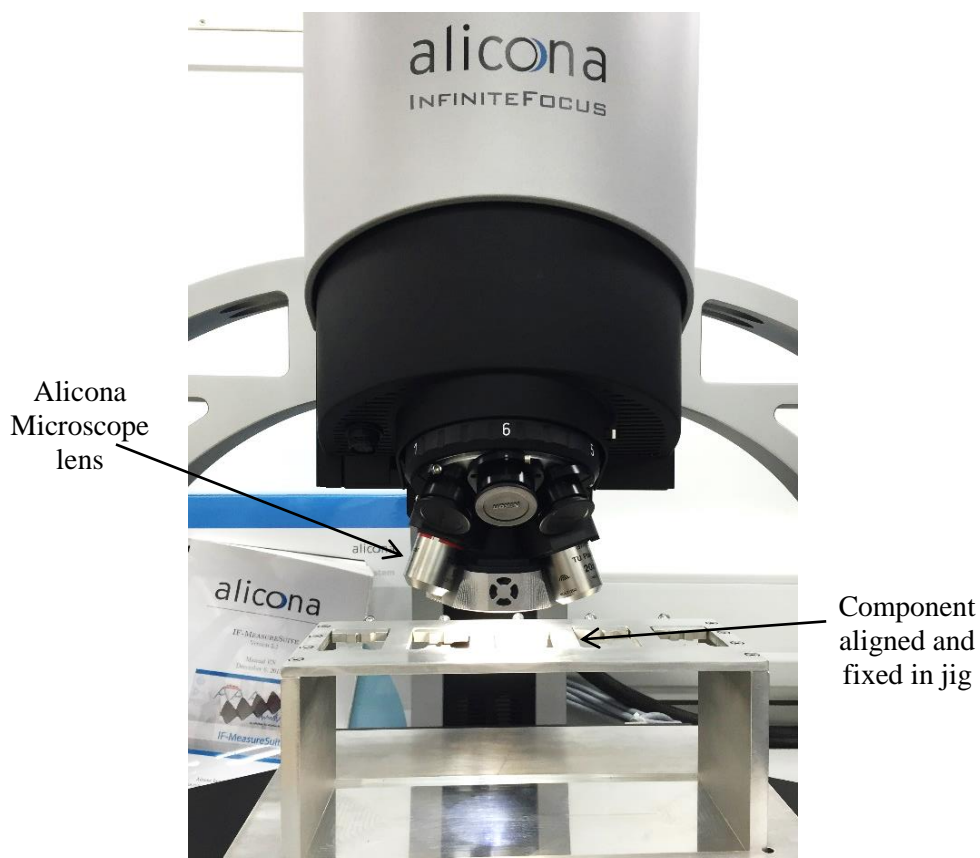


Figure 6.7 Infintefocus microscope (Alicona, AT) measurement set up

The Alicona scanning parameters were adopted from the methodology developed by (Stratton-Powell et al. 2017). To specifically image the Zenith TAR the measurement parameters had to be refined by optimising the contrast setting until the same quality measurement was obtained. This ensured the complete surface could be imaged with minimal lost data. The lowest available objective lens, 10x was used to reduce the scanning time. For the Zenith an exposure time of 130 μ s and contrast of 1.5 were required to obtain a detailed surface scan. To successfully image the complete insert surface without exceeding the data point limit a vertical resolution of 300nm and lateral resolution of 5 μ m were considered sufficient to obtain a high-resolution surface map without exceeding the data point limit.

In post processing the Alicona file format was exported as a surround map file (.sur) which could be used within Talymap Gold software (Taylor Hobson, Leicester, UK). The area was cropped to fit just the superior surface, removing any measurement of the fixture from the analysis and the tilt was removed using a straight line algorithm within the software. Manually the data was thresholded to remove any erroneous data from the fixturing. Relevant outputs such as the surface height maps and mean medial-lateral profile were obtained from the filtered data. Bearing curves have been previously used to represent the surface roughness as a cumulative form graph based on the surface height distribution histogram (Gadelmawla et al. 2002). In this case it was applied to the inset form. The Abbott-Firestone bearing curve was captured to aid comparison to retrievals using existing methodology which uses this surface characterisation parameter to describe and categorise an edge-loaded surface (Stratton-Powell et al. 2017).

6.2.7 SSKS3 validation

As the multi-station pneumatic simulator did not replicate the desired inputs (Chapter 4.4.1) as closely as the single station electromechanical simulator (Figure 6.8) a one Mc wear test was carried out in this simulator under the same coronal malalignment conditions as the extended wear test. To bypass the bedding in effects a worn insert from the first wear test was used in combination with tibial and talar component from the biomechanical study which had been subjected to a relatively low number of cycles so had not experienced the same polishing effect which is seen with the bedding in.

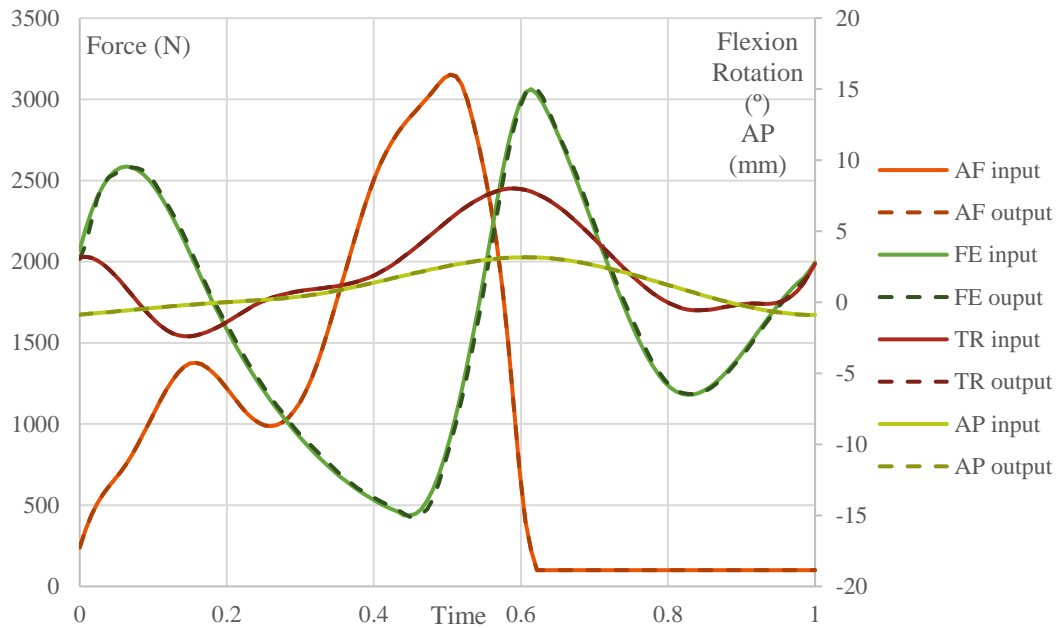


Figure 6.8 SSKS3 Profile input (solid) compared to average output profile (dashed) for 100N swing load

6.3 Results

6.3.1 Measured lift-off

The simulator had to be altered in order to improve the freedom of the ab/adduction cradle, shims were placed under the base of the stations to improve the alignment. The lift-off measured varied between stations (Figure 6.9), greatest at station four with minimal change in abduction in stations two and five. The lift-off was defined as the change in ab/adduction angle as this brought the tibial component out of contact with the insert.

For the stations which experienced a swing the general trend was comparable to that observed in the biomechanical investigation with the majority of lift-off occurring as the peak load reduces (Figure 5.19). Due to the higher swing phase loads the same secondary lift off can be observed around the first loading peak.

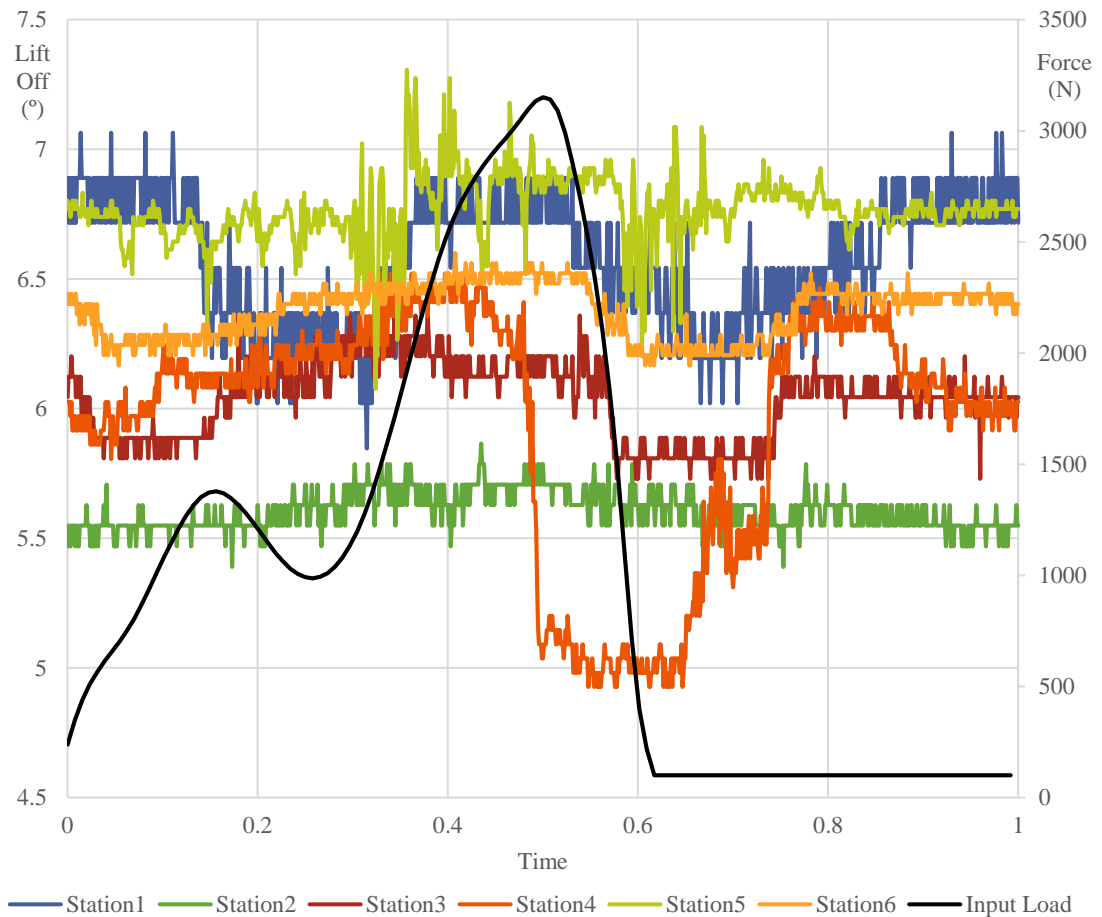


Figure 6.9 Abduction/adduction cradle motion as measured with a potentiometer

6.3.2 Coronal malalignment

As presented in Chapter 4 there was an initial bedding in wear rate of $31.2 \pm 5.4 \text{mm}^3/\text{Mc}$ with neutral alignment. For the following two Mc this decreased significantly to $18.9 \pm 3.8 \text{mm}^3/\text{Mc}$ ($P < 0.001$). The introduction of a 7.5° coronal malalignment saw the wear rate decrease to $11.4 \pm 2.3 \text{mm}^3/\text{Mc}$, significantly different to the prior condition ($P = 0.014$). This is comparable to the same malalignment condition tested on one insert in the single station which had a wear rate of $13.4 \text{mm}^3/\text{Mc}$ (Figure 6.10).

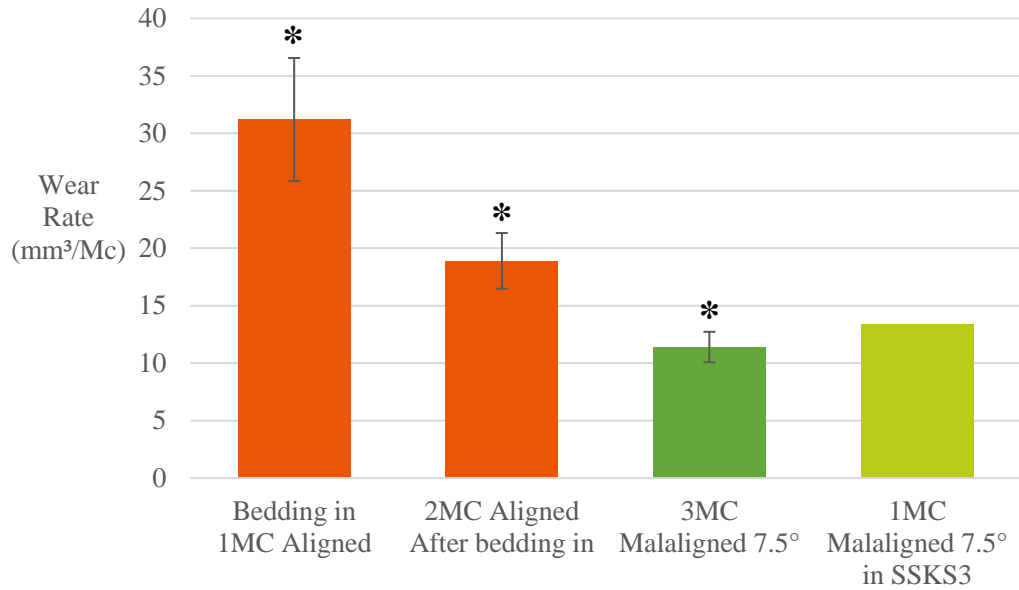


Figure 6.10 Mean measured wear rates under aligned and malaligned conditions

The mean wear rate reduced significantly despite some of the stations not experiencing measurable lift off. Moving though stations will negate some of this effect. Considering the wear rate at each individual station (Figure 6.11 the effect of lift-off is apparent. With the minimal swing on stations two and five there is not the same noticeable reduction in wear rate from the three Mc well aligned (grey) to the further three malaligned as there is for the other stations.

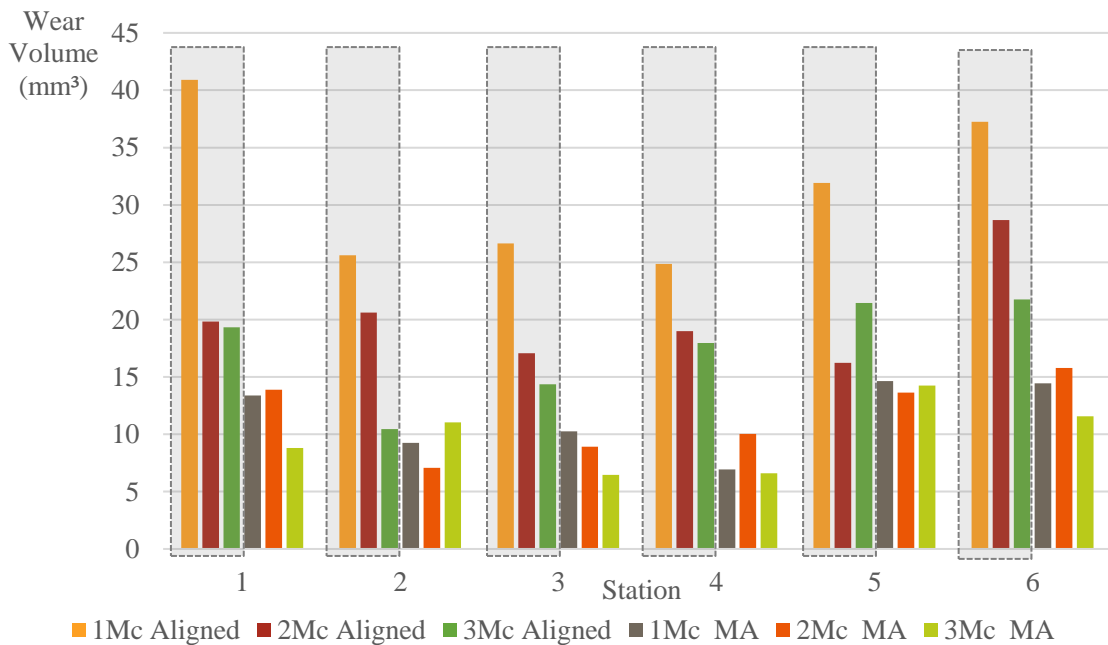


Figure 6.11 Wear volume at each station under each condition with the well aligned Mcs highlighted in grey

Between the aligned and malaligned conditions the changes in surface roughness were measured (Table 6.2). The changes were generally minimal with the tibial component experiencing a continued reduction in Ra. Conversely, the talar roughness, both medial and lateral, increased but only the inferior insert lateral trace saw the Ra increase.

Table 6.2 Changing roughness measurements from well aligned to coronal malalignment with 95% confidence limits

| | | Aligned | | | Malaligned (MA) | | | | | |
|----------|-----------------|-----------------|-----------------|-----------------|-------------------------|-----------------|-----------------|------------------------|-----------------|-----------------|
| | | 3Mc | | | 2Mc | | | 3Mc | | |
| Ra (µm) | | centre | medial | lateral | centre | medial | lateral | centre | medial | lateral |
| Average | Talar | 0.124 ±0.009 | 0.042 ±0.004 | 0.048 ±0.005 | 0.128 ±0.009 | 0.053 ±0.006 | 0.058 ±0.007 | 0.119± 0.011 | 0.060 ±0.007 | 0.070± 0.012 |
| | Inferior Insert | 1.479 ±0.160 | 0.773 ±0.111 | 0.749 ±0.086 | 1.291 ±0.145 | 0.699 ±0.100 | 0.673 ±0.083 | 1.278± 0.132 | 0.613 ±0.092 | 0.872± 0.171 |
| | Superior Insert | 0.116 ± 0.030 | | | 0.134 ± 0.033 | | | 0.112 ± 0.025 | | |
| | Tibial | 0.020 ± 0.002 | | | 0.018 ± 0.002 | | | 0.016 ± 0.002 | | |
| | | | | | Aligned → 2Mc MA | | | 2Mc MA → 3Mc MA | | |
| % Change | Talar | - | - | - | 2.7 | 26.0 | 20.8 | -7.2 | 13.3 | 21.2 |
| | Inferior Insert | - | - | - | -12.7 | -9.5 | -10.1 | -1.1 | -12.4 | 29.5 |
| | Superior Insert | | - | | | 15.3 | | | -16.3 | |
| | Tibial | | - | | | -10.8 | | | -6.9 | |

The wear rate was not the only observed change with the coronal malalignment condition. For the components in neutral alignment there is generally a well-defined raised central region. In the coronally malaligned components there was a lateral shift in this raised region apparent in inserts one, two, three and five (Figure 6.12), however, the change is not visible on all components.

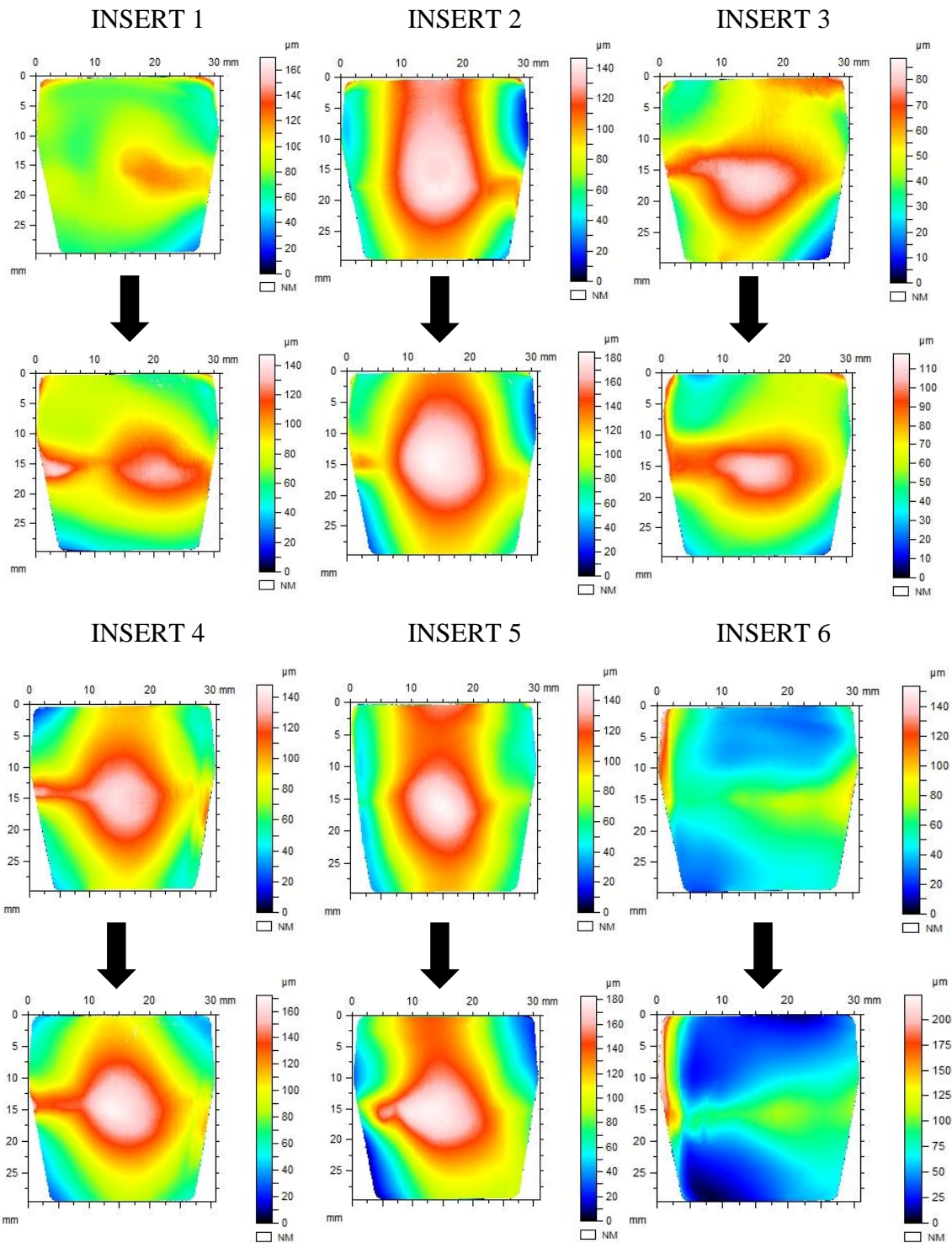


Figure 6.12 Changes in insert form after 3Mc aligned compared to 3Mc coronal malalignment

One of the inserts (six) exhibited edge loading even in the neutral alignment (Figure 6.12) either as a result of the initial component set up or as a result of small variations between the individual stations. As previously highlighted the insert width has minimal clearance with the tibial component (Figure 6.4), any small deviation from optimal component set-up will impact the alignment. With a step height of approximately 200 μm this is not much greater than the increase height due to the rotational centre. Removing the edge loaded profile of insert six the mean medial/lateral surface profiles of the other five inserts were compared (Figure 6.13). The mean profile quantifies this visible change at the lateral side of the insert form but the effects are subdued as the change was most prominent just at the middle of the insert.

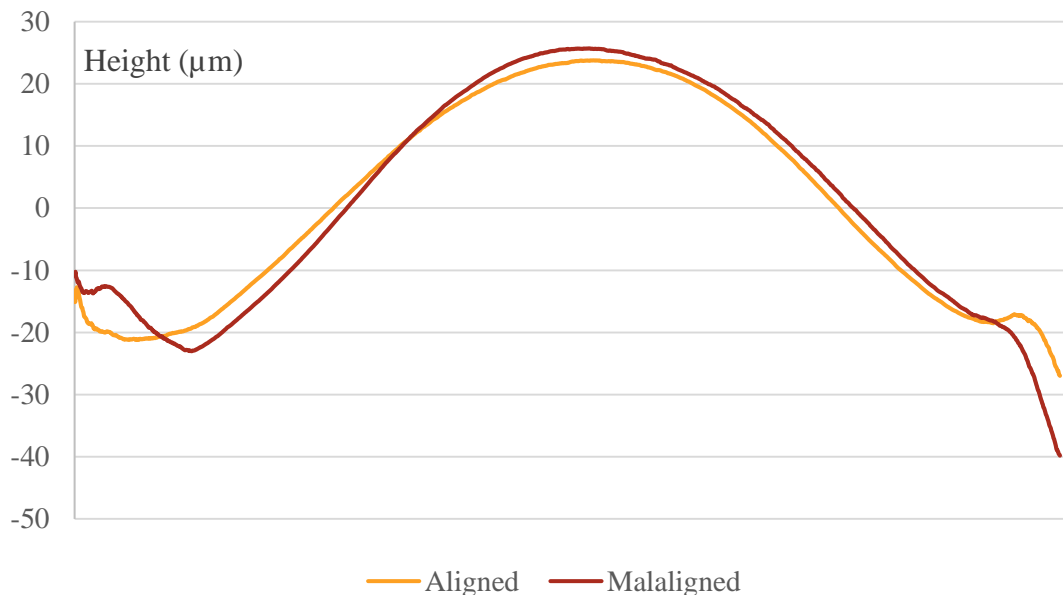


Figure 6.13 Mean medial/lateral surface profile of inserts 1-5

6.3.4 Coronal malalignment with translational Offset

With the additional translational offset creating 'edge loading' the wear measured $9.89 \pm 0.98 \text{ mm}^3/\text{Mc}$. There was no significant difference ($P=0.458$) between the wear rate with solely coronal offset and that in combination with a 3mm translational offset (Figure 6.14). Likewise, for this condition the wear rate was significantly lower ($P<0.001$) than the earlier stages.

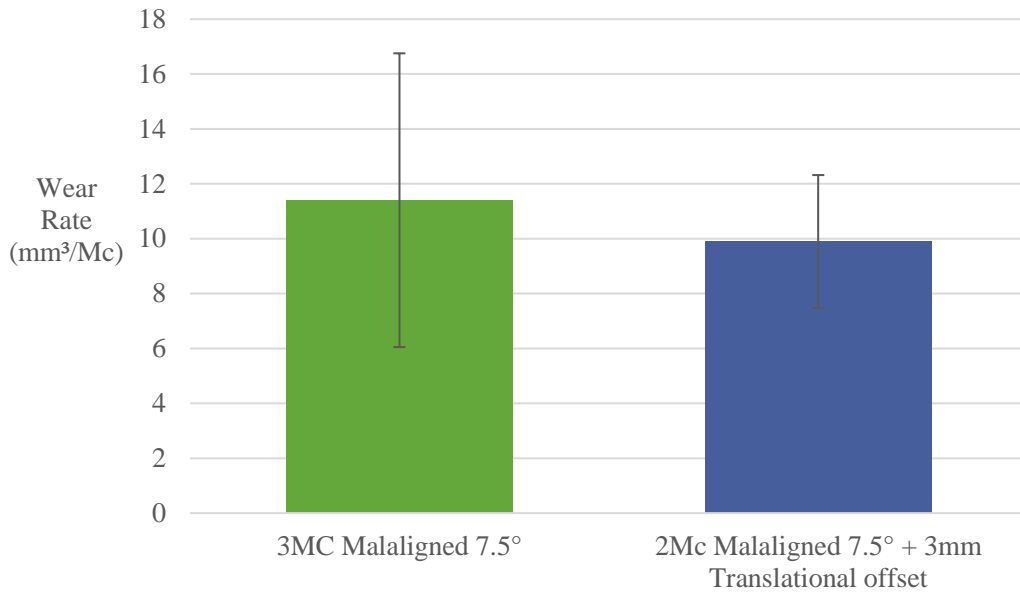


Figure 6.14 Wear rate for coronal malalignment with and without translational offset

The surface roughness measurements saw a general trend of increasing Ra across on the talar and superior insert while the lateral inferior insert surface reduces in roughness substantially and the medial side increases (Table 6.3).

Table 6.3 Change in surface roughness, Ra with the addition of translational offset and 95% confidence limits

| | | Malaligned | | | MA + TO | | |
|----------|--------------------|---------------------------|-----------------|-----------------|-----------------|-----------------|-----------------|
| | | 3Mc | | | 2Mc | | |
| | | centre | medial | lateral | centre | medial | lateral |
| Average | Talar Ra | 0.119 ±0.011 | 0.060 ±0.007 | 0.070 ±0.012 | 0.158 ±0.047 | 0.063 ±0.011 | 0.073 ±0.019 |
| | Inferior Insert Ra | 1.278 ±0.132 | 0.613 ±0.092 | 0.872 ±0.171 | 1.253 ±0.133 | 0.721 ±0.137 | 0.478 ±0.037 |
| | Superior Insert Ra | 0.112 ± 0.025 | | | 0.121±0.031 | | |
| | Tibial Ra | 0.016 ± 0.002 | | | 0.015 ± 0.003 | | |
| | | 3Mc MA→3Mc MA + EL | | | | | |
| % Change | Talar Ra | - | - | - | 33.1 | 5.3 | 4.4 |
| | Inferior Insert Ra | - | - | - | -2.0 | 17.6 | -45.2 |
| | Superior Insert Ra | | | | | 7.9 | |
| | Tibial Ra | | | | | -6.25 | |

Despite no significant changes in the wear rate the inserts underwent a deformation caused by the 3mm translational offset resulting in edge loading (Figure 6.15).

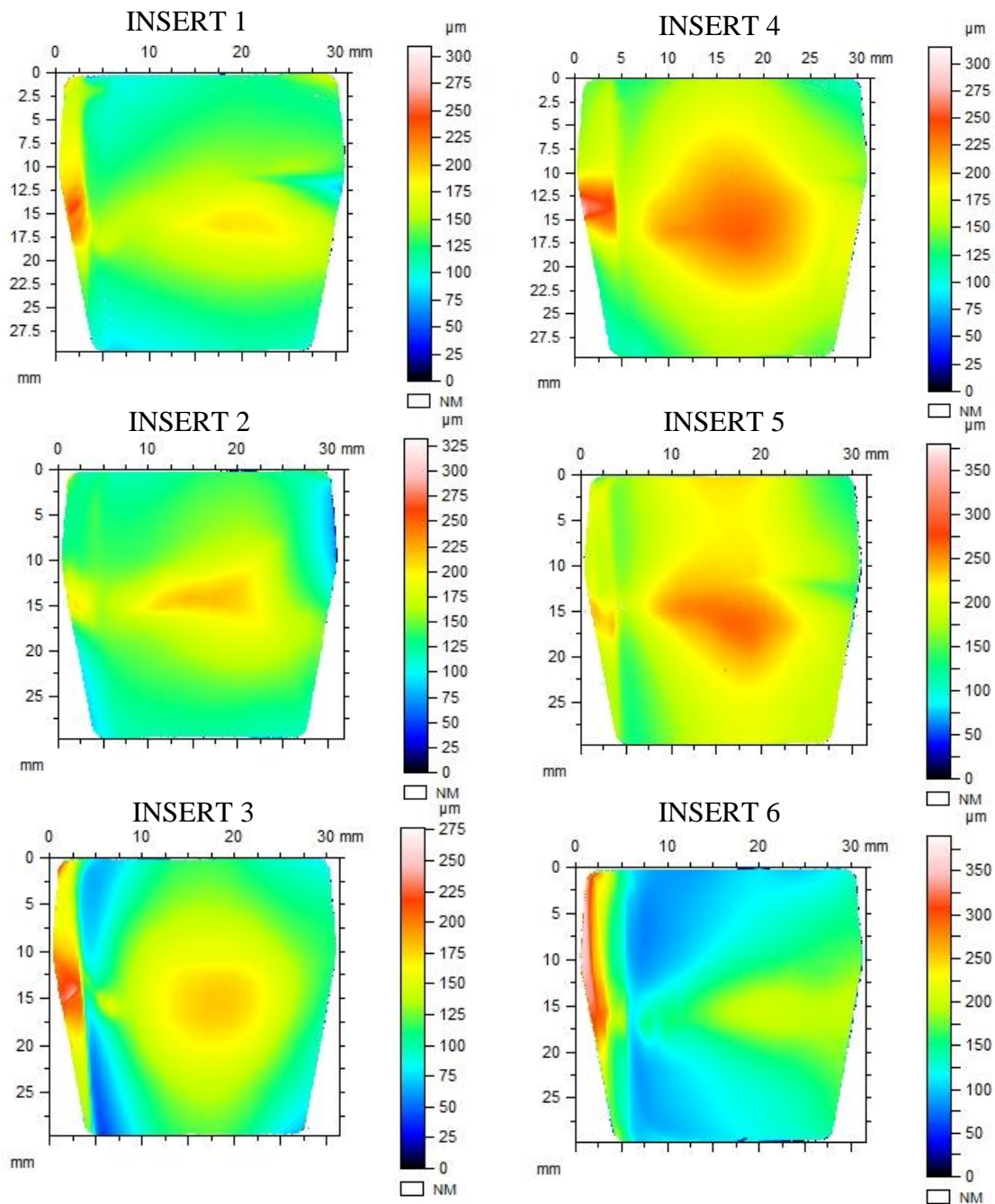


Figure 6.15 Coronally malaligned and edge loaded insert height maps

There is some variability in the severity of the deformation caused by the translational offset. The step height for insert six is more severe than the rest due to the initial alignment, however, insert three showed a similar magnitude. Again,

excluding insert six the mean medial/lateral profiles can be compared to the measurements after the earlier test conditions (Figure 6.16).

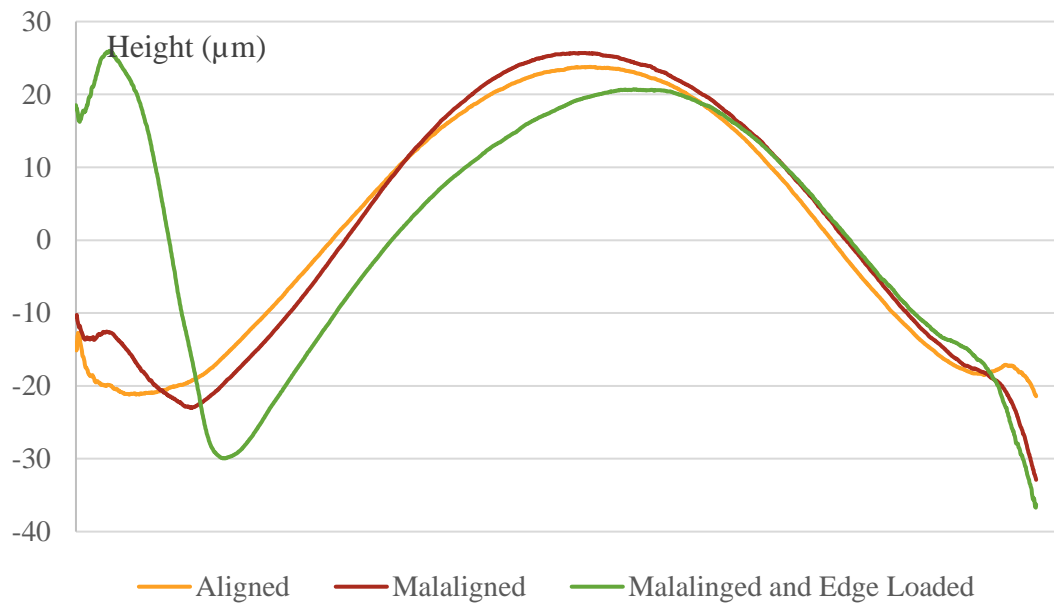


Figure 6.16 Mean medial/lateral profile from the five inserts

The mean profile shows a typical step height of 55µm (Figure 6.16) caused by the translational offset across the length of the surface whereas at points the step height was greater than 100µm (Figure 6.15). From the profile the polyethylene deformation caused by edge loading occurs between 1mm and 4.5mm from the lateral edge. Some of this slope will be caused by the variation between the insert profiles and the displacement controlled rotation causing a slight curved deformation rather than a very definite step.

6.3.5 Translational offset

In order to assess the effects of edge load without the coronal malalignment condition in a comparable way new inserts were tested in neutral alignment first. The same bedding in elevated wear of $21.52 \pm 4.38 \text{ mm}^3/\text{Mc}$ was measured (Figure 6.17). This reduced significantly ($P=0.002$) to $11.73 \pm 3.27 \text{ mm}^3/\text{Mc}$ in the second Mcs of this condition. During this bedding in there was an overall decrease in the surface roughness (Table 6.4). Despite the decrease in the mean wear rate to $5.85 \pm 1.12 \text{ mm}^3/\text{Mc}$ under the edge loaded condition this change was not considered significant ($P=0.056$). As the components were not moved stations in the edge

loaded condition to keep the edge loaded region fixed the effects of the varying kinematics between each station will be amplified at this stage producing greater confidence intervals. There was an initial decrease in the inferior insert Ra with the addition of edge loading and minimal change after. Whereas there was a continued increase in the medial talar Ra for the same time period (Table 6.4). There was also an unexpected increase in the tibial component Ra after four Mc edge loading.

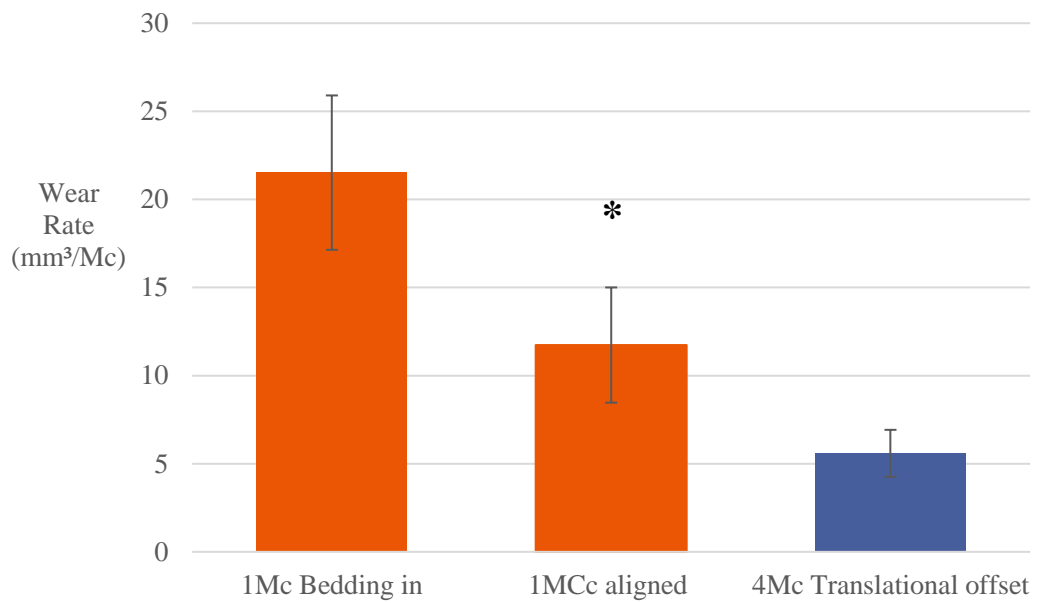


Figure 6.17 Comparing wear rate in neutral alignment to that after 4Mc translational offset

Table 6.4 Mean Ra roughness measurements for translational offset test with 95% confidence limits

| | | Pretest | | | Aligned | | |
|----------|--------------------|-----------------------------|-----------------|-----------------|------------------------|-----------------|-----------------|
| | | | | | 2Mc | | |
| | | centre | medial | lateral | centre | medial | lateral |
| Average | Talar Ra | 0.156 ±0.015 | 0.053 ±0.016 | 0.060 ±0.027 | 0.118 ±0.007 | 0.030 ±0.005 | 0.047 ±0.005 |
| | Inferior Insert Ra | 2.169 ±0.133 | 1.870 ±0.092 | 1.694 ±0.068 | 2.008 ±0.105 | 0.797 ±0.078 | 0.73 ±0.054 |
| | Superior Insert Ra | 0.904 ± 0.043 | | | 0.167 ± 0.052 | | |
| | Tibial Ra | 0.036 ± 0.003 | | | 0.016 ± 0.003 | | |
| | | | | | Pretest → 2Mc | | |
| % Change | Talar Ra | - | - | - | -24.1 | -43.3 | -21.6 |
| | Inferior Insert Ra | - | - | - | -7.5 | -57.4 | -56.6 |
| | Superior Insert Ra | | - | | | -81.5 | |
| | Tibial Ra | | - | | | -55.6 | |
| | | Translational Offset | | | | | |
| | | 2Mc | | | 4Mc | | |
| | | centre | medial | lateral | centre | medial | lateral |
| Average | Talar Ra | 0.147 ±0.010 | 0.039 ±0.003 | 0.047 ±0.004 | 0.137 ±0.007 | 0.050 ±0.007 | 0.068 ±0.006 |
| | Inferior Insert Ra | 1.968 ±0.115 | 0.760 ±0.050 | 0.629 ±0.046 | 2.246 ±0.353 | 0.768 ±0.050 | 0.622 ±0.049 |
| | Superior Insert Ra | 0.101±0.030 | | | 0.134±0.039 | | |
| | Tibial Ra | 0.018±0.001 | | | 0.030±0.002 | | |
| | | 2Mc → 2Mc TO | | | 2Mc TO → 4Mc TO | | |
| % Change | Talar Ra | 24.1 | 58.0 | -17.2 | -6.7 | 28.2 | 44.7 |
| | Inferior Insert Ra | -2.0 | -4.6 | -13.8 | 14.1 | 1.0 | -1.1 |
| | Superior Insert Ra | | -39.5 | | | 32.8 | |
| | Tibial Ra | | 12.5 | | | 62.0 | |

On this occasion, a number of the inserts tested experienced an element of edge loading when they should have been in neutral alignment. After revisiting the data there was no clear indication of what caused the offset. This highlighted the difficulty with such tight clearance to achieve a confidence in the component alignment by eye (Figure 6.18).

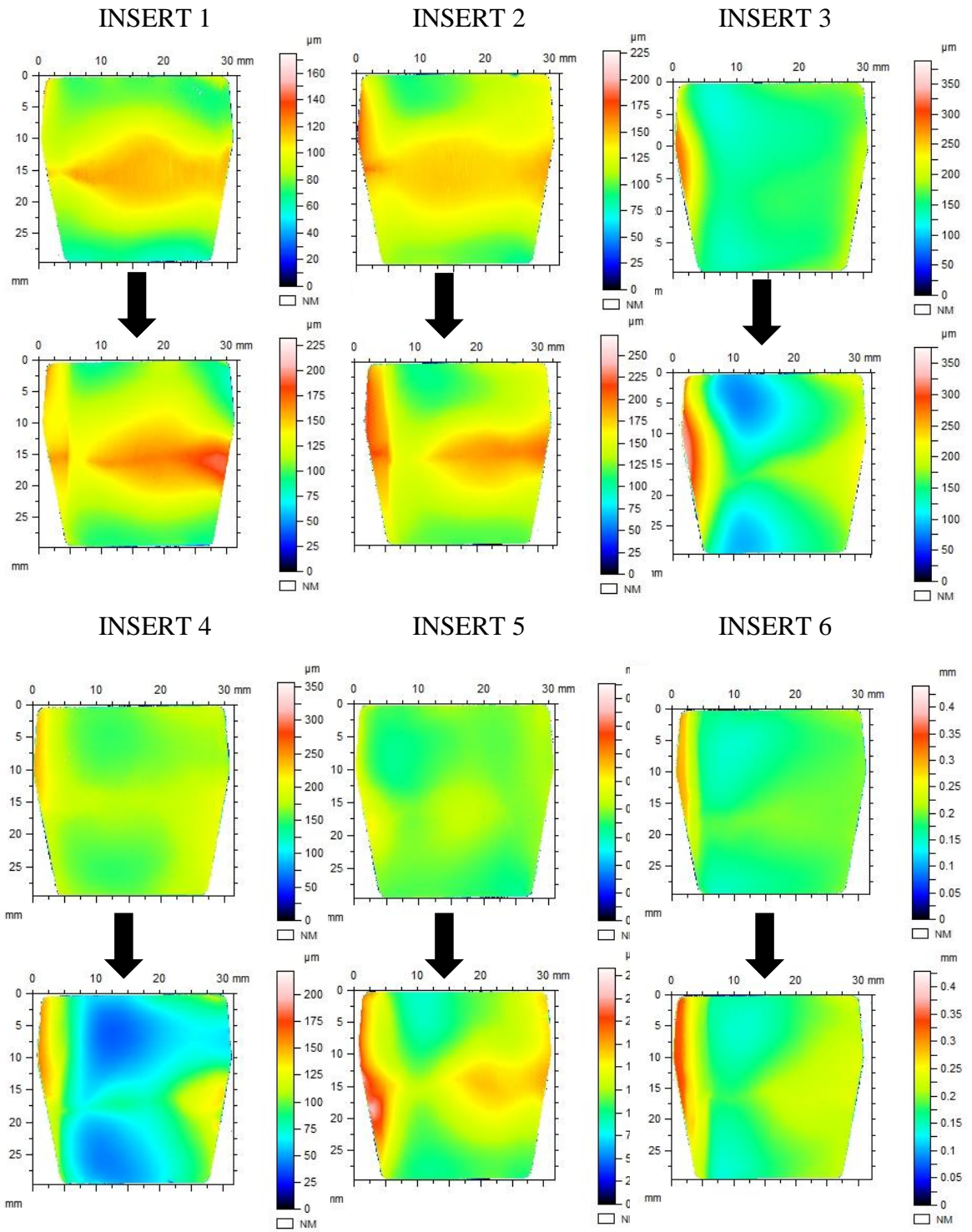


Figure 6.18 Comparing height maps after 2Mc neutral alignment to after 4Mc with 3mm translational offset

The implemented edge loading achieved with the components in neutral coronal alignment appears to be less well defined than that with the coronal malalignment, with the effects of the rotational component of motion more apparent (Figure 6.19).

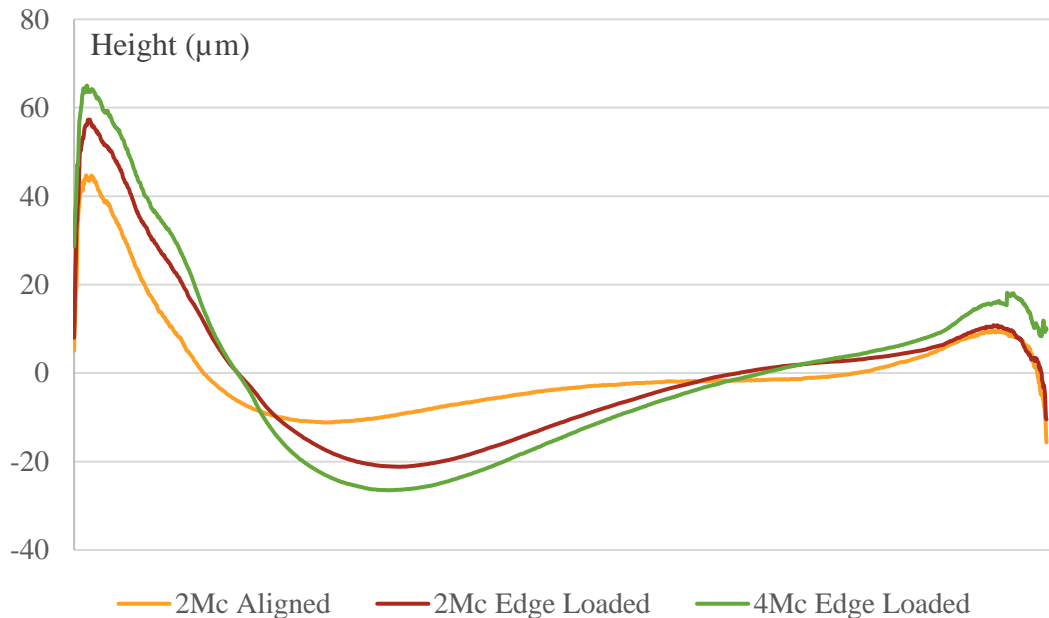


Figure 6.19 Mean medial lateral profiles comparing the surface after 2Mc bedding in to the effects of 4Mc edge loading

As previously mentioned some inserts experienced a degree of edge loading when they should have been aligned in the neutral position. As a result, the edge loading occurs more laterally than with an intentional 3mm offset. The magnitude of plastic deformation is also less measuring $\sim 54\mu\text{m}$ (Figure 6.), this will be because two of the inserts were correctly aligned thus reducing the average. The plastic deformation increased with the talar offset to create a mean step height the length of the surface of $\sim 75\mu\text{m}$ and further to $\sim 90\mu\text{m}$ after a second two Mc with translational offset.

6.3.6 Comparison to retrievals

In order to ensure the simulated conditions were producing physiologically relevant outcomes they were compared to retrievals. Abbott-Firestone bearing curves were used as an approximation for the surface form, calculated by integrating the profile trace. The mean Abbott-Firestone curves for the simulator samples both after well aligned wear testing and a translational offset were compared to the retrievals. Within the retrievals collection cohorts were defined as

‘edge loaded’ or ‘normal’. Edge loaded were defined to have a polyethylene deformation due to component translational offset causing a lip, whereas, ‘normal’ were those which did not show signs of edge loading or impingement on bone. These provided a means of comparison (Figure 6.20). The well aligned simulator insert bearing curve (orange) showed similar but more evenly distributed height to the ‘normal’ retrievals. Similarly, for edge loading, the simulator tested condition (black) demonstrated a profile moving towards that of the mean of the 21 retrievals which experienced edge loading (blue). The profile for both of these shows the majority of the surface was below the mean height caused by the deformation. While the initial inflection shows a small percentage of material above the mean height representing the material lip caused by edge loading. This suggests the typical height of this deformation is much greater than that which the simulator was able to recreate in the testing time frame. As would be expected for the controlled conditions of a simulator the variability amongst the simulator samples is much less than that for the retrievals in the edge loaded condition.

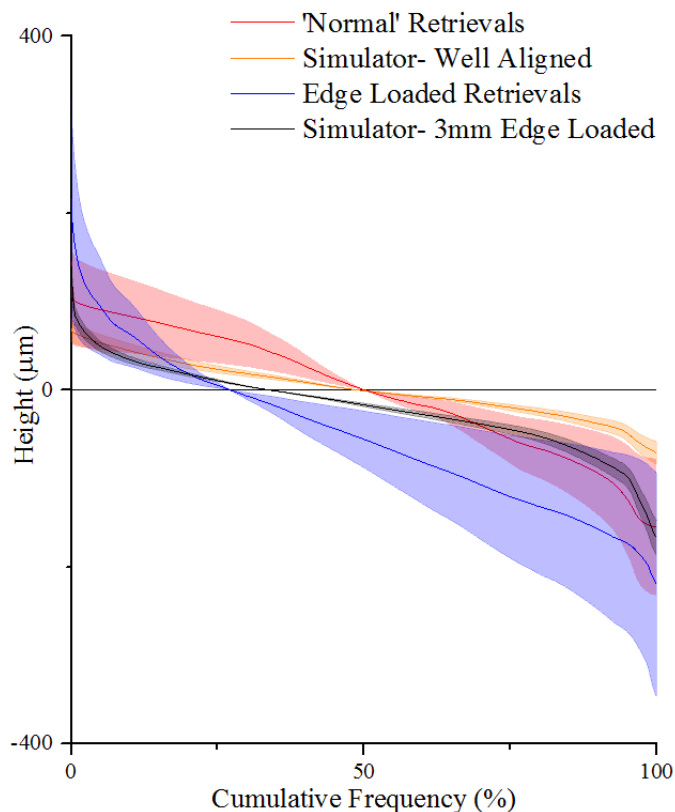


Figure 6.20 Abbott Firestone curves comparing retrievals surface profiles of those categorised as normal (n=9) and Edge loaded (n=25) to simulator samples under well aligned (TARs 1-6) and after 4Mc neutral coronal alignment and translational offset (TARs 7-12)

6.4 Discussion

6.4.1 Coronal malalignment

A coronal malalignment resulted in a significant reduction in the wear rate for this TAR design. In applying a coronal malalignment to the tibial component there was a lift off created between the components. In knee replacements femoral lift off has been associated with excessive loads and premature polyethylene wear (Dennis et al. 2001). A wear study testing total knee replacements under condylar abduction/adduction lift-off conditions showed a significant increase in wear for both fixed bearing and rotating platform designs (Jennings et al. 2007). This increase was explained by the higher contact stresses and the medial-lateral motion created by the lift off increasing the cross-shear effects especially apparent in the rotating platform design which aims to decouple rotation and displacement. The same relationship was not observed for this TAR design. This may be because the talar conformity kept the insert in contact causing a lift off at the flat articulation whereas in the TKR it was believed to be more of a medial lateral roll due to the reduced conformity.

This reduction in the wear rate may be in part a result of the reduced contact area. Both Mazzucco & Spector (2003) and Liu et al. (2011) have defined proportional relationships between wear and the product of sliding distance and contact area with the addition of a constant. While Mazzucco & Spector (2003) stated this constant would relate to the materials and test parameters without being specific, Liu et al. (2011) proposed it would incorporate the cross-shear ratio and be independent from contact pressure which saw better agreement than Archard's law in predicting experimental wear rates. This independence from contact pressure contradicts the historical belief wear increases exponentially with contact stress (Rostoker & Galante 1979) and the more recent correlation between wear factor and maximum contact stress showing a decrease in wear factor with increasing stress (Wang et al. 2001). However, it must be remembered these conclusions were drawn based on the constant load of pin on plate tests so it is unknown how a changing load further impacts these relationships.

From the Tekscan measurements (Chapter 5) it was possible to quantify the contact area under similar gait conditions. As the output swing phase loading profile for KS4 was closer to 300N than the 100N input, Tekscan results from a swing phase of 300N were considered. The contact areas for two cycles were plotted for the neutral alignment and 7.5° malalignment with this swing phase load. The same malalignment condition with a reliable 100N swing phase load was tested in SSKS3 and produced a comparable wear rate. The contact area for this condition was also compared (Figure 6.21).

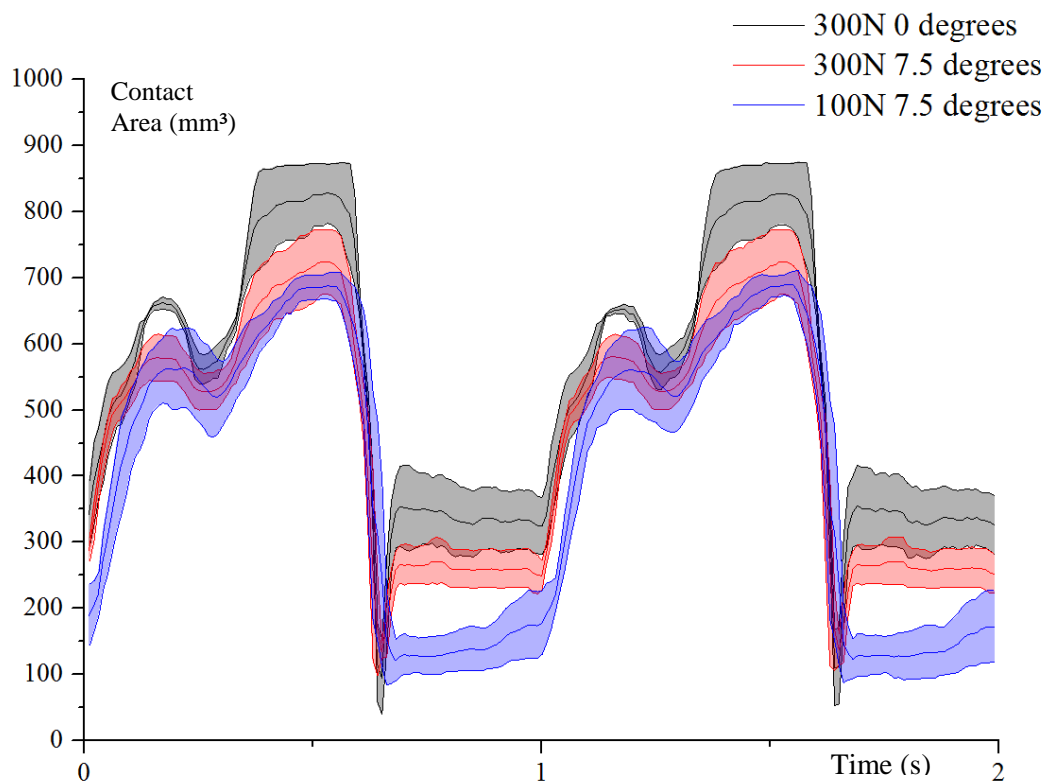


Figure 6.21 Comparing mean contact area measurement from TAR tested in SSKS3 (n=3) for the equivalent tested conditions with standard deviation

The malalignment condition with 300N swing resulted in a 13% decrease in the maximum contact area with a similar offset throughout the gait cycle. However, this corresponded with a 40% reduction in the wear rate. It must be remembered that as contact areas were obtained under static conditions but dynamic loading there could be further differences which are not represented here. The lift off may also have allowed for better lubrication for the components which could reduce the wear. This relationship corresponds with that published by Williams et al.

(2003) looking at ceramic-on-polyethylene hip replacements under micro separation which resulted in a fourfold decrease in the wear rate.

There were also differences between the single station condition and the multi-station wear simulator, visible in the swing phase where the contact area remained low throughout (Figure 6.21). However, the load at this stage is significantly reduced. The better replication of force and motion phase achieved by the electromechanical simulator are the likely reason for the slightly elevated wear rate despite reduced contact areas.

Under neutral alignment there was generally a well-defined raised central region about which the rotation is assumed to occur, causing less wear in this region. When coronally malaligned two thirds of the components experienced a lateral shift in this raised centre of rotation. This change was not visible on all components which may have been a result of station variability. Despite this form change the measured roughness values under the coronal malalignment condition did not vary substantially. However, both of these factors may still affect the long-term wear. The change in centre of rotation may mean despite the same kinematic inputs there is a change in the local kinematics which may impact the surface wear rate. For TKR Brockett et al. (2016) showed the centre of rotation to significantly affect the wear rates observed under identical kinematic conditions when tested on the same design in the same simulator. As the rest of the factors were unchanged it was the local kinematics resulting from the centre of rotation influencing the wear rates a similar mechanism may be at play here.

6.4.2 Translational offset

The translational offset caused a plastic deformation of the surface due to the edge loading. In hard on hard hip replacements edge loading has been shown to result in the increase in wear (Williams et al. 2008; Al-Hajjar et al. 2013). Similar simulator studies have reported both reduced and elevated wear for the hard-on-soft bearing combination in hip edge-loaded conditions (Williams et al. 2003; Ali et al. 2017). Brockett et al. (2011) also noted unintended edge loading in one of their wear tested mobile bearing oxford uni-compartmental knee replacements which claimed to result in elevated wear.

Although edge loading alone saw a reduction in the wear rate this was not deemed significant due to the variability. This will also be affected by the initial edge loading occurring in what should have been a neutrally aligned condition. Furthermore, at this stage the components were not moved between the stations so it is likely the kinematic effects of the individual stations heightened the variability and the single Mc after bedding in of the inserts may have provided further uncertainty. The wear rates for TARs 7-12 were generally lower than TARs 1-6 even during the bedding in period. It is possible this was an effect of the unintended set up edge loading.

In combination with the coronal malalignment no significant change in wear rate was observed with the additional translational offset. However, there are observable differences in the contact areas between the edge loaded and those without translational offset for both of these conditions (Figure 6.22). Tekscan measurements showed edge loading further reduced the contact area during the swing phase in both tested coronal alignments, 7.5° and neutral when compared to the equivalent neutrally aligned 100N swing phase load. It is likely this extra lift-off is also occurring with the 300N swing phase loads simulated in KS4 which may be providing further improved lubrication.

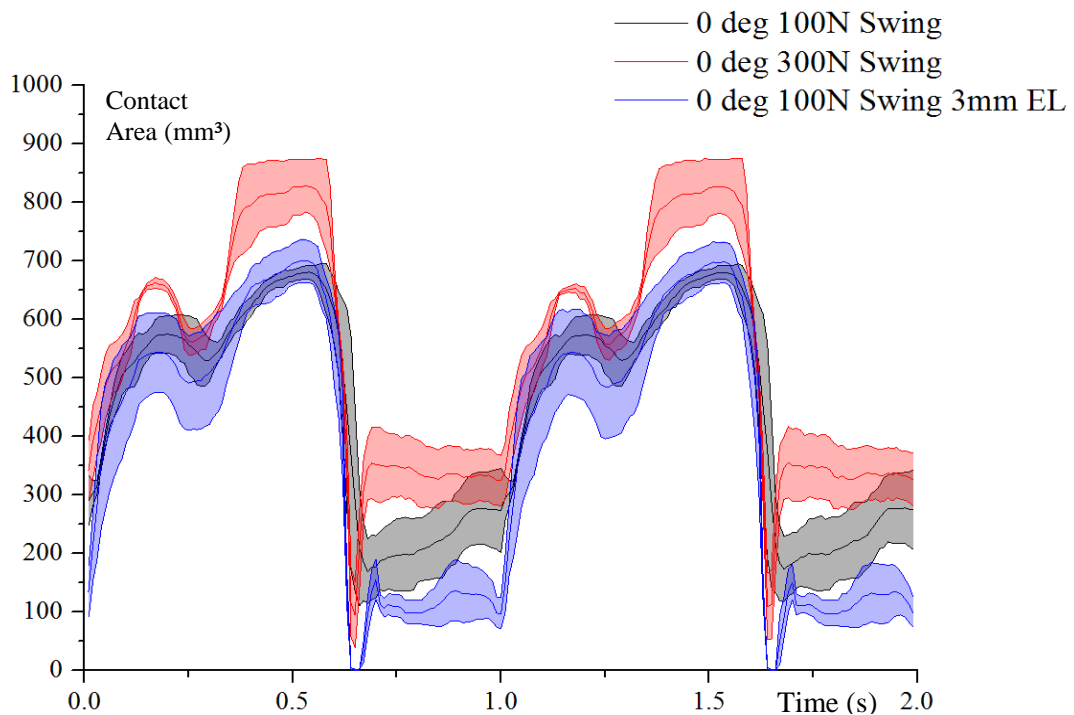


Figure 6.22 Effect of edge loading on the measured contact area in neutral coronal malalignment with standard deviation

As there is no increase in wear the change in surface form must be explained by plastic deformation rather than surface wear. Polyethylene is known for its two phase response with loading, the initial linear elastic reaction followed by the strain hardening at larger deformations (Bergström 2002). As the changes did not recover over time, after the wear simulation finished it can be considered plastic deformation.

As the number of edge loading cycles increased the step height also increased. Due to the initial unintended edge loading in neutral condition and the limited test time. It is not possible to identify whether this would continue at such a rate with every additional Mcs, however because plastic deformation is a time dependent factor it is likely this will continue (Bergström 2002).

With both of the malalignment conditions the peak contact pressure was elevated compared to neutral alignment. The other concern from high contact pressures highlighted in Chapter 5, shown to encroach on the yield stress of polyethylene is the possibility repeated cyclic loading results in polyethylene fracture (Pruitt 2005). In the timeframe of these tests this did not appear to be a risk, however insert fracture related to edge loading has been observed clinically (Karantana et al. 2010). The polyethylene thickness increases this risk, historically Bartel et al. (1986) recommended the polyethylene thickness should remain greater than 8-10mm to avoid an exponential increase in stress but TAR thickness is typically below this. With decreased thickness the structural stiffness of the polyethylene increases while the elastic modulus remains the same increasing the stress on the material.

6.4.3 Comparison to retrievals

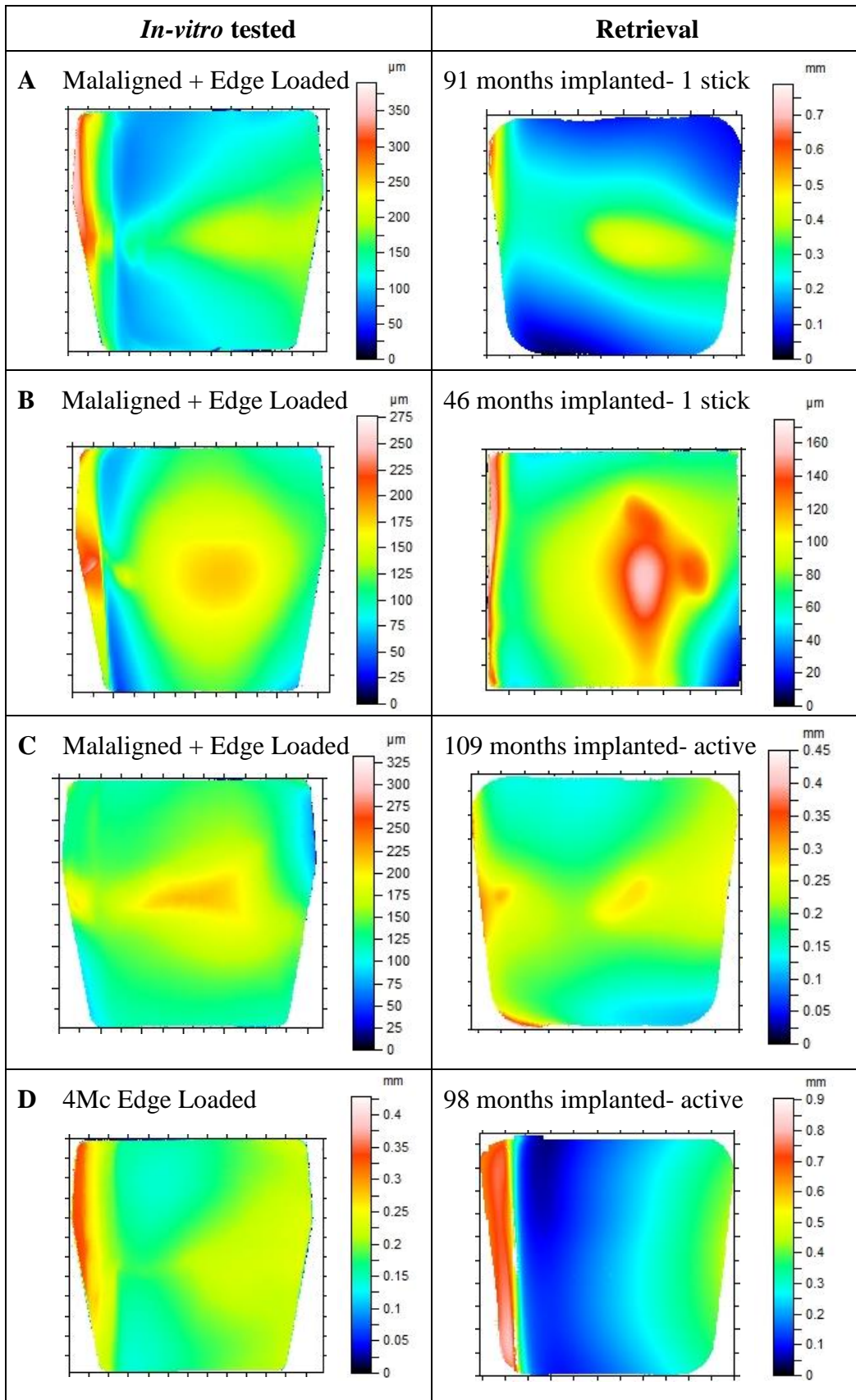
The comparison to retrievals suggests the application of a translational offset was able to create clinically relevant edge loading to a certain degree. The Abbott Firestone curves (Figure 6.20) suggested that the peak inflection caused by the edge loading condition *in-vivo* was much greater than that caused by the simulator. This variability could be caused by a number of factors such as the maximum force capacity reached by the simulator being less than the potential maximum force estimated by Stauffer et al. (1977). The individuals' weight, activity level and number of years the device was implanted may also come into play. The nature of

a displacement controlled simulator ensures the kinematic inputs are applied irrespective of the component alignment. It is highly plausible that when this is experienced clinically the insert could be stuck due to surrounding tissues or it may not experience a full range of motion. This lack of motion may further augment the magnitude of the edge loading.

Within the retrievals collection there were 44 TARs. These specimens were visually investigated in order to look for specific features which aligned with the simulator results. More of the inserts presented with similar conditions but these four were chosen to represent a range of edge loading severities and two device designs. These designs were similar three component unconstrained AES (Biomet, UK) and Hintegra (Integra Lifesciences, USA) TAR retrievals. It was apparent in comparing the height maps that there were similar wear mechanisms in play both *in-vivo* and *in-vitro* (Table 6.5).

Most of the examples show the same raised centre of rotation (Table 6.5) about which the rotation is assumed to occur. Example A shows comparable surface maps between the simulator and chosen retrieval but the magnitude of the retrieval is almost twice that of the simulator sample. Example B shows a retrieval with a less straight edge loading which may mean this was more mobile while example D has a highly defined straight step of almost 1mm which suggests minimal motion was occurring. Meanwhile example C exhibits comparable low points at the edges. Three of these retrievals were implanted for more than seven years and the height of the edge loading seems to be greater for these compared to patient B whose TAR survived less than four years. This potentially supports the time dependent increase in plastic deformation hypothesis. Despite the edge loading the patients all remained active to an extent. In general, the 3mm offset applied to the components has created an edge loading within the range seen clinically, the difference in clearance between the insert and tibial component between TAR designs would vary the size of the edge loading with 3mm translational offset.

Table 6.5 Comparison between some retrieval height maps with their implantation time and activity level and those from in-vitro testing.



6.4.4 Limitations

The pneumatic simulator had limitations in its ability to follow the desired input profile which might have affected the finite wear rate but still provides comparable data. Variation between stations in terms of lift-off will have had some bearing on the wear rates during the coronal malalignment test but in moving the inserts through the stations the effects of this were largely negated.

The limitation with the biggest impact in this instance was the tibial components set-up by eye which in the second group of TARs resulted in multiple set up errors making conclusions from the translational offset test more difficult to draw upon. In future, this could be controlled by fixturing, if a collar was applied around the footprint of the tibial components it would ensure there was no overlap at the component edge.

Assumptions were made in defining the malalignment conditions tested due to the general lack of publications surrounding TAR. These were considered to be reasonable as they were considered within a range seen clinically and their individual effects were understood through the biomechanical investigation prior to wear testing.

The other three component TAR retrievals have provided a useful comparison however, there are no Corin Zenith retrievals in the collection to compare them to. Assumptions have been made that three component TARs will generally behave the same *in-vivo*. Considering the similarities between these devices (Figure 6.23), this is believed to be a reasonable theory.



Figure 6.23 Retrieval Hingtegra and AES TARs compared to simulator Zenith components

6.5 Conclusion

Again, this mobile bearing TAR has not followed the convention set by published TKR and THR research when measuring wear in suboptimal alignment. Under both tested malalignment conditions the contact area was reduced and there was an element of component lift off. This has resulted in a reduction in surface wear despite the association with elevated peak contact pressures shown biomechanically.

Although malalignment in TAR has been associated with failure this investigation suggests, at least for translational and coronal malalignment, this is not a surface wear problem. Concerns arise from the potential for fatigue wear mechanisms over time *in-vivo* due to the resulting peak pressures. More investigation is required to understand the other factors at play and develop a suitable adverse condition TAR preclinical wear test.

CHAPTER 7
OVERALL DISCUSSIONS, CONCLUSIONS
AND FUTURE WORK

CHAPTER 7

OVERALL DISCUSSIONS, CONCLUSIONS AND FUTURE WORK

7.1 Overall discussion

While the prevalence of osteoarthritis in ankles is eight to ten times less common than for knees this still represents a substantial proportion of the population. The majority of ankle osteoarthritis cases are post-traumatic thus affecting a much younger patient demographic. Most post-traumatic cases are the result of fracture or instability (Saltzman et al. 2005). Current government initiatives aim to increase the physical activity levels across the UK population with the hope of creating a healthier, more productive work force and relieving the burden on the National Health Service (Speake et al. 2016). One such example is the mobile application ‘Couch to 5k’ which aims to train people to run 5km (NHS Choices 2014). While there are benefits there is also greater risk of injury associated with high impact activities and repeated ankle sprain especially common in running (Yeung et al. 1994). With a younger more active population it is likely the incidence of ankle arthritis will rise over coming decades. There is a need for a treatment option to allow these younger patients to continue their active lifestyles. Total ankle replacements (TARs) have the potential to provide this relief, however, rates of survivorship for TARs are highly variable depending on a variety of factors from the specific device designs, the positioning and the experience of the surgeon (Henricson et al. 2007).

As a result of the success of total hip replacements (THR) and total knee replacements (TKR) patient expectations for TARs are high. These patients expect to be able to return to not just their typical day to day life pain free but also their passions, be that hiking, cycling, swimming, gymnastics or skiing (Naal et al. 2008). This places great demands on the device.

Hip and knee replacements have benefitted greatly from the standardisation of wear testing encouraging new bearing material combinations to be developed, fully evaluated and adopted clinically to generate better patient outcomes. There is no such standard in place for TARs.

This thesis aimed to develop a standard methodology to simulate the clinical performance of a mobile bearing total ankle replacement. The objectives included development of a physiologically relevant wear simulation to understand the effects of kinematics on wear, followed by an investigation into the biomechanics associated with adverse alignment and how this translates into wear.

The objectives were met through a series of studies. As the existing information on ankle gait was limited this was carried out with a stratified approach, by varying the combination of inputs to observe their individual effects. The component surfaces were compared to retrievals of similar three component designs. This part of the thesis confirmed that representative surface wear mechanisms were generated in the simulator and helped validate the methodology. This wear simulation method also opened up the opportunity to investigate the effects of adverse conditions. This was first addressed through a biomechanical investigation, considering the effect of coronal malalignment on the degree of lift off between components and how the corresponding contact areas and pressures changed. This process defined the most relevant condition to be extrapolated to a wear simulation. Alongside coronal malalignment the wear simulation also provided a platform to introduce edge loading through translational offset between components based on observations from the retrievals collection at the University of Leeds. To the authors knowledge this was the first investigation of the effects of component malalignment in terms of wear for a TAR.

7.1.1 Development of a wear simulation methodology

In-vitro wear simulation is a well-established methodology across joint replacement providing a controlled environment for rigorous pre-clinical assessment of a device (ISO14242-2 2016). This allows the wear performance to be investigated relative to design, material choice and kinematics and can help define the functional envelop for a particular design. Such methods have known limitations, assuming a standardised gait input despite patient variation, only considering continuous walking and use of bovine serum to approximate synovial joint fluid. The methodology developed in earlier chapters is no exception, with the additional effects of inversion of the TAR for testing and the lack of TAR instrumented force data. Regardless of these limitations wear simulation is known

to provide a good approximation for clinical wear rates under a range of conditions. Such estimates can predict, to an extent, the risks of wear induced osteolysis and adverse immune reactions.

In this study, a simulation methodology for investigating wear of a mobile bearing TAR was developed and a stratified approach taken to understand the effects of kinematic gait inputs in terms of wear. The aim was to create a robust methodology applicable to any joint replacement design with minimal modification. A gait input was defined from literature. This process was limited by the existing literature as the ankle is a complex and under-researched joint. The input profile relied on historic data for the natural ankle (Stauffer et al. 1977; Procter et al. 1982; Conti et al. 2006). Ideally the TAR design should be capable of replicating the healthy joint kinematics thus these inputs were used. This is rarely fully achieved in patients with TAR so there is also a strong argument for using the specific joint replacement kinematics as these are likely to be a better approximation of what the joint replacement will be subjected to. Typically joint replacements experience contact forces less than those derived from mathematical calculations (Bergmann et al. 1993; Zhao et al. 2007). In addition the range of plantarflexion/dorsiflexion motion is often reduced by TAR compared to controls but the rotation and inversion/eversion can remain unchanged (Valderrabano et al. 2003). By applying the higher range of loads and kinematics seen in the natural ankle more severe higher wear conditions have been investigated for the TAR design.

By varying the combination of the different components of the gait inputs applied it allowed the biomechanics of the three-component device to be better understood. It appeared some of the flexion occurred at the flat-on-flat tibial articulation which stopped the device from isolating flexion to the talar articulation and rotation to the tibial articulation when displacement was not included. As a result of this, displacement had no significant effect on the wear rate of this TAR at any magnitude. Conversely, the wear rate was highly dependent on the inclusion of internal/external rotation. The increased wear as a result of the rotation suggests that the most severe condition would be one with greater rotation. Incorporation of broader activities of daily living, such as sitting and stair climbing in TAR simulation would probably see minimal change in the wear rate as the ankle does not go to the same motion extremes as hips and knees for these actions.

Alternatively, activities such as skiing or team sports involving running and sidestepping which can require extremes of ankle rotation could create a worst case wear condition (Stoffel et al. 2010; Bronner et al. 2015).

While providing some insight into the wear trends of mobile bearing TARs this research focused on a single device design, with a material bearing combination of titanium nitride (TiN) and conventional ultra-high molecular weight polyethylene (UHMWPE) uncommon across TARs and joint replacement generally. Some coating damage was observed on two tested components. Whilst of concern, this did not seem to result in elevated wear rates. The damage observed was a smooth transition comparable to a clinical report of one knee retrieval which saw “coating breakthrough” after articulation with the natural patella. A further two retrievals saw coating damage as a result of metal-on-metal contact but this was much more irregular and rougher (Fabry et al. 2017).

The wear rate measured for the TAR was comparable to that of TKR with similar conventional polyethylene (Fisher et al. 2004; Muratoglu et al. 2004). Cited as the cause for revision in 38% of cases (Sadoghi et al. 2013), aseptic loosening is already a relatively big concern in TAR, however, the association with wear is not clear. For TKR it was postulated that wear rates of 5-20mm³/Mc may be sufficient to “provide adequate osteolytic-free lifetimes”. However, this also relied on the low specific biological activity (Fisher et al. 2004). *In-vivo*, the TAR particle properties have been shown to be comparable to that of knee replacements for two component designs (Kobayashi et al. 2004). While there has been just one investigation of simulator wear particles in TARs, this found the majority of particles to be in the highly biologically active, submicron size range and found no significant difference in size range compared to *in-vivo* particles (Reinders et al. 2015). Despite this, the same degree of wear debris mediated osteolytic immune response has not been reported in TAR. Typically ankle replacements seem to experience osteolysis at between five and ten years post operatively (Kokkonen et al. 2011), whereas, for knee replacements this is much later. This suggests there may more factors at play for TARs. However, if the design of TAR devices can improve to reduce the incidence of early cyst formation this would result in better clinical outcomes in which case wear mediated osteolysis could become a concern over time. However, it must be remembered the environment surrounding the TAR

cavity is very different to that of THR and TKR. Whether the wear debris is trapped surrounding the ankle or whether it travels is unknown, this will impact the osteolytic potential.

While other joint replacements have widely adopted highly cross linked UHMWPE and furthermore vitamin-E polyethylene in order to reduce the wear and thus the prevalence of wear-induced osteolysis, its presence in TAR is limited. It is hoped the newest generations of TARs are providing better success rates than earlier generations but that is still inconclusive. Meanwhile there is some focus on improving the understanding of the ankle anatomy and biomechanics. As this information becomes more widely available the knowledge can hopefully be combined with informative computational models of the ankle to see improvements in the TAR design. With more considered design alongside the necessary surgical instrumentation it is hoped success rates could finally improve. The longer these devices last the greater the risk associated with wear-debris mediated aseptic loosening may become.

7.1.2 Biomechanical effects of adverse alignment

Initially a biomechanical investigation addressing the lift-off effects associated with malalignment was carried out. Using the standardised gait profile developed throughout the course of this research TARs were tested under a range of alignment conditions. To the authors knowledge this was the second study considering the effect of component lift-off for TAR. The first of these was a computational study by Espinosa et al. (2010) looking at stress and contact area. This did not consider the potential for component realignment throughout the gait cycle. Instead this investigation allowed the malalignment to be corrected whilst also considering the effects of the ankle kinematics throughout the gait cycle. This correction is important as the author believes the surrounding joints of the ankle would compensate for this malalignment which may be occurring in those with smaller degrees of malalignment and central insert alignment to the sulcus. The model could also represent a ligament imbalance as a result of correcting the existing deformity. There have just been a few reports of severe coronal malalignment in weight bearing x-rays in which the components have not been able to realign themselves to the talar component condyles to ensure maximum

function (Morgan et al. 2010; Kim et al. 2016). This is confounded by results from Wood & Deakin (2003) in which 130 out of 200 TAR tibial components were shown to lie within $\pm 5^\circ$ of the tibial axis in the coronal plane. Despite 70 TARs lying outside this range, only nine were identified as at risk due to migration of the component. In some cases this will be because the components are aligned with each other but not the joint loading axis. As Mann et al. (2011) found 25% of patients with coronal plane deformity ended up with malalignment greater than 2° between the tibial and talar components in this plane.

Whilst allowing component realignment the biomechanics testing highlighted the changes in contact area and stress throughout the gait cycle. The degree of lift-off varied depending on the direction of the malalignment with valgus appearing to cause greater lift-off due to the direction of external rotation. Yet the ankle is considered to cope better with valgus malalignment compared to varus, therefore, a TAR may last longer in this orientation (Conti et al. 2001). To create what was anticipated to be a worst-case model valgus component malalignment was used throughout the following testing to amplify the lift-off.

The effect of joint tension in combination with component malalignment was also investigated. There have been no estimations of swing force in TAR so a range of values were tested. The joint tension proved more important than the degree of malalignment itself in terms of controlling the lift-off and increasing the contact area. While TKR systems have extensive intra-operative ligament balancing technologies this process in TAR is primitive using a ratchet to distract the joint and manually judging the appropriate tension (Giannini et al. 2010). Quantifiably balanced ligament tensioning with the use of pressure sensors have seen significant clinical improvements at one year post operation (Gustke et al. 2014). In not taking similar steps of improvement through surgical technique there is an increased chance of surgical error and potential for reduced clinical success. Improving this technique could see a reduction in the peak contact pressures should malalignment occur either as a result of surgical technique, adjacent joint degeneration or lift-off as a result of ligament imbalance.

The peak contact pressure measurements were found to be encroaching on the yield stress of polyethylene especially at the maximum malalignment angles and

at low swing phase loads. From the measurements taken the alternating stress could be measured from the maximum difference between the peak stress and mean stress. For the tested conditions the alternating stress was approximately 10.5MPa. Using a S-N curve for UHMWPE (Rawal et al. 2016) it has been predicted it would be 60-70Mc for 10.5MPa alternating stress before fracture. For an individual meeting the 10,000 recommended steps a day, fracture would be predicted at 16 years. Furthermore, computational simulation predicted these would be greater at the talar interface, even at neutral alignment where the sulcus of the talus and insert are aligned which would reduce this time frame dramatically (Espinosa et al. 2010). Due to limitations of the Tekscan sensor this could not be quantified in this study but this suggests the risks of exceeding the polyethylene yield stress are elevated at the talar component surface. Moreover, when considering the direction of the alignment the rotation proved to impact the degree of lift-off. Measurement of the changing contact areas and stress under static conditions and dynamic loading may be underestimating the severity of the changing contact area and pressure due to the lack of rotation. If this is the case the risk of initiation of the fatigue wear process is elevated which may result in early failure of the polyethylene. This is believed to be a concern as there has been polyethylene fracture of three component designs reported at 4-5% of TARs in numerous clinical follow ups of 50-100 patients, which works out around one quarter of revisions (Anderson et al. 2003; Karantana et al. 2010; Bonnin et al. 2011). Yet Sadoghi et al. (2013) cites implant fracture (including all components) to be responsible for just 5.3% of revisions and the National Joint Registry for England and Wales recorded no incidences of polyethylene fracture resulting in revision in either 2014 or 2015 (NJR 2016). While reports of the occurrence of polyethylene fracture are variable it is important the risk of polyethylene fracture is not amplified further by malalignment or joint tensioning.

7.1.3 Wear effects of adverse alignment

The clinical definition of malalignment in the coronal plane is greater than 5° Hintermann et al. (2013). Considering this and the limitations of the multi-station simulation, a 7.5° malalignment condition was implemented in a wear simulation. While this angle would be unlikely to equate to the same degree of malalignment *in-vivo* it was chosen for the degree of lift-off it generates in the adverse condition

model. This angle allowed component lift-off with the 300N swing phase of the simulator. The relationship between wear rate and component alignment in both the coronal plane and with translational offset between the components in the medial/lateral direction were explored.

Technical error including malalignment is cited as a reason for failure in 15% of cases (Sadoghi et al. 2013). Malalignment has been associated with a greater risk of polyethylene wear without quantitative evidence (Conti et al. 2001; Mann et al. 2011; Usuelli et al. 2016). However, in this wear investigation the additional component malalignment did not create a more severe wear model. Instead a significant reduction in the wear rate was observed, the opposite effect of TKR lift-off (Jennings et al. 2007). These findings aligned with the proportional relationship between contact area and wear rates independent of contact stress (Liu et al. 2011). However, it is possible that if this adverse model were not able to correct for the malalignment uneven wear would have been more of a problem. As the ankle joint complex relies on a number of articulations to facilitate gait, especially the subtalar joint which is thought to ensure the relative orientation between the tibia and talus, the ankle has the capability to correct for such malalignment (Ting et al. 2016).

Clinically translational offset between components resulting in edge loading has been associated with premature polyethylene wear and the subsequent osteolysis in one case (Buechel Sr. et al. 2003). Karantana et al. (2010) also reported two incidences of polyethylene fracture due to edge loading but whether this was displacement or rotational edge loading was not specified. While implementing a translational offset between the TAR components successfully recreated the lip deformation which has been observed in the retrieval collection at University of Leeds (Stratton-Powell et al. 2017) there was no significant change in the wear rate. This was the case when applied in combination with coronal malalignment and in otherwise neutral alignment. The severity of deformation varied but was typically a larger step height in the retrievals. This could be a result of the test duration, the magnitudes of the forces applied or the fact in the simulator the TAR was forced to rotate whereas in this situation *in-vivo* the motion may be very limited all of which would increase the deformation.

While surface wear has shown not to increase the wear rate there appears to be a high prevalence of comparable edge loading in retrievals at 53% (Stratton-Powell et al. 2017). In an *in-vitro* setting the edge loading is solely a deformation and load distribution problem. By contrast the environment for the TAR *in-vivo* is much more complex, the translational offset between the components is likely to result in secondary problems such as, the insert impinging on the surrounding hard and soft tissues or heterotrophic ossification in the open space. This may cause additional pain or instability resulting in earlier device failure.

This wear investigation has shown malalignment to be very much a multifactorial problem with surface wear unlikely to be the root cause of failure for these malaligned TARs. Neither condition tested has created the worst case wear model that testing of malalignment in THR has though their edge-loading model (Al-Hajjar et al. 2013). Further exploration of TAR failure is required to develop something similar for the rigorous testing of TARs.

Clearly it is important to have a standard in place for new devices and new material combinations. This research has taken some steps in order to reach this overarching goal. Through development into ISO standards and engaging manufacturers to go beyond compliance with the pre-clinical testing of these devices just as they do with THR and TKR designs better patient outcomes could be possible.

7.2 Overall Conclusions

The research questions set out in the aims and objectives have been addressed throughout this thesis and the following set of conclusions could be drawn:

7.2.1 Development of a Wear Simulation Methodology

- This study has established a method and furthered the understanding of the effects of the kinematic inputs in mobile bearing TAR devices
- For the TiN on UHMWPE bearing combination in a three-component total ankle replacement there is a significantly increased wear rate for up to two million cycles (Mc) while the components bed in, it is important this is accounted for when designing pre-clinical wear investigations.
- In this instance the magnitude of anterior/posterior displacement appeared to have no significant effect on the measured wear rate making this a less

critical input parameter. Where possible this should still be included as it may have varying effects on the local contact mechanics depending on the conditions investigated.

- Conversely, the wear rate of an unconstrained TAR was most reliant on the addition of rotation which in combination with displacement or flexion at the tibial articulation creates cross shear responsible for elevated wear. As the information surrounding ankle gait expands this should be updated as a priority as it will have the greatest impact on the wear rates.
- A high-rotation gait profile may see further elevated wear rates, creating a worst-case wear model.
- The simulation created wear scars comparable to those observed clinically on similar designs of TAR retrievals which provided confidence in the surface wear mechanisms occurring and the physiological relevance of the gait inputs applied.

7.2.2 Biomechanical effects of adverse alignment

- Imposing a coronal malalignment resulted in component lift-off due to the highly conforming nature of the Zenith TAR.
- The degree of this lift-off depended on the direction of the malalignment and the magnitude of the swing phase load applied and thus the joint tension further highlighting the importance of balanced ligament tensioning during TAR surgery.
- This lift-off resulted in reduced contact areas and increased peak contact pressures, the severity of this related to ligament tensioning and in some instances resulted in dislocation.
- Peak contact stresses encroaching on that of the yield stress of polyethylene created a fatigue failure concern, after four Mcs of this condition this was not observable, however, microcracks may have been forming.
- Tekscan measurements also suggested elevated contact pressures at the edge loaded surface of the polyethylene compared to the same conditions without translational offset, amplifying the potential for fatigue crack initiation.

7.2.3 Wear effects of adverse alignment

- Such changes in contact area resulted in a significant reduction in the wear rate when tested for three Mcs, while malalignment is associated with failure it may not be mediated by surface wear and the resulting osteolysis.
- This reduction may be dependent on the allowance of the wear simulation to compensate for the malalignment. If the ankle did not realign itself to a degree more uneven wear and more severe fatigue wear processes may have been initiated.
- While the wear rate was significantly less *in-vitro* there may be further complications outside of wear. *In-vivo* malalignment has been associated with arthrofibrosis and presumably instability would be more prevalent.
- The addition of a translational offset between the tibial and talar components resulted in edge-loading deformation but had no significant effect on the wear rate when with well aligned components and in combination with coronal malalignment.
- Surface measurements taken with the Alicona were comparable to retrievals showing a similar magnitude of material inflection, proving that the simulation was able to create clinically relevant edge-loading.
- It appears *in-vitro* the edge loading is solely a deformation problem, however, *in-vivo* there is no space for this component mismatch so additionally the insert would be impinging on surrounding bone and soft tissues, potentially causing further problems for the patients and the device.
- While common in failed TARs the edge-loading phenomenon does not appear to be the result of elevated surface wear.
- There is a great need for further investigation in order to understand the other failure mechanisms at play to develop suitable adverse condition TAR pre-clinical test. Increasing understanding would have the potential to reduce the high failure rates of TARs and improve patient outcomes.

7.3 Future Work

Throughout this thesis a methodology for wear testing of TARs has been developed. The gait inputs have, however, been defined from the limited existing literature. The test methodology would benefit from obtaining better quality ankle

force and motion gait data, prioritising the rotation which has shown to have the greatest effect on the wear rate. Furthermore, as wear simulator capabilities have advanced there is a strong drive for inclusion of activities of daily living interspersed with the standard walking cycle. These typically include stair climbing and sitting down (Popoola et al. 2010). While the ankle range of motion is not as great for these activities, stop-dwell-start walking is something which could prove insightful in TAR wear simulation. The addition of dwell periods in the gait cycle have been associated with elevated wear rates for THR (Hadley et al. 2013) but the presence of stop periods did not have the same effect for TKR (Jakubowitz et al. 2009). These are intended to account for pauses in gait, for example waiting at traffic lights or for the kettle to boil. To ensure physiologically relevant wear is measured and any sticking effects or biotribocorrosion associated with the dwell period can be considered this may be a beneficial test methodology to adopt.

Due to constraints of PhD sponsorship this investigation only considered one TAR design with a specific material combination which is, at present, not widely adopted across TAR designs. The combination of TiN and polyethylene follows one of the early mobile bearing TARs, the Buechel Pappas. Upon starting this PhD multiple TAR designs were available as both cobalt chromium and TiN but these have since been phased out. Similarly, TiN has been phased out across joint replacement technology more generally. As a result of this shift comparable data from cobalt chromium or vitamin E polyethylene designs would provide an interesting comparison. The TAR market appears to be starting to swing back towards the two-component design so adjusting the methodology for these devices would further the potential of this clinical assessment tool.

While measurement of the flat insert bearing surface with the Alicona optical microscope provided beneficial insight into the form changes at the superior surface it cannot quantify the changes at the inferior curved surface. The wear test methodology would benefit from development of a geometric wear measurement method, encompassing the full mobile bearing insert. This would provide the opportunity to observe uneven loading changes under a range of conditions.

The investigation has shown component malalignment with both coronal rotation and medial/lateral translational offset does not increase the polyethylene wear rate. While the conditions tested were assumed to be the most severe or the most commonly observed within the cohort of retrievals other malalignment conditions may have more effect on the wear. The developed methodology provides scope to investigate further malalignment conditions. Some TAR devices have been developed with curved surfaces in the coronal plane to allow more flexibility in this plane, comparing this type of design to the standard flat articulation of most mobile bearing TAR designs would provide informative insight for future device designers.

Despite the lower wear rates the measured contact pressures suggest the malalignment may be initiating the fatigue wear process. There may be some value to carrying out an SEM analysis on the malaligned components in order to see whether there is a presence of ripples which have been associated with the micro fatigue process (Shi et al. 2000; Gundapaneni et al. 2016).

Furthermore, the process of developing this methodology as an ISO accredited displacement controlled wear standard is underway. It is important this is followed through to completion as TAR devices should be under the same pre-clinical test scrutiny as the equivalent hip and knee replacements.

While wear is an important factor for joint replacement longevity this investigation and the accompanying retrievals have shown that there are more factors at play, contributing to the failure of TARs. TARs would benefit greatly from wider simulation improvement especially in terms of fixation, stability and biomechanics. Broader insights could see improved devices developed. With such advancements, the future for patients with end stage ankle arthritis could be much brighter.

REFERENCES

|

REFERENCES

- Affatato, S., 2016. Displacement or Force Control Knee Simulators? Variations in Kinematics and in Wear. *Artificial Organs*, 40(2), pp.195–201. Available at: <http://www.ncbi.nlm.nih.gov/pubmed/26147451>
- Affatato, S. et al., 2007. Meniscal wear at a three-component total ankle prosthesis by a knee joint simulator. *Journal of Biomechanics*, 40(8), pp.1871–1876. Available at: <http://www.sciencedirect.com/science/article/pii/S0021929006003022>.
- Affatato, S. et al., 2008. Tribology and total hip joint replacement: Current concepts in mechanical simulation. *Medical Engineering & Physics*, 30(10), pp.1305–1317. Available at: <http://www.sciencedirect.com/science/article/pii/S1350453308001318>
- Affatato, S. et al., 2009. Wear behaviour in total ankle replacement: A comparison between an in vitro simulation and retrieved prostheses. *Clinical Biomechanics*, 24(8), pp.661–669. Available at: <http://www.sciencedirect.com/science/article/pii/S0268003309001545>.
- Affatato, S., 2012. *Wear of orthopaedic implants and artificial joints.*, Woodhead Pub.
- Affatato, S. & Brando, D., 2013. 1 – Introduction to wear phenomena of orthopaedic implants. In *Wear of Orthopaedic Implants and Artificial Joints*. pp. 3–26.
- Ahluwalia, R.S. et al., 2013. Ankle replacement: a 14-year experience. *Orthopaedic Proceedings*, 95–B(SUPP 21).
- Akagi, M. et al., 2007. Effectiveness of Ceramic Femoral Components on Reduction in Tibial Polyethylene Wear: A Simulator Study. *Techniques in Knee Surgery*, 6(4), p.206–212 10.1097/BTK.0b013e31815bd423. Available at: http://journals.lww.com/techknee/Fulltext/2007/12000/Effectiveness_of_Ceramic_Femoral_Components_on.3.aspx.
- Al-Hajjar, M. et al., 2013. Wear of 36-mm BIOLOX(R) delta ceramic-on-ceramic bearing in total hip replacements under edge loading conditions. *Proceedings of the Institution of Mechanical Engineers, Part H: Journal of Engineering in Medicine*, 227(5), pp.535–542. Available at: <http://jih.sagepub.com/lookup/doi/10.1177/0954411912474613>
- Ali, M. et al., 2017. Wear and deformation of metal-on-polyethylene hip replacements under edge loading conditions due to variations in surgical positioning. *Orthopaedic Proceedings*, 99–B(SUPP 3). Available at: http://www.bjjprocs.boneandjoint.org.uk/content/99-B/SUPP_3/12
- Allegra, F. & El Boustany, S., 2016. Ankle Arthritis in Athletes. In *Arthroscopy and Sport Injuries*. Cham: Springer International Publishing, pp. 419–424. Available at: http://link.springer.com/10.1007/978-3-319-14815-1_53
- Anderson, T., Montgomery, F. & Carlsson, A., 2003. Uncemented STAR total ankle prostheses. Three to eight-year follow-up of fifty-one consecutive

- ankles. *The Journal of bone and joint surgery. American volume*, 85–A(7), pp.1321–9. Available at: <http://www.ncbi.nlm.nih.gov/pubmed/12851358>
- Archard, J.F. & Hirst, W., 1956. The Wear of Metals under Unlubricated Conditions. *Proceedings of the Royal Society of London A: Mathematical, Physical and Engineering Sciences*. Available at: <http://rspa.royalsocietypublishing.org/content/236/1206/397>
- Arndt, A. et al., 2004. Ankle and subtalar kinematics measured with intracortical pins during the stance phase of walking. *Foot & Ankle International*, 25(5), pp.357–364.
- Arndt, A. et al., 2007. Intrinsic foot kinematics measured in vivo during the stance phase of slow running. *Journal of Biomechanics*, 40(12), pp.2672–2678. Available at: <http://www.ncbi.nlm.nih.gov/pubmed/17368465>
- de Asla, R.J. et al., 2006. Six DOF in vivo kinematics of the ankle joint complex: Application of a combined dual-orthogonal fluoroscopic and magnetic resonance imaging technique. *Journal of Orthopaedic Research*, 24(5), pp.1019–1027. Available at: <http://www.ncbi.nlm.nih.gov/pubmed/16609963>
- ASTM, 2014. ASTM. <http://www.astm.org>.
- ASTM F1714 - 96, 2013. *Standard Guide for Gravimetric Wear Assessment of Prosthetic Hip Designs in Simulator Devices*, Available at: <https://www.astm.org/Standards/F1714.htm>
- Atkinson, J. et al., 1985. Laboratory wear tests and clinical observations of the penetration of femoral heads into acetabular cups in total replacement hip joints: III: *Wear*, 104(3), pp.225-244. Available at: <http://www.sciencedirect.com/science/article/pii/004316488590050X>
- Baker, D.A., Hastings, R.S. & Pruitt, L., 1999. Study of fatigue resistance of chemical and radiation crosslinked medical grade ultrahigh molecular weight polyethylene. *Journal of Biomedical Materials Research*, 46(4), pp.573–581. Available at: <http://doi.wiley.com/10.1002/%28SICI%291097-4636%2819990915%2946%3A4%3C573%3A%3AAID-JBM16%3E3.0.CO%3B2-A>
- Barg, A. et al., 2013. Ankle osteoarthritis: etiology, diagnostics, and classification. *Foot and ankle International*, 18(3); pp.441-426. Available at: <http://www.sciencedirect.com/science/article/pii/S1083751513000478>
- Barg, A. et al., 2010. Insert position in three-component total ankle replacement. *Foot Ankle International*, 31(9), pp.754–759.
- Barg, A. et al., 2011. The effect of three-component total ankle replacement malalignment on clinical outcome: pain relief and functional outcome in 317 consecutive patients. *Journal of Bone and Joint Surgery-American Volume*, 93(21), pp.1969–1978.
- Barnett, C.H. & Napier, J.R., 1952. The axis of rotation at the ankle joint in man; its influence upon the form of the talus and the mobility of the fibula. *Journal of anatomy*, 86(1), pp.1–9. Available at: <http://www.ncbi.nlm.nih.gov/pubmed/14907546>

- Barnett, P.I. et al., 2002. Investigation of wear of knee prostheses in a new displacement/force-controlled simulator. *Proceedings of the Institute of Mechanical Engineering-Part H*, 216(1), pp.51–61.
- Bartel, D.L., Bicknell, V.L. & Wright, T.M., 1986. The effect of conformity, thickness, and material on stresses in ultra-high molecular weight components for total joint replacement. *The Journal of bone and joint surgery. American volume*, 68(7), pp.1041–51. Available at: <http://www.ncbi.nlm.nih.gov/pubmed/3745241>
- Bauer, G. et al., 1996. Total ankle replacement. Review and critical analysis of the current status. *Foot and Ankle Surgery*, 2(2), pp.119–126. Available at: <http://www.sciencedirect.com/science/article/pii/S1268773105800104>.
- Bell, C.J. & Fisher, J., 2007. Simulation of polyethylene wear in ankle joint prostheses. *Journal of Biomedical Materials Research Part B: Applied Biomaterials*, 81B(1), pp.162–167. Available at: <http://dx.doi.org/10.1002/jbm.b.30649>.
- Belvedere, C. et al., 2017. Experimental Evaluation of a New Morphological Approximation of the Articular Surfaces of the Ankle Joint. *Journal of Biomechanics*, 53, pp.97-104. Available at: <http://www.sciencedirect.com/science/article/pii/S0021929017300039>
- Benson, L.C., DesJardins, J.D. & LaBerge, M., 2001. Effects of in vitro wear of machined and molded UHMWPE tibial inserts on TKR kinematics. *Journal of Biomedical Materials Research*, 58(5), pp.496–504. Available at: <http://dx.doi.org/10.1002/jbm.1046>.
- Bergmann, G., Graichen, F. & Rohlmann, A., 1993. Hip joint loading during walking and running, measured in two patients. *Journal of biomechanics*, 26(8), pp.969–90. Available at: <http://www.ncbi.nlm.nih.gov/pubmed/8349721>
- Bergström, J., 2002. Constitutive modeling of ultra-high molecular weight polyethylene under large-deformation and cyclic loading conditions. *Biomaterials*, 23(11), pp.2329–2343. Available at: <http://linkinghub.elsevier.com/retrieve/pii/S0142961201003672>
- Besong, A.A. et al., 1999. The influence of lubricant on the morphology of ultra-high molecular weight polyethylene wear debris generated in laboratory tests. *Proceedings of the Institution of Mechanical Engineers, Part H: Journal of Engineering in Medicine*, 213(2), pp.155–158. Available at: <http://www.ncbi.nlm.nih.gov/pubmed/10333687>
- Besse, J.L., Brito, N. & Lienhart, C., 2009. Clinical evaluation and radiographic assessment of bone lysis of the AES total ankle replacement. *Foot Ankle International*, 30(10), pp.964–975. Available at: <http://www.ncbi.nlm.nih.gov/pubmed/>.
- Biggsby, R.J.A., Hardaker, C.S. & Fisher, J., 1997. Wear of ultra-high molecular weight polyethylene acetabular cups in a physiological hip joint simulator in the anatomical position using bovine serum as a lubricant. *Proceedings of the*

- Institution of Mechanical Engineers, Part H: Journal of Engineering in Medicine*, 211(3), pp.265–269. Available at: <http://www.ncbi.nlm.nih.gov/pubmed/9256003>
- Bills, P. et al., 2005. A metrology solution for the orthopaedic industry. *Journal of Physics: Conference Series*, 13(1), p.316. Available at: <http://stacks.iop.org/1742-6596/13/i=1/a=074>.
- Bischoff, J.E. et al., 2015. Influence of crosslinking on the wear performance of polyethylene within total ankle arthroplasty. *Foot and Ankle International*, 36(4), pp.369–376.
- Blundell, C.M. and A.E.F., 2012. Early to Medium-Term Results of the Mobility Total Ankle Replacement. *British Orthopaedic Foot and Ankle Society-Annual Scientific Meeting*.
- Blunt, L. et al., 2008. Improvement in the assessment of wear of total knee replacements using coordinate-measuring machine techniques. *Proceedings of the Institution of Mechanical Engineers, Part H: Journal of Engineering in Medicine*, 222(3), pp.309–318. Available at: <http://eprints.hud.ac.uk/4085/>.
- Blunt, L. et al., 2009. The role of tribology and metrology in the latest development of bio-materials. *Wear*, 266(3–4), pp.424–431. Available at: <http://www.sciencedirect.com/science/article/pii/S0043164808002226>.
- Bonasia, D.E. et al., 2010. Total ankle replacement: why, when and how? *The Iowa orthopaedic journal*, 30, pp.119–30. Available at: <http://www.ncbi.nlm.nih.gov/pubmed/21045984>
- Bonnin, M. et al., 2011. The Salto Total Ankle Arthroplasty: Survivorship and Analysis of Failures at 7 to 11 years. *Clinical Orthopaedics and Related Research*, 469(1), pp.225–236. Available at: <http://link.springer.com/10.1007/s11999-010-1453->
- Bortel, E., Charbonnier, B. & Heuberger, R., 2015. Development of a Synthetic Synovial Fluid for Tribological Testing. *Lubricants*, 3(4), pp.664–686. Available at: <http://www.mdpi.com/2075-4442/3/4/664>
- Bowden, F.P. & Tabor, D., 2001. *The friction and lubrication of solids*, Clarendon Press.
- Bragdon, C.R. et al., 1996. The importance of multidirectional motion on the wear of polyethylene. *ARCHIVE: Proceedings of the Institution of Mechanical Engineers, Part H: Journal of Engineering in Medicine 1989-1996 (vols 203-210)*, 210(38), pp.157–165. Available at: http://sdj.sagepub.com/lookup/10.1243/PIME_PROC_1996_210_408_02
- Braitto, M. et al., 2015. Effect of Coronal and Sagittal Alignment on Outcome After Mobile-Bearing Total Ankle Replacement. *Foot & Ankle International*, 36(9), pp.1029–1037. Available at: <http://www.ncbi.nlm.nih.gov/pubmed/25899099>
- Brand, R.A. et al., 1994. Comparison of hip force calculations and measurements in the same patient. *The Journal of Arthroplasty*, 9(1), pp.45–51. Available at: <http://linkinghub.elsevier.com/retrieve/pii/0883540394901368>

- Brandt, J.-M. et al., 2011. Commissioning of a displacement-controlled knee wear simulator and exploration of some issues related to the lubricant. *Proceedings of the Institution of Mechanical Engineers, Part H: Journal of Engineering in Medicine*, 225(8), pp.736–752. Available at: <http://pih.sagepub.com/lookup/doi/10.1177/0954411911406061>
- Brandt, J.-M. et al., 2012. Retrieval analysis of modular total knee replacements: Factors influencing backside surface damage. *The Knee*, 19(4), pp.306–315.
- Brockett, C. & Chapman, G., 2016. Biomechanics of the ankle. *Orthopaedics and trauma*, 30(3), pp.232–238. Available at: <http://www.sciencedirect.com/science/article/pii/S1877132716300483>
- Brockett, C.L. et al., 2016. The influence of simulator input conditions on the wear of total knee replacements: An experimental and computational study. *Proceedings of the Institution of Mechanical Engineers, Part H: Journal of Engineering in Medicine*, 230(5), pp.429–439. Available at: <http://journals.sagepub.com/doi/10.1177/0954411916645134>
- Brockett, C.L. et al., 2012. Wear of moderately cross-linked polyethylene in fixed-bearing total knee replacements. *Proceedings of the Institution of Mechanical Engineers, Part H: Journal of Engineering in Medicine*, 226(7), pp.529–535. Available at: <http://pih.sagepub.com/content/226/7/529.abstract>.
- Brockett, C.L., Jennings, L.M. & Fisher, J., 2011. The wear of fixed and mobile bearing unicompartmental knee replacements. *Proceedings of the Institution of Mechanical Engineers, Part H: Journal of Engineering in Medicine*, 225(5), pp.511–519. Available at: <http://pih.sagepub.com/lookup/doi/10.1177/2041303310393824>
- Bronner, S., Ojofeitimi, S. & Woo, H., 2015. Extreme Kinematics in Selected Hip Hop Dance Sequences. *Medical problems of performing artists*, 30(3), pp.126–34. Available at: <http://www.ncbi.nlm.nih.gov/pubmed/26395613>
- Brown, S.S. & Clarke, I.C., 2006. A Review of Lubrication Conditions for Wear Simulation in Artificial Hip Replacements. *Tribology Transactions*, 49, pp.72–78. Available at: <http://www.tandfonline.com/doi/pdf/10.1080/05698190500519223?needAccess=true>
- Buechel Sr., F.F., Buechel Jr., F.F. & Pappas, M.J., 2003. Ten-year evaluation of cementless Buechel-Pappas meniscal bearing total ankle replacement. *Foot Ankle International*, 24(6), pp.462–472.
- Burdett, R.G., 1982. Forces predicted at the ankle during running. *Medicine and Science in Sports and Exercise*, 14(4), pp.308–316.
- Calderale, P.M. et al., 1983. Biomechanical Design of the Total Ankle Prosthesis. *Engineering in Medicine*, 12(2), pp.69–80. Available at: <http://eim.sagepub.com/content/12/2/69.abstract>.
- Catani, F. et al., 2010. The Mark Coventry Award Articular: Contact Estimation in TKA Using In Vivo Kinematics and Finite Element Analysis. *Clinical Orthopaedics and Related Research*, 468(1), pp.19–28. Available at: <http://www.ncbi.nlm.nih.gov/pubmed/19548042>

- Cenni, F. et al., 2013. Functional performance of a total ankle replacement: thorough assessment by combining gait and fluoroscopic analyses. *Clinical Biomechanics*, 28(1), pp.79–87. Available at: <http://www.sciencedirect.com/science/article/pii/S0268003312002513>.
- Chang, J.D. & Billau, K., 2007. *Bioceramics and Alternative Bearings in Joint Arthroplasty: 12th BIOLOX® Symposium Seoul, Republic of Korea September 7 - 8, 2007. Proceedings*, Steinkopff. Available at: <http://books.google.co.uk/books?id=3CrHHaQ4DmUC>.
- Charlton, P. & Blunt, L., 2008. Surface and form metrology of polished “freeform” biological surfaces. *Wear*, 264(5–6), pp.394–399. Available at: <http://www.sciencedirect.com/science/article/pii/S0043164807001718>.
- Choisne, J. et al., 2012. Influence of kinematic analysis methods on detecting ankle and subtalar joint instability. *Journal of Biomechanics*, 45(1), pp.46–52.
- Clarke, I. et al., 2016. Validation of clinical edge-wear in steep-cups using 40–70 dynamic inclinations in novel mom simulator study. *Orthopaedic Proceedings*, 98–B(SUPP 7). Available at: http://bjjprocs.boneandjoint.org.uk/content/98-B/SUPP_7/86
- Clarke, I. et al., 2007. Wear Performance of 36mm Biolox® forte/delta Hip Combinations Compared in Simulated “Severe” Micro-Separation Test Mode. In *Bioceramics and Alternative Bearings in Joint Arthroplasty*. Darmstadt: Steinkopff, pp. 33–43. Available at: http://www.springerlink.com/index/10.1007/978-3-7985-1783-7_4
- Coester, L.M. et al., 2001. Long-term results following ankle arthrodesis for post-traumatic arthritis. *The Journal of Bone & Joint Surgery*, 83(2), p.219.
- Conti, S., Lalonde, K.-A. & Martin, R., 2006. Kinematic Analysis of the Agility Total Ankle during Gait. *Foot & Ankle International*, 27(11), pp.980–984. Available at: <http://journals.sagepub.com/doi/10.1177/107110070602701120>
- Conti, S.F. & Wong, Y.S., 2001. Complications of total ankle replacement. *Clinical orthopaedics and related research*, (391), pp.105–14. Available at: <http://www.ncbi.nlm.nih.gov/pubmed/11603658>
- Cook, R.B. et al., 2013. Pseudotumour Formation Due to Tribocorrosion at the Taper Interface of Large Diameter Metal on Polymer Modular Total Hip Replacements. *The Journal of Arthroplasty*, 28(8), pp.1430–1436.
- Cottrino, S. et al., 2016. Wear study of Total Ankle Replacement explants by microstructural analysis. *Journal of the Mechanical Behavior of Biomedical Materials*, 61, pp.1–11.
- D’Lima, D., Hermida, J. & Chen, P., 2001. Polyethylene wear and variations in knee kinematics. *and related research*, 392, pp.124-130. Available at: http://journals.lww.com/corr/Abstract/2001/11000/Polyethylene_Wear_and_Variations_in_Knee.15.aspx
- D’Lima, D.D., Chen, P.C. & Colwell, C.W., 2001. Polyethylene contact stresses, articular congruity, and knee alignment. *Clinical orthopaedics and related research*, (392), pp.232–8. Available at:

<http://www.ncbi.nlm.nih.gov/pubmed/11716388>

- Danzl, R., Helmlí, F. & Scherer, S., 2011. Focus variation—a robust technology for high resolution optical 3D surface metrology. *Strojníški vestnik-Journal of mechanical engineering*, 57(3), pp.245-256. Available at: <http://ojs.sv-jme.eu/index.php/sv-jme/article/view/sv-jme.2010.175>
- Davidson, J.A., Poggie, R.A. & Mishra, A.K., 1994. Abrasive Wear of Ceramic, Metal, and UHMWPE Bearing Surfaces from Third-Body Bone, PMMA Bone Cement, and Titanium Debris. *Bio-Medical Materials and Engineering*, 4(3), pp.213–229. Available at: <http://content.iospress.com/articles/bio-medical-materials-and-engineering/bme4-3-09>
- Davim, J.P., 2010. *Biotribology*, Wiley. Available at: <http://books.google.co.uk/books?id=a4WrcQAACAAJ>.
- Dennis, D.A. et al., 2001. Femoral condylar lift-off in vivo in total knee arthroplasty. *Journal of Bone and Joint Surgery-British Volume*, 83B(1), pp.33–9. Available at: <http://www.bjj.boneandjoint.org.uk/content/bjbsbr/83-B/1/33.full.pdf>
- Deorio, J.K. & Easley, M.E., 2008. Total ankle arthroplasty. *Instructional course lectures*, 57, pp.383–413. Available at: <http://www.ncbi.nlm.nih.gov/pubmed/18399599>
- Derbyshire, B. et al., 1994. Assessment of the change in volume of acetabular cups using a coordinate measuring machine. *ARCHIVE: Proceedings of the Institution of Mechanical Engineers, Part H: Journal of Engineering in Medicine 1989-1996 (vols 203-210)*, 208(38), pp.151–158. Available at: http://sdj.sagepub.com/lookup/10.1243/PIME_PROC_1994_208_280_02
- DesJardins, J.D., Burnikel, B. & LaBerge, M., 2008. UHMWPE wear against roughened oxidized zirconium and CoCr femoral knee components during force-controlled simulation. *Wear*, 264(3–4), pp.245–256. Available at: <http://www.sciencedirect.com/science/article/pii/S0043164807004917>.
- Doets, H.C. et al., 2007. Gait Analysis After Successful Mobile Bearing Total Ankle Replacement. *Foot & Ankle International*, 28(3), pp.313–322. Available at: http://www.datatrace.com/e-chemtracts/emailurl.html?http://www.newslettersonline.com/user/user.fas/s=563/fp=20/tp=37?T=open_article,955346&P=article
- Dowson, D., 2001. New joints for the Millennium: Wear control in total replacement hip joints. *Proceedings of the Institution of Mechanical Engineers, Part H: Journal of Engineering in Medicine*, 215(4), pp.335–358. Available at: <http://sdj.sagepub.com/lookup/10.1243/0954411011535939>
- Dugan, S.A. & Bhat, K.P., 2005. Biomechanics and analysis of running gait. *Physical Medical Rehabilitation Clinics of North America*, 16(3), pp.603–621.
- Easley, M.E. et al., 2011. Results of Total Ankle Arthroplasty. *The Journal of Bone & Joint Surgery*, 93(15), pp.1455–1468. Available at: <http://dx.doi.org/10.2106/JBJS.J.00126>.

- Endo, M. et al., 2002. Comparison of wear, wear debris and functional biological activity of moderately crosslinked and non-crosslinked polyethylenes in hip prostheses. *Proceedings of the Institution of Mechanical Engineers, Part H: Journal of Engineering in Medicine*, 216(2), pp.111–122. Available at: <http://journals.sagepub.com/doi/10.1243/0954411021536333>
- Espinosa, N. et al., 2010. Misalignment of total ankle components can induce high joint contact pressures. *Journal of Bone and Joint Surgery-American Volume*, 92(5), pp.1179–1187.
- Estok, D.M. et al., 2005. The measurement of creep in ultrahigh molecular weight polyethylene: a comparison of conventional versus highly cross-linked polyethylene. *The Journal of arthroplasty*, 20(2), pp.239–43. Available at: <http://www.ncbi.nlm.nih.gov/pubmed/15902864>
- Fabry, C. et al., 2017. High wear resistance of femoral components coated with titanium nitride: a retrieval analysis. *Knee Surgery, Sports Traumatology, Arthroscopy*, pp.1–10. Available at: <http://link.springer.com/10.1007/s00167-017-4578-7>
- Fisher, J., 2012. A stratified approach to pre-clinical tribological evaluation of joint replacements representing a wider range of clinical conditions advancing beyond the current standard. *Faraday discussions*, 156, pp.59-68-103. Available at: <http://www.ncbi.nlm.nih.gov/pubmed/23285622>
- Fisher, J. et al., 1994. The effect of sliding velocity on the friction and wear of UHMWPE for use in total artificial joints. *Wear*, 175(1–2), pp.219–225. Available at: <http://linkinghub.elsevier.com/retrieve/pii/0043164894901856>
- Fisher, J. et al., 2004. Wear, Debris, and Biologic Activity of Cross-linked Polyethylene in the Knee. *Clinical Orthopaedics and Related Research*, 428, pp.114–119. Available at: <http://content.wkhealth.com/linkback/openurl?sid=WKPTLP:landingpage&an=00003086-200411000-00019>
- Flannery, M. et al., 2008. Analysis of wear and friction of total knee replacements: Part I. Wear assessment on a three-station wear simulator. *Wear*, 265(7–8), pp.999–1008. Available at: <http://www.sciencedirect.com/science/article/pii/S0043164808000781>.
- Flavin, R., Coleman, S. & Tenenbaum, S., 2013. Comparison of gait after total ankle arthroplasty and ankle arthrodesis. *Foot & ankle international*. Available at: <http://journals.sagepub.com/doi/abs/10.1177/1071100713490675>
- Fregly, B.J., Bei, Y. & Sylvester, M.E., 2003. Experimental evaluation of an elastic foundation model to predict contact pressures in knee replacements. *Journal of Biomechanics*, 36(11), pp.1659–1668. Available at: <http://linkinghub.elsevier.com/retrieve/pii/S0021929003001763>
- Frigg, A. et al., 2010. Clinical Relevance of Hindfoot Alignment View in Total Ankle Replacement. *Foot & Ankle International*, 31(10), pp.871–879. Available at: <http://www.ncbi.nlm.nih.gov/pubmed/20964965>

- Funk, J.R., 2011. Ankle injury mechanisms: Lessons learned from cadaveric studies. *Clinical Anatomy*, 24(3), pp.350–361. Available at: <http://doi.wiley.com/10.1002/ca.21112>
- Gadelmawla, E.S. et al., 2002. Roughness parameters. *Journal of Materials Processing Technology*, 123(1), pp.133–145. Available at: <http://www.sciencedirect.com/science/article/pii/S0924013602000602>.
- Galvin, A.L. et al., 2009. Effect of conformity and contact stress on wear in fixed-bearing total knee prostheses. *Journal of biomechanics*, 42(12), pp.1898–902. Available at: <http://www.ncbi.nlm.nih.gov/pubmed/19524245>
- Giannini, S. et al., 2010. Total ankle replacement compatible with ligament function produces mobility, good clinical scores, and low complication rates: an early clinical assessment. *Clinical orthopaedics and related research*, 468(10), pp.2746–53. Available at: <http://www.ncbi.nlm.nih.gov/pubmed/20559763>
- Glazebrook, M.A., Arsenault, K. & Dunbar, M., 2009. Evidence-based classification of complications in total ankle arthroplasty. *Foot Ankle International*, 30(10), pp.945–949.
- Glitsch, U. & Baumann, W., 1997. The three-dimensional determination of internal loads in the lower extremity. *Journal of biomechanics*. Available at: <http://www.sciencedirect.com/science/article/pii/S0021929097000894>
- Glyn-Jones, S. et al., 2015. The John Charnley Award: Highly Crosslinked Polyethylene in Total Hip Arthroplasty Decreases Long-term Wear: A Double-blind Randomized Trial. *Clinical Orthopaedics and Related Research*, 473(2), pp.432–438. Available at: <http://link.springer.com/10.1007/s11999-014-3735-2>
- Goldberg, A. et al., 2012. The demand incidence of symptomatic ankle osteoarthritis presenting to foot and ankle surgeons in the United Kingdom. *The Foot*. Available at: <http://www.sciencedirect.com/science/article/pii/S0958259212000235>
- Gougoulias, N., Khanna, A. & Maffulli, N., 2010. How successful are current ankle replacements: a systematic review of the literature. *Clinical Orthopaedics and Related Research*, 468(1), pp.199–208.
- Gührs, J. et al., 2015. The influence of stem taper re-use upon the failure load of ceramic heads. *Medical Engineering & Physics*, 37(6), pp.545–552.
- Gundapaneni, D., Laughlin, R.T. & Goswami, T., 2016. Characterization of retrieved total ankle replacement liners. *Engineering Failure Analysis*, 70, pp.237–254. Available at: <http://www.sciencedirect.com/science/article/pii/S1350630716302448>
- Gustke, K.A. et al., 2014. Primary TKA Patients with Quantifiably Balanced Soft-Tissue Achieve Significant Clinical Gains Sooner than Unbalanced Patients. *Advances in orthopedics*. Available at: <http://www.ncbi.nlm.nih.gov/pubmed/25210632>

- Haddad, S.L. et al., 2007. Intermediate and long-term outcomes of total ankle arthroplasty and ankle arthrodesis. A systematic review of the literature. *Journal of Bone and Joint Surgery-American Volume*, 89(9), pp.1899–1905.
- Hadley, M. et al., 2013. Development of a Stop-Dwell-Start (SDS) Protocol for In Vitro Wear Testing of Metal-on-Metal Total Hip Replacements. In *Metal-On-Metal Total Hip Replacement Devices*. 100 Barr Harbor Drive, PO Box C700, West Conshohocken, PA 19428-2959: ASTM International, pp. 271–291. Available at: <http://www.astm.org/doiLink.cgi?STP156020120032>
- Hahn, M., Wright, E. & Segal, A., 2012. Comparative gait analysis of ankle arthrodesis and arthroplasty: initial findings of a prospective study. *Foot & ankle International*. Available at: <http://fai.sagepub.com/content/33/4/282>
- Hall, R.M., Bankes, M.J.K. & Blunn, G., 2001. Biotribology for joint replacement. *Current Orthopaedics*, 15(4), pp.281–290. Available at: <http://linkinghub.elsevier.com/retrieve/pii/S0268089001901975?showalltrue>.
- Harris, G.F., Smith, P.A. & Marks, R.M., 2008. *Foot and ankle motion analysis: clinical treatment and technology*, CRC Press.
- Harris, W.H., 2012. Edge Loading Has a Paradoxical Effect on Wear in Metal-on-Polyethylene Total Hip Arthroplasties. *Clinical Orthopaedics and Related Research*®, 470(11), pp.3077–3082. Available at: <http://link.springer.com/10.1007/s11999-012-2330-7>
- Haskell, A. & Mann, R., 2004. Perioperative complication rate of total ankle replacement is reduced by surgeon experience. *Foot & ankle International*. Available at: <http://journals.sagepub.com/doi/abs/10.1177/107110070402500502>
- Henricson, A., Skoog, A. & Carlsson, Å., 2007. The Swedish Ankle Arthroplasty Register: An analysis of 531 arthroplasties between 1993 and 2005. *Acta Orthopaedica*, 78(5), pp.569–574. Available at: <http://informahealthcare.com/doi/abs/10.1080/17453670710014248>.
- Hermida, J.C. et al., 2008. The effect of oxidative aging on the wear performance of highly crosslinked polyethylene knee inserts under conditions of severe malalignment. *Journal of Orthopaedic Research*, 26(12), pp.1585–1590. Available at: <http://doi.wiley.com/10.1002/jor.20686>
- Heuberger, M.P. et al., 2005. Protein-mediated boundary lubrication in arthroplasty. *Biomaterials*, 26(10), pp.1165–1173. Available at: <http://www.sciencedirect.com/science/article/pii/S014296120400496X>
- Hintermann, B. et al., 2013. Hintegra Revision Arthroplasty for Failed Total Ankle Prostheses. *The Journal of Bone and Joint Surgery-American Volume*, 95(13), pp.1166–1174. Available at: <http://www.ncbi.nlm.nih.gov/pubmed/23824384>
- Hintermann, B., 2005. *Total ankle arthroplasty: historical overview, current concepts and future perspectives*, Springer.
- Hintermann, B. & Valderrabano, V., 2003. Total ankle replacement. *Foot and Ankle Clinics*, 8(2), pp.375–405. Available at:

http://s3.amazonaws.com/academia.edu.documents/46642158/S1083-7515_2803_2900015-920160620-31582-1597do7.pdf?AWSAccessKeyId=AKIAIWOWYYGZ2Y53UL3A&Expires=1497119666&Signature=T81E78kSHLV0ZYNBtKvy7hzIpz0=&response-content-disposition=inline; filename=T

Hood, R.W., Wright, T.M. & Burstein, A.H., 1983. Retrieval analysis of total knee prostheses: A method and its application to 48 total condylar prostheses. *Journal of Biomedical Materials Research*, 17(5), pp.829–842. Available at: <http://dx.doi.org/10.1002/jbm.820170510>.

van Hove, R.P. et al., 2015. Titanium-Nitride Coating of Orthopaedic Implants: A Review of the Literature. *BioMed Research International*, 2015, pp.1–9. Available at: <http://www.hindawi.com/journals/bmri/2015/485975/>

Howling, G.I. et al., 2001. Quantitative characterization of polyethylene debris isolated from periprosthetic tissue in early failure knee implants and early and late failure Charnley hip implants. *Journal of Biomedical Materials Research*, 58(4), pp.415–420.

Hua, X. et al., 2014. Contact mechanics of modular metal-on-polyethylene total hip replacement under adverse edge loading conditions. *Journal of Biomechanics*, 47(13), pp.3303–3309. Available at: <http://www.sciencedirect.com/science/article/pii/S0021929014004394>

Hunt, B. & Joyce, T., 2016. A Tribological Assessment of Ultra High Molecular Weight Polyethylene Types GUR 1020 and GUR 1050 for Orthopedic Applications. *Lubricants*, 4(3), p.25. Available at: <http://www.mdpi.com/2075-4442/4/3/25>

Ingham, E. & Fisher, J., 2000. Biological reactions to wear debris in total joint replacement. *Proceedings of the Institution of Mechanical Engineers, Part H: Journal of Engineering in Medicine*, 214(1), pp.21–37. Available at: <http://sdj.sagepub.com/lookup/10.1243/0954411001535219>

Ingrosso, S. et al., 2009. GAIT analysis in patients operated with a novel total ankle prosthesis. *Gait & Posture*, 30(2), pp.132–137. Available at: <http://linkinghub.elsevier.com/retrieve/pii/S0966636209001192>

Inman, V.T., 1969. The influence of the foot-ankle complex on the proximal skeletal structures. *Artificial Limbs*, 13(1), pp.59–65.

Inman, V.T., 1976. *The joints of the ankle*, Williams & Wilkins.

ISO14242-2, 2016. ISO 14242-2:2016 Implants for surgery -- Wear of total hip-joint prostheses -- Part 2: Methods of measurement.

ISO 4288, 1996. *Geometric product specifications (GPS) - surface texture : profile method : rules and procedures for the assessment of surface texture*, British Standards Institution. Available at: <http://shop.bsigroup.com/ProductDetail/?pid=000000000001345614>

Iwasa, K. et al., 2014. Arthroscopic ankle arthrodesis for treating osteoarthritis in a patient with kashin-beck disease. *Case reports in medicine*, 2014, pp.931278. Available at: <https://www.hindawi.com/journals/crim/2014/931278/abs/>

- Jackson, M.P. & Singh, D., 2003. Total ankle replacement. *Current Orthopaedics*, 17(4), pp.292–298. Available at: <http://www.sciencedirect.com/science/article/pii/S0268089002001950>.
- Jakubowitz, E. et al., 2009. The influence of age, bone quality and body mass index on periprosthetic femoral fractures: a biomechanical laboratory study. *Medical science monitor : international medical journal of experimental and clinical research*, 15(11), pp.307-12. Available at: <http://www.ncbi.nlm.nih.gov/pubmed/19865047>
- Jenkyn, T.R. & Nicol, A.C., 2007. A multi-segment kinematic model of the foot with a novel definition of forefoot motion for use in clinical gait analysis during walking. *Journal of Biomechanics*, 40(14), pp.3271–3278. Available at: <http://www.ncbi.nlm.nih.gov/pubmed/17610881>
- Jennings, L.M. et al., 2007. The influence of femoral condylar lift-off on the wear of artificial knee joints. *Proceedings of the Institution of Mechanical Engineers, Part H: Journal of Engineering in Medicine*, 221(3), pp.305–314. Available at: <http://sdj.sagepub.com/lookup/10.1243/09544119JEIM215>
- Jiang, X. et al., 2007. Paradigm Shifts in Surface Metrology. Part I. Historical Philosophy. *Proceedings: Mathematical, Physical and Engineering Sciences*, 463(2085), pp.2049–2070. Available at: <http://www.jstor.org/stable/20209299>.
- Jiang, X.Q., Blunt, L. & Stout, K.J., 1999. Three-dimensional surface characterization for orthopaedic joint prostheses. *Proceedings of the Institution of Mechanical Engineers, Part H: Journal of Engineering in Medicine*, 213(1), pp.49–68. Available at: <http://pih.sagepub.com/content/213/1/49.abstract>.
- Jin, Z.M. et al., 2006. (v) Biotribology. *Current Orthopaedics*, 20(1), pp.32–40. Available at: <http://www.sciencedirect.com/science/article/pii/S026808900500160X>
- Johnson, T.S. et al., 2003. Comparison of wear of mobile and fixed bearing knees tested in a knee simulator. *Wear*, 255(7–12), pp.1107–1112. Available at: <http://linkinghub.elsevier.com/retrieve/pii/S0043164803002722>
- Kakkar, R. & Siddique, M.S., 2011. Stresses in the ankle joint and total ankle replacement design. *Foot and Ankle Surgery*, 17(2), pp.58–63. Available at: <http://www.ncbi.nlm.nih.gov/pubmed/>.
- Kamali, A. et al., 2005. Wear of ultrahigh-molecular-weight polyethylene against titanium-nitride-coated counterfaces. *Proceedings of the Institution of Mechanical Engineers, Part J: Journal of Engineering Tribology*, 219(1), pp.41–47. Available at: <http://journals.sagepub.com/doi/10.1243/135065005X9736>
- Karantana, A., Hobson, S. & Dhar, S., 2010. The Scandinavian Total Ankle Replacement: Survivorship at 5 and 8 Years Comparable to Other Series. *Clinical Orthopaedics and Related Research®*, 468(4), pp.951–957. Available at: <http://link.springer.com/10.1007/s11999-009-0971-y>

- Kendrick, B.J. et al., 2010. Polyethylene wear in Oxford unicompartmental knee replacement: a retrieval study of 47 bearings. *Journal of Bone and Joint Surgery- British Volume*, 92(3), pp.367–373. Available at: <http://www.ncbi.nlm.nih.gov/pubmed/>.
- Kim, D.-R. et al., 2016. Total Ankle Arthroplasty: An Imaging Overview. *Korean journal of radiology*, 17(3), pp.413–23. Available at: <http://www.ncbi.nlm.nih.gov/pubmed/27134529>
- Kim, Y.-H., Ritchie, A. & Hardaker, C., 2005. Surface Roughness of Ceramic Femoral Heads After in Vivo Transfer of Metal: Correlation to Polyethylene Wear. *The Journal of Bone & Joint Surgery*, 87(3), pp.577–582. Available at: <http://dx.doi.org/10.2106/JBJS.D.01790>.
- Kingston, B., 2000. *Understanding joints: a practical guide to their structure and function*, Nelson Thornes.
- Knowlton, C.B., Bhutani, P. & Wimmer, M.A., 2016. Relationship of surface damage appearance and volumetric wear in retrieved TKR polyethylene liners. *Journal of Biomedical Materials Research Part B: Applied Biomaterials*. Available at: <http://doi.wiley.com/10.1002/jbm.b.33684>
- Knowlton, C.B. & Wimmer, M.A., 2012. An autonomous mathematical reconstruction to effectively measure volume loss on retrieved polyethylene tibial inserts. *Journal of Biomedical Materials Research Part B: Applied Biomaterials*, 101B(3), p.n/a-n/a. Available at: <http://doi.wiley.com/10.1002/jbm.b.32782>
- Kobayashi, A. et al., 2004. Ankle Arthroplasties Generate Wear Particles Similar to Knee Arthroplasties. *Clinical Orthopaedics and Related Research*, 424, pp.69–72. Available at: <http://content.wkhealth.com/linkback/openurl?sid=WKPTLP:landingpage&an=00003086-200407000-00010>
- Koivu, H. et al., 2017. Long-term Results of Scandinavian Total Ankle Replacement. *Foot & Ankle International*, p.107110071769869. Available at: <http://journals.sagepub.com/doi/10.1177/1071100717698695>
- Kokkonen, A. et al., 2011. High rate of osteolytic lesions in medium-term follow-up after the AES total ankle replacement. *Foot Ankle International*, 32(2), pp.168–175.
- Komistek, R.D. et al., 2000. A Determination of Ankle Kinematics Using Fluoroscopy. *Foot & Ankle International*, 21(4), pp.343–350. Available at: <http://journals.sagepub.com/doi/10.1177/107110070002100412>
- Krause, F.G. & Schmid, T., 2012. Ankle arthrodesis versus total ankle replacement: how do I decide? *Foot and Ankle Clinics*, 17(4), pp.529–543.
- Kurtz, S., 2009. *UHMWPE biomaterials handbook: ultra high molecular weight polyethylene in total joint replacement and medical devices*.
- Kurtz, S., Gawel, H. & Patel, J., 2011. History and systematic review of wear and osteolysis outcomes for first-generation highly crosslinked polyethylene.

- Clinical Orthopaedics and Related Research*, 469(8), pp.2262-2277. Available at: <http://link.springer.com/article/10.1007/s11999-011-1872-4>
- Kurtz, S.M. et al., 2002. Deconvolution of surface topology for quantification of initial wear in highly cross-linked acetabular components for THA. *Journal of Biomedical Materials Research*, 63(5), pp.492–500. Available at: <http://dx.doi.org/10.1002/jbm.10309>.
- Kurup, H. V. & Taylor, G.R., 2008. Medial impingement after ankle replacement. *International Orthopaedics*, 32(2), pp.243–246. Available at: <http://link.springer.com/10.1007/s00264-006-0300-y>
- Lamoreux, L., 1970. Kinematic measurements in the study of human walking. *Bulletin of prosthetics research*, 10(15), pp.3-84. Available at: <http://europepmc.org/abstract/med/5131748>
- Lamoreux, L.W., 1971. Kinematic measurements in the study of human walking. *Bulletin of prosthetics research*, 10(15), pp.3–84. Available at: <http://www.ncbi.nlm.nih.gov/pubmed/5131748>
- Lappalainen, R. & Santavirta, S., 2005. Potential of coatings in total hip replacement. *Clinical orthopaedics and related research*, 430, pp72-79. Available at: http://journals.lww.com/corr/Abstract/2005/01000/Potential_of_Coatings_in_Total_Hip_Replacement.9.aspx
- Leardini, A., 2001. Geometry and mechanics of the human ankle complex and ankle prosthesis design. *Clinical Biomechanics*, 16(8), pp.706–709. Available at: <http://www.sciencedirect.com/science/article/pii/S0268003301000225>.
- Leardini, A., Stagni, R. & O'Connor, J.J., 2001. Mobility of the subtalar joint in the intact ankle complex. *Journal of Biomechanics*, 34(6), pp.805–809. Available at: <http://www.sciencedirect.com/science/article/pii/S0021929001000318>.
- Lee, C.K., 1988. Accelerated degeneration of the segment adjacent to a lumbar fusion. *Spine*, 13(3), pp.375–7. Available at: <http://www.ncbi.nlm.nih.gov/pubmed/3388124>
- Leszko, F. et al., 2008. In Vivo Kinematics of the Salto Total Ankle Prosthesis. *Foot & Ankle International*, 29(11), pp.1117–1125. Available at: <http://fai.sagepub.com/lookup/doi/10.3113/FAI.2008.1117>
- Liao, Y.-S., Benya, P.D. & McKellop, H.A., 1999. Effect of protein lubrication on the wear properties of materials for prosthetic joints. *Journal of Biomedical Materials Research*, 48(4), pp.465–473. Available at: <http://doi.wiley.com/10.1002/%28SICI%291097-4636%281999%2948%3A4%3C465%3A%3AAID-JBM10%3E3.0.CO%3B2-Y>
- Liau, J.-J. et al., 2002. The effect of malalignment on stresses in polyethylene component of total knee prostheses – a finite element analysis. *Clinical Biomechanics*, 17(2), pp.140–146. Available at: <http://www.sciencedirect.com/science/article/pii/S0268003301001097>

- Liu, A. et al., 2015. Tribology studies of the natural knee using an animal model in a new whole joint natural knee simulator. *Journal of Biomechanics*, 48(12), pp.3004–3011. Available at: <http://linkinghub.elsevier.com/retrieve/pii/S0021929015004406>
- Liu, F. et al., 2011. A New Formulation for the Prediction of Polyethylene Wear in Artificial Hip Joints. *Proceedings of the Institution of Mechanical Engineers, Part H: Journal of Engineering in Medicine*, 225(1), pp.16–24. Available at: <http://journals.sagepub.com/doi/10.1243/09544119JEIM819>
- Liza, S. et al., 2011. Failure analysis of retrieved UHMWPE tibial insert in total knee replacement. *Engineering Failure Analysis*, 18(6), pp.1415–1423. Available at: <http://www.sciencedirect.com/science/article/pii/S1350630711000999>.
- Lundberg, A., Goldie, I. & Kalin, B., 1989. Kinematics of the ankle/foot complex: plantarflexion and dorsiflexion. *Foot & Ankle International*, 9(4), pp.194–200. Available at: <http://fai.sagepub.com/content/9/4/194.short>
- Lundgren, P. et al., 2008. Invasive in vivo measurement of rear-, mid- and forefoot motion during walking. *Gait & Posture*, 28(1), pp.93–100. Available at: <http://www.sciencedirect.com/science/article/pii/S0966636207002640>
- Malikian, R. et al., 2014. In vivo roughening of retrieved total knee arthroplasty femoral components. *Knee*, 21(1), pp.278–282. Available at: <http://www.sciencedirect.com/science/article/pii/S0968016012001603>.
- Maloney, W. et al., 1995. Isolation and characterization of wear particles generated in patients who have had failure of a hip arthroplasty without cement. *Journal of Bone and Joint Surgery- American Volume*, 77(9), pp.1301–1310. Available at: <http://jbjs.org/content/77/9/1301.abstract>
- Mann, J.A., Mann, R.A. & Horton, E., 2011. STAR™ Ankle: Long-Term Results. *Foot & Ankle International*, 32(5), pp.473–484. Available at: <http://fai.sagepub.com/lookup/doi/10.3113/FAI.2011.0473>
- Mann, R.A. & Harrison, M.J., 2012. Total Ankle Arthroplasty: A Brief Review. *Journal of Orthopaedics, Trauma and Rehabilitation*, 16(2), pp.42–44. Available at: <http://www.sciencedirect.com/science/article/pii/S2210491711000819>.
- Mathia, T.G., Pawlus, P. & Wieczorowski, M., 2011. Recent trends in surface metrology. *Wear*, 271(3–4), pp.494–508. Available at: <http://www.sciencedirect.com/science/article/pii/S0043164810002243>.
- Mazzucco, D. & Spector, M., 2003. Effects of contact area and stress on the volumetric wear of ultrahigh molecular weight polyethylene. *Wear*, 254(5), pp.514–522. Available at: <http://www.sciencedirect.com/science/article/pii/S0043164803001352?np=y&npKey=2ca11912f42993a0ace0012a261f23244a751e119374405905532803ee120cc4>
- McEwen, H.M.J. et al., 2005. The influence of design, materials and kinematics on the in vitro wear of total knee replacements. *Journal of Biomechanics*, 38(2), pp.357–365. Available at:

- <http://www.sciencedirect.com/science/article/pii/S002192900400096X>.
- McKellop, H., Clarke, I. & Markolf, K., 1978. Wear characteristics of UHMW polyethylene: a method for accurately measuring extremely low wear rates. *Journal of Biomedical Materials Research*, 12(6) pp.895-927. Available at: <http://onlinelibrary.wiley.com/doi/10.1002/jbm.820120611/full>
- Mckenzie, J. et al., 2012. The Zenith: A New Total Ankle Replacement - First report of early survivorship and radiographic assessment of alignment. In *EFORT*.
- Mengoni, M. et al., 2016. Subject-specific multi-validation of a finite element model of ovine cervical functional spinal units. *Journal of Biomechanics*, 49(2), pp.259–266. Available at: <http://linkinghub.elsevier.com/retrieve/pii/S002192901500706X>
- Michael, J.M. et al., 2008. Biomechanics of the ankle joint and clinical outcomes of total ankle replacement. *Journal of the mechanical behavior of biomedical materials*, 1(4), pp.276–294. Available at: <http://www.sciencedirect.com/science/article/pii/S1751616108000064>.
- Millar, G.S. and T., 2012. The Zenith Total Ankle Replacement- Early Results of the First 50 Cases in a Non-Inventor Series. *British Orthopaedic Foot and Ankle Society- Annual Scientific Meeting*.
- Morgan, S.S., Brooke, B. & Harris, N.J., 2010a. Total ankle replacement by the Ankle Evolution System: medium-term outcome. *Journal of Bone and Joint Surgery- British Volume*, 92(1), pp.61–65.
- Morgan, S.S., Brooke, B. & Harris, N.J., 2010b. Total ankle replacement by the Ankle Evolution System medium-term outcome. *Journal of Bone and Joint Surgery- British Volume*, 92(1), pp.61–5. Available at: <http://www.bjj.boneandjoint.org.uk/content/jbjsbr/92-B/1/61.full.pdf>
- Morris, C. et al., 2015. Articular congruency of the Salto Talaris total ankle prosthesis. *Foot and Ankle Surgery*, 21(3), pp.206-210. Available at: <http://www.sciencedirect.com/science/article/pii/S1268773115000053>
- Moseley, L. et al., 1996. Three-dimensional kinematics of the rearfoot during the stance phase of walking in normal young adult males. *Clinical biomechanics*, 11(1), pp.39–45. Available at: <http://www.ncbi.nlm.nih.gov/pubmed/11415597>
- Müller, S., Wolf, S. & Döderlein, L., 2006. Three-dimensional analysis of the foot following implantation of a HINTEGRA ankle prosthesis: evaluation with the Heidelberg foot model. *Der Orthopade*, 35(5), pp506-512. Available at: <http://europepmc.org/abstract/med/16575603>
- Muratoglu, O.K. et al., 2001. A novel method of cross-linking ultra-high-molecular-weight polyethylene to improve wear, reduce oxidation, and retain mechanical properties. *The Journal of Arthroplasty*, 16(2), pp.149–160. Available at: <http://linkinghub.elsevier.com/retrieve/pii/S0883540301361466>

- Muratoglu, O.K. et al., 2004. Knee-simulator testing of conventional and cross-linked polyethylene tibial inserts. *The Journal of Arthroplasty*, 19(7), pp.887–897. Available at:
<http://www.sciencedirect.com/science/article/pii/S088354030400316X>
- Muratoglu, O.K. et al., 2003. Metrology to Quantify Wear and Creep of Polyethylene Tibial Knee Inserts. *Clinical Orthopaedics and Related Research*, 410, p.155–164 10.1097/01.blo.0000063604.67412.04. Available at:
http://journals.lww.com/corr/Fulltext/2003/05000/Metrology_to_Quantify_Wear_and_Creep_of.18.aspx.
- Myshkin, N.K. et al., 2003. Surface roughness and texture analysis in microscale. *Wear*, 254(10), pp.1001–1009.
- Naal, F.D. et al., 2008. Habitual Physical Activity and Sports Participation After Total Ankle Arthroplasty. *The American Journal of Sports Medicine*, 37(1), pp.95–102. Available at:
<http://ajs.sagepub.com/lookup/doi/10.1177/0363546508323253>
- Naudie, D.D.R. et al., 2007. Wear and osteolysis around total knee arthroplasty. *The Journal of the American Academy of Orthopaedic Surgeons*, 15(1), pp.53–64. Available at: <http://www.ncbi.nlm.nih.gov/pubmed/17213382>
- Nester, C. et al., 2007. In vitro study of foot kinematics using a dynamic walking cadaver model. *Journal of Biomechanics* 40(9) pp1927-1937. Available at:
<http://www.sciencedirect.com/science/article/pii/S0021929006003290>
- Nevelos, J., Ingham, E. & Doyle, C., 2000. Microseparation of the centers of alumina-alumina artificial hip joints during simulator testing produces clinically relevant wear rates and patterns. *The Journal of Arthroplasty*, 15(6), pp793-795.
- NHS Choices, 2014. Couch to 5K - Live Well - NHS Choices. Available at:
<http://www.nhs.uk/LiveWell/c25k/Pages/couch-to-5k.aspx>
- NJR, 2016. National Joint Registry. <http://www.njrcentre.org.uk/>.
- Nordin, M. & Frankel, V.H., 2001. *Basic biomechanics of the musculoskeletal system*, Wolters Kluwer Health.
- Novacheck, 1998. The biomechanics of running. *Gait & posture*, 7(1), pp.77–95. Available at: <http://www.ncbi.nlm.nih.gov/pubmed/10200378>
- O'Brien, S. et al., 2013. Computational development of a polyethylene wear model for the articular and backside surfaces in modular total knee replacements. *Tribology International*, 59(0), pp.284–291. Available at:
<http://www.sciencedirect.com/science/article/pii/S0301679X1200117X>.
- Ounpuu, S., 1994. The biomechanics of walking and running. *Clinics in sports medicine*, 13(4), pp.843–63. Available at:
<http://www.ncbi.nlm.nih.gov/pubmed/7805110>
- Palmieri, R.M. et al., 2006. Peripheral ankle cooling and core body temperature. *Journal of athletic training*, 41(2), pp.185–8. Available at:
<http://www.ncbi.nlm.nih.gov/pubmed/16791304>

- Pappas, M., Makris, G. & Buechel, F., 1995. Titanium Nitride Ceramic Film Against Polyethylene: A 48 Million Cycle Wear Test. *Clinical Orthopaedics and Related Research*, 317, pp.64-70. Available at: http://journals.lww.com/corr/Abstract/1995/08000/Titanium_Nitride_Ceramic_Film_Against.10.aspx
- Philippe, P. et al., 2008. Ankle replacement versus arthrodesis: a comparative gait analysis study. *Foot & Ankle International*, 29(1), pp.3–9.
- Pinar, N. et al., 2012. Total ankle arthroplasty – Total ankle arthroplasty in Western France: Influence of volume on complications and clinical outcome. *Orthopaedics & Traumatology: Surgery & Research*, 98(4, Supplement), pp.S26–S30. Available at: <http://www.sciencedirect.com/science/article/pii/S1877056812000710>.
- Popoola, O.O. et al., 2010. Wear, delamination, and fatigue resistance of melt-annealed highly crosslinked UHMWPE cruciate-retaining knee inserts under activities of daily living. *Journal of Orthopaedic Research*, 28(9), pp.1120–1126. Available at: <http://doi.wiley.com/10.1002/jor.21104>
- Postak, P.D., Rosca, M. & Greenwald, A.S., 2008. Evaluation of the STAR Total Ankle Replacement: An Evolution in Design.
- Procter, P. & Paul, J.P., 1982. Ankle joint biomechanics. *Journal of Biomechanics*, 15(9), pp.627–634. Available at: <http://www.sciencedirect.com/science/article/pii/0021929082900173>.
- Pruitt, L.A., 2005. Deformation, yielding, fracture and fatigue behavior of conventional and highly cross-linked ultra-high molecular weight polyethylene. *Biomaterials*, 26(8), pp.905–915. Available at: <http://www.sciencedirect.com/science/article/pii/S0142961204002820>
- Puloski, S.K. et al., 2001. Tibial post wear in posterior stabilized total knee arthroplasty. An unrecognized source of polyethylene debris. *Journal of Bone and Joint Surgery- American Volume*, 83–A(3), pp.390–397. Available at: <http://www.ncbi.nlm.nih.gov/pubmed/>.
- Queen, R.M. et al., 2013. Differences in Outcomes Following Total Ankle Replacement in Patients with Neutral Alignment Compared with Tibiotalar Joint Malalignment. *The Journal of Bone and Joint Surgery-American Volume*, 95(21), pp.1927–1934. Available at: <http://www.ncbi.nlm.nih.gov/pubmed/24196462>
- Rabinowicz, E., 1965. Friction and wear of materials. Available at: <http://www.citeulike.org/group/13900/article/11884652>
- Rao, S., Saltzman, C. & Yack, H.J., 2006. Ankle ROM and stiffness measured at rest and during gait in individuals with and without diabetic sensory neuropathy. *Gait & Posture*, 24(3), pp.295–301. Available at: <http://www.ncbi.nlm.nih.gov/pubmed/16293415>
- Rawal, B. R., Yadav, A. & Pare, V., 2016. Life estimation of knee joint prosthesis by combined effect of fatigue and wear. *Procedia Technology* 23, pp.60–67.

- Reggiani, B. et al., 2006. Finite element analysis of a total ankle replacement during the stance phase of gait. *Journal of Biomechanics*, 39(8), pp.1435–1443. Available at: <http://www.sciencedirect.com/science/article/pii/S0021929005001788>.
- Reinders, J. et al., 2015. Force-controlled dynamic wear testing of total ankle replacements. *Acta Biomaterialia*, 12, pp.332–340.
- Remes, A. & Williams, D.F., 1992. Immune response in biocompatibility. *Biomaterials*, 13(11), pp.731–743.
- Røkkum, M., Reigstad, A. & Johansson, C.B., 2002. HA particles can be released from well-fixed HA-coated stems. *Acta Orthopaedica Scandinavica*, 73(3), pp.298–306. Available at: <http://www.tandfonline.com/doi/full/10.1080/000164702320155293>
- Rößler, S. et al., 2003. Electrochemically assisted deposition of thin calcium phosphate coatings at near-physiological pH and temperature. *Journal of Biomedical Materials Research Part A*, 64A(4), pp.655–663. Available at: <http://www.ncbi.nlm.nih.gov/pubmed/12601777>
- Rostoker, W. & Galante, J.O., 1979. Contact pressure dependence of wear rates of ultra-high molecular weight polyethylene. *Journal of Biomedical Materials Research*, 13(6), pp.957–964. Available at: <http://www.ncbi.nlm.nih.gov/pubmed/511863>
- Roukis, T.S., 2016. *Primary and Revision Total Ankle Replacement*
- Saari, H. et al., 1993. Differential effects of reactive oxygen species on native synovial fluid and purified human umbilical cord hyaluronate. *Inflammation*, 17(4), pp.403–415. Available at: <http://link.springer.com/10.1007/BF00916581>
- Sadoghi, P. et al., 2013. Revision Surgery After Total Joint Arthroplasty: A Complication-Based Analysis Using Worldwide Arthroplasty Registers. *The Journal of Arthroplasty*, 28(8), pp.1329–1332. Available at: <http://www.sciencedirect.com/science/article/pii/S0883540313001393>.
- Saltzman, C., Mann, R. & Ahrens, J., 2009. Prospective controlled trial of STAR total ankle replacement versus ankle fusion: initial results. *Foot & Ankle*. Available at: <http://journals.sagepub.com/doi/abs/10.3113/FAI.2009.0579>
- Saltzman, C., Salamon, M. & Blanchard, G., 2005. Epidemiology of ankle arthritis: report of a consecutive series of 639 patients from a tertiary orthopaedic center. *The Iowa Orthopaedic Journal*, 25, pp.44-46. Available at: <https://www.ncbi.nlm.nih.gov/pmc/articles/PMC1888779/>
- Sarrafian, S.K., 1993. Biomechanics of the Subtalar Joint Complex. *Clinical Orthopaedics and Related Research*, 290, pp.17–26. Available at: http://journals.lww.com/corr/Fulltext/1993/05000/Biomechanics_of_the_Subtalar_Joint_Complex.3.aspx.
- Scholes, S.C. et al., 2013. Topographical analysis of the femoral components of ex vivo total knee replacements. *Journal of materials science. Materials in medicine*, 24(2), pp.547–554.

- Schwenke, T. et al., 2009. Differences in wear between load and displacement control tested total knee replacements. *Wear*, 267(5–8), pp.757–762. Available at: <http://linkinghub.elsevier.com/retrieve/pii/S0043164809001410>
- Schwenke, T. et al., 2005. Fluid Composition Impacts Standardized Testing Protocols in Ultrahigh Molecular Weight Polyethylene Knee Wear Testing. *Proceedings of the Institution of Mechanical Engineers, Part H: Journal of Engineering in Medicine*, 219(6), pp.457–464. Available at: <http://www.ncbi.nlm.nih.gov/pubmed/16312105>
- Scott, S.H. & Winter, D.A., 1991. Talocrural and talocalcaneal joint kinematics and kinetics during the stance phase of walking. *Journal of Biomechanics*, 24(8), pp.743–752. Available at: <http://linkinghub.elsevier.com/retrieve/pii/002192909190338N>
- Seireg, A. & Arvikar, R.J., 1975. The prediction of muscular load sharing and joint forces in the lower extremities during walking. *Journal of Biomechanics*, 8(2), pp.89–102. Available at: <http://www.sciencedirect.com/science/article/pii/0021929075900895>.
- Sethi, R.K. et al., 2003. Macrophage response to cross-linked and conventional UHMWPE. *Biomaterials*, 24(15), pp.2561–2573.
- Sharkey, N. & Hamel, A., 1998. A dynamic cadaver model of the stance phase of gait: performance characteristics and kinetic validation. *Clinical Biomechanics* 13(6), pp.420-433. Available at: <http://www.sciencedirect.com/science/article/pii/S0268003398000035>
- Sheehan, F.T., 2010. The instantaneous helical axis of the subtalar and talocrural joints: a non-invasive in vivo dynamic study. *Journal of Foot and Ankle Research* 3(13).
- Sheehan, F.T., Seisler, A.R. & Siegel, K.L., 2007. In vivo talocrural and subtalar kinematics: a non-invasive 3D dynamic MRI study. *Foot and Ankle International*, 28(3), pp.323–335.
- Shi, W., Dong, H. & Bell, T., 2000. Tribological behaviour and microscopic wear mechanisms of UHMWPE sliding against thermal oxidation-treated Ti6Al4V. *Materials Science and Engineering A*, 291(1–2), pp.27–36. Available at: www.elsevier.com/locate/msea
- Siegler, S. et al., 2014. New observations on the morphology of the talar dome and its relationship to ankle kinematics. *Clinical Biomechanics* 29(1), pp.1-6. Available at: <http://www.sciencedirect.com/science/article/pii/S0268003313002283>
- Siegler, S., Chen, J. & Schneck, C.D., 1988. The Three-Dimensional Kinematics and Flexibility Characteristics of the Human Ankle and Subtalar Joints—Part I: Kinematics. *Journal of Biomechanical Engineering*, 110(4), pp.364–373. Available at: <http://0-dx.doi.org.wam.leeds.ac.uk/10.1115/1.3108455>.
- Simon, J. et al., 2006. The Heidelberg foot measurement method: Development, description and assessment. *Gait & Posture*, 23(4), pp.411–424. Available at: <http://www.ncbi.nlm.nih.gov/pubmed/16157483>

- Simonsen, E.B. et al., 1995. Bone-on-Bone Forces during Loaded and Unloaded Walking. *Cells Tissues Organs*, 152(2), pp.133–142. Available at: <http://www.karger.com/doi/10.1159/000147692>
- Sinclair, V., Millar, T. & Garg, S., 2015. Medium-term follow-up of the Corin zenith total ankle replacement in an independent non-inventor cohort. *Bone and Joint Journal Orthopaedic Proceedings Supplement*, 97–B(SUPP 14), p.18.
- Singer, S. et al., 2013. Ankle arthroplasty and ankle arthrodesis: gait analysis compared with normal controls. *Journal of Bone and Joint Surgery American Volume* 95(24), pp.1-10. Available at: <http://jbjs.org/content/95/24/e191.abstract>
- Smith, R., Rattanaprasert, U. & O'Dwyer, N., 2001. Coordination of the ankle joint complex during walking. *Human Movement Science*, 20(4–5), pp.447–460. Available at: <http://linkinghub.elsevier.com/retrieve/pii/S0167945701000628>
- Smith, S.L. & Unsworth, A., 1999. A comparison between gravimetric and volumetric techniques of wear measurement of UHMWPE acetabular cups against zirconia and cobalt-chromium-molybdenum femoral heads in a hip simulator. *Proceedings of the Institution of Mechanical Engineers, Part H: Journal of Engineering in Medicine*, 213(6), pp.475–483. Available at: <http://journals.sagepub.com/doi/10.1243/0954411991535086>
- Smyth, A. et al., 2017. Influence of kinematics on the wear of a total ankle replacement. *Journal of Biomechanics*, 53, pp.105–110.
- Snedeker, J.G., Wirth, S.H. & Espinosa, N., 2012. Biomechanics of the normal and arthritic ankle joint. *Foot and ankle clinics*, 17(4), pp.517–528. Available at: <http://europepmc.org/abstract/MED/23158367>.
- Sonntag, R., Reinders, J. & Kretzer, J., 2012. What's next? Alternative materials for articulation in total joint replacement. *Acta Biomaterialia*. Available at: <http://www.sciencedirect.com/science/article/pii/S1742706112001249>
- Speake, H. et al., 2016. Embedding Physical Activity in the Heart of the NHS: The Need for a Whole-System Approach. *Sports Medicine*, 46(7), pp.939–946. Available at: <http://link.springer.com/10.1007/s40279-016-0488-y>
- Spinelli, M. et al., 2009. CMM-based procedure for polyethylene non-congruous unicompartmental knee prosthesis wear assessment. *Wear*, 267(5–8), pp.753–756. Available at: <http://www.sciencedirect.com/science/article/pii/S004316480900091X>.
- Standring, S., Ellis, H. & Healy, J., 2005. Gray's Anatomy: The anatomical basis of clinical practice. Available at: <http://www.ajnr.org/content/26/10/2703.short>
- Stauffer, R.N., Chao, E.Y. & Brewster, R.C., 1977. Force and motion analysis of the normal, diseased, and prosthetic ankle joint. *Clinical Orthopaedics and Related Research*, (127), pp.189–196.

- Stewart, T. et al., 2001. Long-term wear of HIPed alumina on alumina bearings for THR under microseparation conditions. *Journal of Materials Science: Materials in Medicine*, 12(10/12), pp.1053–1056. Available at: <http://link.springer.com/10.1023/A:1012802308636>
- Stoffel, K., Nicholls, R. & Winata, A., 2010. Effect of ankle taping on knee and ankle joint biomechanics in sporting tasks. *Medicine & Science*. Available at: <http://fitasaphysio.com.au/content/Stoffel.pdf>
- Stout, K.J. & Blunt, L.A., 1995. Application of 3-D topography to bio-engineering. *International Journal of Machine Tools and Manufacture*, 35(2), pp.219–229. Available at: <http://www.sciencedirect.com/science/article/pii/0890695594P2376Q>.
- Stratton-Powell, A. et al., 2016. A retrieval analysis of 22 AES total ankle replacement explants. *Foot and Ankle Surgery*, 22(2), pp.88–89. Available at: <http://linkinghub.elsevier.com/retrieve/pii/S126877311630248X>
- Stratton-Powell, A. et al., 2017. Edge loading in explanted total ankle replacements: a polyethylene insert form and volume analysis. *Orthopaedic Proceedings*, 99–B(SUPP 6). Available at: http://www.bjjprocs.boneandjoint.org.uk/content/99-B/SUPP_6/18
- Teeter, M.G. et al., 2011. Determination of Reference Geometry for Polyethylene Tibial Insert Wear Analysis. *The Journal of Arthroplasty*, 26(3), pp.497–503. Available at: <http://www.sciencedirect.com/science/article/pii/S0883540310001294>.
- Teeter, M.G. et al., 2011. In vitro quantification of wear in tibial inserts using microcomputed tomography. *Clinical Orthopaedics and Related Research*, 469(1), pp.107–112. Available at: <http://link.springer.com/10.1007/s11999-010-1490-6>
- Teoh, S.H., 2000. Fatigue of biomaterials: a review. *International journal of fatigue*, 22(10), pp.825–837.
- Teresa Raimondi, M. et al., 2000. The in-vivo wear performance of prosthetic femoral heads with titanium nitride coating. *Biomaterials*, 21(9), pp.907–913. Available at: <http://linkinghub.elsevier.com/retrieve/pii/S014296129900246X>
- Thomas, R.H. & Daniels, T.R., 2003. Ankle Arthritis. *The Journal of Bone & Joint Surgery*, 85(5), pp.923–936. Available at: <http://dx.doi.org/>.
- Ting, A.J. et al., 1987. The Role of Subtalar Motion and Ankle Contact Pressure Changes from Angular Deformities of the Tibia. *Foot and Ankle International*, 7(5), pp.290-299. Available at: <http://journals.sagepub.com/doi/abs/10.1177/107110078700700505>
- Tipper, J. et al., 2000. Quantitative analysis of polyethylene wear debris, wear rate and head damage in retrieved Charnley hip prostheses. *Journal of Materials*, 11(2), pp.117-124. Available at: <http://www.springerlink.com/index/wu08g0256m436456.pdf>
- Tipper, J.L. et al., 2001. Characterisation of wear debris from UHMWPE on zirconia ceramic, metal-on-metal and alumina ceramic-on-ceramic hip

- prostheses generated in a physiological anatomical hip joint simulator. *Wear*, 250(1–12), pp.120–128. Available at:
<http://www.sciencedirect.com/science/article/pii/S0043164801006536>.
- Tochigi, Y. et al., 2005. The effect of accuracy of implantation on range of movement of the Scandinavian Total Ankle Replacement. *Journal of Bone and Joint Surgery- British Volume*, 87(5), pp.736–740.
- Tomlinson, M. & Harrison, M., 2012. The New Zealand Joint Registry: report of 11-year data for ankle arthroplasty. *Foot and ankle clinics*, 17(4), pp.719–723. Available at: <http://europepmc.org/abstract/MED/23158379>.
- Tower, S.S., 2007. Rim Cracking of the Cross-Linked Longevity Polyethylene Acetabular Liner After Total Hip Arthroplasty. *The Journal of Bone and Joint Surgery (American)*, 89(10), p.2212. Available at:
<http://jbjs.org/cgi/doi/10.2106/JBJS.F.00758>
- Tuke, M. et al., 2010. 3D linear and volumetric wear measurement on artificial hip joints—Validation of a new methodology. *Precision Engineering*, 34(4), pp.777–783. Available at:
<http://www.sciencedirect.com/science/article/pii/S0141635910000905>.
- Uselli, F.G. et al., 2016. Posterior Talar Shifting in Mobile-Bearing Total Ankle Replacement. *Foot & Ankle International*, 37(3), pp.281–287. Available at:
<http://www.ncbi.nlm.nih.gov/pubmed/26443698>
- Valderrabano, V. et al., 2003. Kinematic changes after fusion and total replacement of the ankle: part 1: Range of motion. *Foot and Ankle International*, 24(12), pp.881–887.
- Vickerstaff, J.A., Miles, A.W. & Cunningham, J.L., 2007. A brief history of total ankle replacement and a review of the current status. *Medical engineering & physics*, 29(10), pp.1056–1064. Available at:
<http://www.sciencedirect.com/science/article/pii/S1350453306002487>.
- Walter, R. et al., 2015. ¶. *Bone and Joint Journal Orthopaedic Proceedings Supplement*, 97–B(SUPP 14), p.15.
- Wang, A., 2001. A unified theory of wear for ultra-high molecular weight polyethylene in multi-directional sliding. *Wear*, 248(1), pp.38–47. Available at: <http://www.sciencedirect.com/science/article/pii/S0043164800005226>
- Wang, A. et al., 1998. Lubrication and wear of ultra-high molecular weight polyethylene in total joint replacements. *Tribology International*, 31(1), pp.17–33.
- Wang, A., Essner, A. & Klein, R., 2001. Effect of contact stress on friction and wear of ultra-high molecular weight polyethylene in total hip replacement. *Proceedings of the Institution of Mechanical Engineers, Part H: Journal of Engineering in Medicine*, 215(2), pp.133–139. Available at:
<http://journals.sagepub.com/doi/10.1243/0954411011533698>
- Williams, S. et al., 2003. Wear and deformation of ceramic-on-polyethylene total hip replacements with joint laxity and swing phase microseparation. *Proceedings of the Institution of Mechanical Engineers, Part H: Journal of*

- Engineering in Medicine*, 217(2), pp.147–153. Available at: <http://sdj.sagepub.com/lookup/10.1243/09544110360579367>
- Williams, S., Leslie, I. & Isaac, G., 2008. Tribology and wear of metal-on-metal hip prostheses: influence of cup angle and head position. *Journal of Bone Joint*.
- Winter, D.A., 1991. *The biomechanics and motor control of human gait: normal, elderly and pathological*, University of Waterloo Press. Available at: <https://trid.trb.org/view.aspx?id=770965>
- Wood, P.L. et al., 2009. A randomised, controlled trial of two mobile-bearing total ankle replacements. *Journal of Bone and Joint Surgery- British Volume*, 91(1), pp.69–74.
- Wood, P.L.R. & Deakin, S., 2003. Total ankle replacement. *Journal of Bone and Joint Surgery-British volume-*, 85(3), pp.334–341.
- Wu, W.L. et al., 2000. Gait analysis after ankle arthrodesis. *Gait Posture*, 11(1), pp.54–61.
- Yamaguchi, S. et al., 2009. Ankle and subtalar kinematics during dorsiflexion-plantarflexion activities. *Foot Ankle International*, 30(4), pp.361–366.
- Yeung, M.S. et al., 1994. An epidemiological survey on ankle sprain. *British journal of sports medicine*, 28(2), pp.112–6. Available at: <http://www.ncbi.nlm.nih.gov/pubmed/7921910>
- Zhao, D. et al., 2007. In vivo medial and lateral tibial loads during dynamic and high flexion activities. *Journal of Orthopaedic Research*, 25(5), pp.593–602. Available at: <http://doi.wiley.com/10.1002/jor.20362>
- Zhao, H. et al., 2011. A systematic review of outcome and failure rate of uncemented Scandinavian total ankle replacement. *International Orthopaedics*, 35(12), pp.1751–1758. Available at: <http://link.springer.com/10.1007/s00264-011-1339-y>
- Zietz, C. et al., 2015. Experimental testing of total knee replacements with UHMW-PE inserts: impact of severe wear test conditions. *Journal of Materials Science: Materials in Medicine*, 26(3), p.134. Available at: <http://link.springer.com/10.1007/s10856-015-5470-y>

APPENDIX A
PUBLICATIONS

APPENDIX A

PUBLICATIONS

Journal publications

Smyth, A. et al., 2017. Influence of kinematics on the wear of a total ankle replacement. *Journal of Biomechanics*, 53, pp.105–110.

Conference Proceedings

A. Smyth, J. Fisher, A. Traynor, C. Brockett. Wear of Total Ankle Replacements. MEIBioeng, Leeds, UK, 2015. Chapters 2 and 3.

A. Smyth, J. Fisher, A. Traynor, C. Brockett. Wear of Total Ankle Replacements. International Society of Technology in Arthroplasty (ISTA), Vienna, Austria, 2015. Chapters 2 and 3.

A. Smyth, J. Fisher, A. Traynor, C. Brockett. Wear Testing of Total Ankle Replacements. Centre for Innovative Manufacturing in Medical Devices (MeDe) Annual Conference, Leeds, UK, 2015. Chapters 2 and 3.

A. Smyth, J. Fisher, S. Suárez, C. Brockett. Wear of a Total Ankle Replacements. Orthopaedic Research Society (ORS), Orlando, Florida, USA, 2016. Chapters 2 and 3

A. Smyth, J. Fisher, S. Suárez, C. Brockett. The Effect of Total Ankle Replacement Malalignment on Version and Contact Area. FOOT International, Berlin, Germany 2016. Chapter 5.

A. Smyth, J. Fisher, S. Suárez, C. Brockett. Malalignment Biomechanics for a Total Ankle Replacement. International Society of Technology in Arthroplasty (ISTA), Boston, Massachusetts, USA, 2016. Chapter 5.

A. Smyth, J. Fisher, S. Suárez, C. Brockett. The Effect of Malalignment on the Wear of a Total Ankle Replacement. Centre for Innovative Manufacturing in Medical Devices (MeDe) Annual Conference, Bradford, UK, 2016. Chapters 4 and 6.

A. Smyth, J. Fisher, S. Suñer, C. Brockett. The Effect of Malalignment on a Mobile Bearing Total Ankle Replacement. Orthopaedic Research Society (ORS), San Diego, USA, 2017. Chapters 4, 5 and 6.

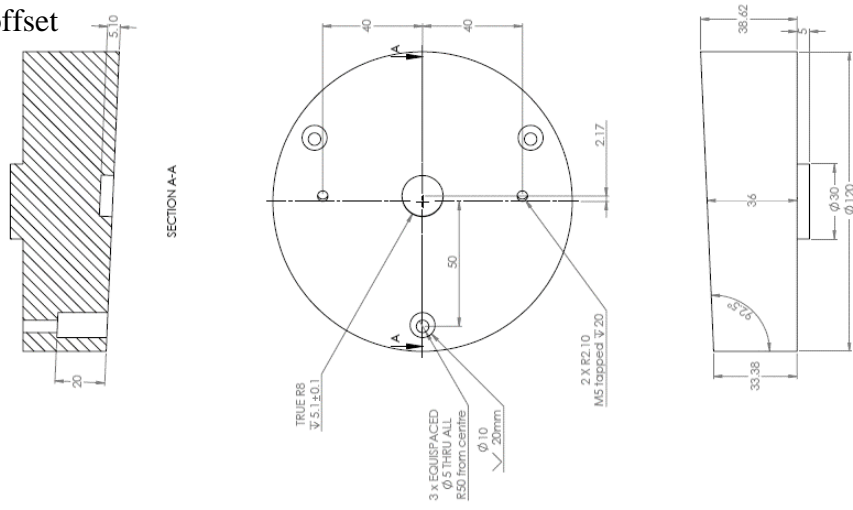
A. A. Stratton-Powell, A. Smyth, S. Williams, A. Redmond, J. L. Tipper, J. Fisher, C. Brockett. Surface Characterisation of Total Ankle Replacement: Retrieved Vs. In-Vitro Simulation. Orthopaedic Research Society (ORS), San Diego, USA, 2017. Chapter 6.

A. A. Stratton-Powell, A. Smyth, S. Williams, A. Redmond, J. L. Tipper, C. Brockett. Surface Characterisation of Total Ankle Replacement: Retrieved vs. In-vitro Simulation. ASTM Standards Meeting, Toronto, Canada, 2017. Chapter 6.

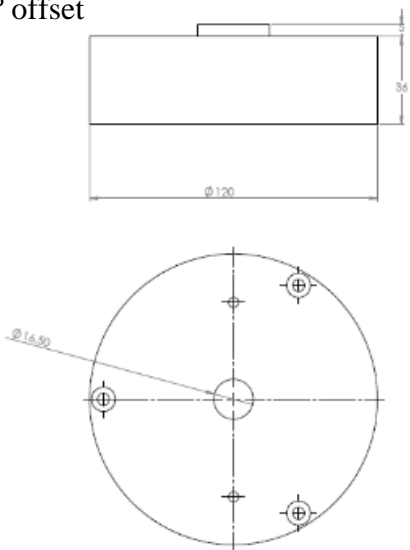
APPENDIX B
ENGINEERING DRAWINGS

Alignment Offset Fixtures

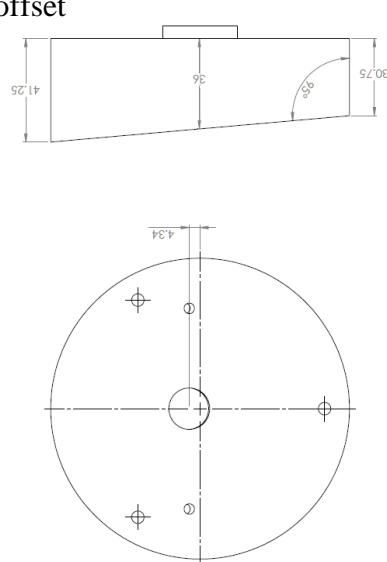
2.5° offset



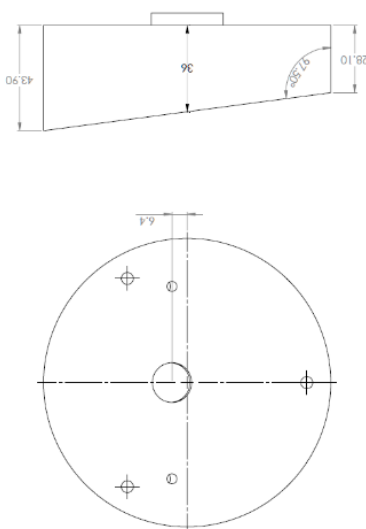
0° offset



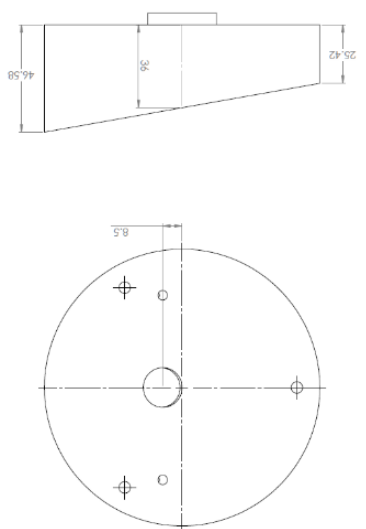
5° offset



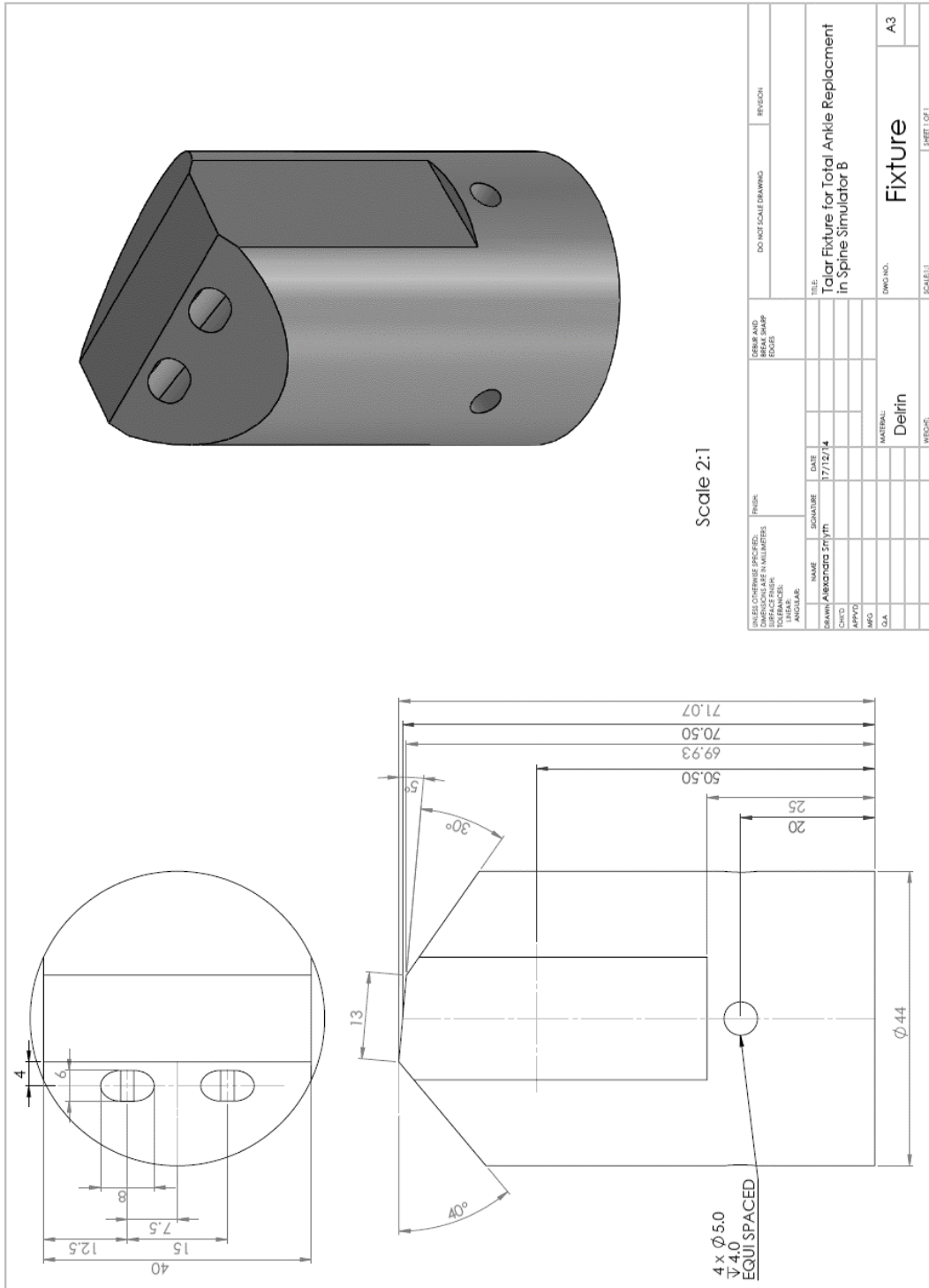
7.5° offset



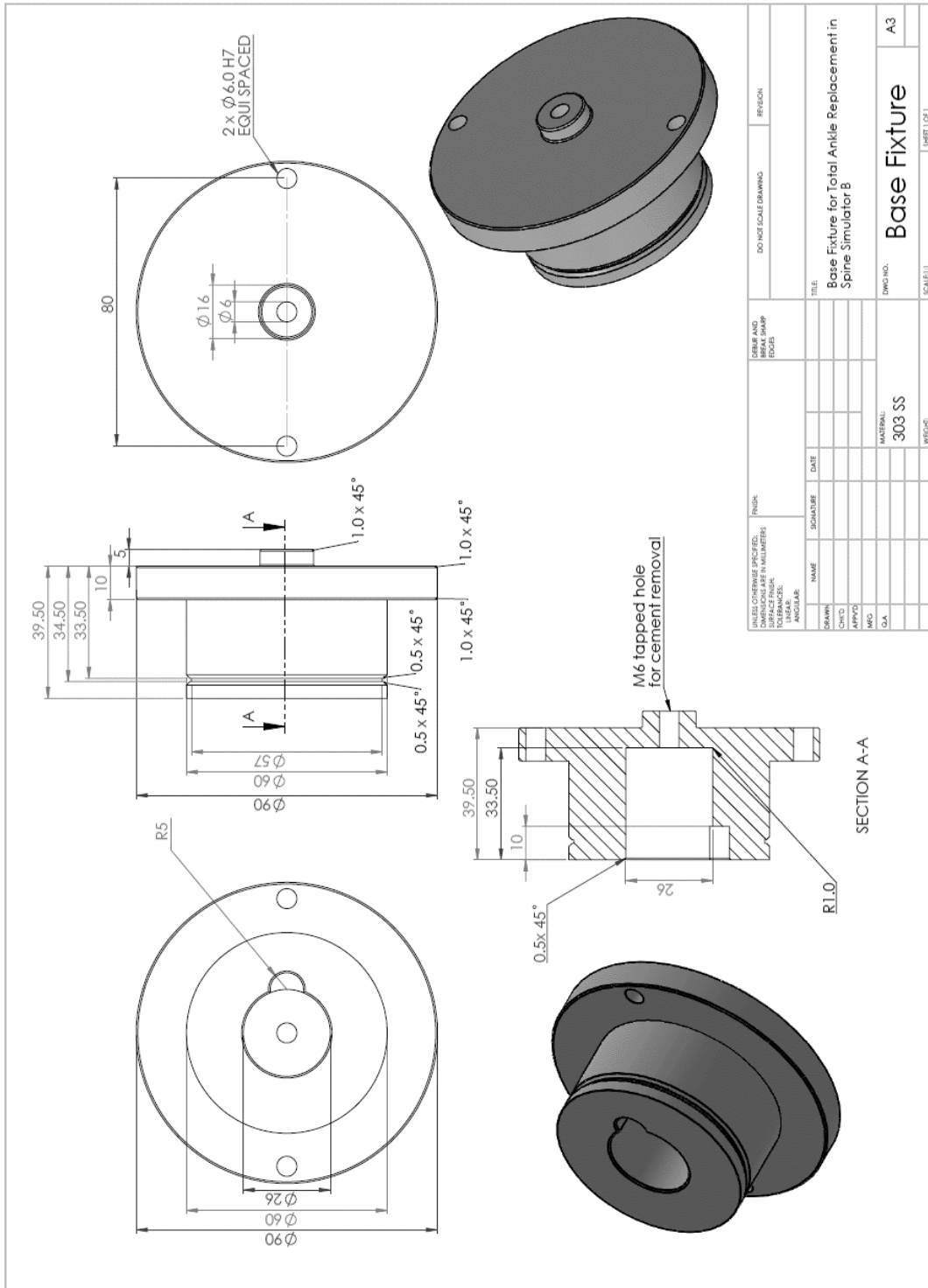
10° offset



Talar Fixture

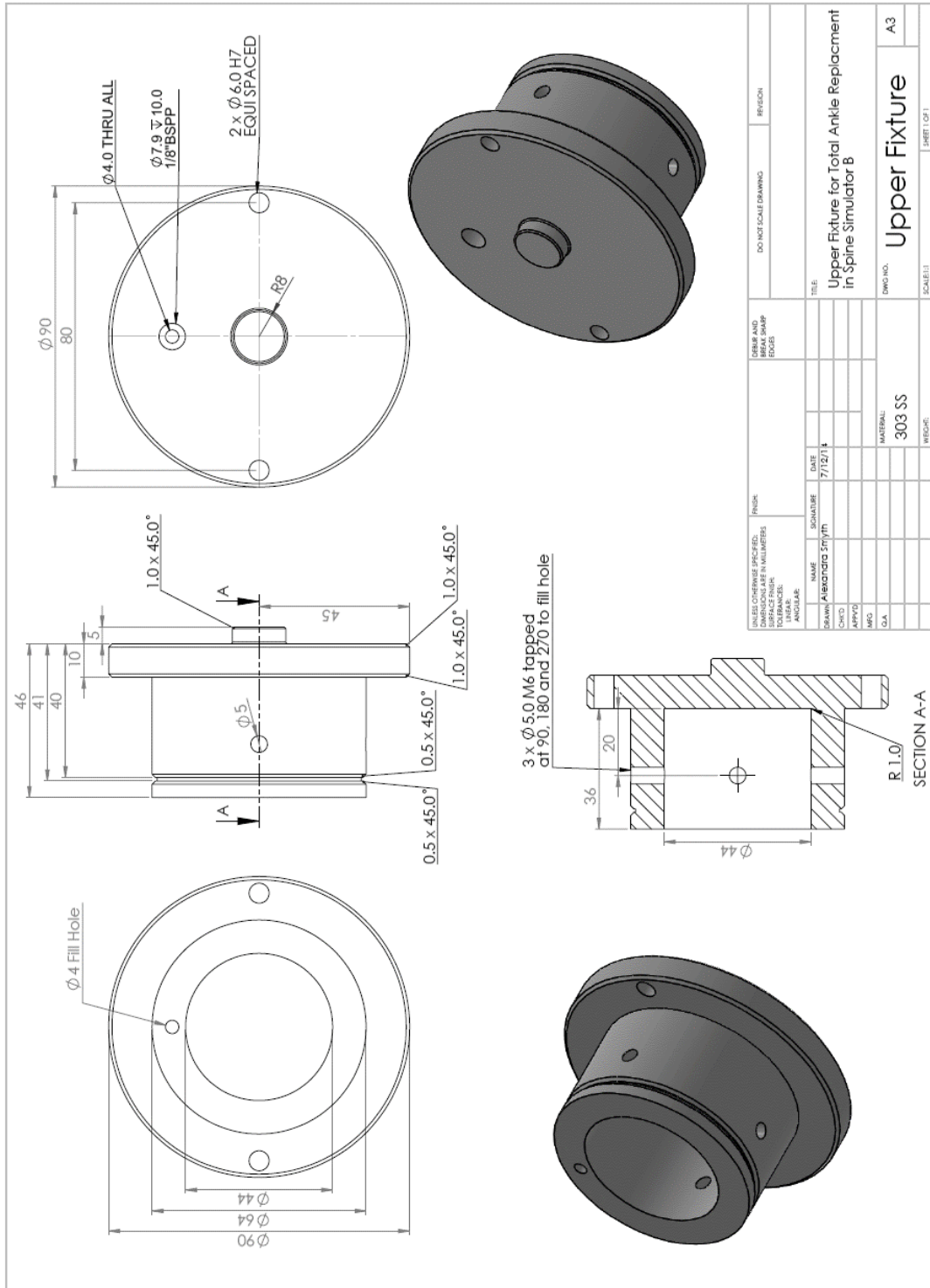


Tibial Holder

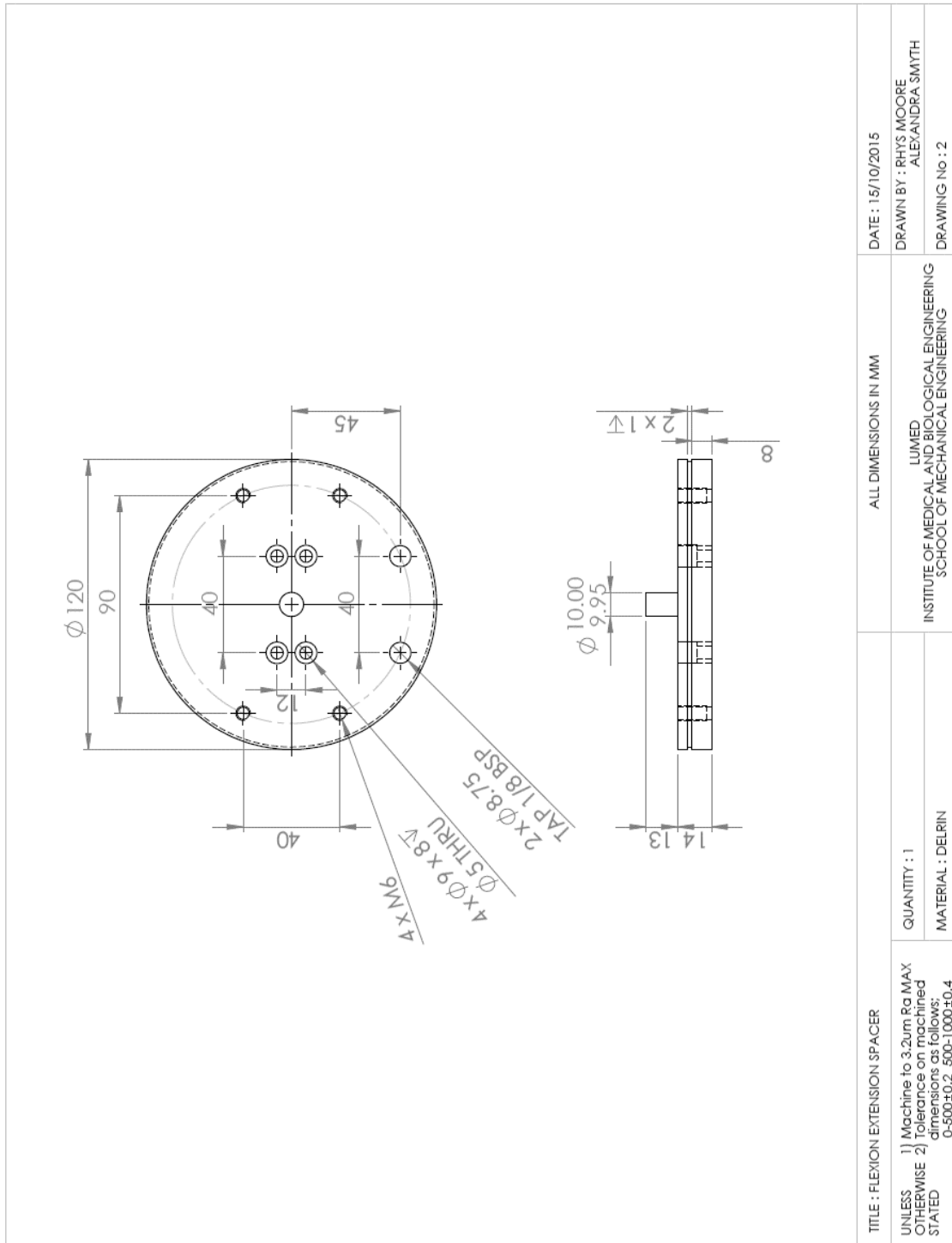


| UNLESS OTHERWISE SPECIFIED, DIMENSIONS ARE IN MILLIMETERS | | FINISH | | DEBARR AND SHARP EDGES | | DO NOT SCALE DRAWING | | REGION | |
|---|----------|--------|-----------|------------------------|-------|----------------------|---|--------------|--------------|
| TOLERANCES: | ANGULAR: | NAME | SIGNATURE | DATE | FRISK | SCALE | TITLE | DWG. NO. | SHEET 1 OF 1 |
| | | | | | | | Base Fixture for Total Ankle Replacement in Spine Simulator B | | |
| | | | | | | | | 303 SS | |
| | | | | | | | | Base Fixture | A3 |
| | | | | | | | | | |

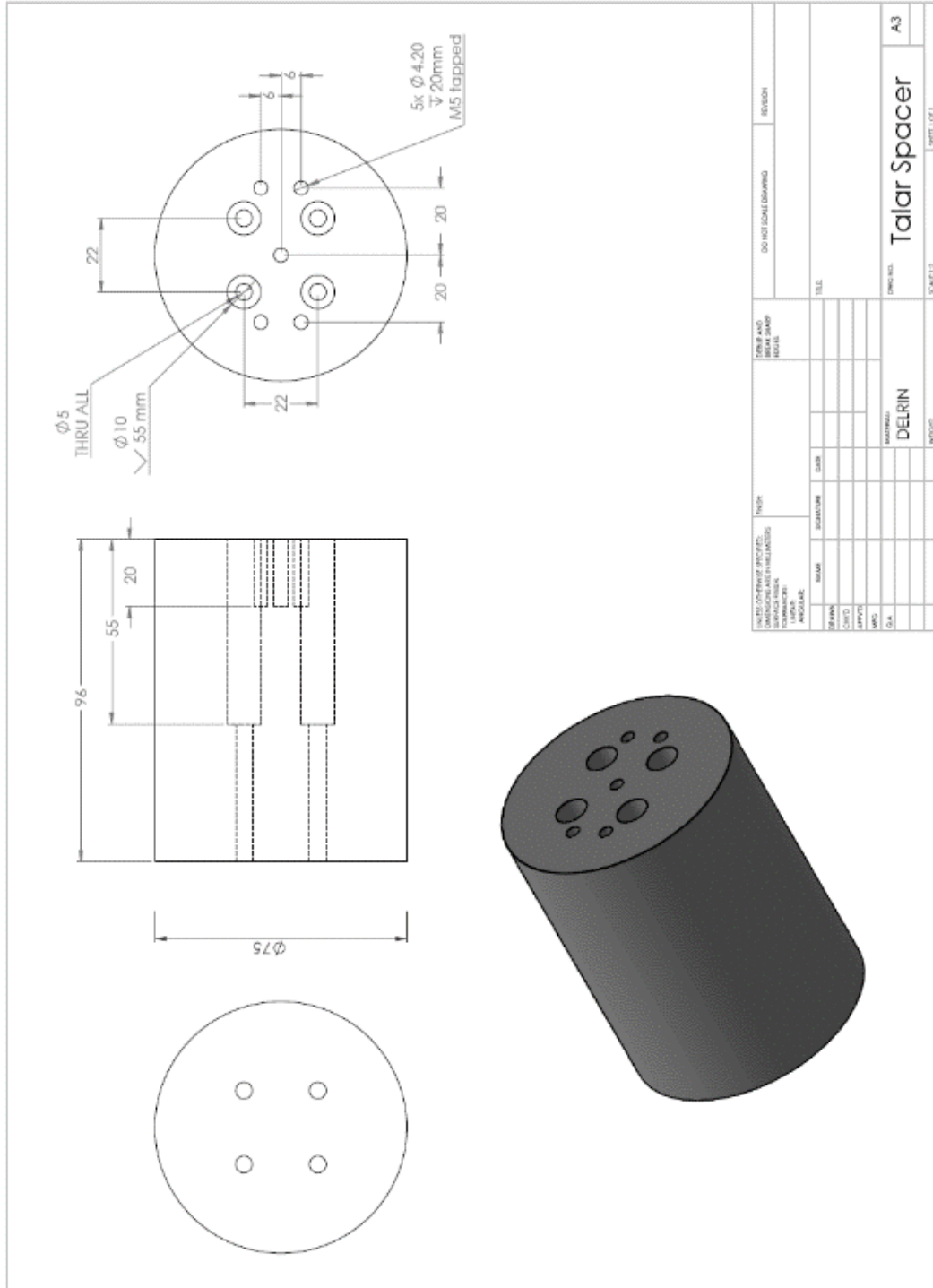
Talar Holder



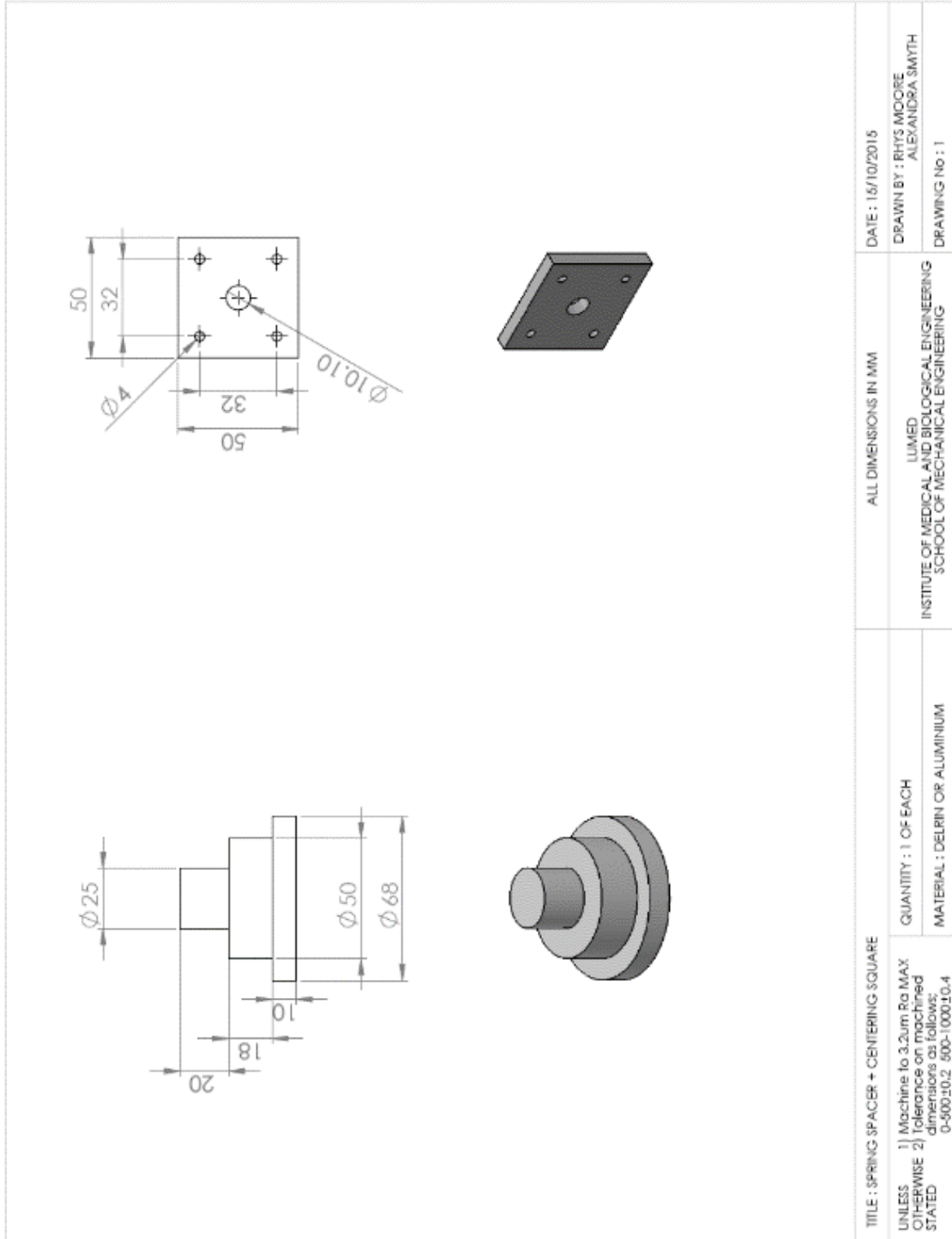
Talar fixation plate



Talar Spacer



Spring Spacer

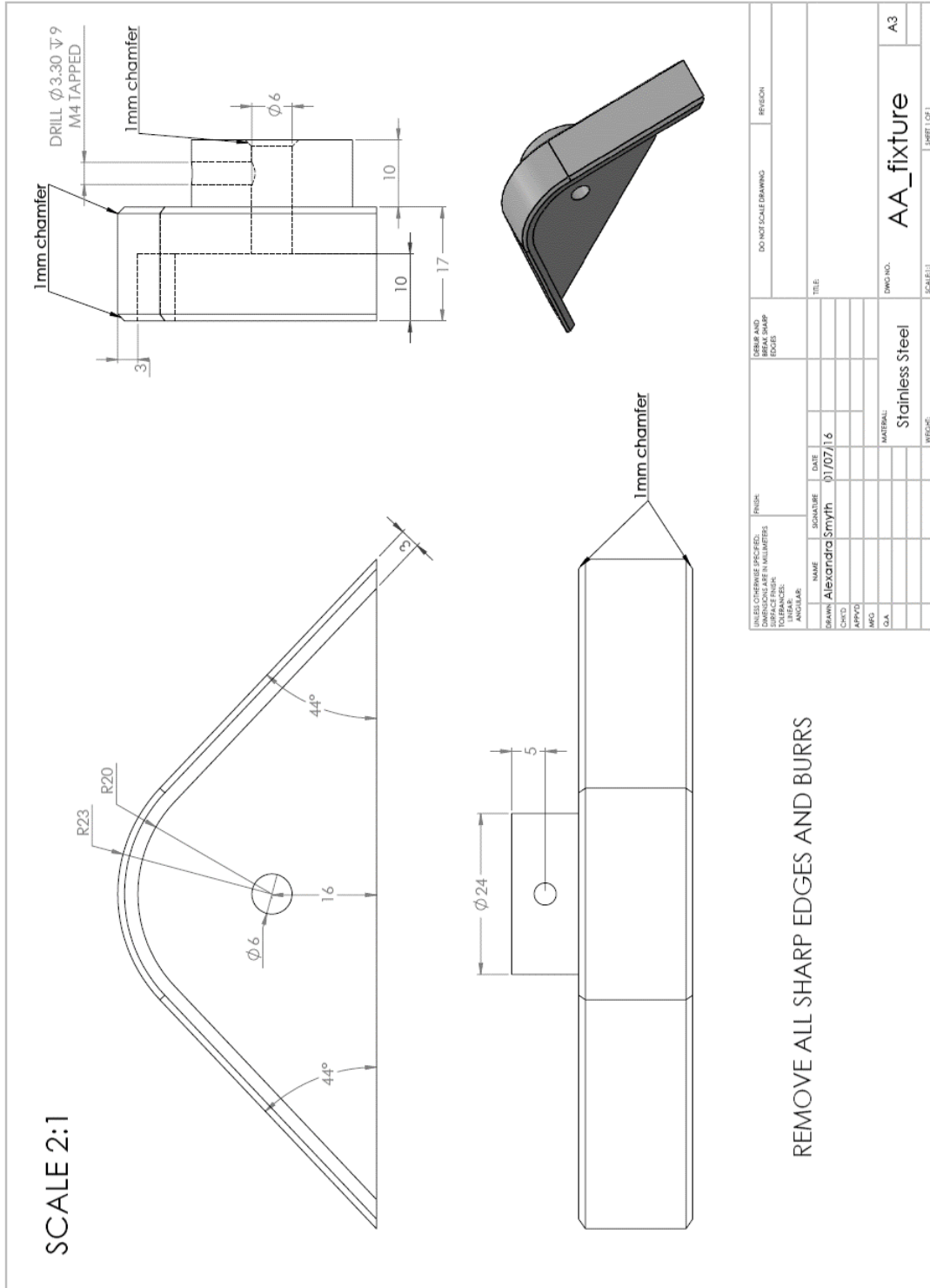


Neural alignment tibial spacer

PLEASE REMOVE ALL SHARP EDGES WITH A 1MM X 45° CHAMFER

| UNDESIGNATED PROTECTIVE FILMS AND/OR RELEASES HELD TOGETHER BY AN ADHESIVE | | FINISH | | TOLERANCE AND SURFACE FINISH | | DO NOT SCALE DRAWING | | REGION | |
|--|---------|------------|------|------------------------------|-----|----------------------|-----|---------------------|-----|
| RAW | SCALING | DATE | DATE | MIN | MAX | MIN | MAX | MIN | MAX |
| 3mm | 0.05mm | 12/01/2016 | | | | | | | |
| CHD | | | | | | | | | |
| APPT | | | | | | | | | |
| MFG | | | | | | | | | |
| QA | | | | | | | | | |
| | | | | MATERIAL | | | | | |
| | | | | Stainless steel | | | | | |
| | | | | NOTE | | | | | |
| | | | | | | | | TibialSpacer_KS4 A3 | |
| | | | | | | | | SCALE: 1:1 | |

Potentiometer Fixture



APPENDIX C
SIMULATOR CALIBRATION RECORD

APPENDIX C

SIMULATOR CALIBRATION RECORD

C.1 KS1



Calibration Record Knee Simulator

| Station Number | Axial load | Internal/External Rotation | Internal/External Rotation Zero | Anterior/Posterior Displacement | Anterior/Posterior Displacement Zero | Anterior/Posterior Load |
|----------------|----------------|----------------------------|---------------------------------|---------------------------------|--------------------------------------|--|
| G1-1 | 0.02796 | 9.24 | 139 | 13 | 139 | Not calibrated – study AP displacement |
| G1-2 | 0.03383 | 11.16 | 142 | 12.8 | 131 | As above |
| G1-3 | 0.03371 | 10.26 | 136 | 12.3 | 123 | As above |
| Average | 0.03186 | 10.22 | 139 | 12.7 | 131 | |
| G2-1 | 0.02475 | 9.38 | 128 | 10.4 | 104 | As above |
| G2-2 | 0.02647 | 11.02 | 131 | 12.6 | 128 | As above |
| G2-3 | 0.02696 | 9.82 | 124 | 12.7 | 128 | As above |
| Average | 0.02608 | 10.07 | 127.7 | 11.9 | 119.7 | |

Simulator: KS1

Calibrated by: Alex Smyth // Raelene Cowie
29/05/2014

Date:

Date Issued: 11/11/2011

Issued by: Louise M. Jennings

CALIBRATION_9_ Issue 1
Page 1 of 1



Calibration Record Single Knee Simulator 4

Calibration performed by: _____ Date: _____ Load cell S/N: _____ Calibration date: _____

| Station | AF Load | AP Force | TR Displacement | AP Displacement | FE Displacement |
|---------|-----------|------------------------|----------------------------|-----------------------------|-----------------|
| 1 | Load cell | Unit/ADC: 0.0711180 | Unit/ADC: 0.00137665198 | Unit/ADC: -0.0008745081 | |
| | Valve | Offset: 68.176469 | Offset: -1.71 | Offset: -0.120 | |
| 2 | Load cell | Unit/ADC: 13.673771 | Unit/ADC: 0.00138274336 | Unit/ADC: -0.00085451827 | |
| | Valve | Offset: -142.844631 | Offset: 0.090 | Offset: 1.34 | |
| 3 | Load cell | Unit/ADC: 0.0840110 | Unit/ADC: 0.00137665198 | Unit/ADC: -0.00085113627 | |
| | Valve | Offset: -34.099370 | Offset: -7.57 | Offset: 1.06 | |

Calibration Record Single Knee Simulator 4

Calibration performed by: _____ Date: _____ Load cell S/N: _____ Calibration date: _____

| Station | | AF Load | AP Force | TR Displacement | AP Displacement | FE Displacement |
|---------|-----------|-----------------------|----------|--------------------------|-----------------|-----------------|
| 4 | Load cell | Unit/ADC: 0.0702250 | | Unit/ADC: 0.00137665198 | -0.00086218045 | |
| | | Offset: 38.9824340 | | | | |
| | Valve | Unit/ADC: 13.85559410 | | Offset: -0.26 | 2.67 | |
| | | Offset: 145.2242620 | | | | |
| 5 | Load cell | Unit/ADC: 0.0604760 | | Unit/ADC: 0.001388888889 | -0.00087807876 | |
| | | Offset: -42.126827 | | | | |
| | Valve | Unit/ADC: 13.8145250 | | Offset: -0.090 | 4.55 | |
| | | Offset: -368.393280 | | | | |
| 6 | Load cell | Unit/ADC: 0.0714060 | | Unit/ADC: 0.00138274336 | -0.00087221980 | |
| | | Offset: 8.5423650 | | | | |
| | Valve | Unit/ADC: 13.8340480 | | Offset: -0.80 | 0.55 | |
| | | Offset: -78.3473570 | | | | |